Advanced control design tools for automotive applications

Tran Anh-Tu Nguyen

Université de Valenciennes et du Hainaut-Cambrésis

Thèse de doctorat

Pour obtenir le grade de Docteur de l'Université de

VALENCIENNES ET DU HAINAUT-CAMBRESIS

Spécialité : Automatique

présentée et soutenue par

Tran Anh-Tu, NGUYEN

le 02 décembre 2013

École doctorale :
Sciences Pour l'Ingénieur (SPI)

Équipe de recherche, Laboratoire :
Laboratoire d'Automatique, de Mécanique et d'Informatique Industrielles et Humaines (LAMIH)

Outils de Commande Avancés pour les Applications Automobiles

JURY

Président du jury
- GUERRA, Thierry-Marie, Professeur, Université de Valenciennes, LAMIH.

Rapporteurs
- SCORLETTI, Gérard. Professeur, École Centrale de Lyon, Ampère.
- SENAME, Olivier. Professeur, Grenoble-INP, GIPSA-Lab.

Examinateur
- ONDER, Christopher. Docteur, ETH Zürich.

Directeurs de thèse
- DAMBRINE, Michel. Professeur, Université de Valenciennes, LAMIH.
- LAUBER, Jimmy. Maître de Conférence, HDR, LAMIH.

Membre invité
- ROUSSEAU, Grégory. Docteur, Responsable des Activités Simulation Véhicules Électriques et Hybrides, Valeo.

ADVANCED CONTROL DESIGN TOOLS FOR AUTOMOTIVE APPLICATIONS

Anh-Tu NGUYEN

Laboratory of Industrial and Human Automation, Mechanics and Computer Science
LAMIH CNRS UMR 8201
E-mail: nguyen.trananhtu@gmail.com

Keywords: Nonlinear systems, Takagi-Sugeno models, robust control, input saturation, anti-windup, Lyapunov design, automotive engine control, Pontryagin's Minimum Principle, energy management strategy, vehicular electric power system.

Mots-clés: Systèmes non linéaires, modèles Takagi-Sugeno, commande robuste, commande saturée, anti-windup, Lyapunov design, contrôle moteur, Principe du Minimum de Pontryagin, stratégie de gestion d'énergie, système électrique du véhicule.

Dedicated to my parents

Kính tặng Bố Mẹ

Outils de Commande Avancés pour les Applications Automobiles

Résumé : Cette thèse est consacrée au développement de techniques de commande avancées pour des classes de systèmes non linéaires en général et pour des applications automobiles en particulier.

Pour répondre au besoin du contrôle moteur, la première partie propose des nouveaux résultats théoriques sur la technique de commande non linéaire à base de modèles de type Takagi-Sugeno soumis à la saturation de la commande. La saturation de la commande est traitée en utilisant sa représentation polytopique ou une stratégie anti-windup.

La deuxième partie porte sur la commande du système d'air d'un moteur turbocompressé à allumage commandé. Deux approches originales sont proposées. Dans la première, l'outil théorique concernant les modèles Takagi-Sugeno à commutation développé dans la première partie est directement appliqué. La seconde approche est basée sur une commande linéarisante robuste. L'originalité de ces approches multivariables consiste dans sa simplicité de mise en œuvre et son efficacité par rapport à celles qui existent dans la littérature.

La dernière partie vise à développer des stratégies pour la gestion énergétique des systèmes électriques d'un véhicule obtenues en se basant sur le Principe du Minimum de Pontryagin. À cet effet, deux approches sont considérées : l'approche hors ligne d'optimisation utilisant les informations du futur concernant les conditions de roulage et l'approche en ligne qui est adaptée de la précédente. Ensuite, ces deux approches sont implémentées et évaluées dans un simulateur avancé.

Advanced Control Design Tools for Automotive Applications

Abstract: This thesis addresses the development of some advanced control design tools for a class of nonlinear systems in general and for automotive systems in particular.

Motivated by automotive applications, Part I proposes some novel theoretical results on control design for nonlinear systems under Takagi-Sugeno form subject to the control input saturation. The input saturation is dealt with by using its polytopic representation or an anti-windup strategy.

Part II deals with our automotive application concerning the control of a turbocharged air system of a spark ignition engine. To this end, two novel control approaches are proposed in this part. For the first one, the theoretical design tool on switching Takagi-Sugeno controller developed in Part I is directly applied. The second one is based on a robust feedback linearization control technique. The originality of these MIMO approaches consist in their simplicity and effectiveness compared to other ones existing in the literature.

Part III aims at developing the strategies, which are based on the Pontryagin's Minimum Principle in optimal control theory, for the energy management of the vehicular electric power systems in a hybrid engine configuration. To this end, both offline optimization approach using the future information of driving conditions and online implementable one have been developed and evaluated in an advanced simulator.

Remerciements

Au terme de ces trois années tellement riches d'expériences scientifiques et humaines passionnantes, passées à travailler sur ma thèse, je tiens à remercier tous ceux qui ont participé à la réussite de ce travail.

En particulier, j'adresse ma sincère et profonde reconnaissance à Michel Dambrine et Jimmy Lauber, pour m'avoir donné la chance de découvrir le monde de recherche. C'est la chose la plus importante à mes yeux dans cette histoire de thèse. Je les remercie également pour leurs remarques constructives qui m'ont permis d'améliorer nettement mon travail. Et leurs qualités humaines exceptionnelles sans aucun doute ont fait que la période de thèse a été un réel plaisir.

Je remercie également Professeur Gérard Scorletti, Professeur Olivier Sename, qui m'ont fait l'honneur d'accepter d'être les rapporteurs de cette thèse. Vos remarques et questions m'ont beaucoup aidé à améliorer ce manuscrit et m'ont fourni de nouvelles pistes de recherche. Merci également à Professeur Thierry-Marie Guerra, Docteur Christophe Onder et Docteur Grégory Rousseau, les examinateurs de mon jury de thèse pour l'intérêt qu'ils ont porté à mon travail.

Je remercie encore le "big boss" du LAMIH de m'avoir permis de réaliser la collaboration avec Professeur Michio Sugeno, d'avoir été le "gentil président" de mon jury de thèse et pour les bons moments que j'ai passés avec lui (je le battrai un jour ... à la piscine).

A la fin de cette thèse, j'ai une énorme chance de collaborer avec Professeur Michio Sugeno, un chercheur "hors norme"! Je le remercie pour les discussions passionnantes qu'on a eues ensemble sur mon travail et aussi sur la recherche appliquée en général. Ces discussions ont énormément boosté ma motivation pour la recherche. J'espère pouvoir continuer les travaux débutés ensemble dans un futur proche.

Je remercie également l'ensemble des personnes que j'ai pu côtoyer durant ces années de thèse au LAMIH. Ils m'ont permis de passer ces trois années dans une ambiance très conviviale. Je pense notamment à mes amis "galériens" du labo de toutes nationalités (français, vietnamiens, kabyles, caballeros españoles et autres), avec qui j'ai pu discuter plus ou moins sérieusement sur tous

problèmes scientifiques en tout genre ... mais pas que de ça non plus. En particulier, merci à Jérémy (celui qui partage avec moi le plus des moments "Fermeeeeeeee!") et Boussaad (celui qui apprécie toujours ma cuisine à moi), les moments passés avec vous sont un de mes meilleurs souvenirs de thèse.

Un très grand merci à Antoine pour la suite de mon aventure de recherche au LAMIH. Je suis vraiment très motivé et j'ai hâte de commencer cette nouvelle aventure.

Je remercie également à la société Valeo, tout d'abord en tant que financeur de la thèse, mais aussi pour de nombreuses discussions intéressantes sur le projet Sural'Hy, en particulier avec Grégory Rousseau et Pascal Ménégazzi. Cela m'a permis d'avancer très vite pour la partie de gestion énergétique.

Je voudrais remercier le grenoblois Jacques Sicard et ma mamette de Paris Marie Scalbert qui fait maintenant partie de ma famille. Ils m'ont tellement aidé pendant les moments les plus difficiles en France. Jamais de ma vie, je vais oublier ce qu'ils m'ont apporté.

Je sais bien que le mot "MERCI" ne suffit jamais pour tous les sacrifices que mes parents m'ont consacrés et mon merci n'est pas non plus nécessaire pour eux. Leur amour inconditionnel est la raison de mes efforts pendant toutes ces années et c'est à eux que je dédie ce travail. Papa, maman, je vais faire de mon mieux pour ne jamais vous décevoir!

Enfin, je voudrais remercier ma copine pour son amour, sa compréhension et son soutien pendant dix ans ensemble. En particulier, elle a su *supporter* mon délire de recherche pendant toutes ces dernières années et je sais bien que ça va continuer dans le futur ... Merci infiniment à toi, ton encouragement est ma force!

TABLE OF CONTENTS

"Success is not final, failure is not fatal: it is the courage to continue that counts."

Winston Churchill, English statesman

Chapter 1. General Introduction

1. General Introduction and Context of the Thesis

Nowadays, modern vehicles must meet several challenges which are often conflicting. On the one hand, the pollutant emissions legislations imposed by governments at the international level are becoming more and more stringent because of environmental concerns. On the other hand, customers' demands in terms of performance and efficiency are also severely increasing. All of these objectives must be delivered at affordable cost and high reliability for series production vehicles. Engine downsizing and electric hybridization are two common technologies in automotive industry which are known as promising solutions to achieve these objectives.

Engine downsizing technique consists in reducing the engine displacement volume while keeping the same performance in terms of torque and power than the initial larger engine, and simultaneously to guarantee an improvement in engine efficiency (Leduc et al., 2003). This technology relies on the use of a turbocharger to increase the gas density at the intake of the engine. Unfortunately, the presence of the turbocharger in the air system causes the well known "turbo lag" phenomenon, i.e. the slow dynamics of intake pressure (and therefore of the engine torque) and the insufficient supercharging capabilities (the lack of torque) at low engine speeds. This phenomenon can be compensated by using variable geometry turbine, or by integrating other devices which aim at assisting the main turbocharger at low engine speeds, such as another turbocharger, mechanical or electrical compressor. Moreover, an adequate control strategy of the turbocharged air systems is also crucial to achieve a fast response time while limiting the overshoots.

Electric hybridization offers many possibilities to improve the overall efficiency of the vehicles:

- kinetic and potential energy can be recovered and stored in the energy storage systems and then it will be used later in the most appropriate ways to minimize the overall consumed energy of the vehicles,

- the engine operating points can be shifted to higher fuel economy regions,
- the engine can be downsized to reduce the engine losses,
- the engine can be shut off during standstill to save fuel and also limit pollutant emissions.

However, this technology leads to two major disadvantages. The first one consists in the additional cost (for more powerful electric machines, energy storage systems, etc.) which may make the vehicle unattractive to potential customers. The second disadvantage is the complexity that the hybrid systems may bring along. Then, the control task of the vehicle becomes more challenging.

The thesis is granted by VALEO Group and the region Nord-Pas de Calais as part of the FUI (Fonds Unique Interministériel) project named Sural'Hy (supercharging hybrid system for highly downsized spark ignition engines) labeled by I-Trans and Moveo. The project aims at developing an innovative technological solution to improve the energy consumption of the automotive engines. The proposed solution is a combination of electric hybridization together with electrical supercharging. This technology is expected to allow taking a further positive step towards engine downsizing so that not only the energy consumption but also the drivability performance of the vehicle can be significantly improved at the same time. To this end, an electrical supercharger (eSC) will be incorporated into the existing turbocharged air system. This electrical device is associated with an advanced electric power system which is able to recover kinetic energy during vehicle braking phases. All the interest of this technological solution comes from the following facts. First, the availability of supercharging air and therefore engine torque is almost instantaneous at low engine speed. Then, the eSC can be used to assist the main turbocharger to reduce the effects of "turbo lag". Hence, the drivability performance is improved. Second, the energy consumption of the eSC can be more or less compensated by "free energy" recovered by the advanced power system with an effective energy management strategy. In this context, two research topics are specifically considered within the thesis:

- The automotive applications concretely concern the control of the turbocharged air system of an automotive SI engine and the energy management for electric vehicle power system.
- Motivated by automotive applications, we have developed in this thesis some novel theoretical design tools using model-based polytopic control techniques involving LMI framework.

For the first topic, it should be noticed that the engine control task in Sural'Hy project is taken care by another industrial partner. Our task for this project is then to design an energy management system for different vehicular electric power systems. In parallel with this work, the control of the

turbocharged air system of the same SI engine is also carried out in the thesis. However, in our case, the eSC is not considered yet in the air system.

In recent years, automotive systems have become an attractive topic for both industrial and academic researchers. Indeed, performance and environmental requirements of these systems have constantly increased, e.g. turbocharged air system of SI engines is a very relevant example for this trend. As a consequence, the considered systems have become more and more sophisticated to cope with these stringent requirements. A low-cost solution to meet those requirements is to propose more and more effective control strategies in terms of accuracy, time response and robustness. In the second thesis topic, polytopic based design tools, which can meet this control challenge, are developed. In general, these control techniques are also very powerful to deal with some class of complex nonlinear systems.

2. Structure of the Thesis

This thesis is divided into three parts:

- Part I: Contributions to stabilization of nonlinear systems subject to input saturation in the Takagi-Sugeno form.
- Part II: Novel control approaches for turbocharged air system of a spark ignition engine.
- Part III: Energy management strategy for vehicular electric power systems.

Each part will begin with its introduction containing a detailed summary of each chapter. In what follows, a quick preview of all three parts and their chapters is given.

Part I focuses on the control approach based on the Takagi-Sugeno models. This part contains three chapters:

Chapter 2 provides some background related to this control approach which will be useful for the theoretical developments proposed in the following chapters.

Motivated by the application on control of the turbocharged air systems, Chapter 3 presents a method to design robust H_∞ controllers that stabilize uncertain and disturbed switching T-S systems subject to control input saturation. For this purpose, the input saturation is represented under its polytopic form. Based on Lyapunov stability theory, both state feedback control and static output feedback control will be addressed.

Chapter 4 presents a new control approach to deal with a class of nonlinear constrained systems. The systems are not only subject to input saturation but also to state constraints. Compared to the approach proposed in Chapter 3, this control approach aims at compensating the saturation effects with an anti-windup strategy. The output feedback controller and its anti-windup strategy will be simultaneously synthesized. The control design can be formulated as a multi-objective convex optimization problem and be effectively solved by using LMI tools.

Part II is devoted to the control of a turbocharged air system of a SI engine. To this end, two novel control approaches are presented.

Chapter 5 is first dedicated to the description of this complex system. Then, a state-of-the-art on its control issues is provided. Finally, this chapter shows how to apply the theoretical design tool developed in Chapter 3 for the considered automotive application.

Chapter 6 presents a new robust control design based on feedback linearization to deal with nonlinear systems subject to model uncertainties/perturbations. The controller gain is easily obtained by solving a convex optimization problem. From this theoretical result, the second nonlinear approach to control the turbocharged air system is presented. This MIMO approach has several great originalities. First, it can offer almost the same performance as the one proposed in Chapter 5 (tracking performance, closed-loop stability of the whole air system, fuel optimal strategy). Second, the controller is very simple and easily implementable. Third, this approach may only need the most common sensors available in series production turbocharged SI engine. We would like to stress that the proposed control approach in this chapter is in particular relevant for industrial context.

Part III contains Chapter 7. This chapter focuses on the work directly related to our task in Sural'Hy project with others industrial partners. Inspired by the research on energy management for hybrid electric vehicles, Chapter 7 presents some strategies to control the electric power system of the vehicle. These strategies aim at generating and storing electric energy in the most appropriate way to reduce the overall energy consumption and eventually the pollutant emissions. To this end, both offline optimal strategies using the information of the future driving conditions and online ones for real-time applications are investigated. Two electric power systems for the same vehicle structure will be considered.

3. Contributions

The research carried out within the framework of this thesis leads to several contributions in both theory and application. These contributions will be detailed in each corresponding part of the thesis. The works presented in this thesis have been the subject of the following publications:

- **Journal publications**
  1. Anh-Tu Nguyen, Michel Dambrine, Jimmy Lauber, "Lyapunov-Based Robust Control Synthesis for a Class of Switching Uncertain Nonlinear Systems Subject to Control Input Saturation", *Submitted for journal publication*.
  2. Anh-Tu Nguyen, Michel Dambrine, Jimmy Lauber, "Simultaneous Output Feedback and Anti-windup Controller Design for Constrained Nonlinear Systems in Takagi-Sugeno Form: An LMI-based Approach", *Submitted for journal publication*.
  3. Anh-Tu Nguyen, Jimmy Lauber, Michel Dambrine, "Optimal Control Based Energy Management for Advanced Automotive Electric Power Systems", *Submitted for journal publication*.
  4. Anh-Tu Nguyen, Michio Sugeno, Michel Dambrine, Jimmy Lauber, "Piecewise Bilinear Modeling: A Novel Approach to Control the Turbocharged Air System of an SI engine", *In preparation for journal publication*.

- **Conference publications**
  1. Anh-Tu Nguyen, Michio Sugeno, Michel Dambrine, Jimmy Lauber, "Feedback Linearization Based Control Approach for Turbocharged Air System of SI Engine: Towards a Fuel-Optimal Strategy", *Submitted.*
  2. Anh-Tu Nguyen, Jimmy Lauber, Michel Dambrine, "Modélisation et Contrôle Flou du Système d'Air d'un Moteur Essence avec Turbocompresseur", in Proc. of the 22ème Rencontres Francophones sur la Logique Floue et ses Applications, Reims, France, October 10-11, 2013.
  3. Anh-Tu Nguyen, Jimmy Lauber, Michel Dambrine, "Multi-Objective Control Design for Turbocharged Gasoline Air System: a Switching Takagi-Sugeno Model Approach", in Proc. of the American Control Conference, Washington DC, USA, June 17-19, 2013.
  4. Anh-Tu Nguyen, Jimmy Lauber, Michel Dambrine, "Robust H_∞ Control Design for Switching Uncertain System: Application for Turbocharged Gasoline Air System

Control", in Proc. of the 51st IEEE Conference on Decision and Control, Maui, Hawaii, December 10-13, 2012.

5. Anh-Tu Nguyen, Jimmy Lauber, Michel Dambrine, "Robust H_∞ Control for the Turbocharged Air System Using the Multiple Model Approach", in Proc. of the 38thAnnual Conference of the IEEE Industrial Electronics Society, Montreal, Canada, October 25-28, 2012. *Best oral presentation for "Robust Control" technical session*.
6. Anh-Tu Nguyen, Jimmy Lauber, Michel Dambrine, "Modeling and Switching Fuzzy Control of the Air Path of a Turbocharged Spark Ignition Engine", in Proc. of the IFAC Workshop on Engine and Powertrain Control, Simulation and Modeling, Rueil-Malmaison, France, October 23-25, 2012.
7. Anh-Tu Nguyen, Jimmy Lauber, Michel Dambrine, "Switching Fuzzy Control of the Air System of a Turbocharged Gasoline Engine", in Proc. of the IEEE International Conference on Fuzzy Systems, Brisbane, Australia, June 10-15, 2012.

- **Others**

1. Anh-Tu Nguyen, Jimmy Lauber, Michel Dambrine, "Commande Robuste H_∞ pour une Classe de Systèmes Incertains à Commutation. Application au Contrôle de la Boucle d'Air d'un Moteur Turbocompressé", Journées Automatique et Automobile, Valenciennes, Novembre, 2012.
2. Anh-Tu Nguyen, Jimmy Lauber, Michel Dambrine, "Commande Multi-objective Basée sur des Modèles Takagi-Sugeno à Commutation pour la Boucle d'Air d'un Moteur Turbocompressée", Journées Automatique et Automobile, Bordeaux, Octobre, 2013.

PART I. CONTRIBUTIONS TO STABILIZATION OF NONLINEAR SYSTEMS SUBJECT TO INPUT SATURATION IN THE TAKAGI-SUGENO FORM

Presentation of Part I

Over the past two decades, control technique based on the so-called Takagi-Sugeno (T-S) models (Takagi & Sugeno, 1985) has become an active research topic (Tanaka & Wang, 2001). In particular, this technique has received more and more significant attention (Sala et al., 2005; Feng, 2006; Guerra et al., 2009), since it has been successfully applied for numerous engineering applications (Tanaka & Wang, 2001; Lauber et al., 2011; Nguyen et al., 2012a). The T-S models are inspired from the historical approach of fuzzy logic (Mamdani, 1974).They can be interpreted as a collection of local linear models interconnected by nonlinear membership functions. Then, based on a T-S model, a model-based control can be designed to guarantee the stability and achieve some performance requirements for nonlinear systems. Such a model presents several advantages. First, the T-S model is a universal approximator (Tanaka & Wang, 2001), and in many cases, this type of models can be used to represent exactly nonlinear systems globally or semi-globally(Ohtake et al., 2001). Second, thanks to its polytopic structure, the T-S control approach makes possible the extension of some powerful linear design tools to the case of nonlinear systems (Tanaka & Wang, 2001). Third, this control technique provides a general and systematic framework to cope with a wide class of nonlinear systems. Indeed, many stability or design conditions in the framework of T-S model are formulated as LMI constraints (Boyd et al., 1994; Scherer & Weiland, 2005), the control problem can then be solved efficiently with some already available numerical algorithms (Tanaka & Wang, 2001).

Among all nonlinear phenomena, actuator saturation is unavoidable in almost all real applications. This effect can severely degrade the closed-loop system performance and in some cases may lead the

system to instability. Motivated by this practical control aspect, a great deal of efforts has been recently focused on saturated systems, see e.g. (Fang et al., 2004; Tarbouriech et al., 2011)and the references therein. However, very few results are available for the nonlinear systems.

In general, there are two main approaches to deal with the input saturation problems. The first one takes directly into account the saturation effect in control design process. To this end, two principal synthesis techniques are considered in the literature: *saturated control law* and *unsaturated control law*. In the latter one, the initial state domain and the design are such that the control law will never reach saturation limits. Presented for instance in (Tanaka & Wang, 2001; Ohtake et al., 2006), this type of low-gain controller is very conservative and often leads to poor closed-loop performance (Tarbouriech et al., 2011; Cao & Lin, 2003). As its name indicates, the saturated control law (Cao & Lin, 2003) allows the saturation of the input signal which results in a better control performance. That is why this type of control laws will be addressed in this thesis. In the second approach, the saturation effect is dealt with by using *anti-windup* compensators. Two types of anti-windup based controllers can be found in the literature: one-step and two-step design. For the *one-step design* method, the anti-windup terms are directly taken into account in the controller. Therefore, the controllers and the anti-windup compensators are simultaneously designed (Wu et al., 2000; Mulder et al., 2009). For the *two-step design* method, the control input law is first computed by ignoring actuator saturation. Once the controller has been designed, an additional anti-windup compensator is included to minimize any undesirable effect of the saturation constraints on closed-loop performance (Hu et al., 2008; Zaccarian & Teel, 2004; Tarbouriech et al., 2011). In this thesis, we deal with the *one-step design* method. In the literature, most of works on anti-windup compensators are available for linear time-invariant (LTI) systems. The book (Tarbouriech et al., 2011) offers an excellent overview of these works. However, very few results exist for nonlinear systems.

Motivated by these facts, Part I presents some contributions to stabilization of nonlinear systems subject to input saturation in the framework of T-S representation. This part is organized as follows.

Chapter 2 provides the background on T-S models and some control issues concerning the control technique based on this kind of models. In this chapter, we review various results to show different possibilities that T-S models may offer in terms of analysis and control design for nonlinear systems. We do not intend to give an exhaustive state-of-the art of this topic but to provide some information directly related to other chapters of this part. More information can be found for example in (Sala et al., 2005; Feng, 2006; Guerra et al., 2009).

Chapter 3 aims at proposing a new method to design robust H_∞ controllers that stabilize uncertain and disturbed switching T-S systems subject to control input saturation. To this end, some motivations on the choice of a switching T-S model instead of a classical one are presented. In this chapter, the input saturation is taken into account in the control design under a polytopic form. Two cases will be investigated: state feedback control and static output feedback control. The Lyapunov stability theory is used to derive control design conditions which are formulated as a linear matrix inequality (LMI) optimization problem. In comparison with previous results, the proposed method not only provides a simple and efficient design procedure but also leads to less conservative controllers by maximizing the domain of attraction.

Chapter 4 is devoted to develop a novel approach dealing with constraint nonlinear systems in the form of T-S model. Here, the systems are subject to both input and state constraints. The *one-step design* method is used to simultaneously synthesize the output feedback controller and its anti-windup strategy. By the means of Lyapunov stability theorem, the control design will be formulated as a multi-objective convex optimization problem. The desired trade-off is fixed by the designer for several conflicting control objectives. An example is also given to illustrate the effectiveness of the proposed approach.

Notations. The following notations will be used in this part:

For an integer number r, Ω_r denotes the set $\{1,2,\ldots,r\}$. $\mathbb{R}^+ = [0,\infty)$ is the set of non-negative real numbers. x_i is the i^{th} element of vector x. $x \succ (\succeq,\prec,\preceq)\, y$ with $x, y \in \mathbb{R}^n$ means that $x_i - y_i > (\geq,<,\leq)\, 0$ for all $i \in \Omega_n$. (*) stands for symmetric matrix blocks and $sym(X) = X + X^T$. $X > (\geq,<,\leq) 0$ is used to denote a symmetric, positive-definite (positive semi-definite, negative definite, negative semi-definite, respectively) matrix. I denotes the identity matrix of appropriate dimensions. For a positive-definite matrix $P \in \mathbb{R}^{n_x \times n_x}$, the ellipsoid $\{x \in \mathbb{R}^{n_x} : x^T P x \leq \rho\}$ will be denoted $\mathcal{E}(P,\rho)$ and for brevity $\mathcal{E}(P) \equiv \mathcal{E}(P,1)$. The set $co\{x^j,\ \forall j \in \Omega_q\}$ is the convex hull of the points $x^j \in \mathbb{R}^{n_x}$. For any value of the argument, the nonlinear functions $\eta_1, \ldots, \eta_r$ are said to verify the convex sum property if $\eta_i \geq 0,\ \forall i \in \Omega_r$ and $\sum_{i=1}^{r} \eta_i = 1$.

"There is nothing more practical than a good theory."

Kurt Lewin, German-American psychologist

Chapter 2. Background on T-S Models

1. Introduction

This chapter aims at presenting a quick tour of various results concerning stability and control design of T-S models. Here, only some basics problems concerning T-S models will be covered. For a more complete state-of-the-art, the reader can refer to (Tanaka & Wang, 2001; Sala et al., 2005; Feng, 2006; Guerra et al., 2009). The chapter starts with a description of T-S models followed by the construction procedure of such a model from another one that may have been obtained from physical principles for instance. In general, design problems based on T-S models can be formulated in terms of LMI constraints (Boyd et al., 1994). To that end, some basics on LMI problems and matrix properties will be reminded.

In T-S model framework, direct Lyapunov method is usually used to derive design conditions. For simplicity, only some standard results on stability and stabilization with quadratic Lyapunov function are presented. A state-of-the-art of output feedback design is also given. Among of numerous results available in the literature concerning performance indexes when dealing with T-S models, we review some of them which are directly related to the thesis work. Finally, some discussions on conservatism of the solutions are also presented in this chapter.

2. T-S Model and Related Control Issues

2.1. Description and Construction of T-S Model

2.1.1. Description of T-S model

In this thesis, the dynamical systems are modeled in the state-space framework and expressed as:

$$\begin{cases} \dot{x}(t) = f\left(\theta(t)\right)x(t) + g\left(\theta(t)\right)u(t) \\ y(t) = h\left(\theta(t)\right)x(t) \end{cases} \tag{2.1}$$

where $f(\cdot)$, $g(\cdot)$ and $h(\cdot)$ are smooth nonlinear matrix functions, $x(t) \in \mathbb{R}^{n_x}$ is the system state vector, $u(t) \in \mathbb{R}^{n_u}$ is the control vector, $y(t) \in \mathbb{R}^{n_y}$ is the measured output vector and $\theta(t) \in \mathbb{R}^{k}$ is the scheduling variable vector that may be functions of the state variables, and/or time. It is assumed that the scheduling variables are bounded and smooth in a compact set $C \subseteq \mathbb{R}^{n_x}$ of the state space including the origin.

For control design purpose, we can exactly represent or approximate the nonlinear system (2.1) under T-S form as:

$$\begin{cases} \dot{x}(t) = \sum_{i=1}^{r} \eta_i(\theta(t)) \left(A_i x(t) + B_i u(t) \right) \\ y(t) = \sum_{i=1}^{r} \eta_i(\theta(t)) C_i x(t) \end{cases} \tag{2.2}$$

For $i \in \Omega_r$, the matrices $A_i \in \mathbb{R}^{n_x \times n_x}$, $B_i \in \mathbb{R}^{n_x \times n_u}$, $C_i \in \mathbb{R}^{n_y \times n_x}$ represent the set of r local linear models and the nonlinear membership functions $\eta_i(\theta(t))$ satisfy the convex-sum property. For simplicity, the explicit time-dependence of the variables is omitted throughout the rest of this part except for confusing situations.

Remark 2.1. Thanks to the convex-sum property of the nonlinear membership functions $\eta_i(\theta)$, the T-S model (2.2) is nothing else than the convex combination of r local linear models. This very nice characteristic is deeply exploited in favor of stability analysis and controller synthesis.

2.1.2. Construction of T-S model

In general, there are two approaches to derive a T-S model from a given nonlinear system (Tanaka & Wang, 2001). The first one is based on system identification algorithms (fuzzy modeling) using input-output data (Sugeno & Kang, 1988; Kim et al., 1997). This approach is suitable for nonlinear systems without mathematical/physical models but with input-output data available. On the contrary, if a preliminary nonlinear model is available, we may use a second approach which is based on the idea of sector nonlinearity concept or local approximation (Tanaka & Wang, 2001). This approach offers a simple and systematic way to obtain the T-S representation of a given nonlinear system. In what follows, we only focus on the second approach which will be exclusively used to obtain the T-S models for all examples and applications in this thesis.

For generality, suppose that there are k nonlinearities $nl_i(\theta)$, $i \in \Omega_k$ in system (2.1). If $x \in C \subseteq \mathbb{R}^{n_x}$, it follows that all nonlinear terms are bounded $nl_i(\theta) \in \left[\underline{nl_i}, \overline{nl_i}\right]$. Then, each nonlinearity can be represented as: $nl_i(\theta) = \omega_i^0(\theta).\underline{nl_i} + \omega_i^1(\theta).\overline{nl_i}$ where $\forall i \in \Omega_k$ and the weighting functions are expressed by:

$$\begin{cases} \omega_i^0(\theta) = \left(\overline{nl_i} - f(\theta)\right) \Big/ \left(\overline{nl_i} - \underline{nl_i}\right) \\ \omega_i^1(\theta) = \left(f(\theta) - \underline{nl_i}\right) \Big/ \left(\overline{nl_i} - \underline{nl_i}\right) \end{cases} \tag{2.3}$$

It is noticed that the weighting functions $\omega_i^0(\theta)$ and $\omega_i^1(\theta)$ satisfy the convex-sum property. Then, the membership functions corresponding to the i^{th} local linear model is computed as follows:

$$\eta_i(\theta) = \prod_{j=1}^{k} w_{ij}(\theta) \tag{2.4}$$

where $w_{ij}(\theta)$ is either $\omega_i^0(\theta)$ or $\omega_i^1(\theta)$, depending on which weighting function is used to obtain the i^{th} local linear model. Of course, the membership functions obtained from (2.4) verify the convex sum property.

The matrices A_i , B_i , C_i are then constructed by substituting the elements corresponding to the weighting functions used for i^{th} local linear model, i.e. $\underline{nl_i}$ for $\omega_i^0(\theta)$ and $\overline{nl_i}$ for $\omega_i^1(\theta)$, respectively, into the matrix functions $f(\cdot)$, $g(\cdot)$ and $h(\cdot)$ of the system (2.1).

Remark 2.2. Using sector nonlinearity approach, we can get an exact T-S representation of nonlinear system in the compact set $C \subseteq \mathbb{R}^{n_x}$. However, this approach inherently causes an important disadvantage. Indeed, the T-S representation is not unique and depends on the choice of the scheduling variables (the nonlinearities). Moreover, the number of local models r increases exponentially with the number of nonlinearities k , i.e. $r = 2^k$. As a consequent, a natural and important question arises: "How to obtain *the best T-S representative* for a given nonlinear system?" The best T-S representative means the model having lowest complexity (minimum number of local linear models) and "still suitable" for design problems. This question is really important for practical applications since a large number of local models may make intractable the design problems with

actual numerical algorithms and/or solvers. Interested reader is referred to (Taniguchi et al., 2001) for more details.

2.1.3. Illustrative example

In order to illustrate how to derive directly the T-S model from the nonlinear system, we consider the following example:

$$\dot{x} = \begin{bmatrix} 2 & \sin(x_2) \\ -x_1^2 x_2 & 7 \end{bmatrix} x + \begin{bmatrix} 5 \\ \sin(x_2) \end{bmatrix} u \tag{2.5}$$

where $x \triangleq [x_1 \quad x_2]^T$ and the nonlinearities are $\sin(x_2)$ and $-x_1^2 x_2$. For simplicity, we assume that $x_1 \in [-1,1]$ and $x_2 \in [-\pi, \pi]$. Of course, we can assume any range of x_1 and x_2 to construct the T-S model for the nonlinear system (2.5).

For the nonlinear terms, let us define $\theta \triangleq [\theta_1 \quad \theta_2]^T$ where $\theta_1 = \sin(x_2)$ and $\theta_2 = -x_1^2 x_2$, then system (2.5) becomes:

$$\dot{x} = \begin{bmatrix} 2 & \theta_1 \\ \theta_2 & 7 \end{bmatrix} x + \begin{bmatrix} 5 \\ \theta_1 \end{bmatrix} u \tag{2.6}$$

Now, we compute the bounds of each nonlinearity with $x_1 \in [-1,1]$ and $x_2 \in [-\pi, \pi]$:

$$\begin{aligned} &\min_{x_1, x_2} \theta_1 = -1; \quad \max_{x_1, x_2} \theta_1 = 1 \\ &\min_{x_1, x_2} \theta_2 = -\pi; \quad \max_{x_1, x_2} \theta_2 = \pi \end{aligned} \tag{2.7}$$

The two nonlinearities can be represented as in (2.3):

$$\theta_1 = \omega_1^0(\theta).(-1) + \omega_1^1(\theta).(1) \quad \text{and} \quad \theta_2 = \omega_2^0(\theta).(-\pi) + \omega_2^1(\theta).(\pi) \tag{2.8}$$

and

$$\begin{aligned} &\omega_1^0(\theta) = \frac{1 - \sin(x_2)}{2}; \quad \omega_1^1(\theta) = \frac{1 + \sin(x_2)}{2} \\ &\omega_2^0(\theta) = \frac{\pi + x_1^2 x_2}{2\pi}; \quad \omega_2^1(\theta) = \frac{\pi - x_1^2 x_2}{2\pi} \end{aligned} \tag{2.9}$$

The membership functions are computed as:

$$\eta_1(\theta)=\omega_1^0(\theta).\omega_2^0(\theta);\quad \eta_2(\theta)=\omega_1^0(\theta).\omega_2^1(\theta)$$
$$\eta_3(\theta)=\omega_1^1(\theta).\omega_2^0(\theta);\quad \eta_4(\theta)=\omega_1^1(\theta).\omega_2^1(\theta) \tag{2.10}$$

Then, the representation T-S of the system (2.5) is given as follows:

$$\dot{x}=\sum_{i=1}^{4}\eta_i(\theta)\left(A_i x+B_i u\right) \tag{2.11}$$

where $A_1=\begin{bmatrix}2 & -1\\ -\pi & 7\end{bmatrix}, A_2=\begin{bmatrix}2 & -1\\ \pi & 7\end{bmatrix}, A_3=\begin{bmatrix}2 & 1\\ -\pi & 7\end{bmatrix}, A_4=\begin{bmatrix}2 & 1\\ \pi & 7\end{bmatrix}$ and $B_1=B_2=\begin{bmatrix}5\\ -1\end{bmatrix}, B_3=B_4=\begin{bmatrix}5\\ 1\end{bmatrix}$.

It is worth noting that the T-S model (2.11) with the expressions in (2.9) and (2.10) represents exactly the nonlinear system (2.5) in the region $(x_1,x_2)\in[-1,1]\times[-\pi,\pi]$ of the state space.

2.2. A Quick Tour of LMI-based Control Synthesis

Analysis and control synthesis results concerning T-S models are essentially based on optimization under LMI constraints. Hence, some basic notions on LMI tool and some useful lemmas are reminded here to facilitate the reading of theoretical results involved in this thesis. Readers can refer to the excellent references (Boyd et al., 1994; Scherer & Weiland, 2005) for details on how using LMI in control system.

2.2.1. Some basic definitions

Definition 2.1. A function $f:\mathbb{R}^m\mapsto\mathbb{R}$ is convex if and only if for all $x,y\in\mathbb{R}^m$ and $\lambda\in[0,1]$:

$$f\left(\lambda x+(1-\lambda)y\right)\le\lambda f(x)+(1-\lambda)f(y) \tag{2.12}$$

◊

Definition 2.2. A linear matrix inequality (LMI) constraint has the following form:

$$F(x)\triangleq F_0+\sum_{i=1}^{m}F_i x_i<0 \tag{2.13}$$

where the vector $x\in\mathbb{R}^m$ has for components the decision variables and the symmetric matrices $F_i=F_i^T\in\mathbb{R}^{n\times n}$, $i\in\Omega_m$ are given.

◊

A simple example of an LMI constraint is given by the necessary and sufficient condition for the stability of an autonomous system $\dot{x} = Ax$ expressed as the existence of a definite-positive matrix P satisfying the Lyapunov inequality

$$A^T P + PA < 0 \tag{2.14}$$

The so-called feasibility set of the LMI (2.13) (that is the set of solutions), denoted by $S = \{x \in \mathbb{R}^m : F(x) < 0\}$, is a convex subset of $\mathbb{R}^m$. Finding a solution for (2.13) is a convex optimization problem (Boyd et al., 1994). There are three generic LMI problems (Gahinet et al., 1995) which are briefly described below.

Definition 2.3. The *feasibility problem* concerns the search of a solution $x \in \mathbb{X}$ such that the LMI constraints $F(x) < 0$ are verified. The LMI $F(x) < 0$ is called *feasible* if such an element x exists, otherwise it is said to be *infeasible*.

◊

Definition 2.4. The *eigenvalue problem* for which objective function is a linear and has to be minimized under some LMI constraints:

$$\text{Minimize } c^T x \text{ subject to } F(x) < 0 \tag{2.15}$$

where the vector c has the same dimension as x.

◊

Definition 2.5. The *generalized eigenvalue problem* which is stated as follows:

$$\text{Minimize } \lambda \text{ subject to } \begin{cases} G(x) < \lambda H(x) \\ H(x) > 0 \\ F(x) < 0 \end{cases} \tag{2.16}$$

where λ is real and the matrices $F(x)$, $G(x)$ and $H(x)$ are symmetric and of appropriate dimensions.

◊

It is worth noting that many control problems and design specifications can be transformed into these LMI problems, especially for Lyapunov-based analysis and design case (Boyd et al., 1994; Scherer et al., 1997). Moreover, the LMI framework offers a wonderful ability to combine various control objectives in an efficiently tractable manner by using some numerical solvers, e.g. SEDUMI, SDPT3, LMILAB, etc. within Matlab LMI Control Toolbox (Gahinet et al., 1995) or Yalmip Toolbox (Lofberg, 2004).

2.2.2. Some useful matrix properties

In this section, some useful lemmas for the rest of the thesis are given. These lemmas are essentially used to transform a nonlinear optimization problem (derived from control design conditions) into LMI formulations.

Lemma 2.1. *Congruence property*

Given two matrices P and Q, if $P > 0$ and Q is a nonsingular matrix, the matrix QPQ^T is positive definite.

♦

Lemma 2.2. *Schur complement lemma*

Given two symmetric matrices $P \in \mathbb{R}^{m\times m}$, $Q \in \mathbb{R}^{n\times n}$ and a matrix $X \in \mathbb{R}^{n\times m}$. The following statements are equivalent:

$$\begin{bmatrix} Q & X^T \\ X & P \end{bmatrix} > 0 \tag{2.17}$$

$$\begin{cases} Q > 0 \\ P - XQ^{-1}X^T > 0 \end{cases} \tag{2.18}$$

$$\begin{cases} P > 0 \\ Q - X^T P^{-1} X > 0 \end{cases} \tag{2.19}$$

It can be noticed that the Schur complement lemma can be used to transform the nonlinear inequalities (2.18) and (2.19) into the LMI (2.17).

♦

Lemma 2.3. (Petersen, 1987) Let X, Y and Δ be real matrices of appropriate dimensions and $\Delta^T\Delta \le I$. Then, for any scalar $\varepsilon > 0$, the following inequality holds:

$$X\Delta Y + Y^T\Delta^T X^T \le \varepsilon XX^T + \varepsilon^{-1}Y^TY \tag{2.20}$$

The same inequality holds with a matrix $Q > 0$ of appropriate dimensions:

$$X\Delta Y + Y^T\Delta^T X^T \le XQX^T + Y^TQ^{-1}Y \tag{2.21}$$

As will be seen later, Lemma 2.3 is very useful when dealing with parametric uncertain matrices for the synthesis of robust control law.

♦

Lemma 2.4. *S-procedure*

Given matrices $T_i = T_i^T \in \mathbb{R}^{n\times n}$, $i \in \Omega_p \cup \{0\}$ and vector $\xi \in \mathbb{R}^n$. A sufficient condition for the property:

$$\xi^T T_0 \xi > 0 \text{ for all } \xi \ne 0 \text{ such that } \xi^T T_i \xi \ge 0,\ \forall i \in \Omega_p \tag{2.22}$$

is:

there exist $\tau_i \ge 0$, $i \in \Omega_p$ such that:

$$T_0 - \sum_{i=1}^{p} \tau_i T_i > 0. \tag{2.23}$$

Note that (2.23) is an LMI in the variables T_0 and $\tau_i \ge 0$, $i \in \Omega_p$.

The S-procedure allows formulating a problem described by a quadratic constraint verified under other quadratic constraints. The S-procedure leads generally to more conservative formulation than the original problem. However, it is often useful for constraint approximation in control theory and robust optimization analysis (Boyd et al., 1994).

♦

When dealing with design problems based on T-S model, many analysis and stabilization problems can be summarized in some parameterized LMI, expressed in the form of a single sum:

$$\sum_{i=1}^{r} \eta_i(\theta)\Upsilon_i < 0 \tag{2.24}$$

or a double sum

$$\sum_{i=1}^{r}\sum_{j=1}^{r} \eta_i(\theta)\eta_j(\theta)\Upsilon_{ij} < 0 \tag{2.25}$$

where the matrices Υ_i and Υ_{ij} are linearly dependent on the unknown variables.

The following lemmas will be used to ensure the negative nature of the sums assuming that the unique available information on the scalar functions η_i is the convex sum property.

Lemma 2.5. *Relaxation for simple sum*

Given matrices Υ_i of appropriate dimensions, (2.24) is verified if:

$$\Upsilon_i < 0, \quad \forall i \in \Omega_r \tag{2.26}$$

♦

It can be easily seen that one trivial sufficient condition for the case of double sum (2.25) is that $\Upsilon_{ij} < 0$, $\forall (i,j) \in \Omega_r \times \Omega_r$. However, this solution is very conservative. Different relaxation results are available in the literature. In what follows, three significant lemmas which offer a good tradeoff between complexity and quality of solutions for actual numerical solvers will be presented.

Lemma 2.6. (Tanaka et al., 1998) Given matrices Υ_{ij} of appropriate dimensions, the condition (2.25) is verified if:

$$\begin{aligned} &\Upsilon_{ii} < 0, \quad \forall i \in \Omega_r \\ &\Upsilon_{ij} + \Upsilon_{ji} < 0, \quad \forall (i,j) \in \Omega_r \times \Omega_r, \quad i < j \end{aligned} \tag{2.27}$$

♦

The result in the following lemma leads to less conservatism than the one in Lemma 2.6 without adding slack variables.

Lemma 2.7. (Tuan et al., 2001) Given matrices Υ_{ij} of appropriate dimensions, the condition (2.25) is verified if:

$$\begin{aligned} &\Upsilon_{ii} < 0, \quad \forall i \in \Omega_r \\ &\frac{2}{r-1}\Upsilon_{ii} + \Upsilon_{ij} + \Upsilon_{ji} < 0, \quad \forall (i,j) \in \Omega_r \times \Omega_r, \quad i \neq j \end{aligned} \tag{2.28}$$

♦

The conditions in the following result are more relaxed compared to the previous ones by introducing some slack variables.

Lemma 2.8. (Liu & Zhang, 2003) Given the matrices Υ_{ij} of appropriate dimensions, the condition (2.25) is verified if there exist matrices $Q_i = Q_i^T$, $i \in \Omega_r$ and $Q_{ij} = Q_{ji}^T$, $(i,j) \in \Omega_r \times \Omega_r$ such that:

$$\begin{aligned} &\Upsilon_{ii} + Q_i < 0, \quad \forall i \in \Omega_r \\ &\Upsilon_{ij} + \Upsilon_{ji} + Q_{ij} + Q_{ji} < 0, \quad \forall (i,j) \in \Omega_r \times \Omega_r, \quad i < j \\ &\begin{bmatrix} Q_1 & Q_{12} & \cdots & Q_{1r} \\ Q_{21} & Q_2 & & \vdots \\ \vdots & & \ddots & Q_{(r-1)r} \\ Q_{r1} & \cdots & Q_{r(r-1)} & Q_r \end{bmatrix} > 0 \end{aligned} \tag{2.29}$$

♦

Remark 2.3. The result in Lemma 2.8 has been further improved, at the expense of higher computational cost, in (Sala & Arino, 2007).

Remark 2.4. Certain control design conditions encountered in this thesis are represented as a triple sum negativity form:

$$\sum_{k=1}^{s}\sum_{i=1}^{r}\sum_{j=1}^{r} \mu_k(\cdot)\eta_i(\cdot)\eta_j(\cdot)\Upsilon_{ij}^k < 0 \tag{2.30}$$

where the matrices Υ_{ij}^{k} are of appropriate dimensions and the scalar functions $\mu_k(\cdot)$ and $\eta_i(\cdot)$ share the convex sum property. Suppose that the functions $\mu_k(\cdot)$ and $\eta_i(\cdot)$ are independent, applying Lemma 2.5 for $\mu_k(\cdot)$, the condition (2.30) is verified if:

$$\sum_{i=1}^{r}\sum_{j=1}^{r}\eta_i(\cdot)\eta_j(\cdot)\Upsilon_{ij}^{k}<0, \quad \forall k\in\Omega_s \tag{2.31}$$

Then, Lemma 2.7 or Lemma 2.8 can be directly applied to get relaxation results for the triple sum negativity problem (2.30).

2.3. Stability and Stabilization of T-S Model

2.3.1. Lyapunov stability

Stability analysis and control design of T-S model are mainly based on the direct Lyapunov method (Tanaka & Sugeno, 1992). Therefore, some recalls on Lyapunov stability are necessary. To this end, let consider the following system:

$$\dot{x}=f(x,t) \tag{2.32}$$

where $x\in\mathbb{R}^n$ is the system state vector. Without loss of generality, we assume from now that the equilibrium point x^* of a given system is the origin, i.e. $x^*=0$.

Definition 2.6. The scalar function $V:\mathbb{R}^n\times\mathbb{R}\mapsto\mathbb{R}$ is said to be:

- *Positive definite* (with respect to x^*) if there exists a continuous, strictly increasing function $\alpha:\mathbb{R}_+\mapsto\mathbb{R}_+$ with $\alpha(0)=0$ such that: $V(x,t)\geq\alpha\left(\left\|x-x^*\right\|\right)$ for all (x,t) and $V(x^*,t)=0$ for all t.
- *Positive semi-definite* if $V(x,t)\geq 0$ for all (x,t) and $V(x^*,t)=0$ for all t.
- *Decrescent* (with respect to x^*) if there exists a continuous, strictly increasing function $\beta:\mathbb{R}_+\mapsto\mathbb{R}_+$ with $\beta(0)=0$ such that: $V(x,t)\leq\beta\left(\left\|x-x^*\right\|\right)$ for all (x,t).

◊

Theorem 2.1. Consider system (2.32) with its equilibrium point x^*, if there exists a continuously differentiable function $V:\mathbb{R}^n\times\mathbb{R}\mapsto\mathbb{R}$ that is positive definite, decrescent and such that the time derivative of $V\left(x-x^*,t\right)$ along the trajectories of (2.32)is negative definite then x^* is globally asymptotically stable.

♦

Definition 2.7. A function $V\left(x,t\right)$ satisfying all the assumptions in the Theorem 2.1 is called a Lyapunov function.

◊

In the framework of T-S models, the choice of the Lyapunov functions is crucial for solution relaxation. Several forms of Lyapunov function are proposed in the literature such as piecewise quadratic Lyapunov function (Johansson et al., 1999; Feng, 2003), non-quadratic or fuzzy Lyapunov function (Guerra & Vermeiren, 2004; Mozelli et al., 2009), line integral function (Rhee & Won, 2006), polynomial Lyapunov function (Sala & Arino, 2009). These Lyapunov functions try to take into account some "knowledge" in order to reduce conservatism. However, the main drawback when using these types of Lyapunov functions is that the LMI design conditions derived from them are usually very complex and costly in terms of computation. This fact may make practical applications intractable with actual LMI solvers. Moreover, some of them are only valid for a restrictive class of T-S models.

In this thesis, the well-known quadratic Lyapunov function will be adopted. Given the nonlinear system (2.1), the quadratic Lyapunov function associated with this system is given as follows:

$$V\left(x\right)=x^TPx,\quad P>0 \tag{2.33}$$

When quadratic Lyapunov function is used to study system stability, we refer to *quadratic stability*. Clearly, using a quadratic Lyapunov function of the form (2.33) is stringent and conservative for design method. However, the synthesis technique based on this type of Lyapunov function has some valuable advantages over previously listed alternatives. First, it is numerically tractable since it leads to convex optimization problems. Second, resulting controllers are of reasonable complexity. Furthermore, all theoretical results developed in this thesis aim to be applied to real industrial applications. Therefore, simple and efficient control algorithms are needed. Finally, all degrees of freedom in the common Lyapunov matrix P will be exploited. Indeed, LMI optimization will shape

this matrix until either all specifications are met or all degrees of freedom are exhausted (Scherer et al., 1997).

2.3.2. Stability of T-S model

Consider the following autonomous T-S model:

$$\dot{x} = \sum_{i=1}^{r} \eta_i(\theta) A_i x \tag{2.34}$$

The time derivative of quadratic Lyapunov function (2.33) is given by:

$$\dot{V}(x) = \dot{x}^T P x + x^T P \dot{x} \tag{2.35}$$

Computing (2.35) along the trajectories of the system (2.34), we get:

$$\dot{V}(x) = \left(\sum_{i=1}^{r} \eta_i(\theta) A_i x \right)^T P x + x^T P \left(\sum_{i=1}^{r} \eta_i(\theta) A_i x \right) \tag{2.36}$$

or

$$\dot{V}(x) = x^T \left(\sum_{i=1}^{r} \eta_i(\theta) \left(A_i^T P + P A_i \right) \right) x \tag{2.37}$$

The theorem below gives the stability conditions for the zero solution of T-S model (2.34):

Theorem 2.2. (Tanaka & Sugeno, 1992) The zero solution of T-S model (2.34) is globally asymptotically stable if:

$$\exists P > 0, \quad A_i^T P + P A_i < 0, \quad \forall i \in \Omega_r \tag{2.38}$$

Proof. The proof of this theorem can be directly derived from the Lemma 2.5.

♦

It is clear that the Theorem 2.2 gives only sufficient conditions since there is no information on $\eta_i(\cdot)$, $i \in \Omega_r$ taken into account.

2.3.3. Stabilization of T-S model

Consider now the T-S model:

$$\begin{cases} \dot{x} = \sum_{i=1}^{r} \eta_i(\theta)\left(A_i x + B_i u\right) \\ y = \sum_{i=1}^{r} \eta_i(\theta) C_i x \end{cases} \tag{2.39}$$

The stabilization problem is to find a control law u for system (2.39) which satisfies some closed-loop performance. A lot of control laws are available in state-of-the-art. We can classified them into two categories: state feedback control law $u = F(x)$ and output feedback control law $u = F(y)$.

a. State feedback control

In this case, the well-known control law PDC (Parallel Distributed Compensation) first proposed in (Wang et al., 1996) is often used. This nonlinear feedback law shares the same membership functions as the T-S model and given as:

$$u = \sum_{j=1}^{r} \eta_j(\theta) L_j x \tag{2.40}$$

The control design task is to determine the constant feedback matrix gains L_j, $\forall j \in \Omega_r$. It can be easily noticed that, if $L_j = L$, $\forall j \in \Omega_r$, the classical linear feedback control law is recovered.

Using the PDC law (2.40), the closed-loop system of T-S model becomes:

$$\begin{cases} \dot{x} = \sum_{i=1}^{r}\sum_{j=1}^{r} \eta_i(\theta)\eta_j(\theta)\left(A_i + B_i L_j\right) x \\ y = \sum_{i=1}^{r} \eta_i(\theta) C_i x \end{cases} \tag{2.41}$$

Then, with the same argument as in the case of stability analysis, the time derivative of the Lyapunov function (2.33) along the trajectories of the closed-loop system (2.41) is negative, i.e. $\dot{V}(x) \le 0$ if:

$$\sum_{i=1}^{r}\sum_{j=1}^{r} \eta_i(\theta)\eta_j(\theta)\left(\left(A_i + B_i L_j\right)^T P + P\left(A_i + B_i L_j\right)\right) < 0 \tag{2.42}$$

Using the congruence property, condition (2.42) is equivalent to:

$$\sum_{i=1}^{r}\sum_{j=1}^{r}\eta_i(\theta)\eta_j(\theta)\left(XA_i^T + A_iX + XL_j^TB_i^T + B_iL_jX\right) < 0 \tag{2.43}$$

where $X = P^{-1}$. Note that inequality (2.43) is a bilinear matrix inequality (BMI) due to the existence of bilinear terms B_iL_jX and $XL_j^TB_i^T$. Using the change of variable $M_j = L_jX$, $j \in \Omega_r$, the condition (2.43) is converted into the following equivalent condition expressed in terms of parameterized LMI:

$$\sum_{i=1}^{r}\sum_{j=1}^{r}\eta_i(\theta)\eta_j(\theta)\left(XA_i^T + A_iX + M_j^TB_i^T + B_iM_j\right) < 0 \tag{2.44}$$

The control design development can be summarized in the following theorem.

Theorem 2.3. (Tanaka & Sugeno, 1992) If there exists a matrix $X > 0$, the matrices M_j, $j \in \Omega_r$ such that, for the quantities Υ_{ij}, $(i,j) \in \Omega_r \times \Omega_r$ defined by:

$$\Upsilon_{ij} \triangleq XA_i^T + A_iX + M_j^TB_i^T + B_iM_j$$

the conditions (2.27) are verified, then the zero solution of system (2.39) is globally asymptotically stabilizable. Moreover, the feedback gains of a stabilizing PDC law (2.40) are given as $L_j = M_jX^{-1}$, $j \in \Omega_r$.

♦

Remark 2.5. In Theorem 2.3, we use the result of Lemma 2.6. Similar quadratic stability results can be done with relaxation results in Lemma 2.7 or Lemma 2.8. The most important thing is to obtain the quantities Υ_{ij}, $(i,j) \in \Omega_r \times \Omega_r$ in LMI form so that the control design can be efficiently solved with some numerical toolboxes.

b. Output feedback control

All the states of the dynamical system are not always available for real-world applications. The output feedback control has to be used in these cases. Output feedback control can be considered through three methods: observer-based control (Tanaka et al., 1998; Yoneyama et al., 2000; Lin et al., 2005; Mansouri et al., 2009), static output feedback control (Lo & Lin, 2003; Xu & Lam, 2005), dynamic output feedback control (Li et al., 2000). However, the separation principle is no longer applicable for the first method in the case of non-measurable scheduling variables. Then, it becomes

much more complicated to deal with control design problems (Nguang & Shi, 2003; Guerra et al., 2006). That is why only static and dynamic output feedback control will be considered in this thesis.

A static output feedback of the T-S model (2.39) is based on the idea of PDC law and expressed as follows (Kau et al., 2007):

$$u = \sum_{j=1}^{r} \eta_j(\theta) L_j y = \sum_{i=1}^{r} \sum_{j=1}^{r} \eta_j(\theta) L_j C_i x \tag{2.45}$$

where $L_j \in \mathbb{R}^{n_u \times n_y}$, $j \in \Omega_r$, are controller matrix gains to be designed. From (2.39) and (2.45), the closed-loop system becomes:

$$\dot{x} = \sum_{i=1}^{r} \sum_{j=1}^{r} \sum_{k=1}^{r} \eta_i(\theta) \eta_j(\theta) \eta_k(\theta) \left(A_i + B_i L_j C_k \right) x \tag{2.46}$$

Several results exist in the literature on this control law (Lo & Lin, 2003; Huang & Nguang, 2006; Xu & Lam, 2005; Chadli & Guerra, 2012).

A dynamic output feedback of the T-S model (2.39) can be written as (Li et al., 2000):

$$\begin{cases} \dot{x}_c = \sum_{i=1}^{r} \sum_{j=1}^{r} \eta_i(\theta) \eta_j(\theta) A_c^{ij} x_c + \sum_{i=1}^{r} \eta_i(\theta) B_c^i y \\ u = \sum_{i=1}^{r} \eta_i(\theta) C_c^i x_c + D_c y \end{cases} \tag{2.47}$$

where $x_c \in \mathbb{R}^{n_x}$ is the state vector of the controller. The controller matrices A_c^{ij}, B_c^i, C_c^i, D_c, $(i, j) \in \Omega_r \times \Omega_r$, to be designed, are of appropriate dimensions. From (2.39) and (2.48), the closed-loop system becomes:

$$\begin{cases} \dot{x}_{cl} = \sum_{i=1}^{r} \sum_{j=1}^{r} \eta_i(\theta) \eta_j(\theta) A_c^{ij} x_{cl} \\ y_{cl} = \sum_{i=1}^{r} \eta_i(\theta) C_{cl}^i x_{cl} \end{cases} \tag{2.49}$$

where $x_{cl}^T = \begin{bmatrix} x^T & x_c^T \end{bmatrix}$ and:

$$A_{cl}^{ij} = \begin{bmatrix} A_i + B_u^i D_c C_y^j & B_u^i C_c^j \\ B_c^i C_y^j & A_c^{ij} \end{bmatrix}; \qquad C_{cl}^i = \begin{bmatrix} C_y^i & 0 \end{bmatrix} \tag{2.50}$$

Some existing results in the literature concerning this type of control law can be found in (Li et al., 2000; Dong & Yang, 2008; Ding, 2009).

The controller matrix gains directly obtained from the stabilization conditions often give poor closed-loop performance. This fact is sometimes unacceptable for real applications. To this end, a great deal of efforts has been investigated to take into account various kinds of performance specifications in TS control design. In general, these performance specifications are also represented in terms of LMI constraints so that control design problem can be efficiently solved, see (Tanaka & Wang, 2001; Sala et al., 2005; Feng, 2006) for overviews. Hereafter, some closed-loop performance directly related to this thesis will be introduced in the case of state feedback control for brevity reason. In fact, the development of dynamic output feedback control laws is quite complex and tedious, especially when dealing with performance index. In Chapter 3, static output feedback will be discussed in more detail and Chapter 4 is devoted to deal with dynamic output feedback control with some closed-loop performance.

3. Closed-Loop Performance Specifications

3.1. α-stability

When we are interested in the time-domain performance improvement, imposing the criterion of α-stability is a very interesting and simple technique. Generally speaking, the idea is to make the closed-loop trajectory from a given initial state convergent as fast as possible towards the equilibrium point 0.

Definition 2.8. System (2.1) is said to be *quadratically stable* with *decay rate* α if there exists $\alpha > 0$ and matrix $P > 0$ such that the time derivative $\dot{V}(x)$ of the quadratic function $V(x)$ defined in (2.33) satisfies the inequality:

$$\dot{V}(x) \le -2\alpha V(x), \quad \forall x \in \mathbb{R}^{n_x} \tag{2.51}$$

for all trajectories of system (2.1).

◊

From Bellman's inequality, it can be deduced from (2.51) that, for all T_0 :

$$V\left(x(t)\right) \le V\left(x(T_0)\right) e^{-2\alpha(t-T_0)} \tag{2.52}$$

Since, for any $P>0$: $\lambda_{\min}(P)\|x\|^2 \le x^T P x \le \lambda_{\max}(P)\|x\|^2$ with $\lambda_{\min}(P)>0$. It follows that:

$$\lambda_{\min}(P)\|x(t)\|^2 \le V(x(t)) \le V(x(T_0))e^{-2\alpha(t-T_0)} \le \lambda_{\max}(P)\|x(T_0)\|^2 e^{-2\alpha(t-T_0)} \tag{2.53}$$

or

$$\|x(t)\|^2 \le \frac{\lambda_{\max}(P)}{\lambda_{\min}(P)}\|x(T_0)\|^2 e^{-2\alpha(t-T_0)} \tag{2.54}$$

Therefore, the closed-loop trajectories exponentially converge to 0 with the decay rate α.

From (2.39), (2.40) and (2.51), the stabilization condition becomes:

$$\sum_{i=1}^{r}\sum_{j=1}^{r}\eta_i(\theta)\eta_j(\theta)\Upsilon_{ij} = \sum_{i=1}^{r}\sum_{j=1}^{r}\eta_i(\theta)\eta_j(\theta)\left(XA_i^T + A_iX + M_j^T B_i^T + B_iM_j + 2\alpha X\right) < 0 \tag{2.55}$$

Theorem 2.4. If there exists a matrix $X>0$, the matrices M_j, $j\in\Omega_r$ and a scalar $\alpha>0$ such that, the quantities Υ_{ij}, $(i,j)\in\Omega_r\times\Omega_r$ defined by:

$$\Upsilon_{ij} \triangleq XA_i^T + A_iX + M_j^T B_i^T + B_iM_j + 2\alpha X$$

the conditions (2.27) are verified, then the closed-loop system (2.41) with the PDC law (2.40) is globally asymptotically stable with the decay rate α. Moreover, the feedback gains of the PDC law are given as $L_j = M_jX^{-1}$, $j\in\Omega_r$.

♦

Remark 2.6. Of course, the Remark 2.5 is also valid for Theorem 2.4. It is worth noting that the design of PDC controller with the decay rate α reduces to the stable PDC control design when $\alpha=0$. Indeed, the design conditions in Theorem 2.3 are special cases of those in Theorem 2.4. A more general approach, called *LMI region*, used to introduce closed-loop performance can be found in (Hong & R., 2000). LMI region approach is an extension version of Pole Placement method in linear systems (Gahinet et al., 1995).

3.2. H_∞ Control Design

Consider the following disturbed T-S model:

$$\begin{cases} \dot{x} = \sum_{i=1}^{r} \eta_i(\theta)\left(A_i x + B_u^i u + B_w^i w\right) \\ y = \sum_{i=1}^{r} \eta_i(\theta) C_i x \end{cases} \tag{2.56}$$

where $w \in \mathbb{R}^{n_w}$ is an energy-bounded disturbance signal, that is $w \in W_\delta$ of the system, where:

$$W_\delta = \left\{ w : \mathbb{R}^+ \mapsto \mathbb{R}^{n_w};\quad \int_0^\infty w^T w dt \le \delta^{-1} \right\} \tag{2.57}$$

Definition 2.9. Given $\gamma > 0$, the system (2.56) is said to have $\mathcal{L}_2$ gain less than or equal to γ if:

$$\int_0^\infty y^T y dt \le \gamma^2 \int_0^\infty w^T w dt \tag{2.58}$$

Note that the zero initial condition $x(0) = 0$ is required in (2.58). Nonzero initial condition can be dealt with by using the technique described in (Khargonekar et al., 1990).

◊

Theorem 2.5. (Tanaka & Wang, 2001) If there exists a matrix $X > 0$, the matrices M_j, $j \in \Omega_r$ such that, for any quantities Υ_{ij}, $(i, j) \in \Omega_r \times \Omega_r$ defined as:

$$\Upsilon_{ij} \triangleq \begin{bmatrix} XA_i^T + A_i X + M_j^T B_i^T + B_i M_j & B_w^i & XC_i^T \\ * & -\gamma^2 I & 0 \\ * & * & -I \end{bmatrix}$$

the conditions (2.27) are verified, then the closed-loop system (2.41) with the PDC law (2.40) is globally asymptotically stable and achieves the disturbance attenuation level less than $\gamma > 0$. Moreover, the PDC feedback gains are given as $L_j = M_j X^{-1}$, $j \in \Omega_r$.

♦

3.3. Robustness

In the literature, robustness performance can be taken into account in many ways. However, parametric uncertainty is generally considered in the framework of T-S model:

$$\begin{cases} \dot{x} = \sum_{i=1}^{r} \eta_i(\theta)\left(\left(A_i + \Delta A_i\right)x + \left(B_i + \Delta B_i\right)u\right) \\ y = \sum_{i=1}^{r} \eta_i(\theta)\left(C_i + \Delta C_i\right)x \end{cases} \tag{2.59}$$

where the time-varying uncertain matrices ΔA_i, ΔB_i, ΔC_i are assumed to be bounded as (Kau et al., 2007):

$$\left[\Delta A_i \quad \Delta B_i \quad \Delta C_i\right] = F_i \Theta_i(t)\left[E_{A,i} \quad E_{B,i} \quad E_{C,i}\right], \quad i \in \Omega_r \tag{2.60}$$

where F_i, $E_{A,i}$, $E_{B,i}$, $E_{C,i}$, $i \in \Omega_r$ are known, constant matrices with appropriate sizes characterizing the structure of the uncertainties, and the matrices $\Theta_i(t)$ with unknown, measurable elements satisfy:

$$\Theta_i^T(t)\Theta_i(t) \le I, \quad i \in \Omega_r \tag{2.61}$$

From the T-S model (2.59), it is possible to derive LMI design conditions by using Lemma 2.3. Indeed, numerous results on this subject are available (Tanaka & Wang, 2001; Taniguchi et al., 2001; Lee et al., 2001; Yoneyama, 2006).

3.4. Tracking Performance

In general, Lyapunov stability in Theorem 2.1 studies the stability of equilibrium points. When there are some exogenous inputs involved in system (as it is the case of tracking problem), input-to-state (ISS) stability has to be considered (Sontag & Wang, 1995). When dealing with T-S models, since the vector field $\sum_{i=1}^{r} \eta_i(\theta) B_i$ is bounded, it can be deduced that the ISS property holds for systems which are globally asymptotically stable in the sense of Lyapunov (Lendek et al., 2010). This fact implies that a conventional solution obtained from LMI design conditions will guarantee the ISS stability.

In trajectory tracking framework where the reference signal is constant, an integral control structure is necessary to eliminate the slow variation disturbance. The control scheme is depicted in Figure 2.1:

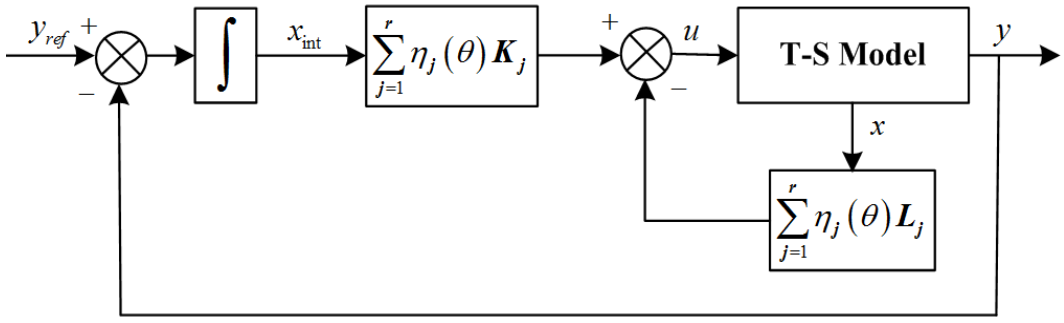

Figure 2.1. PDC control law with integral structure

Adding an integrator amounts to introduce a new system state associated with the dynamic defined as $\dot{x}_{\text{int}} = y_{ref} - y$ where y_{ref} is the reference signal of the system. Then, the closed-loop system becomes:

$$\begin{cases} \dot{\bar{x}} = \sum_{i=1}^{r}\sum_{j=1}^{r} \eta_i(\theta)\eta_j(\theta)\left(\bar{A}_i - \bar{B}_i\bar{F}_j\right)\bar{x} + By_{ref} \\ y = \sum_{i=1}^{r} \eta_i(\theta)\bar{C}_i\bar{x} \end{cases} \tag{2.62}$$

where $\bar{x}^T = \begin{bmatrix} x^T & x_{\text{int}}^T \end{bmatrix}$ and the matrices of the extended systems are given by:

$$\bar{A}_i = \begin{bmatrix} A_i & 0 \\ -C_i & 0 \end{bmatrix}, \quad \bar{B}_i = \begin{bmatrix} B_i \\ 0 \end{bmatrix}, \quad \bar{C}_i = \begin{bmatrix} C_i & 0 \end{bmatrix}; \quad B = \begin{bmatrix} 0 \\ I \end{bmatrix} \tag{2.63}$$

Consequently, the extended PDC can be written as:

$$u = \sum_{i=1}^{r} h_j(\theta)\bar{F}_j\bar{x} \tag{2.64}$$

where $\bar{F}_j = \begin{bmatrix} -L_j & K_j \end{bmatrix}$ are the extended gains. Now, all previous results can be applied with the extended T-S model (2.62) and extended PDC controller (2.64) while ensuring ISS stability with respect to reference signal y_{ref}.

3.5. T-S Model Subject to Input Saturation

As previously said, saturation of control inputs has to be avoided in real control problems. Here, the results existing in (Tanaka & Wang, 2001) are briefly recalled. More effective and relaxed results will be presented in Chapter 3 and Chapter 4.

Theorem 2.6. (Tanaka & Wang, 2001) Given the saturation level $u_{\max} \in \mathbb{R}_+^{n_u}$ and suppose that initial condition $x(0)$ is known. If there exists a matrix $X > 0$, and matrices M_j (for $j \in \Omega_r$) such that the conditions in Theorem 2.3 and the following LMI constraints are verified:

$$\begin{bmatrix} 1 & * \\ x(0) & X \end{bmatrix} \geq 0 \tag{2.65}$$

$$\begin{bmatrix} X & * \\ M_i & u_{\max}^2 I \end{bmatrix} \geq 0 \tag{2.66}$$

then the closed-loop system (2.41) with the PDC law (2.40) and feedback gains given as $L_j = M_j X^{-1}$, $j \in \Omega_r$ is globally asymptotically stable and the input constraint $|u(t)| \leq u_{\max}$ is enforced for $\forall t \geq 0$.

♦

Remark 2.7. In the case where initial condition $x(0)$ is unknown but bounded, i.e. $|x(0)| \leq \phi$, the LMI constraint (2.65) of Theorem 2.6 can be replaced by $\phi^2 I \leq X$. A larger quantity ϕ encompasses a larger set of initial states but of course it may lead to conservative solutions.

4. Concluding Remarks

This chapter aims to provide a brief overview of T-S model and its interest in nonlinear control theory. Two main points are pointed out. The first point concerns the conservatism of the solutions. One has to keep in mind that only sufficient conditions are obtained when dealing with T-S model. The conservatism comes from the following sources:

- No information on nonlinear membership functions is exploited except for the convex sum property.
- Conditions used for sum negativity problems.
- The choice of the Lyapunov candidate functions.

Different efforts have been investigated in the literature to reduce the conservatism, see (Sala et al., 2005; Feng, 2006) for more detail. We will not focus on this research direction in the thesis. The second point concerns the possibility to recast most of design problems as LMI constraints. Therefore, the control design can be effectively solved as convex optimization problem (with some specific numerical toolboxes). For brevity, this chapter presents the stability and state feedback control of a particular class of T-S model with a common quadratic Lyapunov candidate function. Some results on performance, robustness, input constraints and ISS property for tracking control problem are shortly given. Most of them can be extended for more general classes of T-S model, e.g. uncertain systems with/without H_2, H_∞ performance (Liu & Zhang, 2003; Delmotte et al., 2008); system in a descriptor form (Taniguchi et al., 2000; Guelton et al., 2009), delayed systems (Yoneyama, 2007), etc. Moreover, a state-of-the art of output feedback control is also provided. These control design problems will be deeply discussed in Chapter 3 and Chapter 4.

"If you can't explain it simply, you don't understand it well enough."

Albert Einstein, German-born theoretical physicist

Chapter 3. Stabilization of T-S Model under Input Saturation: Polytopic Representation Approach

1. Introduction

This chapter presents a new method to design robust H_∞ controllers stabilizing a switching uncertain and disturbed T-S systems subject to control input saturation. To that end, saturation nonlinearity is directly taken into account in the design control under its polytopic representation. Two cases will be investigated: state feedback control (SFC) and static output feedback control (SOFC). The Lyapunov stability theory is used to derive design conditions, which are formulated as a linear matrix inequality (LMI) optimization problem. The controller design amounts to solving a set of LMI conditions with some numerical tools. In comparison with previous results, the proposed method not only provides a simple and efficient design procedure but also leads to less conservative controllers by maximizing the domain of attraction. In such a way, the closed-loop performance can be enhanced.

The control scheme is based on a parallel distributed compensation (PDC) concept (Tanaka & Wang, 2001) and the consideration of H_∞ performance which guarantees the γ-disturbance attenuation. By using Lyapunov stability theory, the design conditions are derived for the two classes of control laws: SFC and SOFC. The key point of the proposed method is to achieve conditions in LMI (linear matrix inequalities) form. Thus, the controller gains can be efficiently computed with some numerical tools (Gahinet et al., 1995). To our knowledge, very few results deal with the switching uncertain and disturbed T-S models, especially with SOFC approach. The proposed method can be applied for a large class of switching nonlinear systems which is the major contribution of this work.

The chapter is organized as follows. Section 2 introduces the motivation of using switching T-S model with respect to classical one and presents a state-of-the-art concerning the control problem. In

Section 3, the stabilization problem of a switching uncertain T-S system subject to input saturation is first described and some useful preliminaries results needed for the control design are then given. Section 4 is devoted to the main results of the chapter and the stability of the closed-loop system is also proved based on Lyapunov theory. Finally, a conclusion is given in Section 5.

The following notations will be occasionally used:

$$X_\sigma = \sum_{k=1}^{s} \mu_k X^k; \quad Y_{\sigma\theta} = \sum_{k=1}^{s}\sum_{i=1}^{r} \mu_k \eta_i^k Y_i^k; \quad Z_{\sigma\theta\theta} = \sum_{k=1}^{s}\sum_{i=1}^{r}\sum_{j=1}^{r} \mu_k \eta_i^k \eta_j^k Z_{ij}^k \tag{3.1}$$

where X^k, Y_i^k, Z_{ij}^k are matrices of appropriate dimensions, and μ_k, η_i^k are scalar functions sharing the convex sum property with $(k,i,j) \in \Omega_s \times \Omega_r \times \Omega_r$.

2. Motivations and Related Works

As have been shown in the literature, control technique based on T-S model is a powerful approach to deal with complex nonlinear systems. Nevertheless, it is not always possible from a theoretical or practical point of view to use the classical T-S approach for some specific cases such as systems with singularity points (Tanaka et al., 2001) or systems with a too large number of sub-systems (Taniguchi et al., 2001) (this number increases exponentially with the number of nonlinearities of the original nonlinear system when using the sector nonlinear approach). Based on these remarks, a new switching T-S approach which allows overcoming these drawbacks has been proposed in (Tanaka et al., 2001). In this chapter, we focus on this class of switching T-S models. Indeed, a switching T-S model is composed by local T-S models and switches between them according to scheduling variables depending or not on system states. Its structure has two levels: a regional level and a local one with the associated T-S model. In Figure 3.1 is illustrated the concept of switching T-S control approach, the supervisor decides which controller has to be connected in closed loop in function of the actual operating region of the nonlinear system. It is worth noting that it inherits some essential features of hybrid systems (Liberzon, 2003) and retains all the information and knowledge representation capacity of T-S systems.

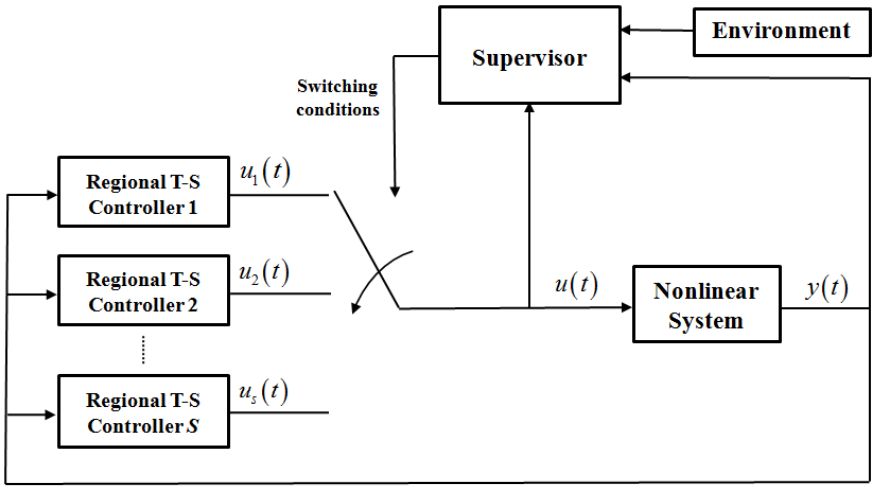

Figure 3.1. Concept of switching T-S control approach

Over the years, many studies have investigated the robust stability and stabilization of uncertain and disturbed T-S systems (Feng, 2006; Lee et al., 2001; Yoneyama, 2006) and references therein. Most of these works often concern the control design based on either state feedback control (SFC) (Lee et al., 2001; Yoneyama, 2006; Guerra & Vermeiren, 2004) or observer-based control (Mansouri et al., 2009; Lin et al., 2005). However, all the system states are not always available for real-world applications in the first case. In the second case, observer-based control design leads to high-order controllers which may increase the complexities/difficulties when dealing with model uncertainties, disturbance attenuation, etc. (Chen et al., 2005). Thus, static output feedback control (SOFC) seems to be a very interesting solution to avoid working with a complex control scheme. The advantages of SOFC are well discussed in (Syrmos et al., 1997). Some studies concerning SOFC in the framework of T-S control are available in the literature (Lo & Lin, 2003; Huang & Nguang, 2006; Xu & Lam, 2005; Chadli & Guerra, 2012).

Among all the nonlinear phenomena, actuator saturation is unavoidable in almost real applications. It can severely degrade the closed-loop system performance and in some cases may lead to the system instability. Motivated by this practical control aspect, a great deal of effort has been recently focused on saturated systems, see e.g. (Tarbouriech et al., 2011; Fang et al., 2004; Cao & Lin, 2003) and the references therein. In general, there are two main approaches to deal with the saturation problems. The first one considers implicitly the saturation effect. In this approach, called *anti-windup*, the control input is first computed by ignoring actuator saturation. Once the controller has been designed, an additional anti-windup compensator is included to handle the saturation constraints. In the second approach, the saturation effect in control design process is taken directly into account. For this, two principal synthesis techniques are considered: *saturated control law* and *unsaturated control*

law. In the latter one, the initial state domain and the design are such that the control law will never reach saturation limits. Presented for instance in (Tanaka & Wang, 2001), this type of low-gain controller is very conservative and often leads to poor system performance (Tarbouriech et al., 2011; Cao & Lin, 2003). As its name indicates, the saturated control law (Cao & Lin, 2003) allows the saturation of the input signal which results in a better control performance. That is why this type of control laws will be addressed in this chapter.

3. Problem Position and Preliminary Results

3.1. Switching T-S System Description

Consider the following uncertain nonlinear switched system of the form:

$$\begin{cases} \dot{x} = f_\sigma(x,u,w) \\ z = g_\sigma(x,u,w) \\ y = h_\sigma(x) \end{cases} \tag{3.2}$$

where $x \in \mathbb{R}^{n_x}$ is the state vector, $u \in \mathbb{R}^{n_u}$ the control input, $w \in \mathbb{R}^{n_w}$ the disturbance vector, $y \in \mathbb{R}^{n_y}$ the measured output vectors, and $z \in \mathbb{R}^{n_z}$ is the controlled output vector used for performance purpose. The switching signal σ takes value in Ω_s and may depend on exogenous signals, on the system state value, etc. which constitutes the components of a vector denoted θ, so that we can write with a slight abuse of notation $\sigma = \sigma(\theta)$.

Under standard assumptions on the field vectors in (3.2) and using sector nonlinearity approach (Tanaka & Wang, 2001), an equivalent representation of (3.2) (at least locally) may be obtained on the form of a switched T-S model:

$$\begin{cases} \dot{x} = \sum_{k=1}^{s}\sum_{i=1}^{r} \mu_k(\theta)\eta_i^k(\theta)\left[\left(A_i^k + \Delta A_i^k\right)x + \left(B_{w,i}^k + \Delta B_{w,i}^k\right)w + \left(B_{u,i}^k + \Delta B_{u,i}^k\right)u\right] \\ z = \sum_{k=1}^{s}\sum_{i=1}^{r} \mu_k(\theta)\eta_i^k(\theta)\left[\left(C_{z,i}^k + \Delta C_{z,i}^k\right)x + \left(D_{w,i}^k + \Delta D_{w,i}^k\right)w + \left(D_{u,i}^k + \Delta D_{u,i}^k\right)u\right] \\ y = \sum_{k=1}^{s}\sum_{i=1}^{r} \mu_k(\theta)\eta_i^k(\theta) C_{y,i}^k x \end{cases} \tag{3.3}$$

where $\mu_k(\theta)$ for $k \in \Omega_s$ are the indicator functions defined by:

$$\mu_k(\theta)=\begin{cases}1, & \text{if} \quad \theta\in\sigma^{-1}(\{k\})\\ 0, & \text{else}\end{cases} \tag{3.4}$$

The real matrices A_i^k, $B_{w,i}^k$, $B_{u,i}^k$, $C_{z,i}^k$, $D_{w,i}^k$, and $D_{u,i}^k$ are constant of appropriate dimensions and describe the nominal system; and the time-varying matrices ΔA_i^k, $\Delta B_{w,i}^k$, $\Delta B_{u,i}^k$, $\Delta C_{z,i}^k$, $\Delta D_{w,i}^k$, and $\Delta D_{u,i}^k$ represent the uncertain part. These matrices are assumed to be bounded as:

$$\begin{bmatrix}\Delta A_i^k & \Delta B_{w,i}^k & \Delta B_{u,i}^k\\ \Delta C_{z,i}^k & \Delta D_{w,i}^k & \Delta D_{u,i}^k\end{bmatrix}=\begin{bmatrix}F_x^k\Theta_x\begin{bmatrix}E_{A,i}^k & E_{Bw,i}^k & E_{Bu,i}^k\end{bmatrix}\\ F_z^k\Theta_z\begin{bmatrix}E_{Cz,i}^k & E_{Dw,i}^k & E_{Du,i}^k\end{bmatrix}\end{bmatrix} \tag{3.5}$$

where F_x^k, F_z^k, $E_{A,i}^k$, $E_{Bw,i}^k$, $E_{Bu,i}^k$, $E_{Cz,i}^k$, $E_{Dw,i}^k$, $E_{Du,i}^k$, $(k,i)\in\Omega_s\times\Omega_r$ are known constant matrices of appropriate dimensions characterizing the structure of the uncertainties, and the matrices Θ_x, Θ_z with unknown, measurable elements satisfy:

$$\Theta_x^T\Theta_x\le I;\quad \Theta_z^T\Theta_z\le I \tag{3.6}$$

Finally, the nonlinear membership functions $\eta_i^k(\theta)$ in (3.3) verify the convex sum property.

Remark 3.1. It is worth noting that to avoid multiplying notations and without loss of generality, we assume that the scheduling variables needed to transform model (3.2) into model (3.3) are components of the vector θ.

The following assumptions are considered in this chapter:

Assumption 3.1. It is assumed that θ is a known quantity (measured or estimated) independent of the control input value u.

Assumption 3.2. The control input u is subject to actuator saturation:

$$sat(u_i)=sign(u_i)\min\{u_{\max,i},|u_i|\},\ \forall i\in\Omega_{n_u} \tag{3.7}$$

where $u_{\max}\in\mathbb{R}_+^{n_u}$ denotes the saturation level vector. Note that, for sake of simplicity, the above saturation constraints are symmetric. In case of asymmetric ones — that is, when the input signals satisfy inequalities of the form $u_{\min,i}\le u_i\le u_{\max,i}$ with $u_{\min,i}\ne -u_{\max,i}$ — symmetry can be restored by

removing and then adding a constant input $C = \frac{u_{\min,i} + u_{\max,i}}{2}$ in the upstream and downstream of the saturation.

3.2. Control Problem Formulation

Our goal in this chapter is to propose a systematic method to design a switching controller of SFC or SOFC type for the constrained system (3.3) such that the closed-loop system satisfies the following properties:

(P.1) *Regional quadratic α-stability*: When $w = 0$, for a given positive real number α, there exists a quadratic function $V(x) = x^T P x$, with $P > 0$, such that $\dot{V}(x) < -2\alpha V(x)$ along the trajectories of closed-loop system for any initial state in the ellipsoid $\mathcal{E}(P)$. This fact implies that these trajectories of the closed-loop system will converge exponentially to 0 with a decay rate α.

(P.2) *Performance*: For a given $\gamma > 0$, there exists positive real numbers δ, ρ such that, for any energy-bounded signal $w \in W_\delta = \left\{ w : \mathbb{R}^+ \to \mathbb{R}^{n_w};\ \int_0^\infty w^T w dt \le \delta^{-1} \right\}$ and for all initial states in $\mathcal{E}(P, \rho)$, the trajectories of the closed-loop system will never escape the ellipsoid $\mathcal{E}(P) \supset \mathcal{E}(P, \rho)$. Furthermore, the $\mathcal{L}_2$-norm of the output signal z is bounded:

$$\int_0^\infty z^T z dt \le \gamma^2 \int_0^\infty w^T w dt + \rho \tag{3.8}$$

3.3. Switching T-S Control Design

3.3.1. Polytopic model for the saturation nonlinearity

In this chapter, the polytopic representation proposed in (Cao & Lin, 2003) will be used in order to model the saturation effect. For that, let $\Gamma = \left\{ \Gamma_p^+ \right\}_{p \in \Omega_{2^m}}$ be the set of $(m \times m)$ diagonal matrices whose diagonal elements take the value 0 or 1, each element of Γ being indexed by an integer number in Ω_{2^m}. For any $p \in \Omega_{2^m}$, Γ_p^- denotes the element of Γ associated with Γ_p^+ such that:

$$\Gamma_p^- = I - \Gamma_p^+ \tag{3.9}$$

Lemma 3.1 (Cao & Lin, 2003) Let $u,\ v \in \mathbb{R}^m$. Suppose that $-u_{\max} \preceq v \preceq u_{\max}$, it follows that:

$$sat(u) \in co\left\{ \Gamma_p^+ u + \Gamma_p^- v :\ \forall p \in \Omega_{2^m} \right\} \tag{3.10}$$

Consequently, $sat(u)$ can be represented as:

$$sat(u) = \sum_{p=1}^{2^m} \xi_p \left(\Gamma_p^+ u + \Gamma_p^- v \right) \tag{3.11}$$

where the numbers ξ_p verify the convex sum property.

♦

3.3.2. State feedback control law

The switching SFC of the system (3.3) is naturally extended from the PDC concept (Tanaka & Wang, 2001) and represented by:

$$u = \sum_{k=1}^{s} \sum_{j=1}^{r} \mu_k(\theta) \eta_j^k(\theta) L_j^k x \tag{3.12}$$

Note that the switching PDC law (3.12) shares the same indicator and membership functions as the switching T-S model (3.3). Let $\tilde{H} = \left\{ H_j^k \right\}_{\substack{j \in \Omega_r \\ k \in \Omega_s}}$ be a finite family of $(m \times n)$ matrices, the polyhedral set $\Xi(\tilde{H}, u_{\max})$ is defined by:

$$\Xi\left(\tilde{H}, u_{\max}\right) = \bigcap_{k=1}^{s} \bigcap_{j=1}^{r} \Xi\left(H_j^k, u_{\max}\right) \tag{3.13}$$

where $\Xi\left(H_j^k, u_{\max}\right)$ denotes the polyhedron:

$$\Xi\left(H_j^k, u_{\max}\right) = \left\{ x \in \mathbb{R}^n : -u_{\max} \preceq H_j^k x \preceq u_{\max} \right\} \tag{3.14}$$

By Lemma 3.1, it is simple to prove that, for any $x \in \Xi\left(\tilde{H}, u_{\max}\right)$, the input saturation can be expressed as:

$$sat(u) = \sum_{k=1}^{s} \sum_{j=1}^{r} \sum_{p=1}^{2^m} \mu_k(\theta) \eta_j^k(\theta) \xi_p \left(\Gamma_p^+ L_j^k + \Gamma_p^- H_j^k \right) x \tag{3.15}$$

By substituting (3.15) into (3.3) and using the notations (3.1), the closed-loop system can then be rewritten on the following form:

$$\begin{cases} \dot{x} = \left[\left(A_{\sigma\theta} + \Delta A_{\sigma\theta} \right) + \left(B_{u,\sigma\theta} + \Delta B_{u,\sigma\theta} \right) \left(\Gamma_{\xi}^{+} L_{\sigma\theta} + \Gamma_{\xi}^{-} H_{\sigma\theta} \right) \right] x + \left(B_{w,\sigma\theta} + \Delta B_{w,\sigma\theta} \right) w \\ z = \left[\left(C_{z,\sigma\theta} + \Delta C_{z,\sigma\theta} \right) + \left(D_{u,\sigma\theta} + \Delta D_{u,\sigma\theta} \right) \left(\Gamma_{\xi}^{+} L_{\sigma\theta} + \Gamma_{\xi}^{-} H_{\sigma\theta} \right) \right] x + \left(D_{w,\sigma\theta} + \Delta D_{w,\sigma\theta} \right) w \\ y = C_{y,\sigma\theta} x \end{cases} \tag{3.16}$$

where

$$\Gamma_{\xi}^{+} = \sum_{p=1}^{2^m} \xi_p \Gamma_p^{+}; \quad \Gamma_{\xi}^{-} = \sum_{p=1}^{2^m} \xi_p \Gamma_p^{-} \tag{3.17}$$

Remark 5.2. In (3.16), the property that $\mu_k(\theta)\mu_l(\theta) = 0$ if $k \neq l$ has been used.

3.3.3. Static output feedback control law

The switching T-S SOFC is represented under the form:

$$u = \sum_{k=1}^{s} \sum_{j=1}^{r} \mu_k(\theta) \eta_j^k(\theta) L_j^k y = \sum_{k=1}^{s} \sum_{j=1}^{r} \sum_{l=1}^{r} \mu_k(\theta) \eta_j^k(\theta) \eta_l^k(\theta) L_j^k C_{y,l}^k x \tag{3.18}$$

As in the case of SFC, if $x \in \Xi\left(\tilde{H}, u_{\max}\right)$, the control input saturation can be expressed as:

$$sat(u) = \sum_{k=1}^{s} \sum_{j=1}^{r} \sum_{l=1}^{r} \sum_{p=1}^{2^m} \mu_k(\theta) \eta_j^k(\theta) \eta_l^k(\theta) \xi_p \left(\Gamma_p^{+} L_j^k C_{y,l}^k + \Gamma_p^{-} H_j^k \right) x \tag{3.19}$$

Then, the closed-loop system (3.3) becomes:

$$\begin{cases} \dot{x} = \left\{ \left(A_{\sigma\theta} + \Delta A_{\sigma\theta} \right) + \left(B_{u,\sigma\theta} + \Delta B_{u,\sigma\theta} \right) \left(\Gamma_{\xi}^{+} L_{\sigma\theta} C_{y,\sigma\theta} + \Gamma_{\xi}^{-} H_{\sigma\theta} \right) \right\} x + \left(B_{w,\sigma\theta} + \Delta B_{w,\sigma\theta} \right) w \\ z = \left\{ \left(C_{z,\sigma\theta} + \Delta C_{z,\sigma\theta} \right) + \left(D_{u,\sigma\theta} + \Delta D_{u,\sigma\theta} \right) \left(\Gamma_{\xi}^{+} L_{\sigma\theta} C_{y,\sigma\theta} + \Gamma_{\xi}^{-} H_{\sigma\theta} \right) \right\} x + \left(D_{w,\sigma\theta} + \Delta D_{w,\sigma\theta} \right) w \\ y = C_{y,\sigma\theta} x \end{cases} \tag{3.20}$$

3.4. Maximization of the Estimate Domain of Attraction

Concerning the undisturbed, closed-loop system, an estimate of the attraction domain of its equilibrium point $x = 0$ will be given in the ellipsoid form $\mathcal{E}(P)$, with $P > 0$, that will be positively invariant. It is worth noting that a larger ellipsoid leads to a less conservative controller. In order to

measure the largeness of the ellipsoid, we adopt here the idea of shape reference set in (Boyd et al., 1994). Let $X_R \subset \mathbb{R}^{n_x}$ be a prescribed bounded convex set containing the origin. Finding the largest ellipsoid $\mathcal{E}(P)$ can be formulated as the following optimization problem:

$$\begin{aligned} &\sup_{\tau, P>0} \quad \tau \\ &s.t. \;\; \tau X_R \subset \mathcal{E}(P) \end{aligned} \tag{3.21}$$

There are two typical choices for reference set X_R. The first one is an *ellipsoid* defined as:

$$X_R = \left\{ x \in \mathbb{R}^{n_x} : \; x^T R x \le 1 \right\} \tag{3.22}$$

where $R > 0$. The second one is a *polyhedron* defined as:

$$X_R = co\left\{ x_0^1, \; x_0^2, \ldots, \; x_0^l \right\} \tag{3.23}$$

where $x_0^1, \; x_0^2, \ldots, \; x_0^l$ are a priori given points in $\mathbb{R}^{n_x}$.

For these two choices of set X_R, problem (3.21) can be expressed as an LMI optimization problem:

- If the reference shape X_R is given by the ellipsoid (3.22), then $\tau X_R \subset \mathcal{E}(P)$ is equivalent to the condition

  $$\frac{R}{\tau^2} \ge P \tag{3.24}$$

  Denoting $\lambda = 1/\tau^2$ and $Q = P^{-1}$, and using Schur complement lemma, the problem (3.21) can be expressed as the LMI optimization problem of finding the minimum value of λ satisfying the inequality

  $$\begin{bmatrix} \lambda R & I \\ I & Q \end{bmatrix} \ge 0 \tag{3.25}$$

- Now, if X_R is the polyhedron (3.23), then $\tau X_R \subset \mathcal{E}(P)$ is equivalent to:

  $$\tau^2 \left(x_0^i \right)^T (P) x_0^i \le 1, \quad \forall i \in \Omega_l \tag{3.26}$$

  This inequality can also be reformulated in LMI form as:

$$\begin{bmatrix} \lambda & \left(x_0^i\right)^T \\ x_0^i & Q \end{bmatrix} \geq 0, \quad \forall i \in \Omega_l \tag{3.27}$$

3.5. Other Preliminary Results

Some other results that will be useful in the proof of our main result are recalled below.

Lemma 3.2 (Cao & Lin, 2003) The ellipsoid set $\mathcal{E}(P)$ is contained in the polyhedral set $\Xi(H, u_{\max})$ if and only if:

$$\left(h_i\right)^T \left(P\right)^{-1} h_i \leq u_{\max,i}^2, \quad \forall i \in \Omega_m \tag{3.28}$$

where h_i^T is the i^{th} row of the matrix H.

♦

4. Main Results

In this section, some LMI-based *sufficient conditions* to solve the problem stated in Section 3.2 are given.

4.1. State Feedback Controller Design

Theorem 3.1. Given positive real numbers α, γ and a set X_R defined as in (3.22) (or (3.23)) , if there exists matrices $Q > 0$, Y_j^k , Z_j^k , and positive real numbers λ , δ , ρ , $\varepsilon_{x,ij}^k$, $\varepsilon_{z,ij}^k$ (for $(k,i,j) \in \Omega_s \times \Omega_r \times \Omega_r$) such that(3.25) (or (3.27)) holds and satisfying also the following inequalities:

$$\begin{bmatrix} u_{\max,i}^2 & z_{j,i}^k \\ * & Q \end{bmatrix} \geq 0, \quad \forall (k,i,j) \in \Omega_s \times \Omega_m \times \Omega_r \tag{3.29}$$

$$\Upsilon_{iip}^k < 0, \quad \forall (k,i,p) \in \Omega_s \times \Omega_r \times \Omega_{2^m} \tag{3.30}$$

$$\frac{2}{r-1} \Upsilon_{iip}^k + \Upsilon_{ijp}^k + \Upsilon_{jip}^k < 0, \quad \forall (k,i,j,p) \in \Omega_s \times \Omega_r \times \Omega_r \times \Omega_{2^m}, \, i \neq j \tag{3.31}$$

$$\begin{bmatrix} 1-\rho & \gamma \\ \gamma & \delta \end{bmatrix} \geq 0 \tag{3.32}$$

where $z_{j,i}^k$ denotes the i^{th} row of matrix Z_j^k, and

$$\Upsilon_{ijp}^{k} \triangleq \begin{bmatrix} sym\left(A_i^k Q + B_{u,i}^k\left(\Gamma_p^+ Y_j^k + \Gamma_p^- Z_j^k\right) + \alpha Q\right) & * & * & * & * & * & * \\ \left(B_{w,i}^k\right)^T & -\gamma^2 I & * & * & * & * & * \\ C_{z,i}^k Q + D_{u,i}^k\left(\Gamma_p^+ Y_j^k + \Gamma_p^- Z_j^k\right) & D_{w,i}^k & -I & * & * & * & * \\ \varepsilon_{x,ij}^k\left(F_x^k\right)^T & 0 & 0 & -\varepsilon_{x,ij}^k I & * & * & * \\ E_{A,i}^k Q + E_{Bu,i}^k\left(\Gamma_p^+ Y_j^k + \Gamma_p^- Z_j^k\right) & E_{Bw,i}^k & 0 & 0 & -\varepsilon_{x,ij}^k I & * & * \\ 0 & 0 & \varepsilon_{z,ij}^k\left(F_z^k\right)^T & 0 & 0 & -\varepsilon_{z,ij}^k I & * \\ E_{Cz,i}^k Q + E_{Du,i}^k\left(\Gamma_p^+ Y_j^k + \Gamma_p^- Z_j^k\right) & E_{Dw,i}^k & 0 & 0 & 0 & 0 & -\varepsilon_{z,ij}^k I \end{bmatrix} \tag{3.33}$$

Then, the switching SFC law (3.12) with:

$$L_j^k = Y_j^k Q^{-1}, \quad \forall (k,j) \in \Omega_s \times \Omega_r \tag{3.34}$$

solves the control problem stated in Section 3.2.

Proof. For brevity, let us introduce the following notations:

$$\begin{aligned} &Q = P^{-1}; \quad Z_j^k = H_j^k Q; \quad \mathbb{A}_{\sigma\theta} = A_{\sigma\theta} + \Delta A_{\sigma\theta}; \quad \mathbb{B}_{u,\sigma\theta} = B_{u,\sigma\theta} + \Delta B_{u,\sigma\theta}; \quad \mathbb{B}_{w,\sigma\theta} = B_{w,\sigma\theta} + \Delta B_{w,\sigma\theta} \\ &Y_j^k = L_j^k Q; \quad \mathbb{C}_{z,\sigma\theta} = C_{z,\sigma\theta} + \Delta C_{z,\sigma\theta}; \quad \mathbb{D}_{u,\sigma\theta} = D_{u,\sigma\theta} + \Delta D_{u,\sigma\theta}; \quad \mathbb{D}_{w,\sigma\theta} = D_{w,\sigma\theta} + \Delta D_{w,\sigma\theta} \end{aligned} \tag{3.35}$$

Considering the positive-definite function $V(x) = x^T P x$ and assuming $x \in \Xi\left(\tilde{H}, u_{\max}\right)$, the following expression is obtained from (3.16):

$$\Lambda \triangleq \dot{V}(x) + 2\alpha V(x) + z^T z - \gamma^2 w^T w = \begin{bmatrix} x \\ w \end{bmatrix}^T \Phi \begin{bmatrix} x \\ w \end{bmatrix} \tag{3.36}$$

where

$$\begin{aligned} \Phi \triangleq &\begin{bmatrix} sym\left(\left(\mathbb{A}_{\sigma\theta} + \mathbb{B}_{u,\sigma\theta}\left(\Gamma_\xi^+ L_{\sigma\theta} + \Gamma_\xi^- H_{\sigma\theta}\right)\right)^T P + \alpha P\right) & * \\ \mathbb{B}_{w,\sigma\theta}^T P & -\gamma^2 I \end{bmatrix} \\ &+ \begin{bmatrix} \left(\mathbb{C}_{z,\sigma\theta} + \mathbb{D}_{u,\sigma\theta}\left(\Gamma_\xi^+ L_{\sigma\theta} + \Gamma_\xi^- H_{\sigma\theta}\right)\right)^T \\ \mathbb{D}_{w,\sigma\theta}^T \end{bmatrix} \begin{bmatrix} \left(\mathbb{C}_{z,\sigma\theta} + \mathbb{D}_{u,\sigma\theta}\left(\Gamma_\xi^+ L_{\sigma\theta} + \Gamma_\xi^- H_{\sigma\theta}\right)\right)^T \\ \mathbb{D}_{w,\sigma\theta}^T \end{bmatrix}^T \end{aligned} \tag{3.37}$$

Then, applying the Schur complement lemma for (3.37), the condition $\Lambda < 0$ holds if and only if:

$$\Psi \triangleq \begin{bmatrix} sym\left(\left(\mathbb{A}_{\sigma\theta}+\mathbb{B}_{u,\sigma\theta}\left(\Gamma_{\xi}^{+}L_{\sigma\theta}+\Gamma_{\xi}^{-}H_{\sigma\theta}\right)\right)^{T}P+\alpha P\right) & * & * \\ \mathbb{B}_{w,\sigma\theta}^{T}P & -\gamma^{2}I & * \\ \mathbb{C}_{z,\sigma\theta}+\mathbb{D}_{u,\sigma\theta}\left(\Gamma_{\xi}^{+}L_{\sigma\theta}+\Gamma_{\xi}^{-}H_{\sigma\theta}\right) & \mathbb{D}_{w,\sigma\theta} & -I \end{bmatrix} < 0 \tag{3.38}$$

From (3.5) and (3.38), Ψ can be decomposed into two parts: a *nominal* part Ψ_0 and an *uncertain* part $\Delta\Psi$ as:

$$\Psi \triangleq \Psi_0 + \Delta\Psi \tag{3.39}$$

with

$$\Psi_0 = \begin{bmatrix} sym\left(\left(A_{\sigma\theta}+B_{u,\sigma\theta}\left(\Gamma_{\xi}^{+}L_{\sigma\theta}+\Gamma_{\xi}^{-}H_{\sigma\theta}\right)\right)^{T}P+\alpha P\right) & * & * \\ B_{w,\sigma\theta}^{T}P & -\gamma^{2}I & * \\ C_{z,\sigma\theta}+D_{u,\sigma\theta}\left(\Gamma_{\xi}^{+}L_{\sigma\theta}+\Gamma_{\xi}^{-}H_{\sigma\theta}\right) & D_{w,\sigma\theta} & -I \end{bmatrix} \tag{3.40}$$

and

$$\begin{aligned} \Delta\Psi = & sym\left\{\begin{bmatrix} PF_{x,\sigma} \\ 0 \\ 0 \end{bmatrix}\Theta_{x}\begin{bmatrix} E_{A,\sigma\theta}+E_{Bu,\sigma\theta}\left(\Gamma_{\xi}^{+}L_{\sigma\theta}+\Gamma_{\xi}^{-}H_{\sigma\theta}\right) & E_{Bw,\sigma\theta} & 0 \end{bmatrix}\right\} \\ & + sym\left\{\begin{bmatrix} 0 \\ 0 \\ F_{z,\sigma} \end{bmatrix}\Theta_{z}\begin{bmatrix} E_{Cz,\sigma\theta}+E_{Du,\sigma\theta}\left(\Gamma_{\xi}^{+}L_{\sigma\theta}+\Gamma_{\xi}^{-}H_{\sigma\theta}\right) & E_{Dw,\sigma\theta} & 0 \end{bmatrix}\right\} \end{aligned} \tag{3.41}$$

Given $\varepsilon_{x,ij}^{k} > 0,\ \varepsilon_{z,ij}^{k} > 0,\ \forall(k,i,j) \in \Omega_s \times \Omega_r \times \Omega_r$, using the notations (3.1), Lemma 2.3 and again the Schur complement lemma, inequality (3.38) holds if:

$$\begin{bmatrix} sym\left(\mathbb{U}_1\right) & * & * & * & * & * & * \\ B_{w,\sigma\theta}^T P & -\gamma^2 I & * & * & * & * & * \\ C_{z,\sigma\theta}+D_{u,\sigma\theta}\left(\Gamma_\xi^+ L_{\sigma\theta}+\Gamma_\xi^- H_{\sigma\theta}\right) & D_{w,\theta} & -I & * & * & * & * \\ \varepsilon_{x,\sigma\theta\theta}F_{x,\sigma}^T P & 0 & 0 & -\varepsilon_{x,\sigma\theta\theta}I & * & * & * \\ E_{A,\sigma\theta}+E_{Bu,\sigma\theta}\left(\Gamma_\xi^+ L_{\sigma\theta}+\Gamma_\xi^- H_{\sigma\theta}\right) & E_{Bw,\sigma\theta} & 0 & 0 & -\varepsilon_{x,\sigma\theta\theta}I & * & * \\ 0 & 0 & \varepsilon_{z,\sigma\theta\theta}F_{z,\sigma}^T & 0 & 0 & -\varepsilon_{z,\sigma\theta\theta}I & * \\ E_{Cz,\sigma\theta}+E_{Du,\sigma\theta}\left(\Gamma_\xi^+ L_{\sigma\theta}+\Gamma_\xi^- H_{\sigma\theta}\right) & E_{Dw,\sigma\theta} & 0 & 0 & 0 & 0 & -\varepsilon_{z,\sigma\theta\theta}I \end{bmatrix} < 0 \tag{3.42}$$

where $\mathbb{U}_1 \triangleq \left(A_{\sigma\theta}+B_{u,\sigma\theta}\left(\Gamma_\xi^+ L_{\sigma\theta}+\Gamma_\xi^- H_{\sigma\theta}\right)\right)^T P+\alpha P$. From (3.35) and using congruence with the matrix $diag\left[Q,I,I,I,I,I,I\right]$, the condition (3.42) is equivalent to:

$$\begin{bmatrix} sym\left(\mathbb{U}_2\right) & * & * & * & * & * & * \\ B_{w,\sigma\theta}^T & -\gamma^2 I & * & * & * & * & * \\ C_{z,\sigma\theta}Q+D_{u,\sigma\theta}\left(\Gamma_\xi^+ Y_{\sigma\theta}+\Gamma_\xi^- Z_{\sigma\theta}\right) & D_{w,\sigma\theta} & -I & * & * & * & * \\ \varepsilon_{x,\sigma\theta\theta}F_{x,\sigma}^T & 0 & 0 & -\varepsilon_{x,\sigma\theta\theta}I & * & * & * \\ E_{A,\sigma\theta}Q+E_{Bu,\sigma\theta}\left(\Gamma_\xi^+ Y_{\sigma\theta}+\Gamma_\xi^- Z_{\sigma\theta}\right) & E_{Bw,\sigma\theta} & 0 & 0 & -\varepsilon_{x,\sigma\theta\theta}I & * & * \\ 0 & 0 & \varepsilon_{z,\sigma\theta\theta}F_{z,\sigma}^T & 0 & 0 & -\varepsilon_{z,\sigma\theta\theta}I & * \\ E_{Cz,\sigma\theta}Q+E_{Du,\sigma\theta}\left(\Gamma_\xi^+ Y_{\sigma\theta}+\Gamma_\xi^- Z_{\sigma\theta}\right) & E_{Dw,\sigma\theta} & 0 & 0 & 0 & 0 & -\varepsilon_{z,\sigma\theta\theta}I \end{bmatrix} < 0 \tag{3.43}$$

where $\mathbb{U}_2 \triangleq A_{\sigma\theta}Q+B_{u,\sigma\theta}\left(\Gamma_\xi^+ Y_{\sigma\theta}+\Gamma_\xi^- Z_{\sigma\theta}\right)+\alpha Q$. Now, applying Lemma 2.7 with inequalities (3.30)-(3.31), inequality (3.43) is proved. Hence, we have shown that, if $x\in\Xi\left(\tilde{H},u_{\max}\right)$, then:

$$\dot{V}\left(x\right)+2\alpha V\left(x\right)+z^T z-\gamma^2 w^T w<0 \tag{3.44}$$

Using Schur complement lemma on (3.29), it follows that:

$$\left(z_{j,i}^k\right)^T z_{j,i}^k \le u_{\max,i}^2 Q, \quad \forall\left(i,j,k\right)\in\Omega_m\times\Omega_r\times\Omega_s, \tag{3.45}$$

which, applying Lemma 3.2, is equivalent to $\mathcal{E}\left(P\right)\subset\Xi\left(\tilde{H},u_{\max}\right)$.

- Assume $w=0,\ \forall t\ge 0$, it follows from (3.44) that:

$$\dot{V}\left(x\right)<-2\alpha V\left(x\right) \tag{3.46}$$

This inequality implies that the set $\mathcal{E}(P)$ is positively invariant for the closed-loop system, and that, for any initial state in this set, the trajectory will converge exponentially to 0 with a decay rate α. This fact proves the property (P.1) stated in Subsection 3.2.

- Assume now that $w \in W_\delta$, integrating both sides of (3.44) from 0 to T_f, where $T_f \in \mathbb{R}^+$, yields:

$$V\left(x\left(T_f\right)\right) - V\left(x(0)\right) + 2\alpha\int_0^{T_f} V(x)\,dt - \gamma^2\int_0^{T_f} w^T w dt + \int_0^{T_f} z^T z dt < 0 \tag{3.47}$$

From (3.32), it can be deduced that $V\left(x\left(T_f\right)\right) \le V\left(x(0)\right) + \gamma^2\int_0^{T_f} w^T w dt \le \rho + \gamma^2\delta^{-1} < 1$. So, it can be easily shown that, for any initial state in $\mathcal{E}(P,\rho)$, the closed-loop trajectory is confined in the set $\mathcal{E}(P) \subset \Xi\left(\tilde{H}, u_{\max}\right)$. Furthermore, from (3.47) and considering the limit case $T_f \to \infty$, we obtain $\int_0^{\infty} z^T z dt \le \gamma^2\int_0^{\infty} w^T w dt + V\left(x(0)\right)$, this means that the $\mathcal{L}_2$-norm of the output signal z is upper bounded by $\|z\|_2^2 \le \gamma^2\|w\|_2^2 + \rho$. These facts prove the statement (P.2) stated in Subsection 3.2.

♦

Remark 3.3. If $x(0) \neq 0$, there is a tradeoff between the size of the set of admissible initial conditions and the maximal level energy of disturbances, given by δ. Indeed, the lower is the admissible δ (i.e. the lower is the disturbance admissible energy), the larger is the admissible set of initial conditions (Castelan et al., 2006).

Next, the design of a static output feedback control is considered.

4.2. Static Output Feedback Controller Design

Theorem 3.2. Given positive real numbers α, γ and a set X_R defined as in (3.22) (or (3.23)), if there exists a nonsingular matrix M, matrices $Q > 0$, Y_j^k, Z_j^k, and positive real numbers λ, δ, ρ, $\varepsilon_{x,ij}^k$, $\varepsilon_{z,ij}^k$ (for $(k,i,j) \in \Omega_s \times \Omega_r \times \Omega_r$) such that(3.25) (or (3.27)) holds and satisfying also the following inequalities:

$$\begin{bmatrix} u_{\max,i}^2 & z_{j,i}^k \\ * & Q \end{bmatrix} \ge 0, \quad \forall (k,i,j) \in \Omega_s \times \Omega_m \times \Omega_r \tag{3.48}$$

$$\Upsilon_{iilp}^k < 0, \quad \forall (k,i,l,p) \in \Omega_s \times \Omega_r \times \Omega_r \times \Omega_{2^m} \tag{3.49}$$

$$\frac{2}{r-1}\Upsilon^k_{iilp}+\Upsilon^k_{ijlp}+\Upsilon^k_{jilp}<0,\quad \forall(k,i,j,l,p)\in\Omega_s\times\Omega_r\times\Omega_r\times\Omega_r\times\Omega_{2^m},\ i\neq j \tag{3.50}$$

$$MC^k_{y,l}=C^k_{y,l}Q,\quad \forall(k,l)\in\Omega_s\times\Omega_r \tag{3.51}$$

$$\begin{bmatrix}1-\rho & \gamma\\ \gamma & \delta\end{bmatrix}\geq 0 \tag{3.52}$$

where $z^k_{j,i}$ denotes the i^{th} row of matrix Z^k_j, and

$$\Upsilon^k_{ijlp}\triangleq\begin{bmatrix}
sym\left(W^k_{ijlp}\right) & * & * & * & * & * & *\\
\left(B^k_{w,i}\right)^T & -\gamma^2 I & * & * & * & * & *\\
C^k_{z,i}Q+D^k_{u,i}\left(\Gamma^+_pY^k_jC_{y,l}+\Gamma^-_pZ^k_j\right) & D^k_{w,i} & -I & * & * & * & *\\
\varepsilon^k_{x,ij}\left(F^k_x\right)^T & 0 & 0 & -\varepsilon^k_{x,ij}I & * & * & *\\
E^k_{A,i}Q+E^k_{Bu,i}\left(\Gamma^+_pY^k_jC_{y,l}+\Gamma^-_pZ^k_j\right) & E^k_{Bw,i} & 0 & 0 & -\varepsilon^k_{x,ij}I & * & *\\
0 & 0 & \varepsilon^k_{z,ij}\left(F^k_z\right)^T & 0 & 0 & -\varepsilon^k_{z,ij}I & *\\
E^k_{Cz,i}Q+E^k_{Du,i}\left(\Gamma^+_pY^k_jC_{y,l}+\Gamma^-_pZ^k_j\right) & E^k_{Dw,i} & 0 & 0 & 0 & 0 & -\varepsilon^k_{z,ij}I
\end{bmatrix} \tag{3.53}$$

where $W^k_{ijlp}\triangleq A^k_iQ+B^k_{u,i}\left(\Gamma^+_pY^k_jC_{y,l}+\Gamma^-_pZ^k_j\right)+\alpha Q$.

Then the switching SOFC law (3.18) with:

$$L^k_j=Y^k_jM^{-1},\quad \forall(k,j)\in\Omega_s\times\Omega_r \tag{3.54}$$

solves the problem stated in Section 3.2.

Proof. Following the same scheme of proof as for Theorem 3.1, the condition (3.44) holds in this case if the condition (3.55) is verified, where $\mathbb{V}_1\triangleq\left(A_{\sigma\theta}+B_{u,\sigma\theta}\left(\Gamma^+_\xi L_{\sigma\theta}C_{y,\sigma\theta}+\Gamma^-_\xi H_{\sigma\theta}\right)\right)^TP+\alpha P$:

$$\begin{bmatrix} sym(\mathbb{V}_1) & * & * & * & * & * & * \\ B_{w,\sigma\theta}^T P & -\gamma^2 I & * & * & * & * & * \\ C_{z,\sigma\theta}+D_{u,\sigma\theta}\left(\Gamma_\xi^+ L_{\sigma\theta}C_{y,\sigma\theta}+\Gamma_\xi^- H_{\sigma\theta}\right) & D_{w,\sigma\theta} & -I & * & * & * & * \\ \varepsilon_{x,\sigma\theta\theta}F_{x,\sigma}^T P & 0 & 0 & -\varepsilon_{x,\sigma\theta\theta}I & * & * & * \\ E_{A,\sigma\theta}+E_{Bu,\sigma\theta}\left(\Gamma_\xi^+ L_{\sigma\theta}C_{y,\sigma\theta}+\Gamma_\xi^- H_{\sigma\theta}\right) & E_{Bw,\sigma\theta} & 0 & 0 & -\varepsilon_{x,\sigma\theta\theta}I & * & * \\ 0 & 0 & \varepsilon_{z,\sigma\theta\theta}F_{z,\sigma}^T & 0 & 0 & -\varepsilon_{z,\sigma\theta\theta}I & * \\ E_{Cz,\sigma\theta}+E_{Du,\sigma\theta}\left(\Gamma_\xi^+ L_{\sigma\theta}C_{y,\sigma\theta}+\Gamma_\xi^- H_{\sigma\theta}\right) & E_{Dw,\sigma\theta} & 0 & 0 & 0 & 0 & -\varepsilon_{z,\sigma\theta\theta}I \end{bmatrix} < 0 \tag{3.55}$$

Using congruence propriety with the matrix $diag[Q,I,I,I,I,I,I]$ and then replacing $MC_{y,l}^k = C_{y,l}^k Q$, $Y_j^k = L_j^k M$ therein, the condition (3.55) is equivalent to:

$$\begin{bmatrix} sym(\mathbb{V}_2) & * & * & * & * & * & * \\ B_{w,\sigma\theta}^T & -\gamma^2 I & * & * & * & * & * \\ C_{z,\sigma\theta}Q+D_{u,\sigma\theta}\left(\Gamma_\xi^+ Y_{\sigma\theta}C_{y,\sigma\theta}+\Gamma_\xi^- Z_{\sigma\theta}\right) & D_{w,\sigma\theta} & -I & * & * & * & * \\ \varepsilon_{x,\sigma\theta\theta}F_{x,\sigma}^T & 0 & 0 & -\varepsilon_{x,\sigma\theta\theta}I & * & * & * \\ E_{A,\sigma\theta}Q+E_{Bu,\sigma\theta}\left(\Gamma_\xi^+ Y_{\sigma\theta}C_{y,\sigma\theta}+\Gamma_\xi^- Z_{\sigma\theta}\right) & E_{Bw,\sigma\theta} & 0 & 0 & -\varepsilon_{x,\sigma\theta\theta}I & * & * \\ 0 & 0 & \varepsilon_{z,\sigma\theta\theta}F_{z,\sigma}^T & 0 & 0 & -\varepsilon_{z,\sigma\theta\theta}I & * \\ E_{Cz,\sigma\theta}Q+E_{Du,\sigma\theta}\left(\Gamma_\xi^+ Y_{\sigma\theta}C_{y,\sigma\theta}+\Gamma_\xi^- Z_{\sigma\theta}\right) & E_{Dw,\sigma\theta} & 0 & 0 & 0 & 0 & -\varepsilon_{z,\sigma\theta\theta}I \end{bmatrix} < 0 \tag{3.56}$$

where $\mathbb{V}_2 \triangleq A_{\sigma\theta}Q + B_{u,\sigma\theta}\left(\Gamma_\xi^+ Y_{\sigma\theta}C_{y,\sigma\theta}+\Gamma_\xi^- Z_{\sigma\theta}\right)+\alpha Q$. Using the same argument as previously, the proof of Theorem 3.2 can be concluded.

♦

Remark 3.4. Theorem 3.1 and Theorem 3.2 provide conditions to find matrices Q, Y_j^k, Z_j^k, and real numbers λ (or τ), δ, ρ, $\varepsilon_{x,ij}^k$, $\varepsilon_{z,ij}^k$ (for $(k,i,j)\in\Omega_s\times\Omega_r\times\Omega_r$) such that $\tau X_R \subset \mathcal{E}(P)$. As shown in Subsection 3.2, maximization of the estimate domain of attraction amounts to maximize τ (or to minimize λ). Hence, the problem of maximizing the estimate domain of attraction can be formulated as the following convex optimization problem (Boyd et al., 1994):

$$\begin{aligned} &\min \lambda \\ &\text{subject to} \\ &\text{LMI constraints in Theorem 3.1 (resp. Theorem 3.2)} \end{aligned} \tag{3.57}$$

It is worth noting that X_R defines the directions in which we want to maximize $\mathcal{E}(P)$.

5. Concluding Remarks

The purpose of this chapter is to develop a novel approach to design robust H_∞ controllers for a class of switching uncertain systems under the effects of control input saturation based on switching T-S models. The class of uncertain, disturbed switching T-S models with control input saturation was first presented. Based on Lyapunov stability theory, a constructive control design procedure is given for two cases: SFC and SOFC. In this paper, the control input saturation is dealt with by using a polytopic representation and the guaranteed domain of attraction is maximized in order to relax the design conditions. The controller gains in the both cases can be efficiently computed with some numerical tools since all design conditions are formulated as LMI optimization problems.

The effectiveness of the proposed method will be performed via a real industrial example concerning the turbocharged air system control of a SI engine in Chapter 5.

"It always seems impossible until it's done."

Nelson Mandela, South African anti-apartheid revolutionary, politician

Chapter 4. Stabilization of T-S Model under Input Saturation: Anti-Windup Based Approach

1. Introduction

In the last years, control of nonlinear systems based on the so-called Takagi-Sugeno (T-S) model (Takagi & Sugeno, 1985) has attracted great interest from researchers and engineers with numerous successful engineering applications (Tanaka & Wang, 2001; Sala et al., 2005; Lauber et al., 2011; Nguyen et al., 2012c). Indeed, T-S model has been widely used to represent complex nonlinear systems as an universal approximator. With a T-S representation, a model-based control may be designed to guarantee the stability and achieve some performance requirements for nonlinear systems. Thanks to its polytopic structure, the main interest of T-S control approach is to make possible the extension of some linear concepts to the case of nonlinear systems (Tanaka and Wang, 2001). This control technique provides a general and systematic framework to cope with complex nonlinear systems.

Among all the nonlinear phenomena, actuator saturation is unavoidable in almost real applications. It can severely degrade closed-loop system performance and in some cases may lead to the system instability. Motivated by this practical control aspect, a great deal of effort has been recently focused on saturated systems; see e.g. (Tarbouriech et al., 2011) for an overview. In general, there are two main approaches to deal with the input saturation problem. The first one explicitly considers the saturation effect by using a polytopic representation (Cao & Lin, 2003; Fang et al., 2004). As seen in previous chapter, this approach often leads to conservative design conditions. The second approach is based on *anti-windup* control scheme (Kothare et al., 1994; Teel & Kapoor, 1997). There are two categories in this case: one-step or two-step design methods. For the two-step method, first a controller is designed without regarding control input nonlinearity and then an additional anti-windup compensator is introduced in order to minimize the undesirable degradation of closed-loop

performance caused by input saturation (Kothare et al., 1994; Grimm et al., 2003; Hu et al., 2008). The one-step method deals with saturation effect by simultaneously designing the controller and its associated anti-windup strategy (Mulder et al., 2009). Numerous results on anti-windup based control are available in the literature for linear systems, but very few works deal with nonlinear cases. Besides control input saturation, the system states are usually bounded in real-world applications. Another point specific to T-S models obtained using the nonlinear sector decomposition approach concerns their validity domain which can be described by additional state constraints. Therefore, it is also important to explicitly consider the state constraints in control design.

In T-S control framework, state-feedback control based on the concepts of parallel distributed compensation (PDC) (Wang et al., 1996) is usually applied to derive the design conditions (Tanaka & Wang, 2001; Guerra & Vermeiren, 2004). However, system states are not always available in many practical cases. Therefore, output feedback control has been intensively investigated in the literature, see (Feng, 2006) for a survey. Most of works concern observer-based controller design (Tanaka et al., 1998; Liu & Zhang, 2003; Lin et al., 2005). However, the separation principle is no longer applicable when some scheduling variables are non-measurable (Nguang & Shi, 2003; Guerra et al., 2006). In particular, the observer-based approach becomes much more complicated when dealing with nonlinear systems subject to control input and system state constraints. This control issue has not been well addressed in the literature (Ding, 2009).

Motivated by these control issues, we propose in this chapter a new LMI-based method to design simultaneously a dynamic output feedback controller (DOFC) and an anti-windup compensator for a given nonlinear system. To this end, the disturbed nonlinear system subject to control input and system state constraints is represented in T-S form and the DOFC proposed in (Li et al., 2000) is adopted. It will be shown that the control design can be formulated as a multi-objective convex optimization problem. In such a way, the obtained controller optimizes several regional closed-loop requirements, often conflicting. Anti-windup based control design in the presence of energy-bounded disturbance and state constraints is quite novel in T-S control framework. This proposed method provides a systematic tool to deal with a very large class of nonlinear systems which is our major contribution.

The chapter is organized as follows. Section 2 describes the design problem and recalls some preliminaries results needed for the control development. The main result is stated in Section 3. In Section 4, a constructive control design is presented as a multi-objective LMI optimization problem.

The effectiveness of the proposed method will be pointed out via an illustrative example in Section 5. Finally, Section 6 gives some conclusions.

The following notations will be occasionally used in this chapter:

$$Y_\theta = \sum_{i=1}^{r} \eta_i(\theta) Y_i; \quad Z_{\theta\theta} = \sum_{i=1}^{r}\sum_{j=1}^{r} \eta_i(\theta)\eta_j(\theta) Z_{ij} \tag{4.1}$$

where Y_i, Z_{ij} are matrices of appropriate dimensions, and $\eta_i(\theta)$ are scalar functions sharing the convex sum property with $i \in \Omega_r$.

2. Problem Definition and Preliminaries Results

2.1. Control Problem Definition

2.1.1. Closed-loop system description

Consider the following time-continuous T-S model described by (Tanaka & Wang, 2001):

$$\begin{cases} \dot{x} = \sum_{i=1}^{r} \eta_i(\theta)\left(A_i x + B_i^u u + B_i^w w\right) \\ y = \sum_{i=1}^{r} \eta_i(\theta)\left(C_i^y x + D_i^{yw} w\right) \end{cases} \tag{4.2}$$

where $x \in \mathbb{R}^{n_x}$, $u \in \mathbb{R}^{n_u}$, $w \in \mathbb{R}^{n_w}$, $y \in \mathbb{R}^{n_y}$ and $\theta \in \mathbb{R}^k$ are respectively the state, the control input, the disturbance, the measured output and the scheduling variable vectors of the system. For $i \in \Omega_r$, the matrices $A_i \in \mathbb{R}^{n_x \times n_x}$, $B_i^u \in \mathbb{R}^{n_x \times n_u}$, $B_i^w \in \mathbb{R}^{n_x \times n_w}$, $C_i^y \in \mathbb{R}^{n_y \times n_x}$, $D_i^{yw} \in \mathbb{R}^{n_y \times n_w}$ represent the set of r local linear subsystems and the nonlinear scalar functions $\eta_i(\theta)$ satisfy the convex sum property.

For the system (4.2), we consider the following assumptions:

Assumption 4.1. The scheduling variable vector $\theta \in \mathbb{R}^k$ is assumed to be known and it may be functions of all signals of interest (states, measurements, external disturbances, and/or time) with the exception of the control input value u.

Assumption 4.2. The input vector u is subject to symmetric magnitude limitations:

$$-u_{\max(i)} \le u_{(i)} \le u_{\max(i)}; \qquad u_{\max(i)} > 0; \qquad \forall i \in \Omega_{n_u} \tag{4.3}$$

Assumption 4.3. The disturbance signal w is energy bounded, i.e. it belongs to the following set of functions:

$$W_\delta = \left\{ w : \mathbb{R}^+ \mapsto \mathbb{R}^{n_w};\quad \int_0^\infty w^T w dt \le \delta \right\}, \tag{4.4}$$

where the bound $\delta > 0$ is given.

Consider now the unconstrained dynamic output feedback controller (DOFC) in the form of (Li et al., 2000):

$$\begin{cases} \dot{x}_c = \sum_{i=1}^{r}\sum_{j=1}^{r} \eta_i(\theta)\eta_j(\theta) A_{ij}^c x_c + \sum_{i=1}^{r} \eta_i(\theta) B_i^c y + v \\ u_c = \sum_{i=1}^{r} \eta_i(\theta) C_i^c x_c + D^c y \end{cases} \tag{4.5}$$

where $x_c \in \mathbb{R}^{n_x}$, $u_c \in \mathbb{R}^{n_u}$ are respectively the state and output vectors of the controller. v is an additional input that will be used to compensate the "windup" effect. The controller (4.5) has to be designed in order to guarantee the stability and some performance requirements for the closed-loop system.

Because of the input limitation, the actual control signal injected into the system is subject to the saturation effect:

$$u = sat(u_c) \tag{4.6}$$

where each component of the saturation function $sat(\cdot)$ is given by:

$$sat(u_c)_{(i)} \triangleq sign(u_{c(i)}) \min\left(\left| u_{c(i)} \right|, u_{\max(i)} \right);\quad i \in \Omega_{n_u} \tag{4.7}$$

Then the interactions between the system (4.2) and the constrained controller are given as:

$$u = sat(u_c);\quad v = \sum_{i=1}^{r} \eta_i(\theta) E_i^c \left(sat(u_c) - u_c \right) \tag{4.8}$$

From (4.5) and (4.8), the DOFC combined with the anti-windup strategy can be expressed as:

$$\begin{cases} \dot{x}_c = \sum_{i=1}^{r}\sum_{j=1}^{r}\eta_i(\theta)\eta_j(\theta)A_{ij}^c x_c + \sum_{i=1}^{r}\eta_i(\theta)\left(B_i^c y - E_i^c \psi(u_c)\right) \\ u_c = \sum_{i=1}^{r}\eta_i(\theta)C_i^c x_c + D^c y \end{cases} \tag{4.9}$$

where E_i^c are the anti-windup gains to be designed and $\psi(u_c) \triangleq u_c - sat(u_c)$. The i^{th} component of the decentralized dead-zone nonlinearity $\psi(u_c)$ is defined as:

$$\psi_i(u_c) = \begin{cases} u_{c(i)} - u_{\max(i)} & \text{if} \quad u_{c(i)} > u_{\max(i)} \\ 0 & \text{if} \quad \left|u_{c(i)}\right| \le u_{\max(i)} \\ u_{c(i)} + u_{\max(i)} & \text{if} \quad u_{c(i)} < -u_{\max(i)} \end{cases} \tag{4.10}$$

The closed-loop system with the anti-windup strategy is depicted in Figure 4.1.

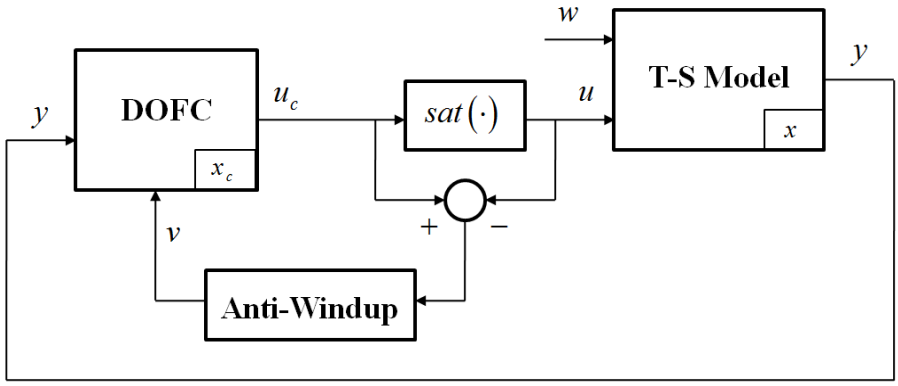

Figure 4.1. Closed-loop system with anti-windup strategy

Let us define $x_{cl} = \begin{bmatrix} x^T & x_c^T \end{bmatrix}^T$. From (4.2) and (4.9), the constrained closed-loop system is represented as:

$$\begin{cases} \dot{x}_{cl} = \sum_{i=1}^{r}\sum_{j=1}^{r}\eta_i(\theta)\eta_j(\theta)\left(\mathbb{A}_{ij}x_{cl} + \mathbb{B}_{ij}^w w - \left(\mathbb{B}_i^\psi + R_\psi E_i^c\right)\psi(u_c)\right) \\ y = \sum_{i=1}^{r}\eta_i(\theta)\left(\mathbb{C}_i x_{cl} + \mathbb{D}_i w\right) \end{cases} \tag{4.11}$$

where

$$\mathbb{A}_{ij}=\begin{bmatrix} A_i+B_i^u D^c C_j^y & B_i^u C_j^c \\ B_i^c C_j^y & A_{ij}^c \end{bmatrix};\quad \mathbb{B}_{ij}^w=\begin{bmatrix} B_i^w+B_i^u D^c D_j^{yw} \\ B_i^c D_j^{yw} \end{bmatrix}$$
$$\mathbb{B}_i^{\psi}=\begin{bmatrix} B_i^u \\ 0 \end{bmatrix};\quad \mathbb{C}_i=\begin{bmatrix} C_i^y & 0 \end{bmatrix};\quad \mathbb{D}_i=\begin{bmatrix} D_i^{yw} \end{bmatrix};\quad R_{\psi}=\begin{bmatrix} 0 \\ I \end{bmatrix} \tag{4.12}$$

and the controller output is given as:

$$u_c=\sum_{i=1}^{r}\eta_i(\theta)\left(\mathbb{K}_i x_{cl}+K_i^w w\right) \tag{4.13}$$

where $\mathbb{K}_i=\begin{bmatrix} D^c C_i^y & C_i^c \end{bmatrix}$ and $K_i^w=D^c D_i^{yw}$.

Then, using the notations (4.1), the closed-loop system (4.11) is rewritten as:

$$\begin{cases} \dot{x}_{cl}=\mathbb{A}_{\theta\theta}x_{cl}+\mathbb{B}_{\theta\theta}^w w-\left(\mathbb{B}_{\theta}^{\psi}+R_{\psi}E_{\theta}^c\right)\psi(u_c) \\ y=\mathbb{C}_{\theta}x_{cl}+\mathbb{D}_{\theta}w \end{cases} \tag{4.14}$$

And the DOFC output (4.13) is rewritten as:

$$u_c=\mathbb{K}_{\theta}x_{cl}+K_{\theta}^w w \tag{4.15}$$

2.1.2. Lyapunov-based stability and closed-loop performance

Stability and performance specifications of the closed-loop system (4.11) will be presented in terms of Lyapunov analysis tools. Our goal is to propose a systematic method to design a dynamic output feedback controller together with its anti-windup strategy of the form (4.9) such that the closed-loop system satisfies the following properties:

(P.1) *State constraints*: The states of the closed-loop system (4.11) are required to remain in the polyhedral region described by linear inequalities:

$$\mathcal{P}_x=\left\{x_{cl}\in\mathbb{R}^{2n_x}:\quad h_k^T x_{cl}\le 1;\quad \forall k\in\Omega_q\right\} \tag{4.16}$$

where $h_k=\begin{bmatrix} h_1^k & h_2^k \end{bmatrix}\in\mathbb{R}^{2n_x}$. In this study, only plant states are constrained, thus $h_2^k=[0]\in\mathbb{R}^{n_x}$, $\forall k\in\Omega_q$.

(P.2) *Regional quadratic α -stability*: When $w=0$, there exists a positive-definite quadratic function $V(x_{cl})=x_{cl}^T P x_{cl}$, with $P>0$ and a real number $\alpha>0$ such that $\dot{V}(x_{cl})<-2\alpha V(x_{cl})$

along the trajectories of closed-loop system for any initial augmented state in the ellipsoid $\mathcal{E}(P)$. This fact implies that these trajectories of the closed-loop system will converge exponentially to 0 with a decay rate α.

(P.3) *Performance*: For a given positive real number δ, there exists positive real numbers γ, ρ such that, for any energy-bounded signal $w \in W_\delta$ and for all initial states in $\mathcal{E}(P,\rho)$, the trajectories of the closed-loop system will never escape the ellipsoid $\mathcal{E}(P) \supset \mathcal{E}(P,\rho)$. Furthermore, the $\mathcal{L}_2$-norm of the output signal y is bounded:

$$\int_0^\infty y^T y dt < \gamma \int_0^\infty w^T w dt + \rho \tag{4.17}$$

2.2. Preliminaries

In this section, some important preliminaries results needed for design problem in Section 3 will be presented.

2.2.1. Generalized sector bound condition for input saturation

Given the matrices $\mathbb{K}_i \in \mathbb{R}^{n_u \times 2n_x}$ and $\mathbb{G}_i = \begin{bmatrix} G_1^i & G_2^i \end{bmatrix} \in \mathbb{R}^{n_u \times 2n_x}$, with $G_1^i \in \mathbb{R}^{n_u \times n_x}$, $G_2^i \in \mathbb{R}^{n_u \times n_x}$, for $i \in \Omega_r$, we define the polyhedral set $\mathcal{P}_u$ as follows:

$$\mathcal{P}_u = \bigcap_{i=1}^{r} \Xi(\mathbb{K}_i - \mathbb{G}_i) \tag{4.18}$$

where

$$\Xi(\mathbb{K}_i - \mathbb{G}_i) \triangleq \left\{ x_{cl} \in \mathbb{R}^{2n_x} : \ \left| \left(\mathbb{K}_{i(l)} - \mathbb{G}_{i(l)} \right) x_{cl} \right| \le u_{\max(l)}; \quad \forall l \in \Omega_{n_u} \right\}. \tag{4.19}$$

The following lemma is an extended version of Lemma 1 of (Gomes da Silva & Tarbouriech, 2005)

Lemma 4.1. Consider the function $\psi(u_c)$ defined in (4.10) with u_c defined in (4.15). If $x_{cl} \in \mathcal{P}_u \cap \mathcal{P}_x$, then the following condition is verified:

$$\psi^T(u_c) T \left[\psi(u_c) - \begin{bmatrix} \sum_{i=1}^{r} \eta_i G_i & \sum_{i=1}^{r} \eta_i K_i^w \end{bmatrix} \begin{bmatrix} x_{cl} \\ w \end{bmatrix} \right] \le 0 \tag{4.20}$$

where $T \in \mathbb{R}^{n_u \times n_u}$ is any positive diagonal matrix and $\eta_1, \cdots, \eta_r$ are scalar functions satisfying the convex sum propriety.

Proof. Assume that $x_{cl} \in \mathcal{P}_u \bigcap \mathcal{P}_x$, it implies $x_{cl} \in \Xi\left(\sum_{i=1}^{r} \eta_i \left(\mathbb{K}_i - \mathbb{G}_i\right)\right)$ since scalar functions η_i, $\forall i \in \Omega_r$, satisfy the convex sum propriety. Hence, it follows that:

$$-u_{\max(l)} \le \sum_{i=1}^{r} \eta_i \left(\mathbb{K}_{i(l)} - \mathbb{G}_{i(l)}\right) x_{cl} \le u_{\max(l)}, \quad \forall (i,l) \in \Omega_r \times \Omega_{n_u} \tag{4.21}$$

Let $l \in \Omega_{n_u}$ and $T_{(l,l)} > 0$, we will show that the inequality:

$$\psi_l\left(u_c\right) T_{(l,l)} \left[\psi_l\left(u_c\right) - \left[\sum_{i=1}^{r} \eta_i \mathbb{G}_{i(l)} \quad \sum_{i=1}^{r} \eta_i K_{i(l)}^{w}\right] \begin{bmatrix} x_{cl} \\ w \end{bmatrix}\right] \le 0 \tag{4.22}$$

holds (implying then obviously (4.20)). For that, note that there exists only three possible cases according to the value of $u_{c(l)}$:

i. **Case 1**: $-u_{\max(l)} \le u_{c(l)} \le u_{\max(l)}$. It follows that $\psi_l\left(u_c\right) = 0$ and so, inequality (4.22) holds trivially.

ii. **Case 2**: $u_{c(l)} > u_{\max(l)}$. Then,

$$\psi_l\left(u_c\right) = u_{c(l)} - u_{\max(l)} = \sum_{i=1}^{r} \eta_i \left(\mathbb{K}_{i(l)} x_{cl} + K_{i(l)}^{w} w\right) - u_{\max(l)} > 0 \tag{4.23}$$

From (4.21), it follows that $\sum_{i=1}^{r} \eta_i \left(\mathbb{K}_{i(l)} - \mathbb{G}_{i(l)}\right) x_{cl} \le u_{\max(l)}$. Hence,

$$\psi_l\left(u_c\right) - \left[\sum_{i=1}^{r} \eta_i \mathbb{G}_{i(l)} \quad \sum_{i=1}^{r} \eta_i K_{i(l)}^{w}\right] \begin{bmatrix} x_{cl} \\ w \end{bmatrix} = \sum_{i=1}^{r} \eta_i \left(\mathbb{K}_{i(l)} - \mathbb{G}_{i(l)}\right) x_{cl} - u_{\max(l)} \le 0 \tag{4.24}$$

Since in this case $\psi_l\left(u_c\right) > 0$, inequality (4.22) holds.

iii. **Case 3**: $u_{c(l)} < -u_{\max(l)}$. It follows that:

$$\psi_l\left(u_c\right) = u_{c(l)} + u_{\max(l)} = \sum_{i=1}^{r} \eta_i \left(\mathbb{K}_{i(l)} x_{cl} + K_{i(l)}^{w} w\right) + u_{\max(l)} < 0 \tag{4.25}$$

Then, from (4.21) it follows that $\sum_{i=1}^{r}\eta_i\left(\mathbb{K}_{i(l)}-\mathbb{G}_{i(l)}\right)x_{cl}\geq -u_{\max(l)}$, and then:

$$\psi_l(u_c)-\left[\sum_{i=1}^{r}\eta_i\mathbb{G}_{i(l)}\quad\sum_{i=1}^{r}\eta_i K^{w}_{i(l)}\right]\begin{bmatrix}x_{cl}\\ w\end{bmatrix}=\sum_{i=1}^{r}\eta_i\left(\mathbb{K}_{i(l)}-\mathbb{G}_{i(l)}\right)x_{cl}+u_{\max(l)}\geq 0 \tag{4.26}$$

Since in this case $\psi\left(y_{c(l)}\right)<0$, inequality (4.22) holds again.

♦

2.2.2. Other preliminary results

Some other results that will be useful in the proof of our main result are recalled below.

Lemma 4.2. (Boyd et al., 1994) The ellipsoid $\mathcal{E}(P)$ is contained in the polyhedral set $\mathcal{P}_u$ defined in (4.18) if and only if:

$$\left(\mathbb{K}_{i(l)}-\mathbb{G}_{i(l)}\right)(P)^{-1}\left(\mathbb{K}_{i(l)}-\mathbb{G}_{i(l)}\right)^{T}\leq u^2_{\max(l)};\quad\forall(i,l)\in\Omega_r\times\Omega_{n_u} \tag{4.27}$$

where $\mathbb{K}_{i(l)}$, $\mathbb{G}_{i(l)}$ are respectively the l^{th} rows of the matrices $\mathbb{K}_i$ and $\mathbb{G}_i$.

♦

Lemma 4.3. (Boyd et al., 1994) The ellipsoid $\mathcal{E}(P)$ is included in the polyhedral region $\mathcal{P}_x$ defined in (4.16) if and only if:

$$\begin{bmatrix}P & h_k\\ h_k^T & 1\end{bmatrix}\geq 0;\quad\forall k\in\Omega_p \tag{4.28}$$

♦

3. Main Results

The theorem below provides LMI conditions to design the DOFC together with its anti-windup strategy of the form (4.9) which solves the control problem defined in Subsection 2.1.2.

Theorem 4.1. Given positive real numbers α and δ, assume there exists positive definite matrices $P_{11} \in \mathbb{R}^{n_x \times n_x}$, $X_{11} \in \mathbb{R}^{n_x \times n_x}$, positive diagonal matrix $S \in \mathbb{R}^{n_u \times n_u}$, matrices $Q_{ij} \in \mathbb{R}^{(2n_x+n_u+n_y+n_w)\times(2n_x+n_u+n_y+n_w)}$, $W_i \in \mathbb{R}^{n_x \times n_u}$, $U_i \in \mathbb{R}^{n_u \times n_x}$, $V_i \in \mathbb{R}^{n_u \times n_x}$, $\hat{\mathcal{A}}_{ij} \in \mathbb{R}^{n_x \times n_x}$, $\hat{\mathcal{B}}_i \in \mathbb{R}^{n_x \times n_y}$, $\hat{\mathcal{C}}_i \in \mathbb{R}^{n_u \times n_x}$ and $\hat{\mathcal{D}} \in \mathbb{R}^{n_u \times n_y}$ for $(i,j) \in \Omega_r \times \Omega_r$, and positive real numbers γ, ρ such that:

$$\begin{bmatrix} X_{11} & I \\ I & P_{11} \end{bmatrix} > 0; \tag{4.29}$$

$$\begin{bmatrix} X_{11} & I & X_{11}h_1^k \\ * & P_{11} & h_1^k \\ * & * & 1 \end{bmatrix} \geq 0; \qquad \forall k \in \Omega_p \tag{4.30}$$

$$\begin{bmatrix} X_{11} & * & * \\ I & P_{11} & * \\ \hat{\mathcal{C}}_{i(l)} - U_{i(l)} & \left(\hat{\mathcal{D}}C_y^i\right)_{(l)} - V_{i(l)} & u_{\max(l)}^2 \end{bmatrix} \geq 0; \qquad \forall (i,l) \in \Omega_r \times \Omega_{n_u} \tag{4.31}$$

$$(1-\rho) - \gamma\delta \geq 0; \tag{4.32}$$

and the conditions (2.29) hold with

$$\Upsilon_{ij} \triangleq \begin{bmatrix} sym\left(\mathbb{H}_{ij}\right) & \mathbb{J}_{ij} & U_i^T - B_i^u S & \mathbb{L}_{ij} & X_{11}\left(C_i^y\right)^T \\ * & sym\left(\mathbb{M}_{ij}\right) & V_i^T - W_i & \mathbb{N}_{ij} & \left(C_i^y\right)^T \\ * & * & -2S & \hat{\mathcal{D}}D_i^{yw} & 0 \\ * & * & * & \left(D_i^{yw}\right)^T\left(D_i^{yw}\right) - \gamma I & 0 \\ * & * & * & * & -I \end{bmatrix} \tag{4.33}$$

and

$$\begin{aligned}
&\mathbb{H}_{ij} \triangleq A_i X_{11} + B_i^u \hat{\mathcal{C}}_j + \alpha X_{11}; \quad \mathbb{J}_{ij} \triangleq \hat{\mathcal{A}}_{ij}^T + A_i + B_i^u \hat{\mathcal{D}} C_j^y + 2\alpha I; \quad \mathbb{M}_{ij} \triangleq P_{11} A_i + \hat{\mathcal{B}}_i C_y^j + \alpha P_{11} \\
&\mathbb{L}_{ij} \triangleq B_i^u \hat{\mathcal{D}} D_j^{yw} + B_i^w + X_{11} \left(C_i^y \right)^T D_i^{yw}; \quad \mathbb{N}_{ij} \triangleq P_{11} B_i^w + \hat{\mathcal{B}}_i D_j^{yw} + \left(C_i^y \right)^T D_i^{yw}.
\end{aligned} \tag{4.34}$$

Let P_{12} and X_{12} be two matrices satisfying the condition

$$P_{11} X_{11} + P_{12} X_{12}^T = I \tag{4.35}$$

Then, the DOFC together with its anti-windup compensation (4.9) given by:

$$\begin{aligned}
E_i^c &= P_{12}^{-1} W_i S^{-1} - P_{12}^{-1} P_{11} B_i^u \\
D^c &= \hat{\mathcal{D}} \\
C_i^c &= \left(\hat{\mathcal{C}}_i - D^c C_i^y X_{11} \right) X_{12}^{-T} \\
B_i^c &= P_{12}^{-1} \left(\hat{\mathcal{B}}_i - P_{11} B_i^u D^c \right) \\
A_{ij}^c &= P_{12}^{-1} \left(\hat{\mathcal{A}}_{ij} - P_{11} \left(A_i + B_i^u D^c C_j^y \right) X_{11} - P_{12} B_i^c C_j^y X_{11} - P_{11} B_i^u C_j^c X_{12}^T \right) X_{12}^{-T}, \quad \forall (i,j) \in \Omega_r \times \Omega_r
\end{aligned} \tag{4.36}$$

solves the control problem stated in Subsection 2.1.2.

Proof. We use the linearizing approach of (Scherer et al., 1997): properties (4.29) and (4.35) imply the existence of two matrices P_{22} and X_{22} such that the block matrices P and X given by:

$$P = \begin{bmatrix} P_{11} & P_{12} \\ P_{12}^T & P_{22} \end{bmatrix}; \qquad X = \begin{bmatrix} X_{11} & X_{12} \\ X_{12}^T & X_{22} \end{bmatrix} \tag{4.37}$$

are such that $P > 0$ and $X = P^{-1}$. Note also that the same properties imply that the matrices P_{12} and X_{12} are regular.

Let us introduce the matrices:

$$\Pi_1 \triangleq \begin{bmatrix} X_{11} & I \\ X_{12}^T & 0 \end{bmatrix}; \qquad \Pi_2 \triangleq P\Pi_1 = \begin{bmatrix} I & P_{11} \\ 0 & P_{12}^T \end{bmatrix} \tag{4.38}$$

By congruence transformation with $diag\left(\Pi_1, I\right)$, inequality (4.28) is shown to be equivalent to (4.30). This implies that the ellipsoid $\mathcal{E}(P)$ is included in the polyhedral set $\mathcal{P}_x$ defined in (4.16). This fact proves the property (P.1).

Similarly, by Schur complement lemma and congruence transformation with $diag\left(\Pi_1, I\right)$, inequality (4.31) is shown to be equivalent to (4.27), so that the ellipsoid $\mathcal{E}(P)$ is included in the polyhedral set $\mathcal{P}_u$ defined in (4.18) with $G_1^i \triangleq V_i$ and $G_2^i \triangleq U_i X_{12}^{-T} - G_1^i X_{11} X_{12}^{-T}$.

Let $T \triangleq S^{-1}$. By Lemma 2.8, inequalities (2.29) imply that $\Upsilon_{\theta\theta} \triangleq \sum_{i=1}^{r}\sum_{j=1}^{r} \eta_i(\theta)\eta_j(\theta)\Upsilon_{ij} < 0$. After a congruence transformation with $diag\left(\Pi_1, S, I, I\right)$, this inequality is proved to be equivalent to:

$$\begin{bmatrix} \mathbb{A}_{\theta\theta}^T P + P\mathbb{A}_{\theta\theta} + 2\alpha P & \mathbb{G}_\theta^T T - P\left(\mathbb{B}_\theta^\psi + R_\psi E_\theta^c\right) & P\mathbb{B}_{\theta\theta}^w + \mathbb{C}_\theta^T \mathbb{D}_\theta & \mathbb{C}_\theta^T \\ * & -2T & TK_\theta^w & 0 \\ * & * & \mathbb{D}_\theta^T \mathbb{D}_\theta - \gamma I & 0 \\ * & * & * & -I \end{bmatrix} < 0 \tag{4.39}$$

which, by Schur complement lemma, is equivalent to:

$$\begin{bmatrix} sym\left(P\mathbb{A}_{\theta\theta} + \alpha P\right) + \mathbb{C}_\theta^T \mathbb{C}_\theta & \mathbb{G}_\theta^T T - P\left(\mathbb{B}_\theta^\psi + R_\psi E_\theta^c\right) & P\mathbb{B}_{\theta\theta}^w + \mathbb{C}_\theta^T \mathbb{D}_\theta \\ * & -2T & TK_\theta^w \\ * & * & \mathbb{D}_\theta^T \mathbb{D}_\theta - \gamma I \end{bmatrix} < 0. \tag{4.40}$$

Pre- and post-multiplying (4.40) by $\begin{bmatrix} x_{cl}^T & w^T & \psi^T(u_c) \end{bmatrix}$ and its transpose, the following condition can be obtained after some algebraic manipulations:

$$\dot{V}(x_{cl}) + 2\alpha V(x_{cl}) + y^T y - \gamma w^T w - 2\psi^T(u_c) T\left[\psi(u_c) - \begin{bmatrix} \mathbb{G}_\theta & K_\theta^w \end{bmatrix}\begin{bmatrix} x_{cl} \\ w \end{bmatrix}\right] < 0 \tag{4.41}$$

Furthermore, since $\mathcal{E}(P) \subset \mathcal{P}_u \bigcap \mathcal{P}_x$, by Lemma 4.1, the condition (4.41) implies that:

$$\dot{V}(x_{cl}) + 2\alpha V(x_{cl}) + y^T y - \gamma w^T w < 0 \tag{4.42}$$

- [Property (P.2)] Assume $w = 0,\ \forall t \geq 0$, it follows from (4.42) that:

  $$\dot{V}(x_{cl}) < -2\alpha V(x_{cl}) \tag{4.43}$$

  This inequality implies that the set $\mathcal{E}(P)$ is positively invariant for the closed-loop system, and that, for any initial state in this set, the trajectory will converge exponentially to 0 with a decay rate α.

- [Property (P.2)] Assume now that $w \in W_\delta$, integrating both sides of (4.42) from 0 to T_f, where $T_f > 0$, it follows that:

$$V\left(x_{cl}\left(T_f\right)\right) - V\left(x_{cl}\left(0\right)\right) + 2\alpha\int_0^{T_f} V\left(x_{cl}\right)dt - \gamma\int_0^{T_f} w^T w dt + \int_0^{T_f} y^T y dt < 0 \qquad (4.44)$$

From (4.32) and (4.44), it can be deduced that, for any initial state in $\mathcal{E}(P,\rho)$, $V\left(x_{cl}\left(T_f\right)\right) < \rho + \gamma\delta \le 1$. This means that the corresponding closed-loop trajectories are confined in the set $\mathcal{E}(P) \subset \mathcal{P}_x$.

- [Property (P.3)] Considering the limit case $T_f \to \infty$ in (4.44), we obtain $\int_0^\infty y^T y dt < \gamma\int_0^\infty w^T w dt + V\left(x(0)\right)$, this means that the $\mathcal{L}_2$-norm of the output signal y is upper bounded by $\|y\|_2^2 < \gamma\|w\|_2^2 + \rho$.

♦

Remark 4.1. When $x_{cl}(0) \neq 0$, there is a tradeoff between the size of the set of initial conditions and the maximal level energy of disturbances characterized by δ. Indeed, the lower is the admissible δ (i.e. the lower is the admissible energy of the disturbance signal), the larger is the set of initial conditions $\mathcal{E}(P,\rho)$, and by extension, the closed-loop estimate domain of attraction $\mathcal{E}(P)$ (Castelan et al., 2006).

4. Anti-Windup Based DOFC Design

This section aims at showing how to derive an anti-windup based DOFC from the result of Theorem 4.1. This DOFC will guarantee the local stability and some performance index of the closed-loop system. The design method can be formulated as a multi-objective convex optimization problem. Two objectives are considered: maximization of the disturbance rejection and the estimate domain of attraction.

Reminding that Theorem 4.1 provides conditions to find positive matrices P_{11}, X_{11}, positive diagonal matrix S, matrices W_i, U_i, V_i, $\hat{\mathcal{A}}_{ij}$, $\hat{\mathcal{B}}_i$, $\hat{\mathcal{C}}_i$ and $\hat{\mathcal{D}}$ for $\forall(i,j) \in \Omega_r \times \Omega_r$, and positive real numbers γ, ρ such that the estimate closed-loop domain of attraction $\mathcal{E}(P)$ is positively invariant. In this case, we have a feasibility problem (Gahinet et al., 1995). For safety issue, the estimate closed-loop domain of attraction should be maximized. To this end, we adopt the idea of shape reference set in

(Boyd et al., 1994). Let $X_R \subset \mathbb{R}^{2n_x}$ be a prescribed bounded convex set containing the origin. Finding the largest ellipsoid $\mathcal{E}(P)$ can be formulated as the following optimization problem:

$$\begin{aligned} &\max_{\tau, P>0} \quad \tau \\ &s.t.\ \tau X_R \subset \mathcal{E}(P) \end{aligned} \tag{4.45}$$

It is worth noting that X_R defines the directions in which we want to maximize $\mathcal{E}(P)$. There are two typical choices for reference set X_R:

- Ellipsoid set defined as:

  $$X_R = \left\{ x_{cl} \in \mathbb{R}^{2n_x} : x_{cl}^T R x_{cl} \le 1 \right\} \tag{4.46}$$

  where $R = R^T > 0$.

- The second one is a *polyhedron* defined as:

  $$X_R = co\left\{ x_0^1, x_0^2, \ldots, x_0^p \right\} \tag{4.47}$$

  where $x_0^1, x_0^2, \ldots, x_0^p$ are a priori given points in $\mathbb{R}^{2n_x}$.

For these two choices of set X_R, problem (4.45) can be expressed as LMI optimization problem (Boyd et al., 1994):

- If the reference shape X_R is given by the ellipsoid (4.46), then $\tau X_R \subset \mathcal{E}(P)$ is equivalent to the condition:

  $$\frac{R}{\tau^2} \ge P \tag{4.48}$$

  Since $X = P^{-1}$, by Schur complement lemma, condition (4.48) is equivalent to, with $\mu = 1/\tau^2$:

  $$\begin{bmatrix} \mu R & I \\ I & X \end{bmatrix} \ge 0 \tag{4.49}$$

  Note that maximization τ amounts to minimize μ. Pre- and post-multiplying condition (4.49) by $diag\left(I, \Pi_2^T\right)$ and its transpose, the condition (4.49) is equivalent to:

$$\left[\begin{array}{c|cc} \mu R & I & P_{11} \\ & 0 & P_{12}^T \\ \hline * & X_{11} & I \\ & I & P_{11} \end{array}\right] \geq 0 \tag{4.50}$$

- Now, if X_R is the polyhedron (4.47), then $\tau X_R \subset \mathcal{E}(P)$ is equivalent to:

$$\tau^2 \left(x_0^i\right)^T (P) x_0^i \leq 1, \quad \forall i \in \Omega_p \tag{4.51}$$

This inequality can also be reformulated in LMI form as:

$$\left[\begin{array}{cc} \mu & \left(x_0^i\right)^T \\ x_0^i & X \end{array}\right] \geq 0, \quad \forall i \in \Omega_p \tag{4.52}$$

As previous case, the condition (4.52) is equivalent to:

$$\left[\begin{array}{c|cc} \mu & \left(x_0^i\right)^T \Pi_2 \\ \hline * & X_{11} & I \\ & I & P_{11} \end{array}\right] \geq 0, \quad \forall i \in \Omega_p \tag{4.53}$$

Based on the result of Theorem 4.1, the following multi-objective convex optimization problem solves the control design problem stated in Subsection 2.1.2 while maximizing the closed-loop domain of attraction of system (4.11) and the admissible set of system state initial conditions:

$$\min_{P_{11}, X_{11}, S, U_i, V_i, W_i, \hat{A}_{ij}, \hat{B}_i, \hat{C}_i, \hat{D}, \gamma, \rho, \mu} \quad \lambda_1 \gamma + \lambda_2 \mu - \lambda_3 \rho \tag{4.54}$$

such that the following LMI conditions hold:

- $\gamma > 0$, $\rho > 0$, $\mu > 0$
- LMIs (2.29) with Υ_{ij} defined in (4.33)
- LMIs (4.29)-(4.32)
- LMI (4.50) (or LMI (4.53))

where positive weighting factors λ_1, λ_2, λ_3 are chosen according to desired trade-off between controller performance (characterized by γ) and the size of the set of admissible system state initial

conditions $\mathcal{E}(P,\rho)$ (characterized by ρ) and the estimate domain of attraction $\mathcal{E}(P)$ of the closed-loop system (characterized by μ).

♦

Remark 4.2. It is noticed that the choice of matrices P_{12}, X_{12} is irrelevant for control design. It corresponds to a change of coordinates of the controller states (El Ghaoui & Scorletti, 1996). However, they should be nonsingular for matrix inversion property. Without loss of generality, we will choose $P_{12} = I$ for (4.36) and (4.50) (or (4.53)). Then X_{12} is deduced from the condition $P_{11}X_{11} + P_{12}X_{12}^T = I$. Now, the DOFC with its anti-windup compensation of the form (4.9) can be computed by (4.36).

Remark 4.3. Note that the condition $X > 0$ is equivalent to $P_{11} > X_{11}^{-1}$. Consequently, the estimate set of initial conditions of the system states $\mathcal{E}(P_{11},\rho)$ is always contained in the ellipsoid $\mathcal{E}(X_{11}^{-1},\rho)$. If we suppose that $x_c(0) = 0$, then $x_{cl}(0)$ always belongs to $\mathcal{E}(P,\rho)$ if $x(0) \in \mathcal{E}(P_{11},\rho)$. In the absence of disturbances (or if the disturbances are vanishing), since the set $\mathcal{E}(P)$ is positively invariant, it follows that $x_{cl}(t) \in \mathcal{E}(P)$ for $\forall t \geq 0$. Therefore, $x(t)$ will never escape the projection of $\mathcal{E}(P)$ onto the plane defined by $x_c = 0$. This projection is nothing but the ellipsoid $\mathcal{E}(X_{11}^{-1})$.

5. Illustrative Example

5.1. System Description

In this section, the effectiveness of the proposed design method is performed via the following nonlinear mass-spring-damper mechanical system:

$$\begin{cases} \dot{x}_1 = -x_1 - (1 + 0.05x_2^2)x_2 + (0.5 + 0.075x_2^3)u + 0.1w \\ \dot{x}_2 = x_1 + 0.1w \\ y = x_2 \end{cases} \tag{4.55}$$

where x_1, x_2 and w are respectively the velocity, the position and the system disturbance.

The following assumptions are considered for this example:

- The state vector $x \triangleq \begin{bmatrix} x_1 & x_2 \end{bmatrix}^T$ always remains in the validity domain described by $\mathcal{P}_x = \left\{ (x_1, x_2) \in \mathbb{R}^2 : \ |x_1| \le 1.5; \ |x_2| \le 1.5 \right\}$.
- The control saturation limit is: $u_{\max} = 0.5$.
- Only the position is measured as system output.

Since $x \in \mathcal{P}_x$, two nonlinearities $f(x_2) = 1 + 0.05x_2^2$ and $g(x_2) = 0.5 + 0.075x_2^3$ of system (4.55) are then bounded:

$$\begin{cases} f_{\min} \le f(\cdot) \le f_{\max} \\ g_{\min} \le g(\cdot) \le g_{\max} \end{cases}; \qquad \begin{cases} f(\cdot) = \omega_1 f_{\min} + \omega_2 f_{\max} \\ g(\cdot) = \omega_3 g_{\min} + \omega_4 g_{\max} \end{cases} \tag{4.56}$$

The normalized nonlinear functions of T-S model are given by:

$$\eta_1 = \omega_1\omega_3; \quad \eta_2 = \omega_1\omega_4; \quad \eta_3 = \omega_2\omega_3; \quad \eta_4 = \omega_2\omega_4 \tag{4.57}$$

where

$$\omega_1 = \frac{f_{\max} - f(\cdot)}{f_{\max} - f_{\min}}; \qquad \omega_2 = 1 - \omega_1; \quad \omega_3 = \frac{g_{\max} - g(\cdot)}{g_{\max} - g_{\min}}; \qquad \omega_4 = 1 - \omega_3 \tag{4.58}$$

Then, the nonlinear system (4.55) can be exactly represented by the following T-S model in the polyhedral set $\mathcal{P}_x$:

$$\begin{cases} \dot{x} = \sum_{i=1}^{4} \eta_i(\theta) \left(A_i x + B_i^u u + B_i^w w \right) \\ y = \sum_{i=1}^{4} \eta_i(\theta) \left(C_i^y x + D_i^{yw} w \right) \end{cases} \tag{4.59}$$

where the subsystem matrices are given by, $\forall i \in \Omega_4$:

$$\begin{aligned} A_1 &= \begin{bmatrix} -1 & -f_{\min} \\ 1 & 0 \end{bmatrix}; \quad B_1^u = \begin{bmatrix} g_{\min} \\ 0 \end{bmatrix}; \quad A_2 = \begin{bmatrix} -1 & -f_{\min} \\ 1 & 0 \end{bmatrix}; \quad B_2^u = \begin{bmatrix} g_{\max} \\ 0 \end{bmatrix}; \quad B_i^w = \begin{bmatrix} 0.1 \\ 0.1 \end{bmatrix} \\ A_3 &= \begin{bmatrix} -1 & -f_{\max} \\ 1 & 0 \end{bmatrix}; \quad B_3^u = \begin{bmatrix} g_{\min} \\ 0 \end{bmatrix}; \quad A_4 = \begin{bmatrix} -1 & -f_{\max} \\ 1 & 0 \end{bmatrix}; \quad B_4^u = \begin{bmatrix} g_{\max} \\ 0 \end{bmatrix}; \quad D_i^{yw} = 1 \end{aligned} \tag{4.60}$$

5.2. *Some Illustrative Results*

In what follows, it will be shown that the DOFC derived from convex optimization problem (4.54) satisfies the all three predefined properties stated in Subsection 2.1.2. To that end, let us take the decay rate $\alpha = 0.01$, the reference shape $X_R = \mathcal{E}(R)$ with $R = diag(1,2,3,4)$, the weighting factors $\lambda_1 = 0$, $\lambda_2 = \lambda_3 = 1$ and the energy-bounded disturbance is defined as, with $\delta \approx 0.08$:

$$w(t) = \begin{cases} 0.1\sin(t) & \text{if} \quad 0 \le t \le 15 \\ 0 & \text{if} \quad t \ge 15 \end{cases} \tag{4.61}$$

5.2.1. *Regional quadratic α-stability*

In the absence of disturbances, i.e. $w(t) = 0$, it can be observed in Figure 4.2 that the projection of $\mathcal{E}(P)$ onto the plane defined by $x_c = 0$, that is $S_1 \triangleq \mathcal{E}(X_{11}^{-1})$, is an invariant set (corresponding to system states) of the closed-loop system, i.e. all system trajectories initialized in this set will never escape it. This set includes, of course, the set of admissible initial conditions projected into x_1 and x_2, namely $S_2 \triangleq \mathcal{E}(P_{11}, \rho)$. Furthermore, as can be seen also, the ellipsoid S_1 is maximized along the direction of the polyhedral set $S_3 \triangleq \mathcal{P}_u \cap \mathcal{P}_x$ which is, in turn, contained in the $S_4 \triangleq \Xi\left(\sum_{i=1}^{r} \eta_i (\mathbb{K}_i - \mathbb{G}_i)\right)$. Finally, all trajectories converge to the origin.

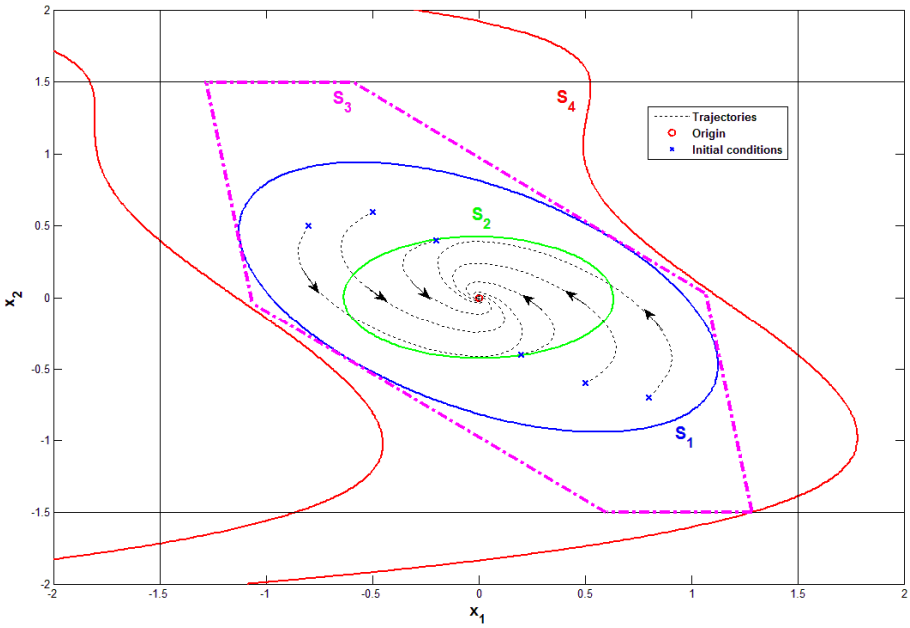

Figure 4.2. Projection of $\mathcal{E}(P)$ onto the plane defined by $x_c = 0$ and system trajectories

5.2.2. *Closed-loop finite $\mathcal{L}_2$-gain performance*

Now, with the presence of the disturbance defined in (4.61), Figure 4.3 shows that this energy-bounded disturbance is well attenuated (top) and the ratio $\int_0^{T_f} y^T y dt \Big/ \left(\gamma \int_0^{T_f} w^T w dt + \rho\right)$, with $T_f > 0$, is always bounded by 1 (bottom).

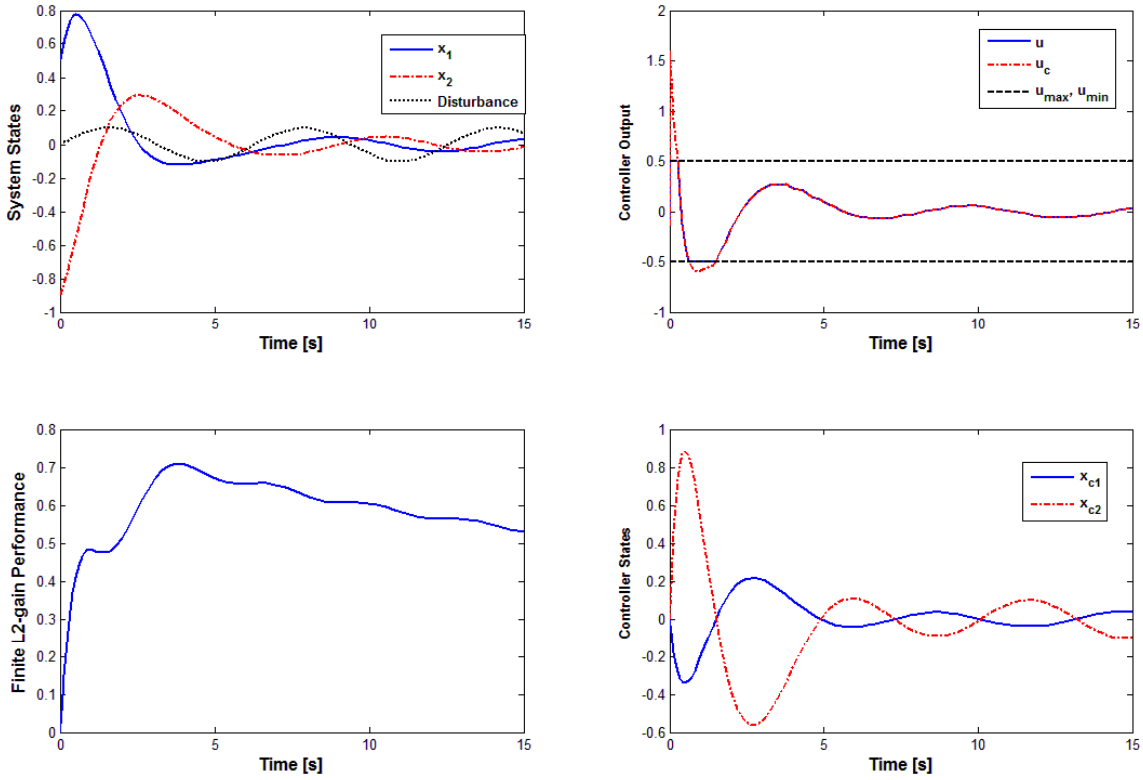

Figure 4.3. Disturbance attenuation and closed-loop $\mathcal{L}_2$-gain performance (left); corresponding control signal response and evolution of the controller state of the DOFC (right)

Note that in this case, the classical DOFC (without anti-windup nor $\mathcal{L}_2$-gain performance) is no longer effective, see Figure 4.4.

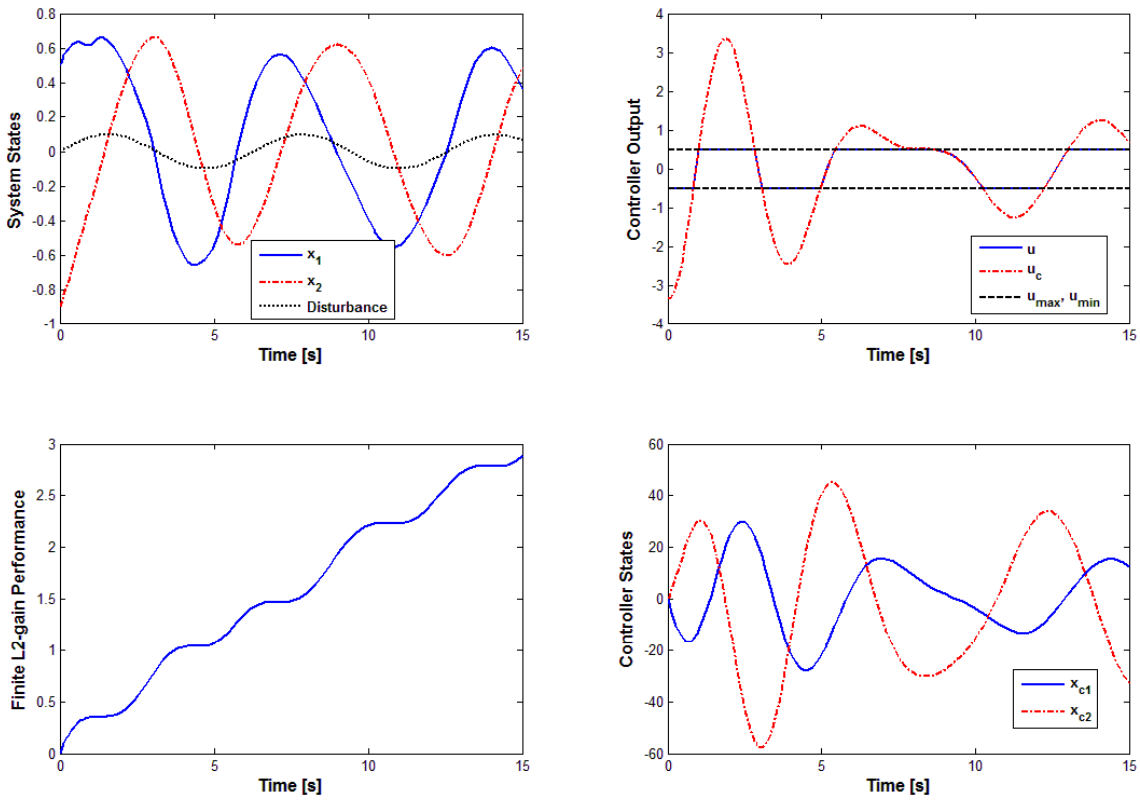

Figure 4.4. Closed-loop state responses (top); control input signal (middle) and evolution of the controller states (bottom) with classical DOFC (Li et al., 2000)

5.2.3. System state constraints

To illustrate this closed-loop property, let us take the limit cases where the initial conditions are four vertex of the polytope of admissible system states, that are $(-1.5,-1.5)$; $(-1.5,1.5)$; $(1.5,-1.5)$ and $(1.5,1.5)$. As shown in Figure 4.5, all corresponding trajectories are enforced to stay inside this polytope even the presence of disturbance signal.

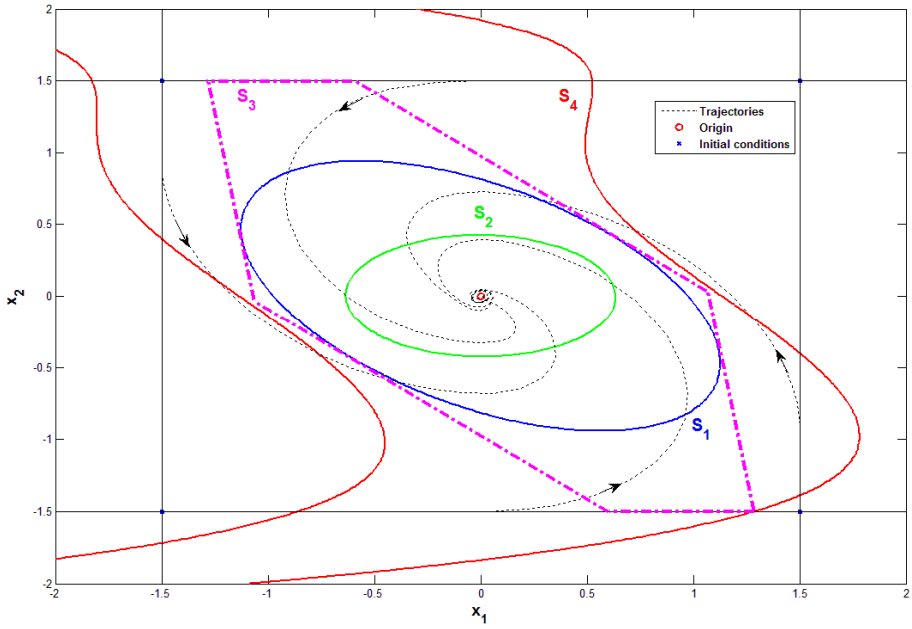

Figure 4.5. Closed-loop state constraint property

6. Concluding Remarks

A novel approach to design a dynamic output feedback controller together with anti-windup strategy for continuous-time nonlinear systems in T-S form has been proposed. In this approach, the disturbed systems are subject to control input and system state constraints. Based on Lyapunov stability theory, a constructive procedure is given to design simultaneously the dynamic output feedback controller and its anti-windup compensator. The control design is formulated as multi-objective LMI optimization problem. In this way, the controller and anti-windup compensator gains can be efficiently computed with some numerical tools. As illustrated via an example, the resulting controller satisfies several closed-loop properties.

The derived conditions may be conservative since the Lyapunov function is common for all control objectives. However, these conditions are relatively simple. The problem of reducing their conservatism is currently under study. This novel LMI design method is in our knowledge one of the first results concerning anti-windup based controller in the T-S control framework. This method may be applied to a wide class of nonlinear disturbed systems.

"Research is to see what everybody else has seen, and to think what nobody else has thought."

Albert Szent-Gyorgyi, Hungarian physiologist

PART II. NOVEL CONTROL APPROACHES FOR TURBOCHARGED AIR SYSTEM OF A SI ENGINE

Presentation of Part II

Nowadays, modern automotive engines have to meet several challenges which are often conflicting. On the one hand, the emissions legislations imposed by governments at the international level are becoming more and more stringent because of environmental concerns. On the other hand, customers' demands in terms of performance and efficiency are also increasingly severe. All of these objectives must be delivered at low cost and high reliability for series vehicles. The downsizing (reduction in engine displacement) is a very promising solution to achieve these objectives. Indeed, combining turbocharging with downsizing has now become a key technology to improve engine performance as fuel economy, pumping loss reduction to increase engine efficiency or drivability optimization in the automotive industry. The technology potential is fully exploited only with an efficient air path management system. In this context, Part II proposes two novel approaches to control the air system of a turbocharged SI engine.

The purpose of Chapter 5 is to show how to control the turbocharged air system of a SI engine applying the theoretical results in Chapter 3. A quick tour on SI engines and on modeling of a turbocharged air system is given. Then, we propose to consider the complex model of a turbocharged air system as a switching system in order to simplify the control model and, at the same time, take into account the strategy to minimize energy pumping losses. Compared to existing results, the proposed method facilitates the analysis and the tuning tasks over the whole operating range of the turbocharged air system with very satisfying closed-loop performance.

Chapter 6 addresses the second control approach, which is based on feedback linearization, for turbocharged air system. To this end, a new robust control design is first proposed to deal with model

uncertainties/perturbations. The controller gain is easily obtained by solving a convex optimization problem. Then, two strategies for turbocharged air system are presented: drivability optimization strategy and fuel-optimal strategy. The simplicity and the effectiveness of both strategies clearly point out that the approach proposed in this chapter is in particular relevant for industrial context. Moreover, through this real-world application, we would like to stress that the robust feedback linearization could be a very powerful nonlinear design tool for industrial applications.

The work in Chapter 6 is our first results carried out in collaboration with Prof. Michio Sugeno, Emeritus Researcher from European Centre for Soft Computing, Spain. We gratefully acknowledge the valuable supports of Prof. Marie-Thierry Guerra, Director of LAMIH.

Chapter 5. Multi-Objective Design for Turbocharged Air System: a Switching Takagi-Sugeno Control Approach

1. Introduction

This chapter deals with the nonlinear modeling of the air system of a turbocharged spark ignition (TCSI) engine and proposes a novel robust H_∞ switching controller for this complex system. The design of this robust controller is directly based on the theoretical results concerning the switching T-S model presented in Chapter 3. The proposed switching controller handles easily the high nonlinearities and facilitates considerably the global stability analysis of the whole turbocharged air system. Moreover, this approach can be generalized for more complex turbocharging structures with some small adaptations.

The chapter is organized as follows. Section 2 introduces some particularities of SI engines and the technology, called *downsizing*. In Section 3, the highlights of modeling of a turbocharged air system of a SI engine are given, some control issues and a state-of-the-art concerning this systems are also presented. Section 4 is devoted to the design of a switching robust T-S controller for this complex system. A series of tests and their analysis are performed in Section 5 to point out the effectiveness of the proposed method. Finally, a summary is drawn in Section 6.

2. Background on SI Engines

In the literature, automotive engines can be classified into two main categories: compression ignition (Diesel) engines and spark ignition (gasoline) engines. The main difference between the two is the way in which the air to fuel mixture is ignited, and the design of the chamber which leads to certain power and efficiency characteristics (Heywood, 1988). Only SI engines will be studied here.

2.1. SI Engine Particularities

The general structure of a classical SI engine is depicted in Figure 5.6. The overall engine system can be divided into three main subsystems:

- The *air path* (air system) determines the mass and composition of the gas in the cylinder before the combustion. The control of this subsystem is fundamental for SI engines because it affects directly on the combustion outputs: torque production, engine efficiency and pollutant emissions (Moulin, 2010).
- The *fuel path* aims at providing, by means of injectors, an appropriate amount of fuel for the cylinder during each stroke. The control of this subsystem is important to reduce the SI engine pollutant emissions.
- The *ignition path* whose goal is to initiate, via electrical spark plug, the combustion at an appropriate timing. The spark angle control is crucial to avoid the knock phenomenon and at the same time it can help to improve the fuel economy as well (Guzzella & Onder, 2004).

In this manuscript, we only focus on the control of SI air system. So, this subsystem is described in details. More information on the two other parts can be found in (Heywood, 1988; Guzzella & Onder, 2004).

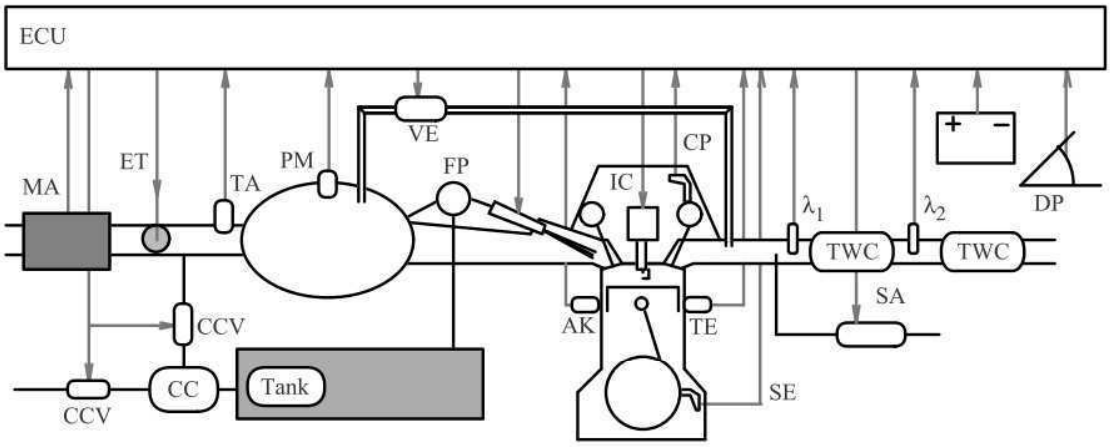

AK	knock sensor	PM	manifold pressure sensor	VE	EGR valve
CP	camshaft sensor	ET	electronic throttle	SA	secondary air valve
IC	ignition command	TA	intake air temperature sensor	TWC	3-way catalyst
MA	air mass-flow sensor	TE	cooling water temperature sensor	ECU	controller
SE	engine speed sensor	CC	active carbon canister	CCV	CC control valves
FP	fuel pressure control	$\lambda_{1,2}$	air/fuel ratio sensors	DP	driver pedal

Figure 5.6. Overview of a typical SI engine system structure (Guzzella & Onder, 2004)

The main objective of an internal combustion engine is to produce some mechanical torque from a chemical energy. Indeed, the engine torque is a result of the expansion of high temperature and pressure gases produced by the combustion of air/fuel mixture in the cylinders. In the case of SI engine, the air/fuel mixture is correctly ignited by an electrical spark plug. An important particularity of SI engine lies in its operation conditions. Actually, SI engines are usually equipped with three-way catalytic converter (TWC) system to reduce pollutant emissions (mainly hydrocarbon (HC), carbon monoxide (CO), and nitrogen oxide (NO_x)) and meet emissions standards. The stationary conversion efficiency of TWC device is depicted in Figure 5.7. It can be observed that pollutant emissions are effectively reduced only when the normalized air/fuel ratio, defined in (5.1), must be kept within this narrow approximately constant at a level determined by the stoichiometry ($\lambda \approx 1$).

$$\lambda = \frac{m_{air}}{m_{fuel}} \lambda_s \tag{5.1}$$

where λ_s is air/fuel stoichiometric ratio.

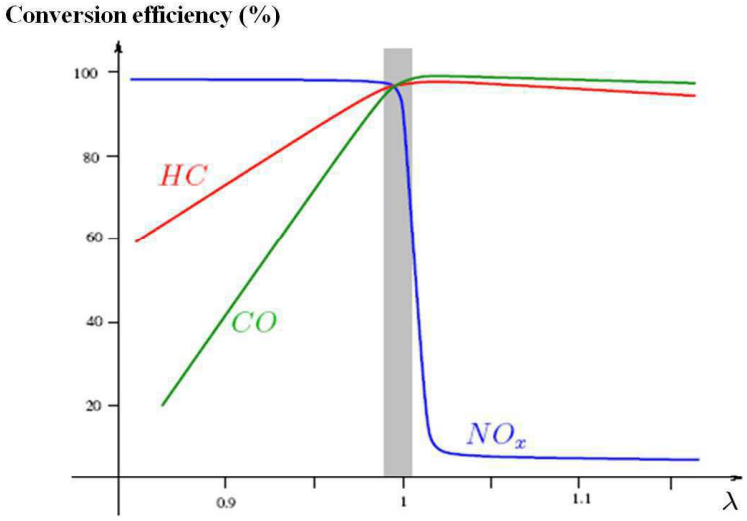

Figure 5.7. Conversion efficiency of a three-way catalytic converter

Due to the stoichiometric operation conditions of SI engines, the produced torque can be directly controlled by the quantity of air/fuel mixture aspirated in the cylinders. Typically, two types of actuator are available for air/fuel ratio control. First, the throttle actuator, located in the upstream of intake manifold, controls the density of the air flow by changing the intake pressure. Second, the injectors, located in the inlet ports or in the chamber for direct injection engines, control the amount of injected fuel. It is worth noting that the dynamics of the injection process is much faster than the

cylinder filling one. Therefore, the engine torque dynamics depends on the dynamics of mass air flow aspirated in the cylinders.

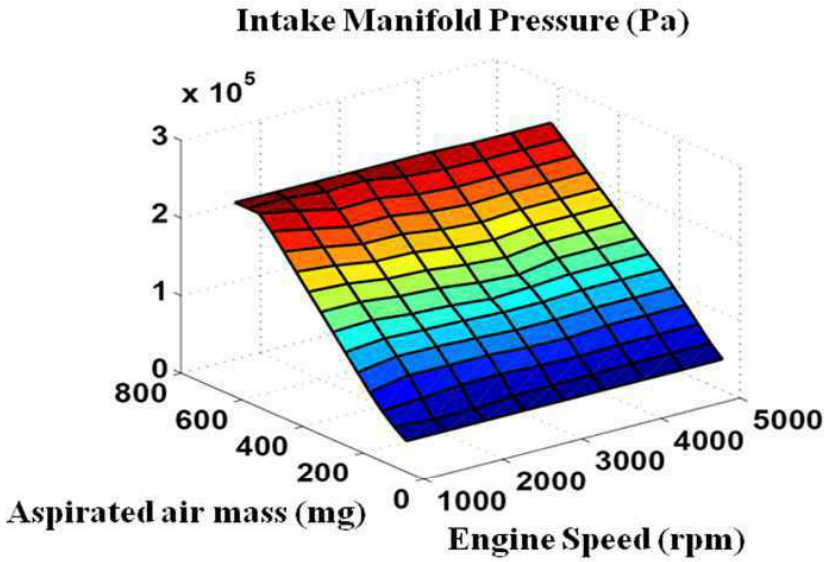

Figure 5.8. High correlation between aspirated air mass and intake manifold pressure

Furthermore, there is a high correlation (almost linear) between the aspirated mass air and the intake manifold pressure, as shown in Figure. This is the reason why we can control the intake pressure in order to control the SI engine torque.

2.2. Combining Turbocharging with Downsizing: a Key Technology to Lower Fuel Consumption and CO_2 Emissions for SI Engines

As highlighted in (Guzzella & Onder, 2004), the reduction of SI engine pollutant emissions can be effectively solved thanks to three-way catalytic converter devices. As a consequence, all attention for this kind of engine is now focused on how to improve the overall fuel economy. It is well known that the critical drawback of SI engine is its poor efficiency at low and partial loads caused by important pumping losses in these situations (Heywood, 1988). Several technologies have been proposed to enhance the engine fuel economy: e.g. variable valve timing systems, downsizing and supercharging systems, variable compression ratio engines, etc. Among these technologies, the technique called *downsizing* (Leduc et al., 2003; Lake et al., 2004) consisting in reducing engine displacement has become unavoidable to improve the fuel consumption and CO_2 emissions in automotive industry. In order to preserve the engine performance as the one of engines with larger capacity, this technology relies on the use of a turbocharger in order to increase the gas density at the engine intake side. Nowadays, almost modern SI engines are associated with turbochargers.

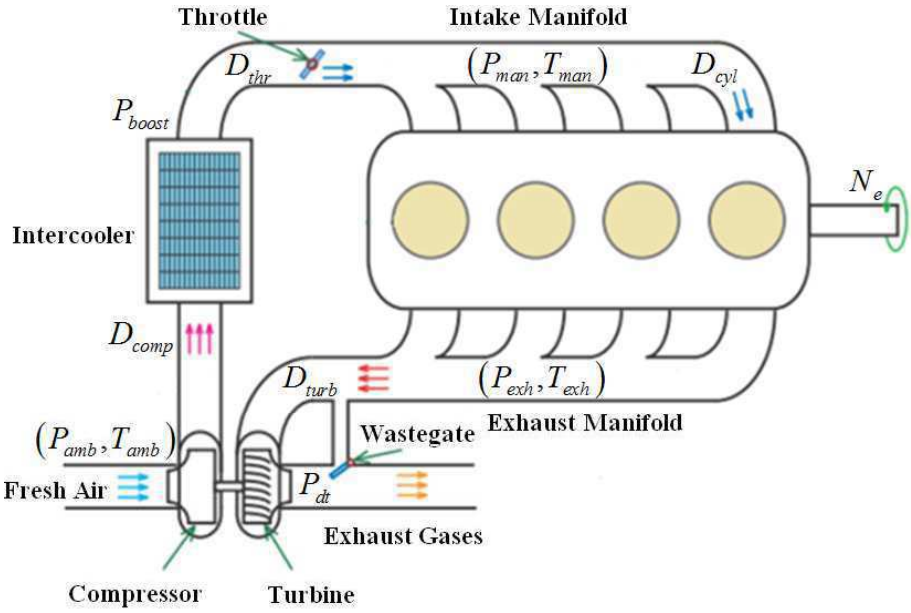

Figure 5.9. Schematic of a turbocharged spark ignited engine

The turbocharged air system consists in the components located upstream the intake valve and downstream the exhaust valve. Main components can be listed as: intercooler, throttle actuator, manifolds (intake and exhaust), turbocharger (composed by wastegate actuator, compressor and turbine) and eventually EGR (Exhaust Gas Recirculation). A sketch of the studied turbocharged air system of a SI engine is depicted in Figure 5.9. The ambient fresh air is boosted when passing through the compressor. This compressed air is used to burn the fuel in the cylinder where the combustion occurs, resulting in the production of the engine torque. The remaining energy (in the form of enthalpy) contained in the exhaust gases exits the system through the turbine. A part of this energy is recovered to drive the compressor via the turbocharger shaft whose dynamics are the consequences of the energy balance between the compressor and the turbine. There are two air actuators available on the studied air system:

- The throttle allows controlling directly the pressure in the intake manifold.
- The wastegate is used to control the exhaust gas flow to the turbine by diverting a part of the flow. It allows controlling indirectly the boost pressure in the upstream of the throttle.

The following variable notations of turbocharged air system will be used in this chapter:

Var.	Quantity	Unit	Var.	Quantity	Unit	Var.	Quantity	Unit
Π_{thr}	Throttle pressure ratio	--	D_{cyl}	In-cylinder air flow	kg/s	T_{exh}	Exhaust manifold temperature	°K
Π_{wg}	Wastegate pressure ratio	--	D_{fuel}	Fuel injected flow	kg/s	D_{thr}	Throttle mass air flow	kg/s
Π_{comp}	Compressor pressure ratio	--	V_{exh}	Exhaust manifold volume	m^3	D_{wg}	Wastegate mass air flow	kg/s
Π_{turb}	Turbine pressure ratio	--	V_{man}	Intake manifold volume	m^3	D_{comp}	Compressor mass air flow	kg/s
P_{boost}	Boost pressure	Pa	V_{cyl}	Cylinder volume	m^3	D_{turb}	Turbine mass air flow	kg/s
P_{man}	Intake pressure	Pa	N_e	Engine speed	rpm	η_{vol}	Engine volumetric efficiency	--
P_{exh}	Exhaust pressure	Pa	$\mathbb{P}_{comp}$	Compressor power	W	λ_s	Stoichiometric air/fuel ratio	--
P_{amb}	Atmospheric pressure	Pa	$\mathbb{P}_{turb}$	Turbine power	W	γ	Ratio of specific heats	--
T_{amb}	Atmospheric temperature	°K	η_{comp}	Compressor isentropic efficiency	--	R	Ideal gas constant	J/kg/°K
T_{man}	Intake manifold temperature	°K	η_{turb}	Turbine isentropic efficiency	--	C_p	Specific heats at constant pressure	J/kg/°K

The common sensors available on series production vehicles are the following:

- Pressure and temperature in the upstream of the compressor (P_{amb}, T_{amb}).
- Boost pressure (pressure in the downstream of the compressor) P_{boost}.
- Intake manifold pressure and temperature (P_{man}, T_{man}).
- Engine speed N_e.

Unfortunately, the turbocharger inertia causes the phenomenon known as *"turbo lag"*, i.e. the slow dynamics of intake pressure (and therefore the brake torque) and the insufficient supercharging capabilities (the lack of torque) at low engine speed. A control strategy achieving a fast response time while limiting the boost pressure overshoot is needed to handle this drawback. In the next section, the control-oriented models of some key components of turbocharged air system are recalled. These models will be used to design our controller in the latter of this chapter.

3. Turbocharged Air System: Modeling and Control Issues

3.1. Turbocharged SI Engine Modeling

We recall here only some main equations governing the turbocharged air system behavior. More details can be found in (Heywood, 1988; Guzzella & Onder, 2004; Eriksson, 2007).

3.1.1. Intake and exhaust manifolds pressure dynamics

The filling-emptying model in (Guzzella & Onder, 2004) is used to model the air pressure dynamics in the manifolds.

a. Intake manifold pressure dynamics

The pressure dynamics in the intake manifold is derived from the ideal gas relationship:

$$\dot{P}_{man} = \frac{RT_{man}}{V_{man}}\left(D_{thr} - D_{cyl}\right) \tag{5.2}$$

b. Exhaust manifold pressure dynamics

Similarly, the dynamics of the exhaust pressure is written as:

$$\dot{P}_{exh} = \frac{RT_{exh}}{V_{exh}}\left(D_{cyl} + D_{fuel} - D_{turb} - D_{wg}\right) \tag{5.3}$$

Next, the mass air flow calculations will be detailed.

3.1.2. Air flows calculations

The mass air flows through the air actuator valves (throttle and wastegate) are modeled using the standard model for compressible isentropic flow through a nozzle (Guzzella & Onder, 2004):

$$D_{act}\left(\phi_{act}, P_{us}, P_{ds}, T_{us}\right) = S_{eff}\left(\phi_{act}\right)\Phi_{act}\left(\Pi_{act}\right) \tag{5.4}$$

where P_{us} and P_{ds} are upstream and downstream pressures, T_{us} is upstream temperature, $S_{eff}\left(\phi_{act}\right)$ is the effective opening surface of the actuator, $\gamma \approx 1.4$ is the isentropic coefficient and $\Pi_{act} \triangleq P_{ds}/P_{us}$ is the actuators pressure ratio. The quantity $\Phi_{act}\left(\Pi_{act}\right)$ is given as follows:

$$\Phi_{act}\left(\Pi_{act}\right) = \frac{P_{us}}{\sqrt{RT_{us}}}\begin{cases}\sqrt{\dfrac{2\gamma}{\gamma-1}\left(\Pi_{act}^{\frac{2}{\gamma}} - \Pi_{act}^{\frac{\gamma+1}{\gamma}}\right)} & \text{if } \Pi_{act} \geq \left(\dfrac{2}{\gamma+1}\right)^{\frac{\gamma}{\gamma-1}} \\ \sqrt{\gamma\left(\dfrac{2}{\gamma+1}\right)^{\frac{\gamma+1}{\gamma-1}}} & \text{otherwise}\end{cases} \tag{5.5}$$

As a consequent, the air flows through the throttle and wastegate in (5.2) and (5.3) are computed as follows:

$$\begin{cases} D_{thr} = \phi_{thr}\Phi_{thr}\left(\Pi_{thr}\right) \\ D_{wg} = \phi_{wg}\Phi_{wg}\left(\Pi_{wg}\right) \end{cases} \tag{5.6}$$

where $\phi_{thr} \triangleq S_{thr}$ and $\phi_{wg} \triangleq S_{wg}$ are respectively throttle and wastegate opening sections satisfying the following physical constraints:

$$\begin{cases} S_{thr,\min} \leq \phi_{thr} \leq S_{thr,\max} \\ S_{wg,\min} \leq \phi_{wg} \leq S_{wg,\max} \end{cases} \tag{5.7}$$

The air flow entering into the cylinders is given as (Heywood, 1988):

$$D_{cyl} = \eta_{vol}\frac{P_{man}V_{cyl}}{RT_{man}}\frac{N_e}{30} \tag{5.8}$$

where the volumetric efficiency $\eta_{vol} = \eta_{vol}\left(N_e, P_{man}\right)$ is given by look-up-table (LUT). Since the SI engine operates under stoichiometric conditions, the fuel injected flow can be deduced by:

$$D_{fuel} = \frac{1}{\lambda_s} D_{cyl} \tag{5.9}$$

where $\lambda_s \approx 14.5$ is the stoichiometric air/fuel ratio.

Finally, the air flow through the turbine D_{turb} is given by a LUT, as shown in Subsection 3.1.4.

3.1.3. Dynamics of air actuators

In our developments, without loss of generality, the electronic controlled throttle and wastegate are considered using a linear first order dynamics:

$$\begin{cases} \dot{\phi}_{thr} = \dfrac{1}{\tau_{thr}} \left(u_{thr} - \phi_{thr} \right) \\ \dot{\phi}_{wg} = \dfrac{1}{\tau_{wg}} \left(u_{wg} - \phi_{wg} \right) \end{cases} \tag{5.10}$$

where τ_{thr} (resp. τ_{wg}) and u_{thr} (resp. u_{wg}) are the time constant and the control signal of the throttle (resp. wastegate). Note that the actuator dynamics are only taken into account in the simulation platforms for the results presented in Section 5. In (Nguyen et al., 2012b), we have also proposed how to consider these actuator dynamics in control design. Note also that the technology of the two valve actuators may change from one engine to another one, e.g. electronic valve, pneumatic valve, etc. That is why the two actuators should be controlled in opening section, not in opening angular position as in our studied engine, i.e. $u_{thr} \triangleq S_{thr}$ and $u_{wg} \triangleq S_{wg}$. This choice leads to less adaptation tasks when the actuator technology changes.

3.1.4. Turbocharger modeling

The rotational speed of the turbocharger is modeled using Newton second law:

$$\frac{d}{dt}\left(\frac{1}{2} J_{tc} N_{tc}^2 \right) = \mathbb{P}_{turb} - \mathbb{P}_{comp} \tag{5.11}$$

where J_{tc} is the inertia of the turbocharger.

The power consumed by the compressor is derived from the first law of thermodynamics:

$$\mathbb{P}_{comp} = D_{comp} C_p T_{amb} \frac{1}{\eta_{comp}} \left(\Pi_{comp}^{\frac{\gamma-1}{\gamma}} - 1 \right) \tag{5.12}$$

where the compressor pressure ratio $\Pi_{comp} \triangleq P_{boost}/P_{amb} > 1$ and the isentropic efficiency of the compressor η_{comp} are mapped and shown in Figure 5.10:

$$\begin{cases} \Pi_{comp} = MAP_{\Pi_{comp}}\left(N_{tc,cor}, D_{comp,cor}\right) \\ \eta_{comp} = MAP_{\eta_{comp}}\left(N_{tc,cor}, D_{comp,cor}\right) \end{cases} \tag{5.13}$$

The variables (air flow, turbocharger speed) are corrected to consider the variations of the thermodynamic conditions in upstream of the compressor (Moraal & Kolmanovsky, 1999):

$$\begin{cases} D_{comp,cor} = D_{comp}\dfrac{\sqrt{T_{amb}}}{P_{amb}} \\ N_{tc,cor} = \dfrac{N_{tc}}{\sqrt{T_{amb}}} \end{cases} \tag{5.14}$$

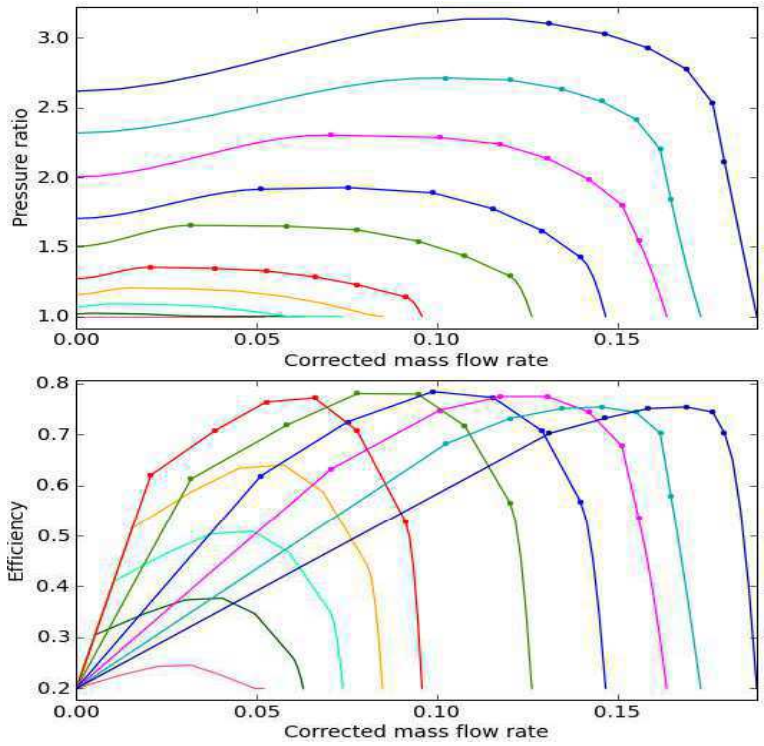

Figure 5.10. Compressor LUTs with different corrected turbocharger speeds. The points correspond to measurements.

Similarly, the power delivered by the turbine can be modeled as follows:

$$\mathbb{P}_{turb} = D_{turb} C_p T_{exh} \eta_{turb} \left(1 - \Pi_{turb}^{\frac{1-\gamma}{\gamma}} \right) \tag{5.15}$$

where the turbine pressure ratio is defined as $\Pi_{turb} \triangleq P_{turb} / P_{exh} < 1$ (P_{turb} is the pressure in downstream of the turbine). The turbine air flow and turbine efficiency are mapped and shown in Figure 5.11:

$$\begin{cases} D_{turb,cor} = MAP_{D_{turb,cor}} \left(N_{tc,cor}, \Pi_{turb} \right) \\ \eta_{turb} = MAP_{\eta_{turb}} \left(N_{tc,cor}, \Pi_{turb} \right) \end{cases} \tag{5.16}$$

The corrected quantities in this case are (Eriksson, 2007):

$$\begin{cases} D_{turb,cor} = D_{turb} \dfrac{\sqrt{\left(T_{exh} / T_{turb,ref} \right)}}{\left(P_{exh} / P_{turb,ref} \right)} \\ N_{tc,cor} = \dfrac{N_{tc}}{\sqrt{\left(T_{exh} / T_{turb,ref} \right)}} \end{cases} \tag{5.17}$$

where $P_{turb,ref}$ and $T_{turb,ref}$ are the reference conditions of the turbine.

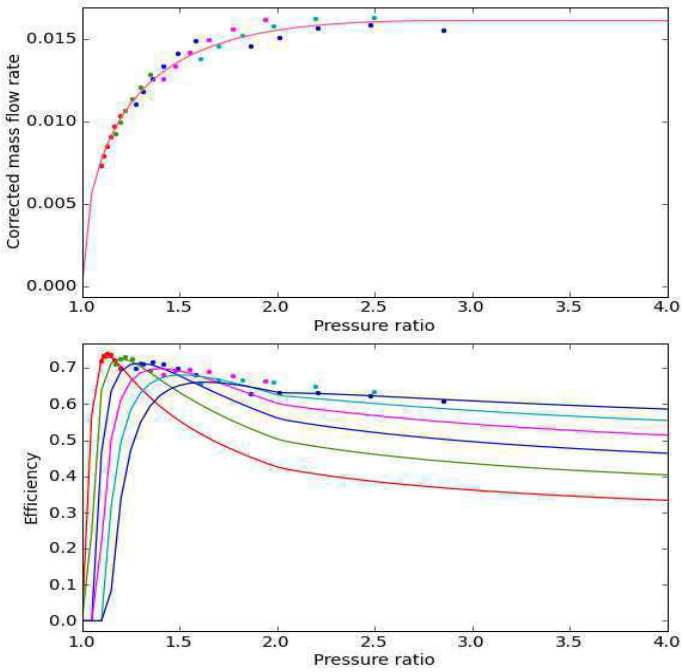

Figure 5.11. Turbine LUTs with different corrected turbocharger speeds. The points correspond to measurements.

3.1.5. Complete control-oriented model

By grouping all the equations (5.2), (5.3), (5.11), (5.12), (5.15), we obtain the following dynamical model of a turbocharged SI air system:

$$\begin{cases} \dfrac{d}{dt}\left(\dfrac{1}{2}J_{tc}N_{tc}^2\right) = D_{turb}C_pT_{exh}\eta_{turb}\left(1-\Pi_{turb}^{\frac{1-\gamma}{\gamma}}\right) - D_{comp}C_pT_{amb}\dfrac{1}{\eta_{comp}}\left(\Pi_{comp}^{\frac{\gamma-1}{\gamma}}-1\right) \\ \dot{P}_{exh} = \dfrac{RT_{exh}}{V_{exh}}\left(D_{cyl}+D_{fuel}-D_{turb}-D_{wg}\right) \\ \dot{P}_{man} = \dfrac{RT_{man}}{V_{man}}\left(D_{thr}-D_{cyl}\right) \end{cases} \tag{5.18}$$

In the framework of the thesis, two simulators of turbocharged air system have been developed with the data of a 4-cylinders SI engine from Renault. The first one, implemented in Matlab/Simulink software, is based on the three main dynamics presented in (5.18), see Figure 5.12.

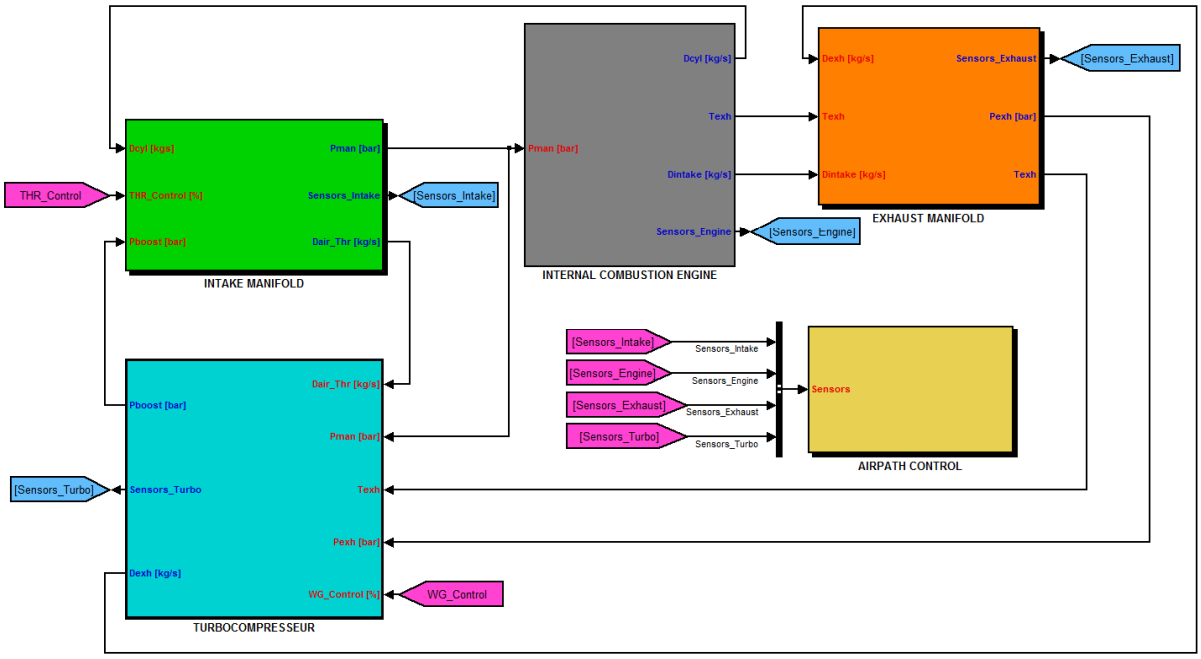

Figure 5.12. Simulink diagram of the turbocharged air system of developed SI engine

The second simulator is implemented in the commercial software LMS Imagine.Lab AMESim, see Figure 5.13. This simulator is more accurate than the previous one because it is able to take into account some complex physical phenomena involved in different components of the whole turbocharged engine.

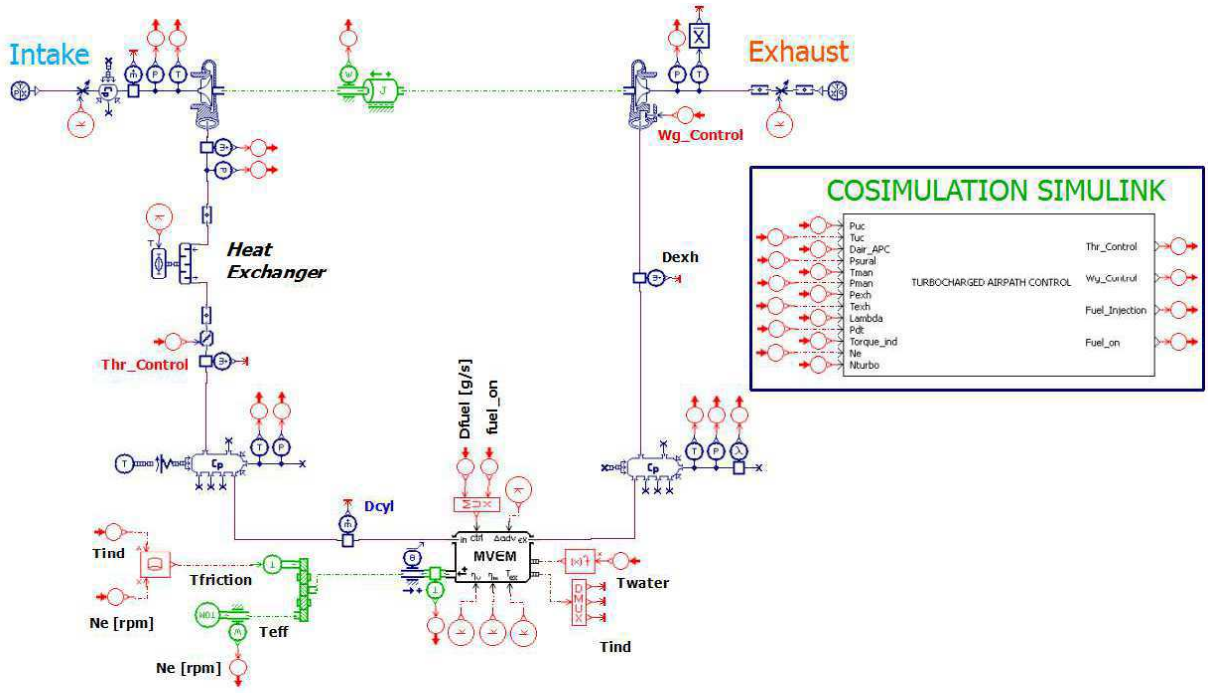

Figure 5.13. Illustration of co-simulation interface between AMESim and Simulink for a turbocharged air system of SI engine

A great advantage when using AMESim is that it is not only a powerful platform for modeling high complex systems but also enables the possibility to couple an AMESim plant model with a controller embedded in Simulink by a co-simulation interface. In our work, all proposed control strategies will be tested with both simulators.

3.2. Turbocharged Air System Control

3.2.1. Engine control structure

In general, the complete vehicle control system can be implemented with a hierarchical structure (Guzzella & Onder, 2004) which is depicted in Figure 5.14. This structure is composed by several modules, the outputs of each upper level module are the inputs of the corresponding lower level module. The driver request is normally the accelerator pedal position. *Vehicle Manager* aims at managing all driving strategies and the interface with others components of the powertrain system. As a result, the driver request is converted into a torque control objective set point. Then, the set points for the air path, the fuel path and the ignition path are inversely given by corresponding static LUTs for which each operating point is defined in terms of engine speed and torque. The calibration of these static LUTs is experimentally carried out by compromising all constraints on pollutants, consumption and drivability. From the corresponding set points, the *engine control* computes the appropriate control signals for all engine actuators from the measurements of the available sensors.

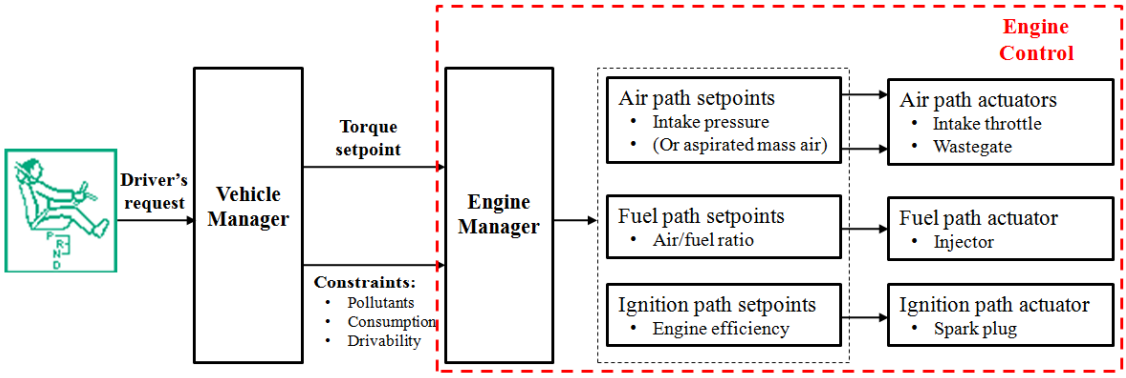

Figure 5.14. Hierarchical structure of the torque control for a turbocharged SI engine

Nowadays, modern engines are usually equipped with an electronic device, namely Electronic Control Unit (ECU), which is in charge of engine control tasks. In the sequel, we are only focusing on the control of air system.

3.2.2. State-of-the-art on turbocharged air system control

As highlighted in (Moulin, 2010), it is very complex and costly to develop and implement a new control strategy in automotive industry since it may change the available software in series. The novel control strategies, generally needed when some new technologies are introduced, have to justify its relevant advantages with respect to the actual versions. As the same time, they have to satisfy several stringent constraints such as control performance/robustness, calibration complexity, software consistency. That is the reason why up to now the conventional control strategy is still largely adopted by automakers. This strategy normally consists in combining the gain-scheduled PID controllers (feedback control) with some static LUTs (feed-forward control used for performance improvement) (Guzzella & Onder, 2004). It is relatively simple to implement conventional control strategy in the ECU. However, this strategy remains some inherent drawbacks. First, when using the technique based on gain-scheduled PID controllers and feed-forward static LUTs, each engine operating point need to be defined. It may leads to heavy calibration efforts. In addition, it is not always clear to define an engine operating point, in particular for complex air system with multiple air actuators (Moulin, 2010). Second, the trade-off between performance and robustness is not easy to achieve for a wide engine operating range when applying a linear control technique to high complex nonlinear system. For all these reasons, conventional control strategy may not be appropriate to cope with new engine generations for which many novel technologies have been introduced to meet more and more stringent legislation constraints. A model-based control approach is a way to overcome these drawbacks.

Since turbochargers are key components in downsizing and supercharging technology, many works have been recently investigated in the design of new control strategies for this system. Indeed, a large numbers of advanced model-based control technique have been studied in the literature, e.g. gain-scheduled PID controllers (Karnik et al., 2005; Daubler et al., 2007), H_∞ control (Jung et al., 2005), Gain-scheduled H_∞ control (Wei & del Re, 2007), sliding mode control (Utkin et al., 2000), predictive control (Colin et al., 2007; Ortner & del Re, 2007), etc. These control techniques are based on engine model linearization in order to apply linear control theory. Again, calibration efforts are expensive and inherent aforementioned drawbacks are still remaining. Nonlinear model-based control techniques seem more relevant for this complex nonlinear system. Most of efforts are dedicated to turbocharged air system of diesel engines (Dabo et al., 2009; Wang et al., 2011) and very few works deal with SI engine. In (Moulin et al., 2008; Moulin, 2010), the authors proposed a very interesting approach based on flatness property of the system which combines feedback linearization and constrained motion planning. This approach limits considerably calibration efforts and is able to meet some closed-loop performance. However, it requires a good model quality. In addition, the author seems to have difficulties when handling model uncertainties.

In this chapter, based on the theoretical results on switching Takagi-Sugeno model developed in Chapter 3, we propose a novel nonlinear approach to control the air system of a turbocharged SI engine. This approach is able to handle easily the number of involved nonlinearities and allows overcoming all aforementioned drawbacks. In addition, the obtained controller, having only two tuning parameters, is easily implementable and achieves very satisfying results. To the best of our knowledge, this is the first nonlinear model-based control approach for which stability of the whole turbocharged air system can be proven while taking into account the strategy to minimize the engine energy losses. Finally, this generic approach can be also generalized for other more complex turbocharging systems with several air actuators (VVT, EGR, etc.). The proposed approach is detailed in next section.

4. Switching Robust T-S Controller Design

4.1. Turbocharged Air System Control Strategy

As mentioned above, SI engines operate under stoichiometric conditions. This leads to the tight connection between the engine torque and the air mass trapped in the cylinders. This air mass, in turn, depends strongly on the pressure in the intake manifold P_{man}. The goal of the air path management is therefore to control this pressure. For high load, since pumping losses are minimized when the

throttle is fully open (Eriksson et al., 2002), the boost pressure $P_{boost} \approx P_{man}$ is controlled by the wastegate in this zone. Only at low load, the throttle is activated to control the intake manifold pressure P_{man}. This strategy results in the switching nature of our nonlinear controller illustrated in Figure 5.15.

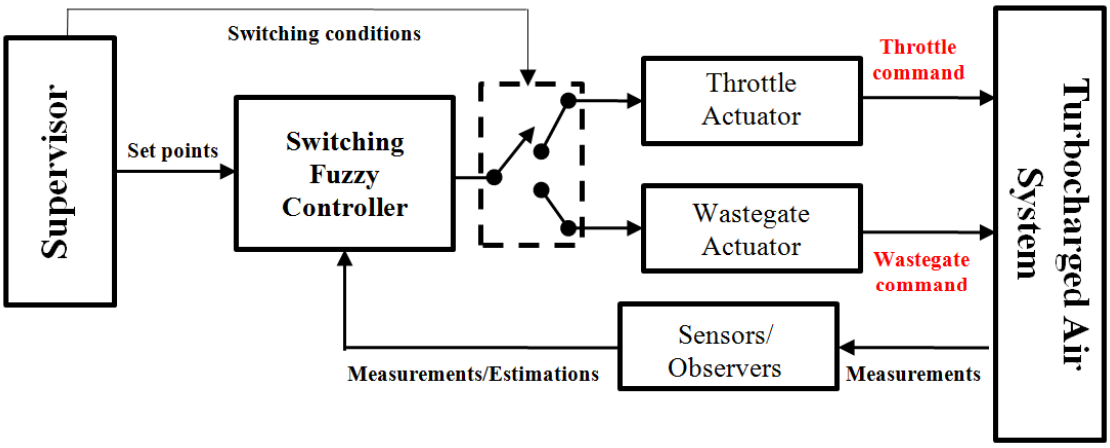

Figure 5.15. Proposed control scheme of turbocharged air system

The supervisor provides intake pressure set point for the proposed controller. In addition, it decides also the switching moments between the two air actuators. The throttle and the wastegate work separately but coordinately according to the fuel-optimal optimization strategy described above. All variables needed for control design are easily measured or estimated with the common sensors on automotive engines.

4.2. How to Simplify the Turbocharged Air System Model?

Let recall the complete model of the turbocharged air system of a SI engine, we obtain the following dynamical system:

$$\begin{cases} \dfrac{d}{dt}\left(\dfrac{1}{2}J_{tc}N_{tc}^2\right) = D_{turb}C_pT_{exh}\eta_{turb}\left(1-\Pi_{turb}^{\frac{1-\gamma}{\gamma}}\right) - D_{comp}C_pT_{amb}\dfrac{1}{\eta_{comp}}\left(\Pi_{comp}^{\frac{\gamma-1}{\gamma}}-1\right) \\ \dot{P}_{exh} = \dfrac{RT_{exh}}{V_{exh}}\left(D_{cyl}+D_{fuel}-D_{turb}-D_{wg}\right) \\ \dot{P}_{man} = \dfrac{RT_{man}}{V_{man}}\left(D_{thr}-D_{cyl}\right) \end{cases} \tag{5.19}$$

The nonlinear model (5.19) describes completely the three dynamics governing the turbocharged air system. However, this highly nonlinear model of 3rd order is too complicated from a control point of

view. Applying directly the classical T-S control technique for this system would not be an appropriate solution due to its large number of nonlinearities. Therefore, this model needs to be simplified for control design purpose. Here, we adopt the model reduction methodology used in (Moulin et al., 2008). The goal is to preserve only the dominant dynamics of the turbocharger by neglecting the fast pressures dynamics according to the theory of singular perturbations. The simplified model is then given by:

$$\begin{cases} \dfrac{d}{dt}\left(\dfrac{1}{2}J_{tc}N_{tc}^2\right) = D_{turb}C_pT_{exh}\eta_{turb}\left(1-\Pi_{turb}^{\frac{1-\gamma}{\gamma}}\right) - D_{cyl}C_pT_{amb}\dfrac{1}{\eta_{comp}}\left(\Pi_{comp}^{\frac{\gamma-1}{\gamma}}-1\right) \\ D_{cyl}+D_{fuel} = D_{turb}+D_{wg} \end{cases} \tag{5.20}$$

The first equation of (5.20) represents the energy balance between the compressor and the turbine and gives the dynamics of the air system. The second one gives the mass balance of gases in the manifolds for which the dynamics are neglected. It can be noticed that the system (5.20) has only one state variable: the turbocharger squared speed N_{tc}^2. However, this quantity is not measurable on series vehicles. At high load, it can be approximated by a linear function of the boost pressure $P_{boost} \approx P_{man}$ as follows, as shown in Figure 5.16(Moulin et al., 2008):

$$N_{tc}^2 = A_{tc}P_{man} + B_{tc} \tag{5.21}$$

This approximation considerably simplifies the control task. After some simple transformations of (5.20), we obtain the following dynamics of the turbocharger depending on the intake pressure:

$$\dot{P}_{man} = g_1(\cdot)P_{man} - g_2(\cdot)u_{wg} \tag{5.22}$$

where the nonlinear functions are:

$$\begin{cases} g_1(\cdot) = \dfrac{2}{J_{tc}A_{tc}}\left[\alpha_1\left(1+\dfrac{1}{\lambda_s}\right)-\alpha_2\right]\alpha_3 \\ g_2(\cdot) = \dfrac{2}{J_{tc}A_{tc}}\alpha_1\Phi_{wg}\left(\Pi_{wg}\right) \end{cases} \tag{5.23}$$

The parameters $(\alpha_1, \alpha_2, \alpha_3)$ depending only on the engine operation conditions are given by:

$$\begin{cases} \alpha_1 = C_p T_{exh} \eta_{turb} \left(1 - \Pi_{turb}^{\frac{1-\gamma}{\gamma}} \right) \\ \alpha_2 = C_p T_{amb} \dfrac{1}{\eta_{comp}} \left(\Pi_{comp}^{\frac{\gamma-1}{\gamma}} - 1 \right) \\ \alpha_3 = \eta_{vol} \dfrac{V_{cyl}}{R T_{man}} \dfrac{N_e}{30} \end{cases} \tag{5.24}$$

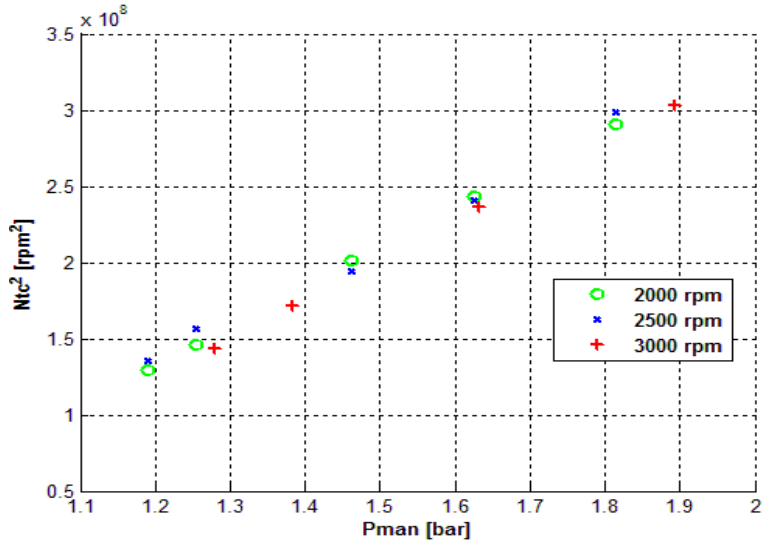

Figure 5.16. Turbocharger square speed N_{tc}^2 with respect to P_{man}

As can be noticed in Figure 5.17, the simplified model (5.22) captures well the boost pressure dynamics during the turbocharger transient phases with some small differences in steady-state phases. This simplified model will be used to control the wastegate actuator in the high load.

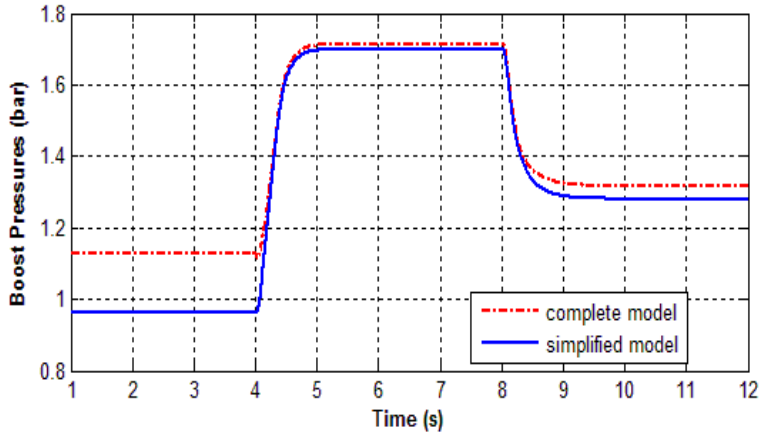

Figure 5.17. Boost pressure validation during the turbocharger transient at $N_e = 2750\,\text{rpm}$

4.3. Switching T-S Control Design for Turbocharged Air System

In accordance with the control strategy stated in Subsection 4.1, we have been proposed to consider the turbocharged air system as a switching system with two operating zones (regions) separated according to the pressure ratio $\Pi \triangleq P_{man}/P_{amb}$. This fact allows reducing the number of subsystems in the final T-S model and, at the same time, the strategy to minimize the engine losses is taken into account in the control design. The two operating zones are defined as follows, with $\varepsilon \approx 1.1$:

- Zone 1: $\Pi \le \varepsilon$ (low load zone), only the throttle is used to track the intake pressure P_{man} .
- Zone 2: $\Pi > \varepsilon$ (high load zone), only the wastegate is activated to track the boost pressure $P_{boost} \approx P_{man}$.

4.3.1. Pressure dynamics in low load zone

From (5.2) and (5.6), the system dynamics in Zone 1 is given by:

$$\dot{P}_{man} = f_2(\cdot)u_{thr} - f_1(\cdot)P_{man} \tag{5.25}$$

where the nonlinearities are:

$$\begin{cases} f_1(\cdot) = \dfrac{RT_{man}}{V_{man}P_{man}} D_{cyl} \\ f_2(\cdot) = \dfrac{RT_{man}}{V_{man}} \Phi_{thr}(\Pi_{thr}) \end{cases} \tag{5.26}$$

4.3.2. Pressure dynamics in high load zone

The reference model in Zone 2 is given by (5.22), (5.23) and (5.24).

4.4. Switching Robust Control Design

As mentioned above, we aim here to track the intake pressure trajectory in order to control the engine torque. It is well known that an integral action in the control law is necessary to ensure a zero steady-state error in the tracking problem. This amounts by adding a new state whose dynamics is defined as follows:

$$\dot{x}_{\text{int}} = y_{ref} - y \tag{5.27}$$

where y_{ref} is the intake pressure set point signal.

It is noted that the two nonlinearities in each local model (5.22) and (5.25) are bounded and can be represented:

$$\begin{cases} \underline{f_i} \le f_i(\cdot) \le \overline{f_i} \\ \underline{g_j} \le g_j(\cdot) \le \overline{g_j} \end{cases} \text{ and } \begin{cases} f_i(\cdot) = \omega_{1i}^1 \overline{f_i} + \omega_{2i}^1 \underline{f_i} \\ g_j(\cdot) = \omega_{1j}^2 \overline{g_j} + \omega_{2j}^2 \underline{g_j} \end{cases} \tag{5.28}$$

where

$$\begin{aligned} &\omega_{1i}^1 = \frac{f_i(\cdot) - \underline{f_i}}{\overline{f_i} - \underline{f_i}}; \quad \omega_{2i}^1 = 1 - \omega_{1i}^1 \text{ with } i = 1,2 \\ &\omega_{1j}^2 = \frac{g_j(\cdot) - \underline{g_j}}{\overline{g_j} - \underline{g_j}}; \quad \omega_{2j}^2 = 1 - \omega_{1j}^2 \text{ with } j = 1,2 \end{aligned} \tag{5.29}$$

Thus, the global switching system has two separated zones and the T-S model in each zone has four linear models. The membership functions in each local zone are given by:

$$\begin{aligned} &\text{Zone 1: } \eta_1^1 = \omega_{11}^1.\omega_{12}^1; \quad \eta_2^1 = \omega_{11}^1.\omega_{22}^1; \quad \eta_3^1 = \omega_{21}^1.\omega_{12}^1; \quad \eta_4^1 = \omega_{21}^1.\omega_{22}^1 \\ &\text{Zone 2: } \eta_1^2 = \omega_{11}^2.\omega_{12}^2; \quad \eta_2^2 = \omega_{11}^2.\omega_{22}^2; \quad \eta_3^2 = \omega_{21}^2.\omega_{12}^2; \quad \eta_4^2 = \omega_{21}^2.\omega_{22}^2 \end{aligned} \tag{5.30}$$

Moreover, the studied system has only one state, the intake pressure, which is also the measured output and the controlled output. We will denote $\overline{x} \triangleq \begin{bmatrix} P_{man} & x_{\text{int}} \end{bmatrix}^T$, $u \triangleq \begin{bmatrix} u_{thr} & u_{wg} \end{bmatrix}^T$, $y \triangleq P_{man}$ and $y_{ref} \triangleq P_{man,ref}$. Then, the global closed-loop system can be represented as follows:

$$\begin{cases} \dot{\overline{x}} = \sum_{k=1}^{2}\sum_{i=1}^{4} \mu_k(P_{man})\eta_i^k(\theta)\left\{\left(\overline{A}_i^k + \Delta\overline{A}_i^k\right)\overline{x} + \overline{B}_{w,i}^k w + \left(\overline{B}_{u,i}^k + \Delta\overline{B}_{u,i}^k\right) sat(u) + B y_{ref}\right\} \\ y = \sum_{k=1}^{2}\sum_{i=1}^{4} \mu_k(P_{man})\eta_i^k(\theta)\overline{C}_i^k\overline{x} + \overline{D}_i^k w \end{cases} \tag{5.31}$$

where the scheduling variable vector θ corresponds to the nonlinearities $f_i(\cdot)$ or $g_i(\cdot)$, $i = 1,2$ according to the considered operating zone the matrices of the extended systems are given by:

$$\begin{aligned} &\overline{A}_i^k = \begin{bmatrix} A_i^k & 0 \\ -C_i^k & 0 \end{bmatrix}; \quad \overline{B}_{u,i}^k = \begin{bmatrix} B_{u,i}^k \\ 0 \end{bmatrix}; \quad \overline{C}_i^k = \begin{bmatrix} C_i^k & 0 \end{bmatrix}; \quad B = \begin{bmatrix} 0 \\ 1 \end{bmatrix}; \\ &\Delta\overline{A}_i^k = \begin{bmatrix} \Delta A_i^k & 0 \\ 0 & 0 \end{bmatrix}; \quad \Delta\overline{B}_{u,i}^k = \begin{bmatrix} \Delta B_{u,i}^k \\ 0 \end{bmatrix}; \quad \overline{B}_{w,i}^k = \begin{bmatrix} B_{w,i}^k \\ 0 \end{bmatrix}; \quad \overline{D}_i^k = \begin{bmatrix} D_i^k \\ 0 \end{bmatrix} \end{aligned} \tag{5.32}$$

In this work, a maximum of 10% parametric uncertainties are considered:

$$\begin{cases} \left|\Delta f_1(\cdot)\right| \le 0.1 f_1(\cdot); & \left|\Delta f_2(\cdot)\right| \le 0.1 f_2(\cdot) \\ \left|\Delta g_1(\cdot)\right| \le 0.1 g_1(\cdot); & \left|\Delta g_2(\cdot)\right| \le 0.1 g_2(\cdot) \end{cases} \tag{5.33}$$

These uncertainties can be seen as modeling errors or system disturbances (Nguyen et al., 2012c). The sub-model matrices are given by, $\forall i \in \Omega_4$:

$$\begin{aligned} &F_{x,i}^1 = F_{x,i}^2 = \begin{bmatrix} 1 & 1 \\ 0 & 0 \end{bmatrix}; \quad B_{w,i}^1 = B_{w,i}^2 = \begin{bmatrix} 0.1 \\ 0 \end{bmatrix}; \\ &C_i^1 = C_i^2 = \begin{bmatrix} 1 & 0 \end{bmatrix}; \qquad D_i^1 = D_i^2 = 0.01 \end{aligned} \tag{5.34}$$

- Zone 1: $\Pi \le \varepsilon$ (low load zone)

$$\begin{aligned} &A_1^1 = A_2^1 = \begin{bmatrix} -\overline{f}_1 & 0 \\ -1 & 0 \end{bmatrix}; \quad B_{u,1}^1 = B_{u,3}^1 = \begin{bmatrix} \overline{f}_2 & 0 \\ 0 & 0 \end{bmatrix}; \quad E_{A,i}^1 = \begin{bmatrix} -1.4 & 0 \\ 0 & 0 \end{bmatrix}; \\ &A_3^1 = A_4^1 = \begin{bmatrix} -\underline{f}_1 & 0 \\ -1 & 0 \end{bmatrix}; \quad B_{u,2}^1 = B_{u,4}^1 = \begin{bmatrix} \underline{f}_2 & 0 \\ 0 & 0 \end{bmatrix}; \quad E_{u,i}^1 = \begin{bmatrix} 0 & 0 \\ 3513 & 0 \end{bmatrix}. \end{aligned} \tag{5.35}$$

- Zone 2: $\Pi > \varepsilon$ (high load zone)

$$\begin{aligned} &A_1^2 = A_2^2 = \begin{bmatrix} \overline{g}_1 & 0 \\ -1 & 0 \end{bmatrix}; \quad B_{u,1}^2 = B_{u,3}^2 = \begin{bmatrix} 0 & -\overline{g}_2 \\ 0 & 0 \end{bmatrix}; \quad E_{A,i}^2 = \begin{bmatrix} 0.075 & 0 \\ 0 & 0 \end{bmatrix}; \\ &A_3^2 = A_4^2 = \begin{bmatrix} \underline{g}_1 & 0 \\ -1 & 0 \end{bmatrix}; \quad B_{u,2}^2 = B_{u,4}^2 = \begin{bmatrix} 0 & -\underline{g}_2 \\ 0 & 0 \end{bmatrix}; \quad E_{u,i}^2 = \begin{bmatrix} 0 & 0 \\ 0 & -164 \end{bmatrix}. \end{aligned} \tag{5.36}$$

Remark 5.1. In the trajectory tracking framework, the reference signal $y_{ref} \neq 0$ is supposed to evolve slowly, i.e. $\dot{y}_{ref} = 0$, then input-to-state stability propriety has to be considered (Sontag & Wang, 1995). Thus, Theorem 3.1 will be directly used to find the feedback gains in our case. Theorem 3.2 can be also applied by considering $\overline{C}_i^k = I$.

Remark 5.2. It should be also noticed that all data concerning the turbocharged air system and controller will not be revealed here for the confidentiality reason with our industrial collaboration partners. However, this does not restrict our observations since we are focusing on the control design and the controller performance.

Remark 5.3. As highlighted in (Tanaka et al., 2001), a typical phenomenon when dealing with switching control is non-continuity of control input at switching boundaries. It may lead to a serious degradation of the controller performance. In order to handle this problem, the "distance" between all the connecting gains in all the zones should be minimized as much as possible. Concretely, the smoothness condition $L_2^1 \approx L_1^2$ will be integrated in the control design to prevent the pressure overshoots in our case. From(3.34), the smoothness LMI condition is fulfilled if:

$$\begin{bmatrix} \beta I & \left(Y_2^1 - Y_1^2\right)^T \\ \left(Y_2^1 - Y_1^2\right) & I \end{bmatrix} \geq 0 \tag{5.37}$$

where $\beta > 0$ is chosen as small as possible.

Remark 5.4. The controller feedback gains $L_j^k,\ \forall (k,j) \in \Omega_2 \times \Omega_4$ are efficiently designed by solving the LMI conditions in Theorem 3.1 and also the smoothness condition (5.37) with some numerical tools, e.g. the Matlab LMI Control Toolbox (Gahinet et al., 1995) or Yalmip Toolbox (Lofberg, 2004).

5. Simulation Results and Analysis

5.1. Controller Implementation

It is important to emphasize that the pressure switching line defined by the ratio $\varepsilon \approx 1.1$ in Subsection 4.3 may slightly change in function of engine speeds and engine characteristics. In order to deal with this problem, we propose here to approximate the indicator functions μ_k, $k = 1,2$ by the following tangent hyperbolic functions:

$$\begin{cases} \mu_2\left(P_{man}\right) \approx \dfrac{1}{2} + \dfrac{1}{2}\tanh\left(p.P_{man}\right) = \dfrac{1}{1+e^{-2pP_{man}}} \\ \mu_1\left(P_{man}\right) = 1 - \mu_2\left(P_{man}\right) \end{cases} \tag{5.38}$$

where p is the function parameter. The two new indicator functions is illustrated in Figure 5.18. It can be obsevered that this approximation introduces virtually the so-called middle load zone (Zone 3) whose largeness can be easily tuned by the parameter p, i.e. a larger p corresponds to a sharper transition.

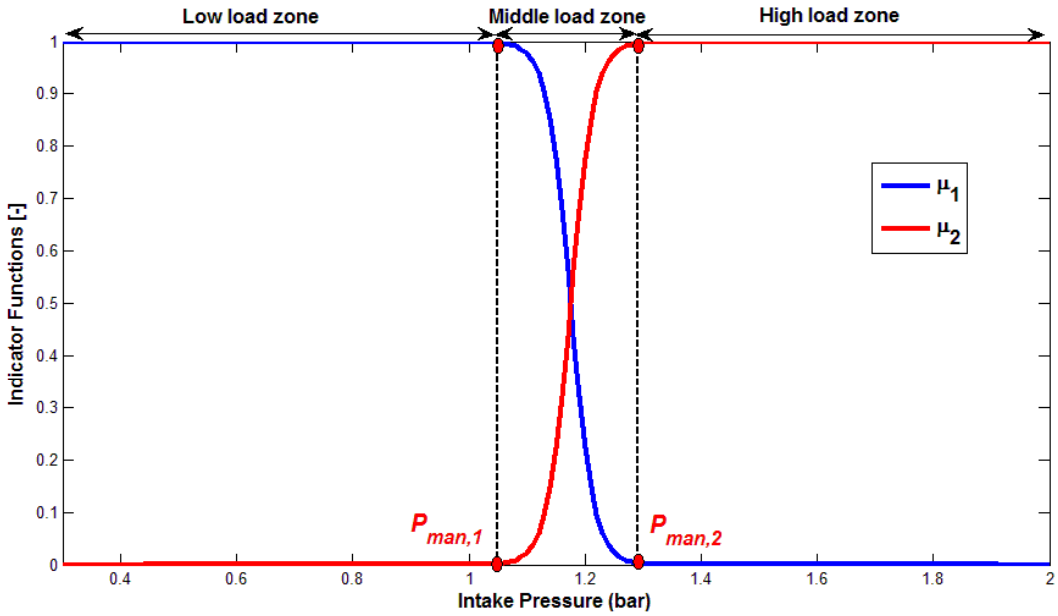

Figure 5.18. Approximation of indicator functions and virtual introduction of middle load zone

As can be seen in see Figure 5.18, the whole engine operating range is now divided into three zones separated by two intake pressure thresholds $P_{man,1}$ and $P_{man,2}$. Then, each operating zone has its own actuator scheduling strategy as described below:

- *Zone 1* (low load zone $P_{man} \leq P_{man,1}$): The wastegate is widely open and only the throttle is used to track the intake pressure reference.
- *Zone 2* (high load zone $P_{man} \geq P_{man,2}$): The throttle is wide-open and only the wastegate is activated to control the intake pressure which is approximate to the boost pressure P_{boost} in this case.
- *Zone 3* (middle load zone $P_{man,1} < P_{man} < P_{man,2}$): Both throttle and wastegate are simultaneously used to control the intake pressure.

It is worth noting that the pressure thresholds $P_{man,1}$ and $P_{man,2}$ separating the three zones are tuned by the parameter p. Indeed, this parameter is chosen so that the two pressure thresholds are very close. This is due to different reasons. First, the indicator functions will be well approximated by the tangent hyperbolic functions. Second, the middle load zone is sufficiently small so that engine pumping losses are minimized.

Hereafter, a series of trials will be performed in order to point out the validity of the proposed method. For the sake of clarity, the two commands (throttle, wastegate) are normalized. The control

inputs constraints in (5.7) become: $0 \le \overline{u}_{thr}, \overline{u}_{wg} \le 100\%$. When $\overline{u}_{thr} = 100\%$ (resp. $\overline{u}_{wg} = 0\%$), it means that the throttle (resp. wastegate) is fully open. On the reverse, when $\overline{u}_{thr} = 0\%$ (resp. $\overline{u}_{wg} = 100\%$), the throttle (resp. wastegate) is fully closed. Before starting, it is noted that the proposed controller is easily tuned with only two parameters, the decay rate α and the disturbance attenuation level γ which are the same for all following simulations.

5.2. Test 1: Control Strategy Validation

This scenario test aims at validating turbocharged air system control strategy stated above. To this end, the intake pressure reference varies in different engine operating zones at a constant engine speed $N_e = 2250$ rpm. The validity of the proposed control strategy is confirmed by the result in Figure 5.19.

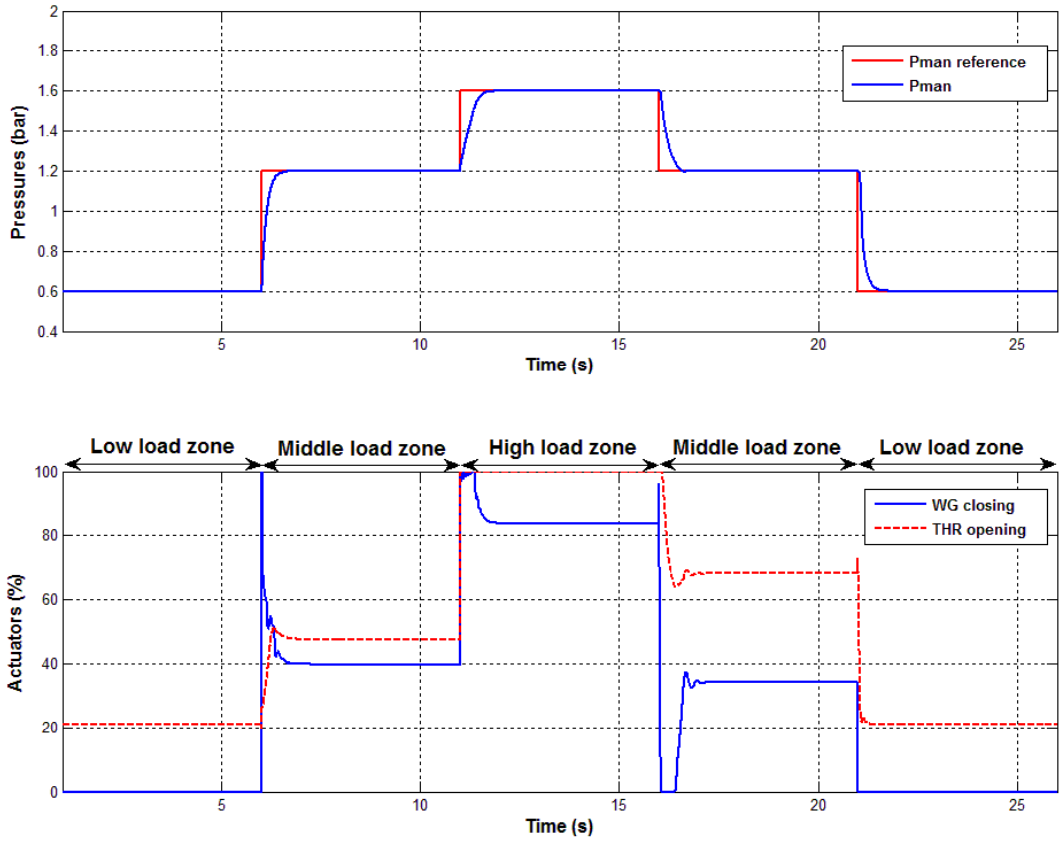

Figure 5.19. Validation of the turbocharged air system control strategy at $N_e = 2250$ rpm

The wastegate is open in low load operating zone. Once the throttle is fully open, the wastegate closes to track the boost pressure. When the turbocharged engine operates in the middle load zone, both actuators are simultaneously activated to control the intake pressure.

Remark 5.5. In low load zone (Zone 1), the wastegate is fully open, i.e. $\overline{u}_{wg} = 100\%$. Note that this imposed constant value does not agree with the one computed from the controller feedback gains L_j^1, $\forall j \in \Omega_4$. However, fortunately, it can be observed from the elements of matrices $B_{u,i}^1$, $\forall i \in \Omega_4$ that this constant control input will never affect on the dynamics of the closed-loop system in this zone. The same remark can be done for high load zone (Zone 2) with $\overline{u}_{thr} = 100\%$.

5.3. Test 2: Tracking Performance at Different Engine Speeds

The trajectory tracking of the intake pressure for different engine speeds (from 2000 up to 3500 rpm) is shown in Figure 5.20.

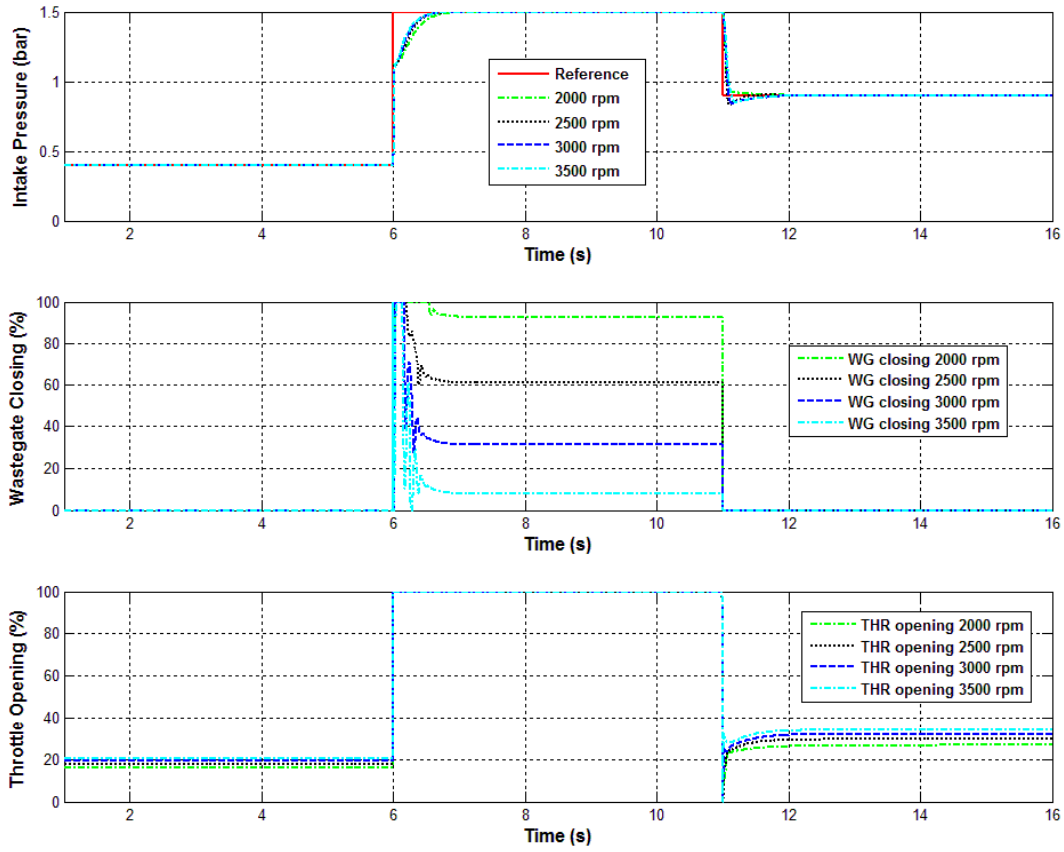

Figure 5.20. Trajectory tracking with different engine speeds

Some remarks about these results can be reported as follows. First, the convergence is ensured over the whole operating range. The wastegate response is very aggressive during the turbocharger transients; it hits the constraints and then stabilizes to track the boost pressure. This behavior which can be tuned easily with the tuning parameter α allows compensating the slow dynamics of the turbocharger. Second, the controller does not generate any overshoot in the considered operating range which is also a very important property for the driving comfort.

5.4. *Test 3: Vehicle Transients*

The closed-loop responses during the vehicle transient are presented in Figure 5.21. It can be noticed that the proposed controller is perfectly able to guarantee a very good tracking performance even with the important variation of the engine speed (which represents the vehicle transient).

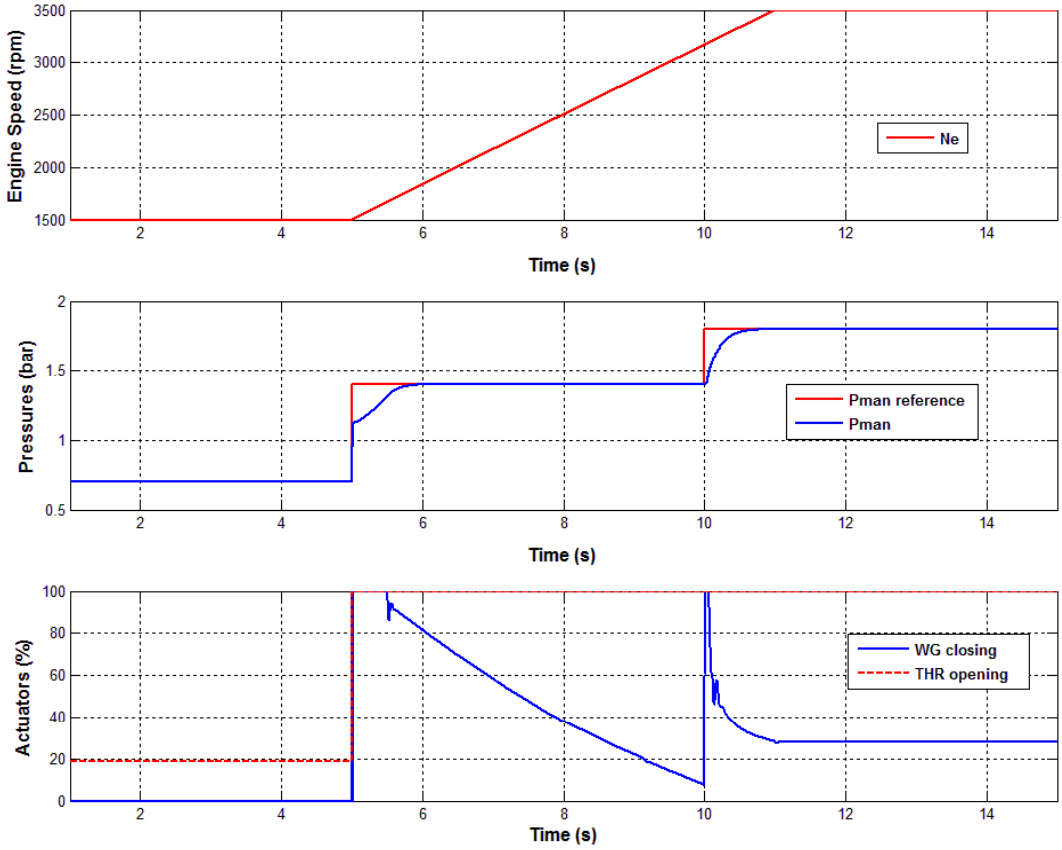

Figure 5.21. Variation of engine speed (up) and pressure tracking performance (middle) with corresponding actuator commands (bottom) for a vehicle transient

5.5. *Test 4: Disturbance Attenuation*

This test aims to point out the robustness performance (w.r.t the exogenous disturbances) and the benefits of the integral action in the control loop. For that, the intake pressure reference varies largely at constant speed, and a bounded noise w, which is the combination of a sampled Gaussian noise with a square wave, is also added (see Figure 5.22- top). Despite the presence of noise, as shown in Figure 5.22 (middle), the tracking is still guaranteed without any offset in steady-state phases and the disturbance is also well attenuated. However, the wastegate solicitation is sensitive to noises Figure 5.22 (bottom). It is due to the non-minimum phase zero in the relation between the wastegate behavior and the boost pressure (Karnik et al., 2005; Nguyen et al., 2012c).

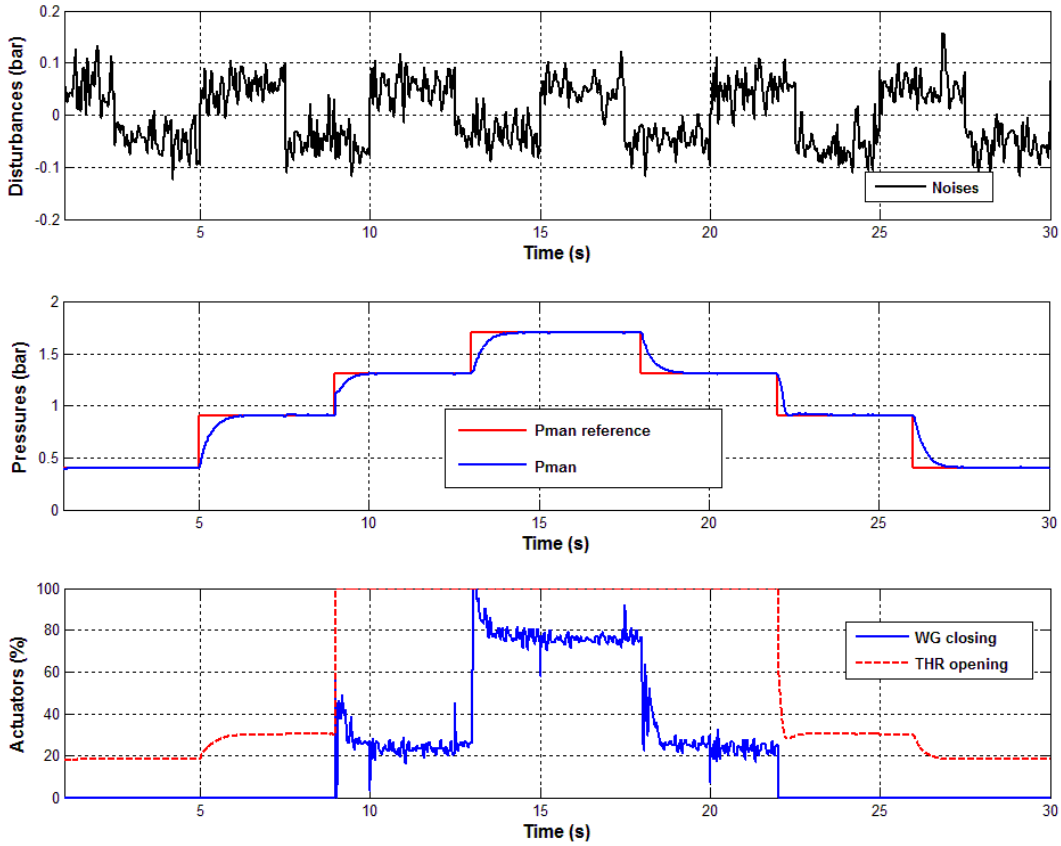

Figure 5.22. Disturbance used for the simulation (top); Intake pressure trajectory tracking (middle); and actuators corresponding solicitation (bottom) at $N_e = 2750$ rpm

5.6. Test 5: With and Without Saturation

Control input saturation is a major control issue of industrial systems. It must be taken into account in the control design in order to guarantee the system stability and enhance the control performance. This fact will be pointed out in this part. Our proposed method will be also compared with the existing results in (Tanaka et al., 2001).

Figure 5.23 shows the system responses with different control approaches. Here, three control approaches are compared: Controller 1 does not take into account the actuator saturation in the control design, Controller 2 is with the unsaturated control approach proposed in (Tanaka et al., 2001) and Controller 3 is with our proposed method. Some observations can be noticed. First, Controller 1 takes much more time to stabilize the system and it leads to important pressure overshoots which must absolutely be avoided to ensure an acceptable driving comfort. Actuator responses of the Controller 2 are over-constrained; control performance is therefore rather poor in terms of time response. Finally, Controller 3 achieves a very satisfying performance (no overshoots, quick time response) and fulfills our control specifications.

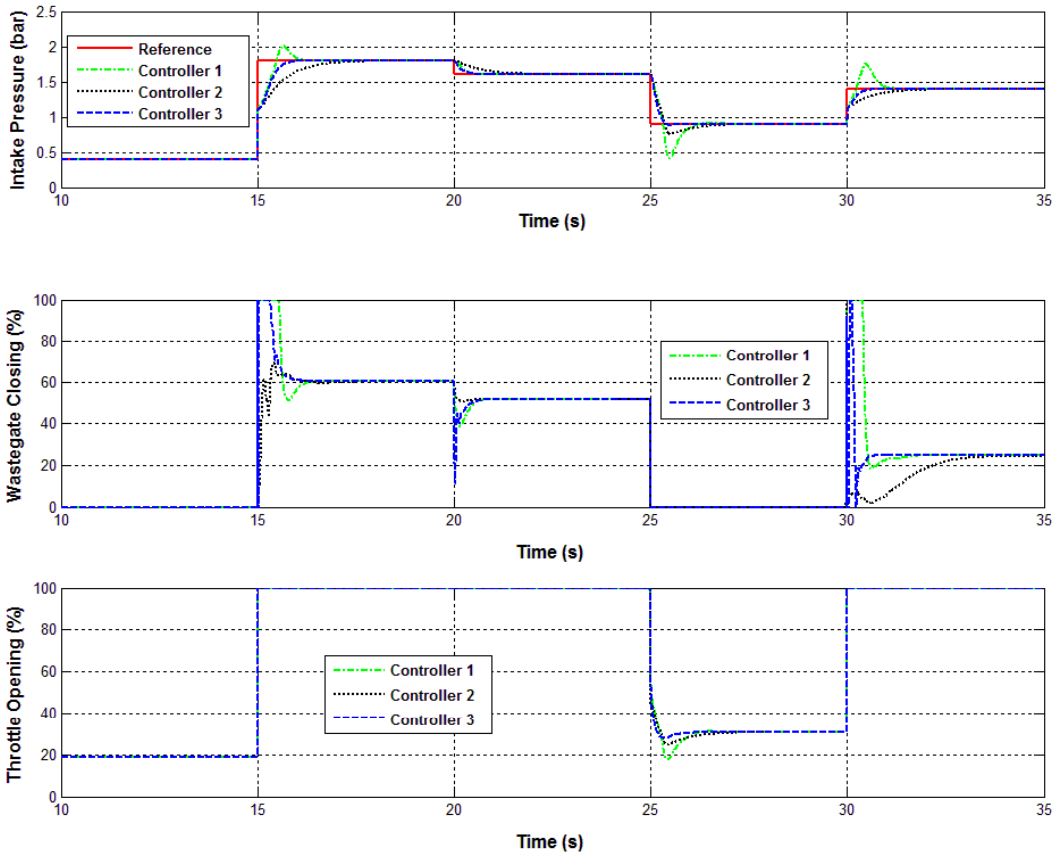

Figure 5.23. Controller performance comparison with different control approaches

6. Concluding Remarks

This chapter aims at applying a new approach to design a robust H_∞ switching controller for a turbocharged air system. To this end, some background on SI engines was first presented. Next, the modeling of a complete air system including the actuators dynamics was given in some detail. Then, after a brief state-of-the-art concerning the control of turbocharged air system, we proposed a switching control strategy for this complex system and showed how to apply the theoretical results proposed in Chapter 3 to control it. Several scenario tests were carried out in order to point out the effectiveness of our method. Finally, as highlighted, the proposed controller is easily tuned with only two parameters and achieves very satisfying performance over a wide operating range of the studied SI engine.

Chapter 6. Robust Feedback Linearization Controller for Turbocharged Air System of SI Engine: Towards a Fuel-Optimal Approach

1. Introduction

Turbocharged air system control of a SI engine is known as a very interesting problem in automotive industry. Over the years, numerous control approaches have been proposed in the literature to deal with this control problem. However, up to now, it is still an active research subject in industry. The difficulties when dealing with turbocharged air system are mainly due to the following facts. First, there are many complex nonlinearities involved in this MIMO system. Second, it is not easy to take into account the *fuel-optimal strategy* (Eriksson et al., 2002) in the control design when considering the whole system. In Chapter 5, a state-of-the-art concerning this control problem is given. We have also proposed a novel control strategy based on switching Takagi-Sugeno model which can get rid of the aforementioned difficulties. Although this powerful nonlinear controller provides satisfying closed-loop performance, it may look complex from industrial point of view. In this chapter, we propose a second control approach based on feedback linearization for the turbocharged air system which is much simpler (in the sense of control design and implementation) and can achieve practically a similar level of performance as the previous one. To the best of our knowledge, this is the second nonlinear MIMO control approach that can guarantee the stability of the whole closed-loop turbocharged air system while taking into account the *fuel-optimal strategy* after (Nguyen et al., 2012a) and the first nonlinear controller which is directly based on the complete model of this system. Furthermore, the control approach proposed in this work could also limit the costly automotive sensors and/or observers/estimators design tasks by exploiting the maximum possible available offline information. The idea is to estimate all variables needed for control design by static look-up-tables issued from the data of the test bench.

Feedback linearization provides a systematic control design procedure for nonlinear systems. The main idea is to algebraically transform nonlinear system dynamics into a (fully or partly) linear one so that the linear control techniques can be applied. However, it is well known that this technique is based on the principle of exact nonlinearity cancellation. Hence, it requires high quality models. This fact is directly related to the closed-loop robustness property with respect to model uncertainties. To this end, a new robust design dealing with model uncertainties/perturbations will be proposed. Compared to some others existing results on robust feedback linearization (Ha & Gilbert, 1987; Kravaris & Palanki, 1988; Khalil, 2002), the proposed method is not only simple and constructive but also maximizes the robustness bound of the closed-loop system through an linear matrix inequality (LMI) optimization problem (Boyd et al., 1994). Furthermore, this method may be applied to a large class of nonlinear systems which are input-output linearizable and possess stable internal dynamics. Finally, the stability analysis of internal dynamics will be also illustrated through a case study on engine control at the end of this chapter.

The chapter is organized as follows. Section 2 reviews some bases on feedback linearization. In Section 3, a new robust control design based on this technique is proposed in some detail. Section 4 is devoted to the control problem of a turbocharged air system of a SI engine. To this end, a brief description of this system is first recalled. Besides a conventional MIMO control approach, a novel idea is also proposed to take into account the strategy for minimizing the engine pumping losses (Eriksson et al., 2002) in the control design. Then, simulation results are presented to show the effectiveness of our proposed method. Finally, some concluding remarks are given in Section 5.

2. Feedback Linearization Control Technique

Control design based on feedback linearization is a vast research topic. Literature related to this control technique is very abundant; some classic books can be cited such as (Isidori, 1989; Sastry, 1999; Khalil, 2002). However, for our control purpose, only input-output linearization for control-affine MIMO nonlinear systems will be considered here.

2.1. Input-Output Linearization for MIMO System

Let consider the following MIMO nonlinear system (Isidori, 1989):

$$\begin{cases} \dot{x} = f(x) + \sum_{i=1}^{m} g_i(x) u_i \\ y = h(x) \triangleq \left[h_1(x), \ldots, h_m(x) \right]^T \end{cases} \tag{6.1}$$

where $x \in \mathbb{R}^n$, $u \in \mathbb{R}^m$ and $y \in \mathbb{R}^m$ are respectively the system state, control input and the output vectors. The vector functions $f(x)$, $g(x)$ and $h(x)$ are assumed to be sufficiently smooth in a domain $D \subset \mathbb{R}^n$. Note that throughout the chapter, the explicit time dependence of the variables is omitted.

The feedback linearization control law of the system (6.1) is given as follows:

$$\begin{aligned} u &= \begin{bmatrix} L_{g_1} L_f^{\rho_1 - 1} h_1(x) & \dots & L_{g_m} L_f^{\rho_1 - 1} h_1(x) \\ \dots & \dots & \dots \\ L_{g_1} L_f^{\rho_m - 1} h_m(x) & \dots & L_{g_m} L_f^{\rho_m - 1} h_m(x) \end{bmatrix}^{-1} \left(\begin{bmatrix} v_1 \\ \vdots \\ v_m \end{bmatrix} - \begin{bmatrix} L_f^{\rho_1} h_1(x) \\ \vdots \\ L_f^{\rho_m} h_m(x) \end{bmatrix} \right) \\ &\triangleq J^{-1}(x)\left(v - l(x)\right) \end{aligned} \tag{6.2}$$

where $[\rho_1 \dots \rho_m]^T$ is the vector of relative degree; $L_f^{\rho_i} h_i(x)$ and $L_{g_i} L_f^{\rho_i - 1} h_i(x)$ are Lie derivatives of the scalar functions $h_i(x)$, $i = 1, \dots, m$; v is a vector of new manipulated inputs. Note that the control law (6.2) is well defined in the domain $D \subset \mathbb{R}^n$ if the *decoupling matrix* $J(x)$ is non-singular at every point $x_0 \in D \subset \mathbb{R}^n$.

The new manipulated input vector v can be designed with any linear control technique, for instance a state feedback law $v = -K\xi$ designed through pole placement approach. The relative degree of the whole system (6.1) in this case is defined as:

$$\rho = \sum_{k=1}^{m} \rho_k \tag{6.3}$$

2.2. Normal Form and Internal Dynamics Analysis

The system relative degree ρ plays an important role in feedback linearization control technique. Indeed, according to its value, the three following cases are considered:

- Case 1: If $\rho = n$, then the nonlinear system (6.1) is fully feedback linearizable.
- Case 2: If $\rho < n$, then the nonlinear system (6.1) is partially feedback linearizable. In this case, there are some internal dynamics of order $(n - \rho)$. In tracking control design, it should be guaranteed that these dynamics are well behaved, i.e. stable or bounded in some sense.

- Case 3: If ρ does not exist on the domain $D \subset \mathbb{R}^n$, then the input-output linearization technique is not directly applicable. In this case, a virtual output $\tilde{y} = \tilde{h}(x)$ is generally introduced in such a manner that the new system will be feedback linearizable. This issue is not considered in this work.

The linearized system for the two first cases can be represented under the following *normal form* (Isidori, 1989):

$$\begin{cases} \dot{\xi} = A\xi + Bv \\ y = C\xi \\ \dot{\omega} = f_0(\omega, \xi, v) \end{cases} \tag{6.4}$$

where ξ and ω are respectively ρ-dimensional and $(n-\rho)$-dimensional state vector which are obtained with a suitable change of coordinates $z \triangleq [\xi \quad \omega]^T = T(x) \triangleq [T_1(x) \quad T_2(x)]^T$; the triplet (A, B, C) is in Brunovsky block canonical form; the last equation in (6.4) characterizes the internal dynamics (Isidori, 1989). It is worth noting that if the system $\dot{\omega} = f_0(\omega, \xi, v)$ is input-to-state stable, then the origin of system (6.4) is globally asymptotically stable (Khalil, 2002) if v is a stabilizing control law for the first subsystem.

In next section, we propose how to design a robust controller for the system (6.4).

3. LMI-based Robust Control Design

As mentioned above, feedback linearization is based on exact mathematical cancellation of the nonlinearities, which theoretically requires exact knowledge on systems. This is impossible for practical applications due to model uncertainties, computational errors, etc. Thus, a robust design is necessary for feedback linearization based controllers. In this section, we propose a new robust control approach to deal with model uncertainties/perturbations. Compared to the one studied in (Taniguchi & Sugeno, 2012), this new approach may be applied to a larger class of nonlinear systems. Moreover, the proposed robust controller is easily obtained by solving an LMI problem with some numerical tools (Gahinet et al., 1995; Lofberg, 2004).

For the sake of convenience, the feedback linearization control law (6.2) is rewritten as follows:

$$u(x) = \alpha(x) + \beta(x)v = \alpha(x) - \beta(x)K\xi = \alpha(x) - \beta(x)KT_1(x) \tag{6.5}$$

where $v = -K\xi$ is a stabilizing state-feedback for the linear subsystem and the corresponding terms $\alpha(x)$ and $\beta(x)$ are easily derived from (6.2), respectively. Due to model uncertainties, the real implemented feedback control law is of the form:

$$u(x) = \tilde{\alpha}(x) - \tilde{\beta}(x) K \tilde{T}_1(x) \tag{6.6}$$

where $\tilde{\alpha}(x)$, $\tilde{\beta}(x)$ and $\tilde{T}_1(x)$ are respectively approximations of $\alpha(x)$, $\beta(x)$ and $T_1(x)$. The closed-loop system (6.4) becomes (Khalil, 2002):

$$\begin{cases} \dot{\xi} = (A - BK)\xi + B\Delta(z) \\ \dot{\omega} = f_0(\omega, \xi, v) \end{cases} \tag{6.7}$$

where

$$\Delta(z) = \beta^{-1}(x)\left\{\tilde{\alpha}(x) - \alpha(x) + \left[\beta(x) - \tilde{\beta}(x)\right] K T_1(x) + \tilde{\beta}(x) K \left[T_1(x) - \tilde{T}_1(x)\right]\right\}\Big|_{x = T^{-1}(z)} \tag{6.8}$$

The uncertain term $\Delta(z)$ can be also seen as a perturbation of the nominal system $\dot{\xi} = (A - BK)\xi$.

Suppose that the internal dynamics is input-to-state stable. Next, the stability of the system:

$$\dot{\xi} = (A - BK)\xi + B\Delta(z) \tag{6.9}$$

with respect to the uncertain term $\Delta(z)$ will be studied. To this end, it is crucial to assume that the uncertain term $\Delta(z)$ satisfies the following quadratic inequality (Šiljak & Stipanović, 2000):

$$\Delta^T(z)\Delta(z) \le \delta^2 \xi^T H^T H \xi\Big|_{z=[\xi,\omega]} \tag{6.10}$$

where $\delta > 0$ is a bounding parameter and the matrix $H \in \mathbb{R}^{l \times \rho}$ is constant for a certain integer l. They both characterize the model uncertainties. In general, the matrix H is chosen according to *a priori* knowledge on system uncertainties. If no special information is available, H can be set equal to the identity matrix.

The inequality (6.10) can be rewritten as follows:

$$\begin{bmatrix} \xi \\ \Delta \end{bmatrix}^T \begin{bmatrix} -\delta^2 H^T H & 0 \\ 0 & I \end{bmatrix} \begin{bmatrix} \xi \\ \Delta \end{bmatrix} \le 0 \tag{6.11}$$

where I denotes identity matrix of appropriate dimension.

Consider the Lyapunov function $V(\xi)=\xi^T P\xi$, where $P\in\mathbb{R}^{\rho\times\rho}$, $P=P^T>0$. The derivative of V along the trajectories of (6.9) is given by:

$$\dot{V}(\xi)=\xi^T\Big((A-BK)^T P+P(A-BK)\Big)\xi+\Delta^T P\xi+\xi^T P\Delta \tag{6.12}$$

If $\dot{V}(\xi)$ is negative definite then the zero solution of the system is robustly stable. This condition is equivalent to:

$$\begin{bmatrix}\xi\\ \Delta\end{bmatrix}^T\begin{bmatrix}(A-BK)^T P+P(A-BK) & P\\ P & 0\end{bmatrix}\begin{bmatrix}\xi\\ \Delta\end{bmatrix}<0 \tag{6.13}$$

for all ξ and Δ satisfying (6.11). By the S-procedure, the condition (6.13) holds if and only if there exists a scalar $\tau>0$ such that:

$$\begin{bmatrix}(A-BK)^T P+P(A-BK)+\tau\delta^2 H^T H & P\\ P & -\tau I\end{bmatrix}<0 \tag{6.14}$$

Pre- and post-multiplying (6.14) with the matrix $diag\left[\tau P^{-1}, I\right]$ and then using the change of variable $Y=\tau P^{-1}>0$, the condition (6.14) is equivalent to:

$$\begin{bmatrix}(A-BK)Y+Y(A-BK)^T+\delta^2 YH^T HY & I\\ I & -I\end{bmatrix}<0 \tag{6.15}$$

By Schur complement lemma, the condition (6.15) is equivalent to:

$$\begin{bmatrix}(A-BK)Y+Y(A-BK)^T & I & YH^T\\ I & -I & 0\\ HY & 0 & -\gamma I\end{bmatrix}<0 \tag{6.16}$$

where $\gamma\triangleq 1/\delta^2$. Using the change of variable $L\triangleq KY$, the control design can be formulated as an LMI problem in Y, L and γ as follows:

$$\begin{bmatrix} AY + YA^T - BL - L^T B^T & I & YH^T \\ I & -I & 0 \\ HY & 0 & -\gamma I \end{bmatrix} < 0 \tag{6.17}$$

As highlighted in (Šiljak & Stipanović, 2000), the system (6.9) satisfies the *matching condition*, i.e. the input matrix B is identical for the control input u and the uncertain term Δ. This fact implies that for any arbitrarily large uncertainty Δ, there always exists a stabilizing feedback v with its arbitrarily large feedback gain matrix K. Therefore, to prevent the controller gains that would be unacceptably high for practical applications, the amplitude of the entries of K should be constraint in the optimization problem. It can be accomplished by including the following LMIs:

$$\begin{bmatrix} -\kappa_L I & L^T \\ L & -I \end{bmatrix} < 0; \quad \begin{bmatrix} Y & I \\ I & \kappa_Y I \end{bmatrix} > 0; \quad \kappa_L > 0; \quad \kappa_Y > 0. \tag{6.18}$$

Indeed, the condition (6.18) implies that $K^T K < \kappa_L \kappa_Y^2 I$ (Šiljak & Stipanović, 2000).

Moreover, in order to guarantee some desired prescribed robustness bound $\overline{\delta}$, the following LMI conditions can be also included:

$$\gamma - 1/\overline{\delta}^2 < 0 \tag{6.19}$$

The above development can be summarized by the following theorem.

Theorem 6.1. Given a real positive number $\overline{\delta}$. If there exists matrices $Y > 0$, L, positive real numbers γ, κ_L, κ_Y such that the following LMI optimization problem is feasible:

$$\text{minimize} \quad \lambda_1 \gamma + \lambda_2 \kappa_L + \lambda_3 \kappa_Y \tag{6.20}$$

subject to LMI conditions (6.17), (6.18), (6.19).

Then, the closed-loop system (6.9) is robustly stable and the state feedback control law is defined as $v = -K\xi$ where $K \triangleq LY^{-1}$.

♦

The weighting factors λ_1, λ_2 and λ_3 are chosen according to the desired trade-off between the guaranteed robustness bound $\bar{\delta}$ and the size of the stabilizing gain matrix K. The LMI optimization problem can be solved with some numerical toolboxes, e.g. (Gahinet et al., 1995; Lofberg, 2004).

In the next section, the effectiveness of this method will be illustrated through an automotive control application.

4. Case Study of SI Engine: Turbocharged Air System Control

The results developed in previous sections will be now applied to control the turbocharged air system of a SI engine which is illustrated in Figure 6.1.

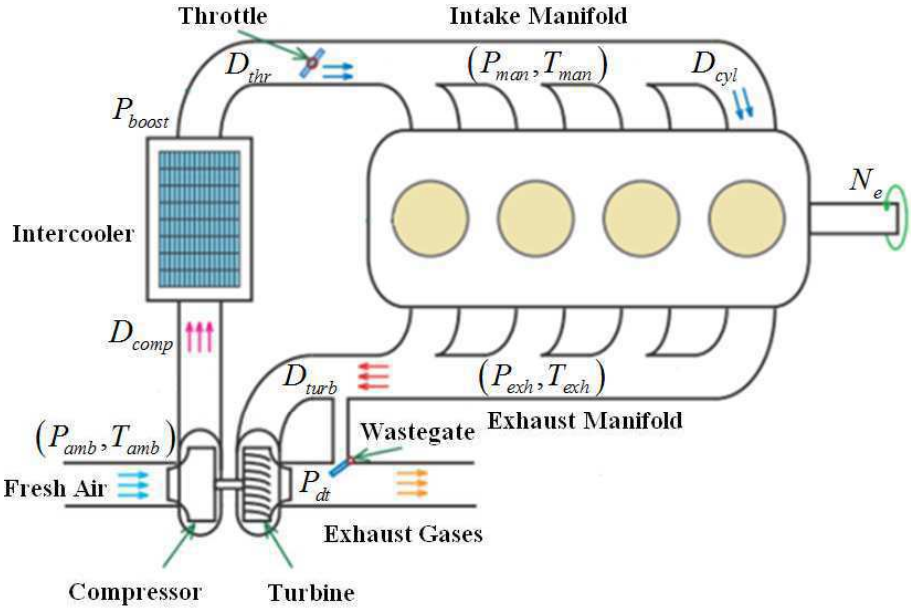

Figure 6.1. Schematic of a turbocharged SI engine

4.1. Turbocharged Air System of SI Engine: a Very Brief Description

In this subsection, a very brief description of a turbocharged air system will be recalled so that the chapter is self-contained, please refer to Chapter 5 for more information. The dynamical model of this system is composed by three main dynamics:

- Intake pressure dynamics:

$$\frac{dP_{man}}{dt} = -\eta_{vol}\frac{V_{cyl}}{V_{man}}\frac{N_e}{30}P_{man} + \frac{P_{boost}\sqrt{RT_{man}}}{V_{man}}\Phi_{thr}\left(\Pi^*_{thr}\right)u_{thr} \tag{6.21}$$

where $\Phi\left(\Pi_{thr}^{*}\right)=\sqrt{\frac{2\gamma}{\gamma-1}\left(\Pi_{thr}^{*\,\frac{2}{\gamma}}-\Pi_{thr}^{*\,\frac{\gamma+1}{\gamma}}\right)}$ with $\Pi_{thr}^{*}\triangleq\max\left(\frac{P_{man}}{P_{boost}},\left(\frac{2}{\gamma+1}\right)^{\frac{\gamma}{\gamma-1}}\right)$ and the volumetric efficiency $\eta_{vol}\triangleq\mathrm{LUT}_{\eta_{vol}}\left(N_e,P_{man}\right)$ is given by LUT.

- Exhaust pressure dynamics:

$$\frac{dP_{exh}}{dt}=\frac{RT_{exh}}{V_{exh}}\left(\left(1+\frac{1}{\lambda_s}\right)\eta_{vol}\frac{P_{man}V_{cyl}}{RT_{man}}\frac{N_e}{30}-D_{turb}-\Phi_{wg}\left(\Pi_{wg}^{*}\right)\frac{P_{exh}}{\sqrt{RT_{exh}}}u_{wg}\right) \tag{6.22}$$

where $\Phi\left(\Pi_{wg}^{*}\right)=\sqrt{\frac{2\gamma}{\gamma-1}\left(\Pi_{wg}^{*\,\frac{2}{\gamma}}-\Pi_{wg}^{*\,\frac{\gamma+1}{\gamma}}\right)}$ with $\Pi_{wg}^{*}\triangleq\max\left(\frac{P_{dt}}{P_{exh}},\left(\frac{2}{\gamma+1}\right)^{\frac{\gamma}{\gamma-1}}\right)$ and the gas flow through the turbine $D_{turb}\triangleq\mathrm{LUT}_{D_{turb}}\left(N_{tc},\frac{P_{dt}}{P_{exh}}\right)$ is given by LUT. Another turbine gas flow model based on the standard equation for compressible flow across an orifice is also available in (Eriksson, 2007).

- Turbocharger dynamics:

$$\frac{d}{dt}\left(\frac{1}{2}J_{tc}N_{tc}^{2}\right)=\mathbb{P}_{turb}-\mathbb{P}_{comp} \tag{6.23}$$

where the powers of the turbine and the compressor are given by:

$$\begin{cases}\mathbb{P}_{turb}=D_{turb}C_pT_{exh}\eta_{turb}\left(1-\Pi_{turb}^{\frac{1-\gamma}{\gamma}}\right)\\ \mathbb{P}_{comp}=D_{comp}C_pT_{amb}\dfrac{1}{\eta_{comp}}\left(\Pi_{comp}^{\frac{\gamma-1}{\gamma}}-1\right)\end{cases} \tag{6.24}$$

In expressions (6.24), the following quantities are given by LUTs $\eta_{turb}\triangleq\mathrm{LUT}_{\eta_{turb}}\left(N_{tc},\frac{P_{dt}}{P_{exh}}\right)$, $\Pi_{comp}\triangleq\mathrm{LUT}_{\Pi_{comp}}\left(N_{tc},D_{comp}\right)$ and $\eta_{comp}\triangleq\mathrm{LUT}_{\eta_{comp}}\left(N_{tc},\frac{P_{boost}}{P_{amb}}\right)$. From (6.23)and (6.24), the turbocharger dynamics can be rewritten as follows:

$$\frac{d}{dt}\left(\frac{1}{2}J_{tc}N_{tc}^2\right)=D_{turb}C_pT_{exh}\eta_{turb}\left(1-\Pi_{turb}^{\frac{1-\gamma}{\gamma}}\right)-D_{comp}C_pT_{amb}\frac{1}{\eta_{comp}}\left(\Pi_{comp}^{\frac{\gamma-1}{\gamma}}-1\right) \tag{6.25}$$

Finally, from (6.21), (6.22) and (6.25), the dynamical model of turbocharged air system is given as:

$$\begin{cases}\dfrac{dP_{man}}{dt}=-\eta_{vol}\dfrac{V_{cyl}}{V_{man}}\dfrac{N_e}{30}P_{man}+\dfrac{P_{boost}\sqrt{RT_{man}}}{V_{man}}\Phi_{thr}\left(\Pi_{thr}^*\right)u_{thr}\\ \dfrac{dP_{exh}}{dt}=\dfrac{RT_{exh}}{V_{exh}}\left(\left(1+\dfrac{1}{\lambda_s}\right)\eta_{vol}\dfrac{P_{man}V_{cyl}}{RT_{man}}\dfrac{N_e}{30}-D_{turb}-\Phi_{wg}\left(\Pi_{wg}^*\right)\dfrac{P_{exh}}{\sqrt{RT_{exh}}}u_{wg}\right)\\ \dfrac{d}{dt}\left(\dfrac{1}{2}J_{tc}N_{tc}^2\right)=D_{turb}C_pT_{exh}\eta_{turb}\left(1-\Pi_{turb}^{\frac{1-\gamma}{\gamma}}\right)-D_{comp}C_pT_{amb}\dfrac{1}{\eta_{comp}}\left(\Pi_{comp}^{\frac{\gamma-1}{\gamma}}-1\right)\end{cases} \tag{6.26}$$

The state-of-the-art concerning the control issue of turbocharged air system can be found in Chapter 5. Here, we would like to emphasize some particular points directly related to our proposed solution:

- This system is highly nonlinear and apparently complex for control design.
- There are two control inputs (throttle and wastegate) and only one output of interest, the intake pressure, which is directly related to the engine torque.
- The relation between the wastegate and the intake pressure is not direct.
- LUTs are widely used in industry, especially for automotive applications, to approximate the nonlinear models of complex physical phenomena. Again, it is not surprising that there are many LUTs in the model of the turbocharged air system.
- For this system, it is necessary to remind that the most commonly available sensors on series production vehicles are found in the intake side of the engine, that are: the pressure and temperature in the upstream of the compressor $\left(P_{amb},T_{amb}\right)$, the boost pressure P_{boost}, the mass air flow through the compressor D_{comp}, the intake pressure and temperature $\left(P_{man},T_{man}\right)$ and the engine speed N_e.

4.2. MIMO Controller Design

First of all, it is very important to highlight the following fact. For almost controllers existing in actual literature, not only aforementioned available measures of engine intake side but also several other signals coming from the exhaust side are needed for controller implementation. These latter signals, i.e. P_{exh}, T_{exh}, P_{dt}, N_{tc}, are not measured in series production vehicles and usually assumed to be given by some observers. To get rid of this assumption, in this work, these variables will be

estimated by their static LUTs issued from the data measured in steady-state conditions in the test bench. As a consequence, the number of sensors or/and complex observers/estimators could be limited. Concretely, the following LUTs will be constructed for control implementation:

$$\begin{cases} P_{exh} = \mathrm{LUT}_{P_{exh}}\left(N_e, P_{man}\right); \quad T_{exh} = \mathrm{LUT}_{T_{exh}}\left(N_e, D_{cyl}\right) \\ P_{dt} = \mathrm{LUT}_{P_{dt}}\left(N_e, D_{cyl}\right); \quad N_{tc} = \mathrm{LUT}_{N_{tc}}\left(\Pi_{comp}, D_{comp}\right) \end{cases} \tag{6.27}$$

Note from (6.27) that all the inputs of respective LUTs P_{exh} , T_{exh} , P_{dt} , N_{tc} can be measured/computed with available sensors. In fact, the approximations in (6.27) are reasonable since SI engines operate at stoichiometric conditions which implies that all exhaust variables are highly correlated to the in-cylinder air mass flow (or intake pressure).

In what follows, we focus on the control design. To this end, apart from the output of interest $y_{man} \triangleq P_{man}$, let us virtually introduce the second output $y_{exh} \triangleq P_{exh}$ to facilitate the control design task. Note that the goal is only to track the intake pressure reference $P_{man,ref}$ and in reality, we do not have the exhaust pressure reference $P_{exh,ref}$. However, by means of LUT in (6.27), we can impose that $P_{exh,ref} = \mathrm{LUT}_{P_{exh}}\left(N_e, P_{man,ref}\right)$ and then if P_{exh} converges to $P_{exh,ref}$, it implicitly makes P_{man} converge to $P_{man,ref}$. As a consequent, both outputs P_{man} and P_{exh} are used with the same control purpose, i.e. intake pressure reference tracking. That is also the reason why $y_{exh} \triangleq P_{exh}$ is called *virtual output*. In order to propose a novel control method for the studied turbocharged air system, let us first consider the two pressure dynamics in (6.21) and (6.22). For brevity, these two equations are rewritten in the following form:

$$\begin{cases} \dot{P}_{man} = K_{man}\left(D_{thr} - D_{cyl}\right) \triangleq f_{thr} + g_{thr}u_{thr} \\ \dot{P}_{exh} = K_{exh}\left(K_{fuel}D_{cyl} - D_{turb} - D_{wg}\right) \triangleq f_{wg} + g_{wg}u_{wg} \\ y_{man} \triangleq P_{man} \\ y_{exh} \triangleq P_{exh} \end{cases} \tag{6.28}$$

where

$$\begin{cases} K_{man} \triangleq \dfrac{RT_{man}}{V_{man}}; \quad K_{exh} \triangleq \dfrac{RT_{exh}}{V_{exh}}; \quad K_{fuel} \triangleq \left(1+\dfrac{1}{\lambda_s}\right); \quad D_{cyl} \triangleq \eta_{vol}\dfrac{V_{cyl}}{V_{man}}\dfrac{N_e}{30}P_{man} \triangleq K_{cyl}P_{man}; \\ f_{thr} \triangleq -K_{man}D_{cyl}; \quad g_{thr} \triangleq K_{man}\dfrac{P_{boost}}{\sqrt{RT_{man}}}\Phi_{thr}\left(\Pi^*_{thr}\right); \\ f_{wg} \triangleq K_{exh}\left(K_{fuel}D_{cyl}-D_{turb}\right); \quad g_{wg} \triangleq -K_{exh}\dfrac{P_{exh}}{\sqrt{RT_{exh}}}\Phi_{wg}\left(\Pi^*_{wg}\right). \end{cases} \tag{6.29}$$

Now, feedback linearization technique will be applied to control the system (6.28). For that, let us compute the time derivatives of the outputs:

$$\begin{cases} \dot{y}_{man} = \dot{P}_{man} = f_{thr} + g_{thr}u_{thr} = v_{man} \\ \dot{y}_{exh} = \dot{P}_{exh} = f_{wg} + g_{wg}u_{wg} = v_{exh} \end{cases} \tag{6.30}$$

It can be observed that the two control inputs u_{thr}, u_{wg} appear respectively in $\dot{y}_{man}$, $\dot{y}_{exh}$; the signals v_{man} and v_{exh} are two new manipulated inputs. By using integral structure for tracking control purpose, the following linearized system:

$$\begin{cases} \dot{y}_{man} = v_{man} \\ \dot{y}_{exh} = v_{exh} \\ \dot{x}_{\text{int}} = y_{man,ref} - y_{man} \end{cases} \tag{6.31}$$

is straightforwardly derived from the system (6.28) with the following feedback linearization control laws:

$$\begin{cases} u_{thr} = -\dfrac{f_{thr}}{g_{thr}} + \dfrac{1}{g_{thr}}v_{man} \\ u_{wg} = -\dfrac{f_{wg}}{g_{wg}} + \dfrac{1}{g_{wg}}v_{exh} \end{cases} \tag{6.32}$$

Let us now define $x \triangleq \begin{bmatrix} y_{man} & y_{exh} & x_{\text{int}} \end{bmatrix}^T$, $v \triangleq \begin{bmatrix} v_{man} & v_{exh} \end{bmatrix}^T$ and suppose that the system (6.28) is subject to modeling errors $\Delta(x)$ caused by nonlinearities f_{thr}, g_{thr}, f_{wg}, g_{wg} and the approximation by using LUTs. Then, the linearized system (6.31) is rewritten as:

$$\dot{x} = \begin{pmatrix} 0 & 0 & 0 \\ 0 & 0 & 0 \\ -1 & 0 & 0 \end{pmatrix} x + \begin{pmatrix} 1 & 0 \\ 0 & 1 \\ 0 & 0 \end{pmatrix} v + \begin{pmatrix} 0 \\ 0 \\ 1 \end{pmatrix} y_{man,ref} + \Delta(x) \tag{6.33}$$

As stated in Section 3, we assume that $\Delta(x) \le \delta^2 x^T H^T H x$. Theorem 6.1 is now applied to design both manipulated inputs v_{man} and v_{exh}. To this end, let us set $H = I$, $\lambda_1 = 1$, $\lambda_2 = \lambda_3 = 0$ and $\bar{\delta} = 0.9$, then we obtain the following control law:

$$v = -Kx = -\begin{bmatrix} 110.3 & 0 & -4052 \\ 0 & 48.9 & 0 \end{bmatrix} x \tag{6.34}$$

and $\delta = 0.9983$, as expected, is larger than prescribed value of $\bar{\delta}$.

The tracking control problem has been solved above accounting only for a part of the closed-loop system. The stability analysis of the internal dynamics is necessary to make sure that the state N_{tc}^2 is well behaved. To do this, the turbocharger dynamics (6.25) is rewritten in the following form:

$$\frac{d}{dt}\left(N_{tc}^2\right) = K_{turb} D_{turb} - K_{comp} D_{comp} \tag{6.35}$$

where

$$K_{turb} \triangleq \frac{2}{J_{tc}} C_p T_{exh} \eta_{turb} \left(1 - \Pi_{turb}^{\frac{1-\gamma}{\gamma}}\right); \quad K_{comp} \triangleq \frac{2}{J_{tc}} C_p T_{amb} \frac{1}{\eta_{comp}} \left(\Pi_{comp}^{\frac{\gamma-1}{\gamma}} - 1\right) \tag{6.36}$$

Furthermore, from (6.28)and (6.30), one gets:

$$D_{turb} = K_{fuel} D_{cyl} - D_{wg} - \frac{v_{exh}}{K_{exh}} \tag{6.37}$$

It follows from (6.35) and (6.37) that:

$$\frac{d}{dt}\left(N_{tc}^2\right) = -K_{turb} D_{wg} - K_{comp} D_{comp} + K_{turb} K_{fuel} D_{cyl} - \frac{K_{turb}}{K_{exh}} v_{exh} \tag{6.38}$$

Note that $P \triangleq \begin{bmatrix} P_{man} & P_{exh} \end{bmatrix}^T$ can be seen as the input vector of system(6.38). Then, one can deduce:

$$\begin{aligned} \frac{d}{dt}\left(N_{tc}^2\right) &< \left(K_{turb} K_{fuel} K_{cyl} P_{man} + \frac{K_{turb}}{K_{exh}} K_{(2,2)} P_{exh}\right) - K_{comp} D_{comp} \\ &\le \sqrt{\left(K_{turb} K_{fuel} K_{cyl}\right)^2 + \left(\frac{K_{turb}}{K_{exh}} K_{(2,2)}\right)^2} \|P\| - K_{comp} D_{comp} \triangleq \alpha_1(\cdot)\|P\| - \beta_1\left(N_{tc}^2\right) \end{aligned} \tag{6.39}$$

Since $\alpha_1(\cdot)$ is bounded and the function $\beta_1(\cdot)$ is of class $\mathcal{K}^\infty$, its curve form is depicted in Figure 6.2. In addition, the dynamics of N_{tc}^2 does not directly depend on the real control inputs u_{thr} and u_{wg} of the turbocharged air system Then, it can be deduced that the system (6.35) is always input-to-state stable with respect to its input vector P (Sontag & Wang, 1995).

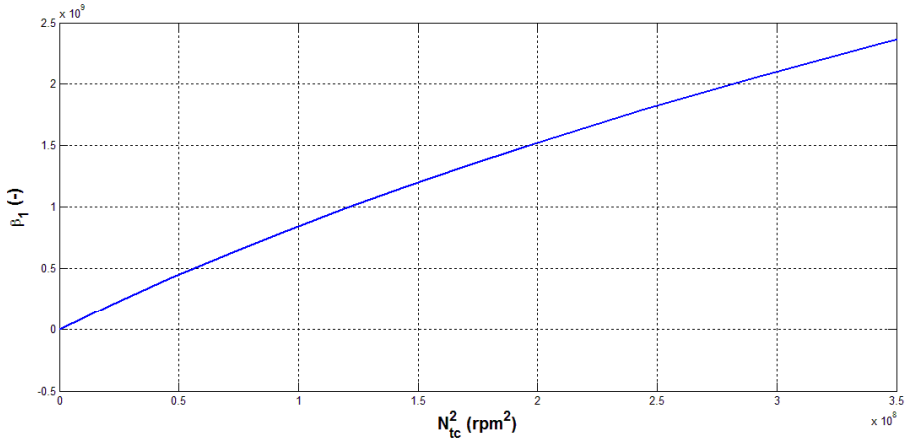

Figure 6.2. $\beta_1\left(N_{tc}^2\right)$ function

In what follows, the controller designed in this subsection will be called *Conventional MIMO controller*.

4.3. Fuel-Optimal Control Strategy

Until now, we have designed in this work *Conventional MIMO controller* with two inputs: throttle, wastegate and two outputs: intake pressure, exhaust pressure for the whole engine operating zone. However, from the viewpoint of energy efficiency, this controller is not *optimal* in the sense of energy losses minimization. Indeed, it is well-known in automotive industry that the wastegate should be opened as much as possible at a given operating point to minimize the pumping losses (Eriksson et al., 2002). Several comments need to be made regarding this *fuel-optimal* concept. First, this concept generally leads to the control strategy proposed in Chapter 5, i.e. in low load zone, only the throttle is used to track the intake pressure, the wastegate is widely open and in high load zone, the wastegate is solely activated to control the pressure and the throttle is widely open in this case. Second, this latter control strategy offers many advantages concerning the fuel economy benefits and also the control design simplification (only one actuator is controlled at a time). Third, as previously mentioned, the relation between the wastegate and the intake pressure is not direct. Then, engine torque response with respect to the wastegate is slower than to the throttle. As a consequence, if only the wastegate is used to control the intake pressure in high load zone, it may be overcharged in some

cases. In order to overcome this eventual difficulty while taking fully into account the above fuel-optimal strategy, we propose in this subsection the so-called *Fuel-optimal controller* for turbocharged air system of a SI engine. This novel controller is directly derived from *Conventional MIMO controller* and they both have the same control law given in (6.34). The idea is presented in the sequel.

Let us consider again the model (6.28):

$$\begin{cases} \dot{P}_{man} = K_{man}\left(D_{thr} - D_{cyl}\right) \triangleq f_{thr} + g_{thr}u_{thr} = v_{man} \\ \dot{P}_{exh} = K_{exh}\left(K_{fuel}D_{cyl} - D_{turb} - D_{wg}\right) \triangleq f_{wg} + g_{wg}u_{wg} = v_{exh} \\ y_{man} \triangleq P_{man} \\ y_{exh} \triangleq P_{exh} \end{cases} \tag{6.40}$$

It can be deduced from the second equation of (6.40) that:

$$D_{cyl} = \frac{v_{exh}}{K_{exh}K_{fuel}} + \frac{D_{turb}}{K_{fuel}} + \frac{D_{wg}}{K_{fuel}} \tag{6.41}$$

With this new expression of the in-cylinder mass air flow, the intake pressure dynamics can be also rewritten as:

$$\dot{P}_{man} = K_{man}\left(D_{thr} - \frac{v_{exh}}{K_{exh}K_{fuel}} - \frac{D_{turb}}{K_{fuel}} - \frac{D_{wg}}{K_{fuel}}\right)$$

or (6.42)

$$\dot{P}_{man} = g_{thr}u_{thr} - \frac{K_{man}}{K_{exh}K_{fuel}}v_{exh} - \frac{K_{man}}{K_{fuel}}D_{turb} + \frac{K_{man}}{K_{exh}K_{fuel}}g_{wg}u_{wg} = v_{man}$$

Note from the expression (6.42) that the intake pressure can be controlled either by the throttle or the wastegate. The novel *Fuel-optimal controller* is directly derived from this expression. To this end, the whole engine operating range is divided into three zones according to two predefined intake pressure thresholds $P_{man,1}$ and $P_{man,2}$. Each operating zone has its own actuator scheduling strategy as described below:

- *Zone 1* (low load zone $P_{man} \le P_{man,1}$): The wastegate is widely open and the throttle is solely used to track the intake pressure reference. Let $S_{wg,\max}$ be the maximal opening section of the wastegate. The implemented actuator control laws are in this case:

$$\begin{cases} u_{thr} = \dfrac{1}{g_{thr}}\left(\dfrac{K_{man}}{K_{exh}K_{fuel}} v_{exh} + \dfrac{K_{man}}{K_{fuel}} D_{turb} - \dfrac{K_{man}}{K_{exh}K_{fuel}} g_{wg} S_{wg,\max} + v_{man} \right) \\ u_{wg} = S_{wg,\max} \end{cases} \tag{6.43}$$

- *Zone 2* (middle load zone $P_{man,1} < P_{man} < P_{man,2}$): Both throttle and wastegate are simultaneously used to control the intake pressure. In this case, the implemented actuator control laws are exactly the feedback linearization laws in (6.32), which are recalled here:

$$\begin{cases} u_{thr} = -\dfrac{f_{thr}}{g_{thr}} + \dfrac{1}{g_{thr}} v_{man} \\ u_{wg} = -\dfrac{f_{wg}}{g_{wg}} + \dfrac{1}{g_{wg}} v_{exh} \end{cases} \tag{6.44}$$

- *Zone 3* (high load zone $P_{man} \geq P_{man,2}$): The throttle is fully opened and only the wastegate is activated to control the intake pressure which is approximated by the boost pressure P_{boost}. The implemented actuator control laws are:

$$\begin{cases} u_{thr} = S_{thr,\max} \\ u_{wg} = \dfrac{K_{exh}K_{fuel}}{K_{man}g_{thr}} \left(\dfrac{K_{man}}{K_{exh}K_{fuel}} v_{exh} + \dfrac{K_{man}}{K_{fuel}} D_{turb} - g_{thr} S_{thr,\max} + v_{man} \right) \end{cases} \tag{6.45}$$

where $S_{thr,\max}$ is the maximal opening section of the throttle.

Several remarks can be reported for this actuator scheduling strategy. First, the new manipulated input vector $v \triangleq \begin{bmatrix} v_{man} & v_{exh} \end{bmatrix}^T$ is kept to be the same for all three zones. Second, when the wastegate is saturated in Zone 1, the exhaust pressure dynamics can be rewritten as follows:

$$\begin{aligned} \dot{P}_{exh} &= K_{exh}K_{fuel}K_{cyl}P_{man} - K_{exh}\left(\frac{P_{exh}}{\sqrt{RT_{exh}}} \Phi_{wg}\left(\Pi_{wg}^*\right) S_{wg,\max} + D_{turb} \right) \\ &< \left(K_{exh}K_{fuel}K_{cyl} \right) P_{man} - \left(\frac{K_{exh}}{\sqrt{RT_{exh}}} \Phi_{wg}\left(\Pi_{wg}^*\right) S_{wg,\max} \right) P_{exh} \triangleq \alpha_2(\cdot) P_{man} - \beta_2(\cdot) P_{exh} \end{aligned} \tag{6.46}$$

Note that the functions $\alpha_2(\cdot)$ and $\beta_2(\cdot)$ are bounded, then the exhaust pressure dynamics is always input-to-state stable with respect to P_{man}. Third, when the throttle is saturated in Zone 3, the intake pressure dynamics in (6.40) can be expressed as:

$$\begin{aligned}\dot{P}_{man} &= \frac{P_{boost}\sqrt{RT_{man}}}{V_{man}}\Phi_{thr}\left(\Pi^{*}_{thr}\right)S_{thr,\max} - \eta_{vol}\frac{V_{cyl}}{V_{man}}\frac{N_e}{30}P_{man} \\ &\triangleq \alpha_3(\cdot)P_{boost} - \beta_3(\cdot)P_{man}\end{aligned} \tag{6.47}$$

Since $\alpha_3(\cdot)$ and $\beta_3(\cdot)$ are bounded and it is known that P_{boost} is a strictly increasing function of P_{exh}, then the intake pressure dynamics is also input-to-state stable with respect to P_{exh}.Fourth, it can be concluded from the above remarks that if the intake pressure tracking performance is guaranteed, then all other variables of the turbocharged air system (6.26) will be well behaved in spite of the fact that the engine operating range is divided into three zones. Fifth, the model-based *Fuel-optimal controller* is based on a "dummy" switching strategy because no switching model has been used in this approach. Sixth, the pressure thresholds $P_{man,1}$ and $P_{man,2}$ separating the three zones are "freely" chosen thanks to the propriety of the above third remark. However, the values of $P_{man,1}$, $P_{man,2}$ are usually chosen very close for engine efficiency benefits.

It is worth noting that *Fuel-optimal controller* is different from other existing approaches in the literature. As the approach proposed in Chapter 5, this novel controller is a MIMO nonlinear controller which can guarantee the closed-loop stability of the whole turbocharged air system. However, the novel *Fuel-optimal controller* is much simpler and the middle-load zone (Zone 2) is very easily introduced to improve the torque response at high load while maintaining the maximum possible the advantage of *fuel-optimal* concept in (Eriksson et al., 2002). The scheduling strategy of *Fuel-optimal controller* has also appeared in (Gorzelic et al., 2012). However, the control approach in (Gorzelic et al., 2012) is based on a decentralized linear scheduling PI controller. In addition, the throttle is only *passively* activated in Zone 2, that is, the throttle control is maintained at a constant value obtained from calibration for each operating point of the engine. Moreover, the authors did not show how to choose the intake pressure thresholds and in particular how this choice will effect on the control design. Compared with the control approach in (Moulin & Chauvin, 2011) which is also based on feedback linearization, our controller does not need any model simplification task, e.g. neglecting pressure dynamics with respect to turbocharger dynamics according to singular perturbation theory and approximating the turbocharger square speed as a linear function of the boost pressure (note also that the same simplification procedure is carried out for the approach in Chapter 5). Moreover, in (Moulin & Chauvin, 2011), the wastegate and the throttle are separately controlled and the approach cannot take into account the mid-load zone.

4.4. Simulation Results and Analysis

Hereafter, a series of trials are performed on an engine simulator designed under commercial AMESim platform to show the effectiveness of the proposed method for both cases: *Conventional MIMO controller* and *Fuel-optimal controller*. For the sake of clarity, the two commands (throttle, wastegate) are normalized. The control inputs constraints become: $0 \le \overline{u}_{thr}, \overline{u}_{wg} \le 100\%$. When $\overline{u}_{thr} = 100\%$ (resp. $\overline{u}_{wg} = 0\%$), it means that the throttle (resp. wastegate) is fully open. On the reverse, when $\overline{u}_{thr} = 0\%$ (resp. $\overline{u}_{wg} = 100\%$), the throttle (resp. wastegate) is fully closed. Before starting, note that the proposed controller is easily tuned with only one parameter, the desired robustness bound $\overline{\delta}$ which is the same for all following simulations. The pressure thresholds are chosen as $P_{man,1} = 0.9$ bar and $P_{man,2} = 1.2$ bar.

4.4.1. Conventional MIMO controller versus Fuel-optimal controller

Figure 6.3 and Figure 6.4 represent the intake pressure tracking performance and the corresponding actuator commands for *Conventional MIMO controller* and *Fuel-optimal controller*, respectively. Several comments can be reported as follows. First, *Conventional MIMO controller* simultaneously uses both actuators to track the intake pressure while these actuators are "optimally" scheduled by the strategy described in subsection 4.3 with *Fuel-optimal controller*. Second, the wastegate is opened very little with *Conventional MIMO controller* so that the boost potential of the turbocharger can be fully exploited. Hence, the closed-loop time response with this controller is faster than the one of *Fuel-optimal controller* in middle and high load zones. Third, although *Conventional MIMO controller* can be used to improve the torque response (drivability), this controller is not optimal in terms of fuel consumption compared with *Fuel-optimal controller* as pointed out in Figure 6.5. The pumping losses with *Fuel-optimal controller* are almost lower than the ones with *Conventional MIMO controller* at every time. Moreover, the pumping losses with *Fuel-optimal controller* are insignificant when the intake pressure is high.

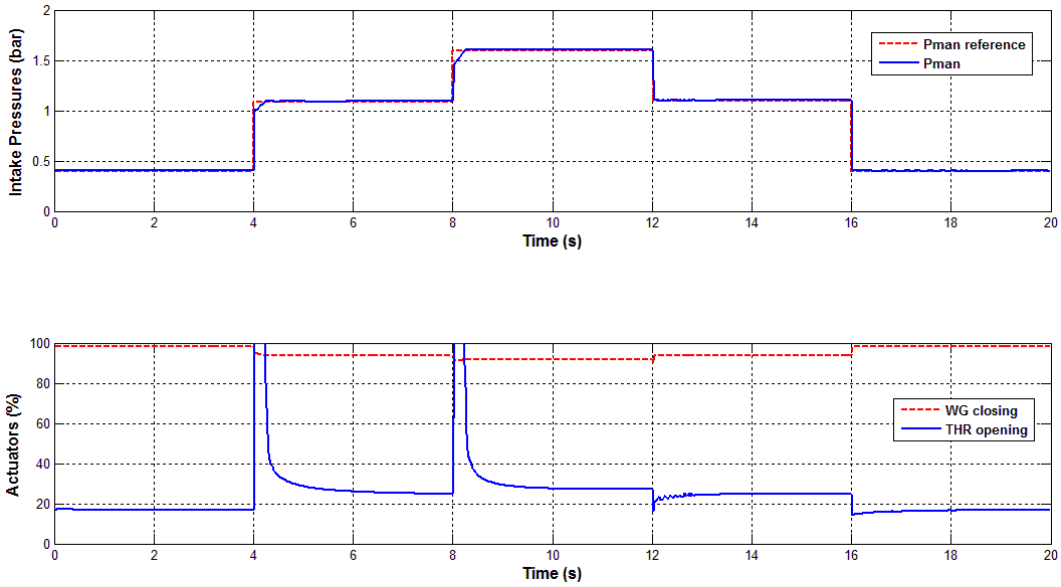

Figure 6.3. Pressure tracking performance (up) and corresponding actuator commands (bottom) with *Conventional MIMO controller* at $N_e = 2000$ rpm

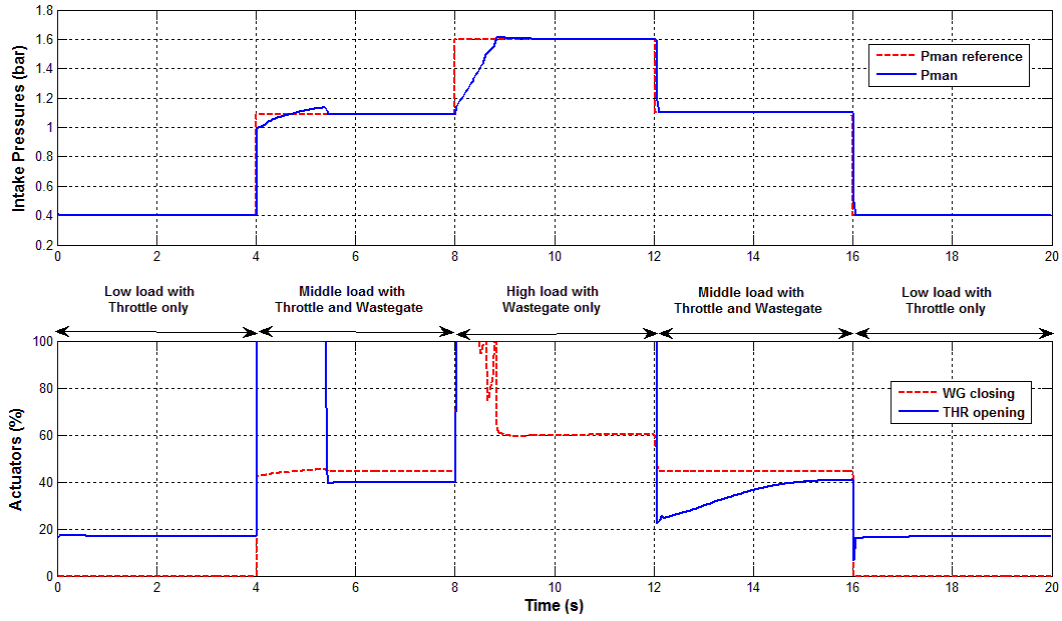

Figure 6.4. Pressure tracking performance (up) and corresponding actuator commands (bottom) with *Fuel-optimal controller* at $N_e = 2000$ rpm

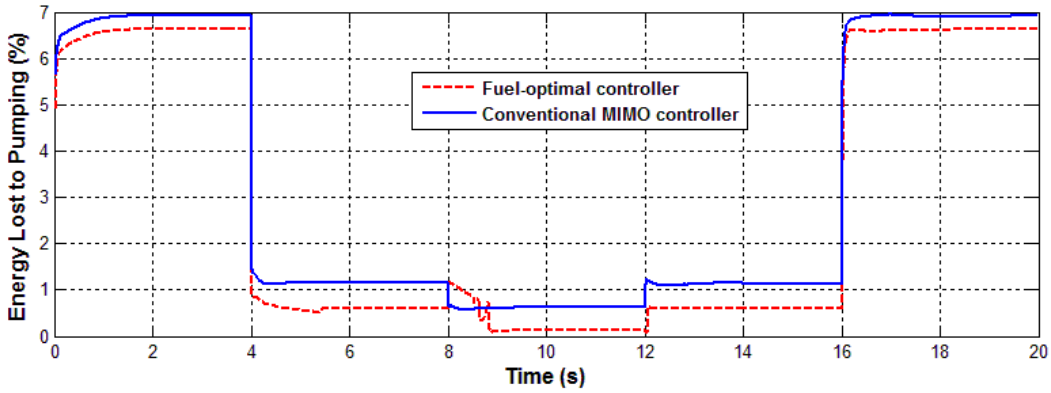

Figure 6.5. Comparison of engine pumping losses between *Conventional MIMO controller* and *Fuel-optimal controller* at $N_e = 2000$ rpm

Figure 6.6 shows the comparison, in the case of *Fuel-optimal controller*, between the exhaust pressure given by the simulator AMESim and its static look-up-table model, i.e. $P_{exh} = \mathrm{LUT}_{P_{exh}}\left(N_e, P_{man}\right)$ which is used to compute the controller. It can be noticed that although some higher dynamics are missing and there are some slight static errors, the intake pressure tracking performance of both controller is very satisfying.

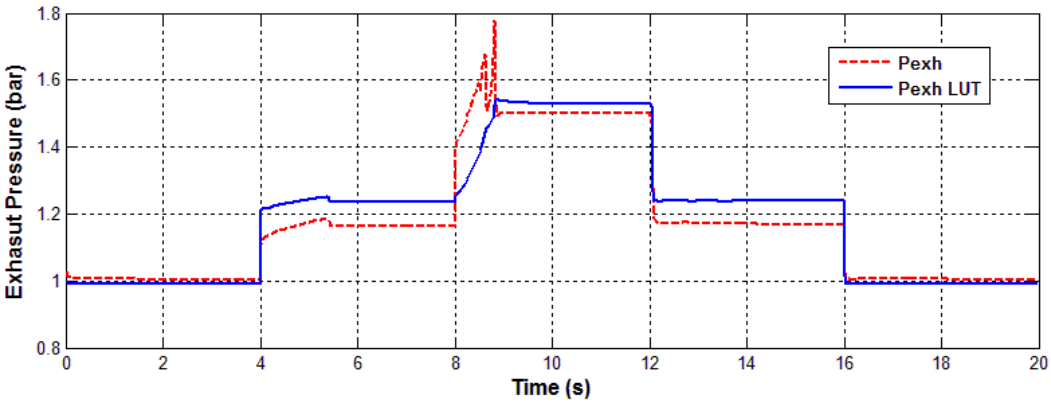

Figure 6.6. Comparison between the exhaust pressure given by the simulator AMESim (solid) and its static LUT model (dotted) at $N_e = 2000$ rpm

Since the goal of this work is to design a controller minimizing the energy losses, only results with the *Fuel-optimal controller* will be presented in the rest of this chapter.

4.4.2. Fuel-optimal controller performance at different engine speeds

The trajectory tracking of the intake pressure at different engine speeds is shown in Figure 6.7. The following comments need to be made regarding these results. First, the tracking performance is

very satisfying over the whole operating range. The wastegate command is very aggressive during the turbocharger transients; it hits the constraints and then stabilizes to track the boost pressure. This fact allows compensating the slow dynamics of the turbocharger. Moreover, this behavior can be easily tuned with the parameter $\overline{\delta}$, i.e. a smaller value of $\overline{\delta}$ leads to the faster time response, however the robustness bound will be reduced. Second, the controller does not generate any overshoot in the considered operating range which is also a very important property for the driving comfort.

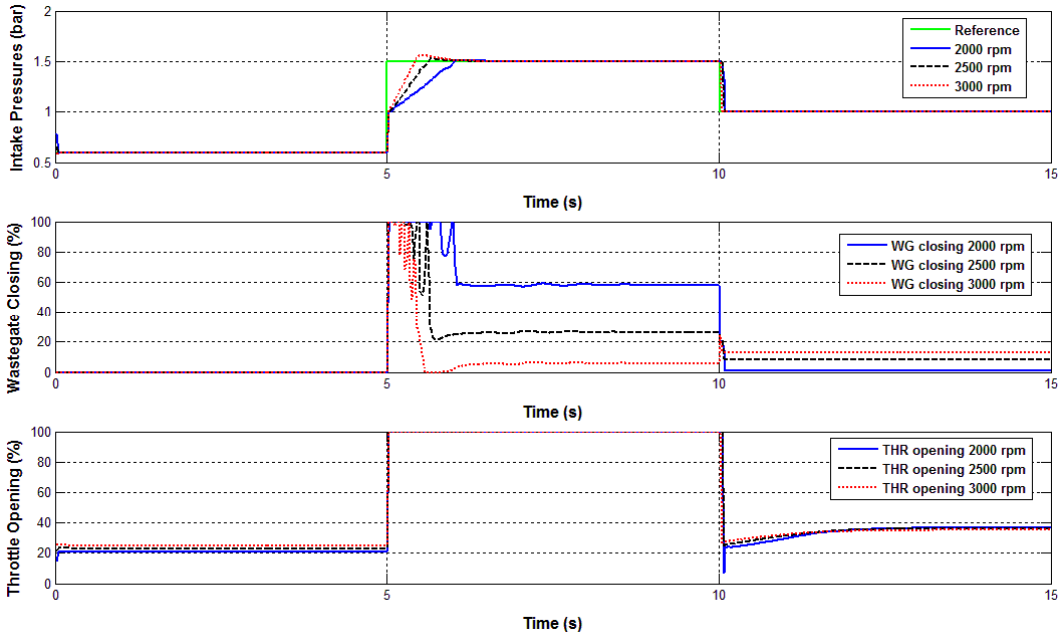

Figure 6.7. Intake pressure tracking performance (up) with corresponding wastegate commands (middle) and throttle commands (bottom) at different engine speeds

4.4.3. Vehicle transients

The closed-loop responses during the vehicle transient are presented in Figure 6.8. It can be noticed that the *Fuel-optimal controller* is perfectly able to guarantee a very good tracking performance even with the important variation of the engine speed (which represents the vehicle transient).

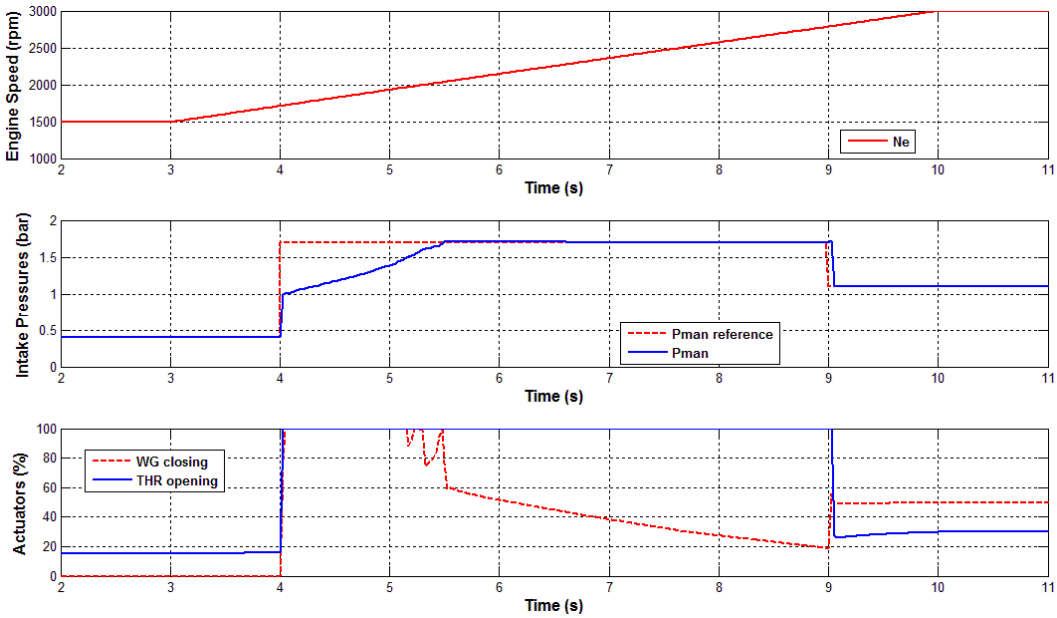

Figure 6.8. Variation of engine speed (up) and pressure tracking performance (middle) with corresponding actuator commands (bottom) for a vehicle transient

All above test scenarios and the corresponding results confirm the effectiveness of the proposed approach over the whole engine operating range. It should be emphasized again that the same controller gain is used for both controllers in all simulations. Therefore, the proposed approach requires very limited calibration effort.

5. Concluding Remarks

In this chapter, a new robust control design has been proposed to handle the model uncertainties/perturbations which is known as one of major drawbacks of feedback linearization. Compared to other existing results, the proposed method provides a simple and constructive design procedure which can be cast as an LMI optimization problem. Hence, the controller feedback gain is effectively computed. However, it is generally quite hard to make a link between the uncertain term $\Delta(z)$ and the mappings $f(x)$, $g_i(x)$, $h_i(x)$, $i=1,\ldots,m$ of the original system (6.1) through expression (6.8).

In terms of application, an original idea has been proposed to control the turbocharged air system of a SI engine. Several advantages of this approach can be summarized as follows. First, the second virtual output $y_{exh} \triangleq P_{exh}$ is introduced by means of LUT and this fact drastically simplifies the control design task. Second, the resulting nonlinear control law is very easily implementable. Third, offline engine data of the test bench is effectively reused and exploited for engine control

development so that the number of sensors and/or observers/estimators could be limited. Finally, the controller is robust with respect to model uncertainties/perturbations and its feedback gain can be effectively computed through a convex optimization problem with some numerical toolboxes. As pointed out, even with its simplicity, the proposed controller performs very promising results for both control strategies of turbocharged air system, i.e. to improve the drivability with *Conventional MIMO controller* or to optimize the fuel consumption with *Fuel-optimal controller*. The above remarks once again confirm that the proposed approach would be in particular relevant for industrial context.

"The mathematician's patterns, like the painter's or the poet's, must be beautiful; the ideas, like the colors or the words, must fit together in a harmonious way. Beauty is the first test: there is no permanent place in the world for ugly mathematics."

Godfrey Harold Hardy, British mathematician

PART III. ENERGY MANAGEMENT STRATEGY FOR VEHICULAR ELECTRIC POWER SYSTEMS

Presentation of Part III

The work in this part is directly related to our tasks for the Sural'Hy project with other industrial partners. The objective is to control the electric power system of the studied vehicle in such a manner that their power flows should be optimized in the sense of energy efficiency. As will be seen, the control problem considered in this work can be formulated as an optimization problem in the presence of several constraints. A systematic approach based on optimal control will be adopted to design the energy management strategies. Then, by means of these strategies, the electric energy will be generated and stored in the most appropriate manner so that the overall energy consumption and eventually the pollutant emissions can be minimized for a given driving cycle. To this end, both non-causal optimization method using the knowledge of the entire driving cycle and causal one are developed for two case studies with different structures of energy storage system. These strategies are then evaluated in an advanced simulation environment to point out their effectiveness.

The energy management problem considered in this work is very similar to the one for hybrid electric vehicles (HEVs). Hence, the developed strategies can be directly applied to parallel HEV. They are also easily generalized to others kinds of HEVs with some slight modifications.

"In theory, theory and practice are the same. In practice, they are not."

Albert Einstein, German-born theoretical physicist

Chapter 7. Optimal Control Based Energy Management

1. Introduction

1.1. Motivation

Over the years, the demand electric power consumption in conventional vehicle has become more and more important. This is due to the fact that automotive customers are more demanding in terms of performance, comfort and safety for their new vehicles. Hence, the number of auxiliary electric-powered devices has been constantly increased in modern vehicles, e.g. active suspension, electric brakes, catalyst heaters, etc. This increasing demand tends to double or triple the current vehicle electric load (Soong et al., 2001). Apart to improve the efficiency of the electric components, an effective energy management strategy (EMS) is also crucial to minimize the overall energy consumption of the vehicle.

In our project, one particularity of the studied vehicle consists in the presence of an electrical supercharger (eSC) in the turbocharged air system of the SI engine. This device aims at assisting the main turbocharger to reduce the effects of "turbo lag", that are: slow engine torque dynamics and lack of torque at low load zones. As a consequent, the drivability performance is significantly improved. The energy consumed by the eSC comes from either the alternator or the energy storage system (ESS) of the vehicular electric power system. To this end, the vehicle is equipped with an advanced alternator which is power controlled. Note that this alternator is directly coupled to the vehicle primary shaft; therefore, the engine operating point can be shifted by controlling the alternator output power. This fact offers one degree of freedom for energy optimization as in the case of classical parallel hybrid electric (Koot, 2006). However, this small capacity alternator is exclusively used to generate the energy for electric power system and cannot assist the internal combustion engine (ICE) to propel the vehicle. Note also that the considered alternator can also recover the kinetic and potential energy during the regenerative braking phases. This "free energy" is then stored in the energy storage system (ESS) and will be used later at appropriate moments.

From the above remarks, it is clear that the energy management becomes very attractive to improve the overall energy efficiency of the studied vehicle. Indeed, one of the objectives of the project is also to know if the energy consumed by the eSC could be fully compensated by the energy gain with an efficient EMS.

1.2. Goals of Part III

The goal of this work is to develop energy management strategies (EMSs) that optimize the power flow of the vehicular electric power system. Thank to these EMSs, the overall energy consumption of the vehicle is minimized under all driving situations. The developed strategies have to satisfy several objectives. First, when the driving conditions are perfectly known *a priori*, they are able to offer a global optimal solution. However, the exact knowledge about the entire future driving cycle is unfortunately not available for real-time applications. Thus, the second objective of these strategies is that their adaptations for real-world driving situations are straightforward and the resulting causal strategies behave closely as the global optimal ones. Third, the developed strategies must be simple in order to be implementable with limited computation and memory resources. Fourth, the strategies are based on a systematic approach so that they can be applicable to a large spectrum of component dimension without the need for extensive calibration. For these all reasons, the developed EMSs will be based on an optimal control approach with physical component models of the vehicle.

In this work, two case studies of the same vehicle configuration are investigated. The vehicle is equipped with a conventional powertrain with 5-speed manual transmission. The alternator is connected to the engine with a fixed gear ratio. The only difference between these case studies consists in their energy storage systems. The power flow of both case studies is described below.

1.2.1. Case study 1: Single storage electric power system

The single ESS consists only of the battery as dynamical system. The components connected to the electric power system in this case are the battery, the alternator, the onboard auxiliaries and the eSC. For simplicity, all onboard electric auxiliaries are modeled as one lumped power consumer. Concerning the eSC, it is controlled by engine control unit (ECU) which is out of the present work scope. However, its energy consumption profile is known and will be considered as an input of the developed EMSs. The power flow in this case is sketched in Figure 7.1. The direction of the arrows corresponds to the direction of the energy exchange between different components.

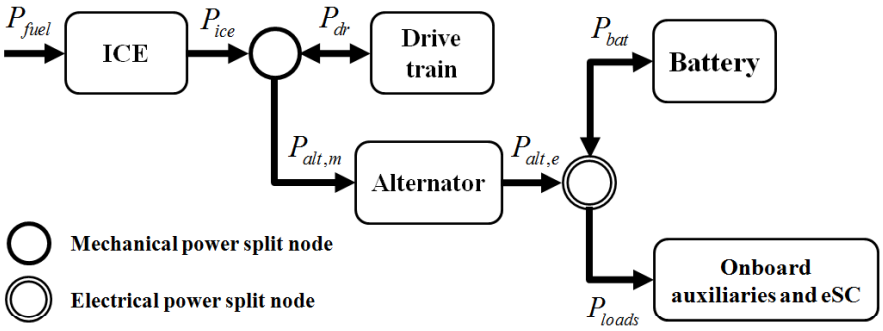

Figure 7.1. Power flow of the studied vehicle with single storage electric power system

The ICE produces the mechanical power P_{ice} from chemical energy (fuel). This mechanical power P_{ice} is divided into two parts. The first part P_{dr} is used for vehicle propulsion. The second one $P_{alt,m}$ is delivered to the alternator and then converted to electrical power $P_{alt,e}$. The alternator generates the power to satisfy the demand P_{loads} of all onboard auxiliaries including the eSC. It is also used to charge the battery when necessary. The battery power P_{bat} can be negative (when it is charged by the alternator) as well as positive (when it provides electric power for all electrical loads).

This case study offers only one degree of freedom for optimization which comes from the mechanical architecture of the vehicle. The EMS aims at controlling the alternator in the most beneficial way in the sense of energy efficiency. As a consequence, the battery will be temporarily charged or discharged to generate the appropriate energy amount to the electric power system. The EMS considers the battery as an energy buffer system and the charge-sustaining condition should hold at the end of the driving cycle, i.e. all consumed energy for vehicle propulsion and for onboard electric demand comes exclusively from the fuel combustion of ICE.

1.2.2. Case study 2: Dual storage electric power system

Apart from the components present in the electric power system of Case study 1, the supercapacitors are also available in this case as a second dynamical storage system. The two energy sources (battery and supercapacitor) are interconnected thank to a DC/DC converter. It is worth noting that Case study 1 is nothing else than a special case of Case study 2 where the supercapacitor and the DC/DC converter are removed from the electric power system. A sketch of the power flow in this case is depicted in Figure 7.2.

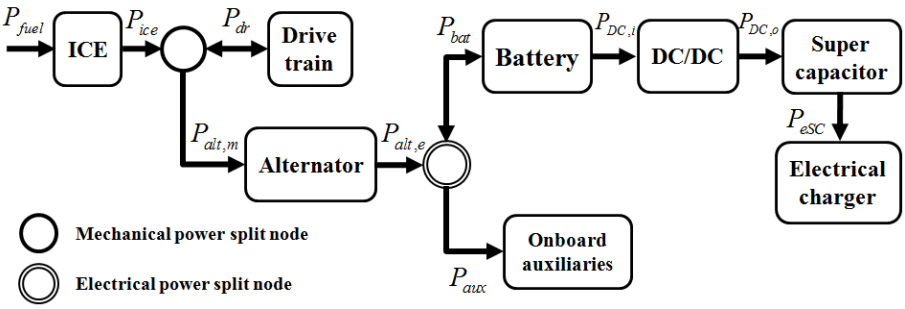

Figure 7.2. Vehicle power flow in the studied dual storage electric power system

It can be observed that the consumption of onboard auxiliaries P_{aux} can be powered either by the alternator or by the battery. The battery is also used to charge the supercapacitor through the DC/DC converter. However, the supercapacitor cannot charge the battery in this electric structure, it is exclusively used to power the eSC.

For Case study 2, two degrees of freedom are available for optimization. The first one comes from the mechanical architecture of the vehicle as in Case study 1, whereas the second one comes from the electric power system. In this case, both battery and supercapacitor are considered as energy buffer systems and the charge-sustaining conditions should hold for both of them. However, the use of the battery should be limited, i.e. it is mainly used for onboard auxiliary demand when necessary.

1.3. Organization

This chapter is organized as follows. Section 2 presents the simulation environment used in this work. To this end, two classes of models are distinguished and some models of the main component used to develop the EMSs are described. In Section 3, a state-of-the-art concerning the energy management is provided. Then, the Pontryagin's Minimum Principle is also briefly recalled. Section 4 is devoted to the development of the optimal strategies for the two cases studied. In Section 5, a simple adaptation idea to obtain causal strategies from optimal ones is first presented. Then, the simulation results are performed to show the effectiveness of the developed strategies. Finally, a conclusion is given in Section 6.

2. Simulation Environment

Hereafter, the simulation environment, which is used for testing and evaluating the different energy management strategies developed in the present work, is presented. It consists of all appropriate models of different elements constituting the vehicle considered, including the driver and the energy management strategy. An overview of the simulation environment in this work is

illustrated in Figure 7.3. As can be seen from it, the considered simulation environment has two separated parts: the vehicle model part and the energy management system part. The first part is developed in the numerical platform LMS Imagine.Lab AMESim. The second one is an optimization algorithm coded in language **C** for time computation efficiency and implemented in Matlab/Simulink as an S-function. The two parts are interconnected by a co-simulation interface. The most advantage of this simulation approach is that it offers at the same time the realistic vehicle model and the great convenience of Matlab/Simulink in terms of control design.

In the sequel, two model classes are considered: simulation model in LMS Imagine.Lab AMESim and control model in Matlab/Simulink. Both of them are used to represent the characteristics of the same vehicle, however, their complexity levels are different.

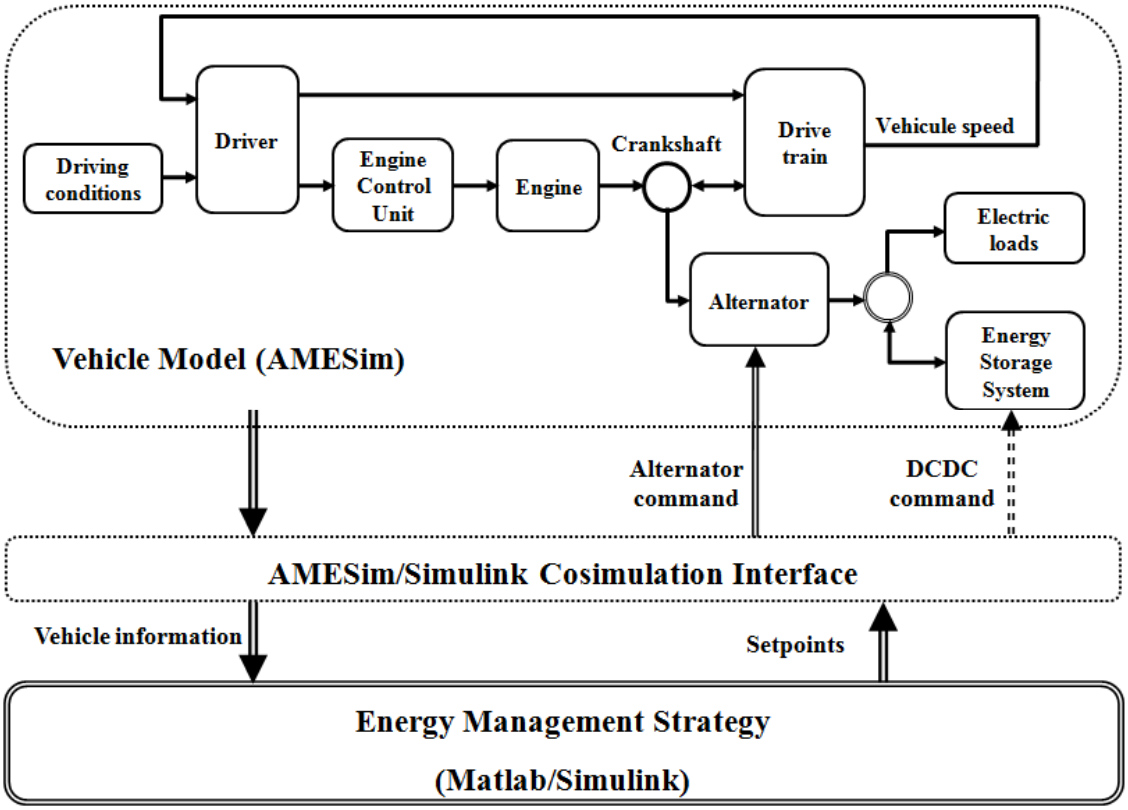

Figure 7.3. Simulation environment in the thesis framework

2.1. Vehicle Model Complexity

2.1.1. Dynamic model for simulation

The simulation model accurately represents all relevant characteristics of the real vehicle. This one is implemented in LMS Imagine.Lab AMESim which is an advanced simulation platform inspired by Bond Graph approach (Borutzky, 2010). This numerical simulation platform offers a powerful tool to

test, analyze and evaluate the energy management strategies. LMS Imagine.Lab AMESim has several libraries holding all necessary components to construct the preferred vehicle configuration (or the complex dynamical systems in general). The library component blocks introduce a modular approach, such that the entire vehicle model is decomposed into sub-models (components) interconnected by causal relationships. Moreover, it offers a great flexibility in terms of modeling, i.e. adding/removing some components does not modify the structure of the entire vehicle model.

The simulation model is obtained from forward modeling approach. The driver model, which is a feedback controller, provides a required torque target and different drive train commands based on required velocity and current vehicle velocity. These commands will be respectively used to control the engine (with the ECU) and the drive train in such a manner that the vehicle behaves as desired by the driver. The model and strategies involved have been developed by VALEO and will not be exposed here for confidentiality.

2.1.2. Simplified model for control

The control model is used to develop the energy optimization algorithm. At each sampling time, this algorithm computes the optimal control sequences that minimize the energy consumption of the vehicle. For real-time applications, the control model should have a very limited complexity. Hence, this model uses simple power-based models for the engine, the alternator, the battery, the supercapacitor, the DC/DC converter and the electric loads, which will be discussed in more detail in the next subsection.

2.2. Vehicle Modeling for Energy Optimization Strategy Design

Hereafter, some components of interest for both case studies will be described. It is worth noting that for confidential reasons, data range of variation characterizing the corresponding component of the system in each figure will be hidden.

2.2.1. Internal combustion engine

Internal combustion engine (ICE) is a complex system where many physical phenomena are not easy to model, e.g. combustion process (Heywood, 1988). However, from an energetic point of view some assumptions can be considered. Here, the temperature dependency and the dynamic behavior of the ICE will be neglected. Then, ICE is characterized by a static look-up-table (LUT) giving the instantaneous fuel consumption in function of the engine torque and the engine speed, see Figure 7.4.

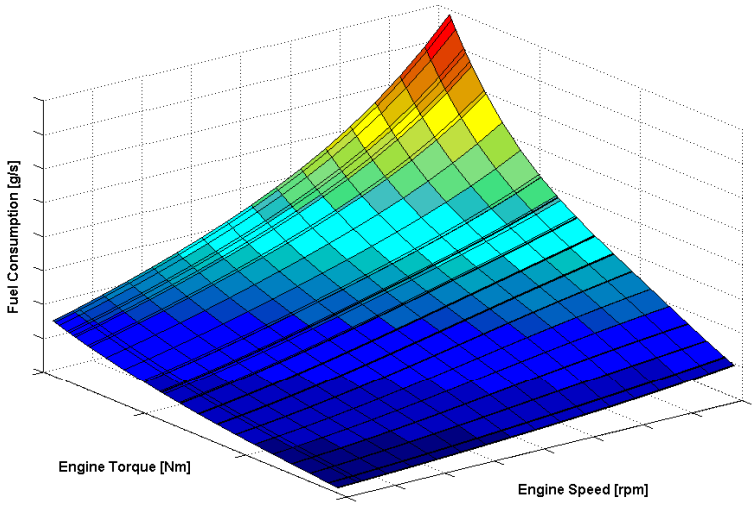

Figure 7.4. Representation of the instantaneous fuel consumption of the studied engine

Moreover, at a given engine speed, the engine torque is physically limited by its maximum available torque. This characteristic is also represented by a static LUT.

2.2.2. Alternator

In this work, an average model will be considered for the alternator. Of course, this kind of model is not able to precisely provide the information on the alternator dynamics; however, it is suitable to represent its energetic behavior. Then, the alternator is characterized by some static LUTs as in the case of ICE. The first one, shown in Figure 7.5, provides the alternator efficiency as a function of the rotary speed and the current.

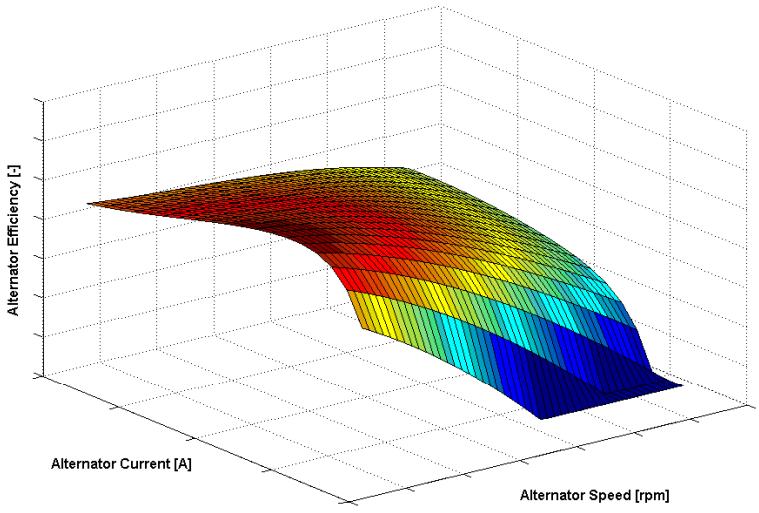

Figure 7.5. Representation of the alternator efficiency

The second LUT needed for the alternator average model provides the maximum current that the alternator can produce as a function of the rotary speed and the current, see Figure 7.6.

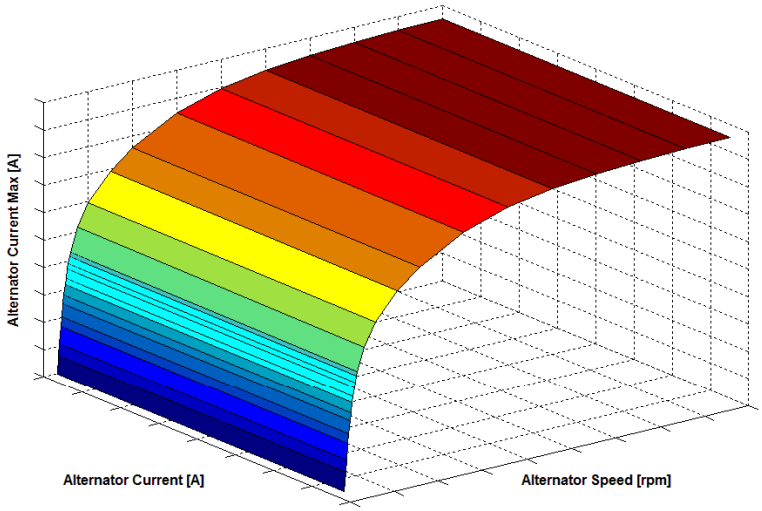

Figure 7.6. Representation of the alternator maximal current

For energy management strategy design, another LUT providing the maximum available torque at a given alternator speed is also needed. This one guarantees that the alternator torque is always within its physical limitation. Note that the alternator only works in generator mode, so its current is conventionally positive and is assumed to be measured for the optimization design problem. Moreover, the studied alternator is equipped with a voltage controller which aims to stabilize the electric power system voltage of the vehicle at a desired value. In such a manner, it controls also the alternator current and its torque.

2.2.3. Battery

Up to now, battery modeling is still an open research subject since its performance (voltage, current and efficiency) dynamically depends on some complex thermal-electrochemical behaviors. However, for control purpose, the thermal-temperature effects and transients (due to internal capacitance) are usually neglected. Then, the battery is electrically modeled with an open circuit voltage U_{oc} and an internal resistance R_{bat} as presented in Figure 7.7.

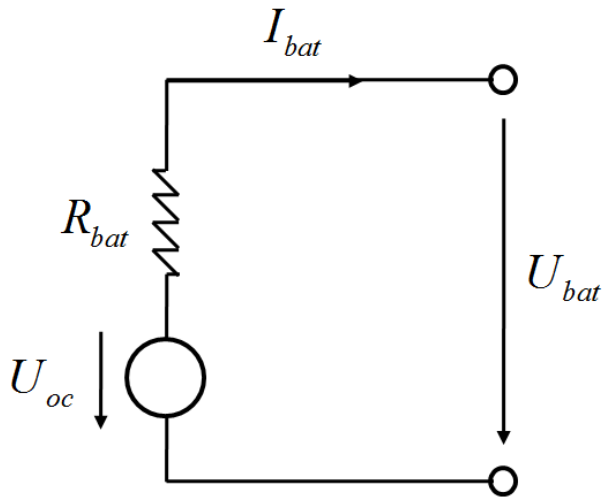

Figure 7.7. Equivalent electrical circuit of a battery

With these assumptions, the only state variable left in the battery is its state of charge (SOC). The battery SOC, expressed in percent, represents the normalized charge level in the battery and defined as follows:

$$SOC_{bat}(t) \triangleq \frac{Q_{bat}(t)}{Q_{bat,0}} \tag{7.1}$$

where $SOC_{bat}(t)$ is the battery SOC, $Q_{bat,0}$ is the nominal battery capacity which is given as battery data and $Q_{bat}(t)$ is the available amount of electric charge in the battery. The battery dynamics equation is given as follows:

$$\dot{SOC}_{bat}(t) \triangleq -\frac{I_{bat}\left(SOC_{bat}(t)\right)}{Q_{bat,0}} \tag{7.2}$$

The internal battery power $P_s(t)$ and the power at the terminal voltage $P_{bat}(t)$ are described as:

$$P_s(t) = U_{oc}\left(SOC_{bat}(t)\right) I_{bat}\left(SOC_{bat}(t)\right) \tag{7.3}$$

$$P_{bat}(t) \triangleq P_s(t) - P_{losses}(t) = U_{oc}\left(SOC_{bat}(t)\right) I_{bat}\left(SOC_{bat}(t)\right) - I_{bat}^2\left(SOC_{bat}(t)\right) R_{bat}\left(SOC_{bat}(t)\right) \tag{7.4}$$

where both open circuit voltage and internal resistance depend on the battery SOC and they are given by LUTs, i.e. $U_{oc} \triangleq U_{oc}\left(SOC_{bat}(t)\right)$ and $R_{bat} \triangleq R_{bat}\left(SOC_{bat}(t)\right)$. The expression of the battery current can be derived from (7.4) as:

$$I_{bat}\left(SOC_{bat}(t)\right)=\frac{U_{oc}\left(SOC_{bat}(t)\right)-\sqrt{U_{oc}^{2}\left(SOC_{bat}(t)\right)-4R_{bat}\left(SOC_{bat}(t)\right)P_{bat}(t)}}{2R_{bat}\left(SOC_{bat}(t)\right)} \tag{7.5}$$

From (7.3) and (7.4), the battery efficiency can be computed as:

$$\eta_{bat}(t)=\frac{P_{bat}(t)}{P_{s}(t)}=\frac{U_{oc}\left(SOC_{bat}(t)\right)I_{bat}\left(SOC_{bat}(t)\right)-I_{bat}^{2}\left(SOC_{bat}(t)\right)R_{bat}\left(SOC_{bat}(t)\right)}{U_{oc}\left(SOC_{bat}(t)\right)I_{bat}\left(SOC_{bat}(t)\right)} \tag{7.6}$$

2.2.4. Supercapacitor

Generally speaking, the specific power of the supercapacitors is much higher than in batteries and their specific energy is substantially lower. Moreover, their charge and discharge losses are also much smaller compared to that of batteries. That is why supercapacitors are very advantageous for high peak power applications. However, the supercapacitors generally have considerable energy leakage, so they are not suitable for long term storage (Koot, 2006).

After neglecting all complex thermal-electrochemical dynamics, the simplest equivalent electrical circuit consists of a capacitor and a resistor in series, which is depicted in Figure 7.8.

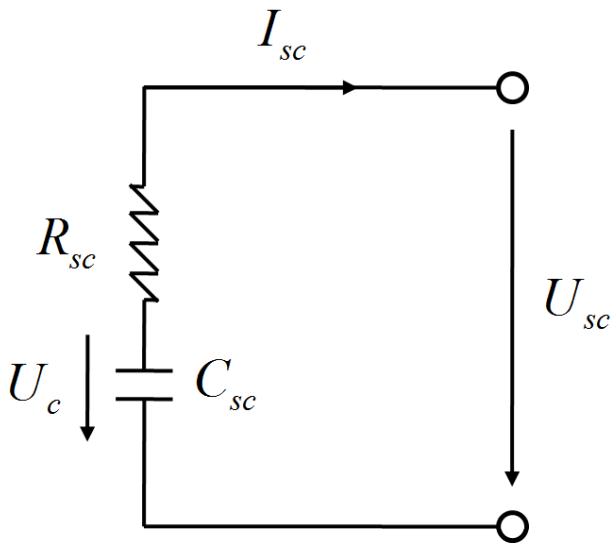

Figure 7.8. Equivalent electrical circuit of a supercapacitor

Then, the only state variable left in the supercapacitor is the voltage U_c which is the image of its available energy amount. From the Kirchhoff's voltage law, it can be obtained:

$$U_{sc}(t)=U_{c}(t)-R_{sc}I_{sc}(t);\qquad I_{sc}(t)=-\dot{Q}_{sc}(t) \tag{7.7}$$

where the internal resistance R_{sc} and the capacitance C_{sc} are constant. Note that the voltage $U_{sc}(t)$ directly depends on the current $I_{sc}(t)$, thus the voltage drop due to the equivalent resistance of the supercapacitor. Hence, the voltage $U_c(t)$ dynamics will be used for control purpose with:

$$\dot{U}_c(t) = -\frac{I_{sc}(U_c(t))}{C_{sc}} \tag{7.8}$$

Similar to the battery, the supercapacitor current expression can be also given as:

$$I_{sc}(U_c(t)) = \frac{U_c(t) - \sqrt{U_c^2(t) - 4R_{sc}P_{sc}(t)}}{2R_{sc}} \tag{7.9}$$

The state of the charge of the supercapacitor is computed by:

$$SOC_{sc}(t) = \frac{Q_{sc,0} - Q_{sc}(t)}{Q_{sc,\max}} \tag{7.10}$$

where $Q_{sc,0}$ and $Q_{sc,\max}$ are respectively the initial and maximal charges of the supercapacitor which are also given.

2.2.5. DC/DC converter

For Case study 2, where the battery and the supercapacitor are both used in the electric power system, a DC/DC converter is needed to link two different power sources. This converter is simply modeled by the following efficiency rate:

$$\eta_{DC} = \frac{P_{DC,o}(t)}{P_{DC,i}(t)} \tag{7.11}$$

where $P_{DC,o}(t)$ and $P_{DC,i}(t)$ are respectively converter output and input powers. The efficiency of the DC/DC converter is given.

3. Energy Management Strategy

3.1. Introduction

The vehicular energy management strategies (EMSs) aim at controlling the amount of power exchange and other available input variables to satisfy the power demand of the drive line in the most beneficial way. The goal of these strategies is to achieve some desired vehicle performance (usually

expressed by overall energy use and/or exhaust emissions) under the presence of various constraints due to drivability requirements and the characteristics of the components. Therefore, the vehicular energy management problem can be formulated as an optimization problem subject to constraints. The performance of any EMS strongly depends on the available driving information. Then, the EMSs can be classified into two categories: *offline strategies* and *online strategies*. The former category requires detailed knowledge on the future driving conditions which may be the case of public transportation vehicles. The latter one deals with the cases where no information on future driving conditions is *a priori* available. It is worth noting that *online strategies* are only sub-optimal solutions. Therefore, the objective is to make them as close as possible to the global optimal solution.

Although *offline strategies* are non causal, they are, however, still developed for different reasons (Sciarretta & Guzzella, 2007). First, it is clear that a global optimal solution for the energy management problem can be obtained only with these kinds of strategies. Then, this solution can be used to compare the performance of different vehicle architectures or different *online strategies*. It can be also used for component sizing purpose. Second, they allow understanding the optimal solution behaviors under various constraints and driving conditions, and in such a manner, some rule-based strategies could be derived for online purposes (Hofman, 2007).

The EMSs developed in this work are very similar to that for hybrid electric vehicles (HEVs). For this reason, a brief state-of-the-art concerning this control issue for HEVs will be provided in what follows.

3.2. A Brief Overview of Optimal Energy Management Strategies

Over the years, many approaches have been tried to solve the problem of vehicle energy optimization. Heuristic based strategies (Schouten et al., 2002; Poursamad & Montazeri, 2008), which relies on empirical knowledge, can be easily implemented and often used for real-time applications. Although they may improve the energy efficiency, these strategies are however not easily generalized and sometimes costly in terms of calibration since they directly depends on the studied vehicle architecture and the acquired expertise. Above all, the heuristic approaches do not guarantee an optimal result in all situations. Therefore, more systematic approaches are needed.

Optimal strategies are model-based approaches and typically derived from optimal control theory. In automotive framework, there are mainly two methods which may both offer globally optimal result for offline situations and under some assumptions, that are: Dynamic Programming (DP) (Bellman, 1957) and Pontryagin's Minimum Principle (PMP) (Pontryagin et al., 1962). DP-based

strategies are known as very costly in terms of computation. Numerous efforts have been devoted to reduce the computation time (Sciarretta & Guzzella, 2007). These strategies are often used for offline purposes (performance evaluation, component sizing) (Hofman, 2007; Sundström, 2009). Some adapted online versions can be found in (Lin et al., 2003; Koot et al., 2005; Hofman, 2007; Kessels, 2007). Concerning the strategies based on PMP, their optimum could not be global as in the case of DP since the PMP only provides necessary optimality conditions. However, they are much more computationally efficient and the online adaptation is more straightforward. This is the main reason why we only deal with PMP approach in this work. In the literature, numerous results exist on PMP-based strategies (Delprat et al., 2004; Rousseau, 2008; Serrao et al., 2009; Ambühl et al., 2010) or the related Equivalent Consumption Minimization Strategies (ECMS) (Paganelli et al., 2002; Sciarretta et al., 2004).

Hereafter, some basis on PMP, which will useful for the EMS design, is recalled.

3.3. Optimal Control Problem and Pontryagin's Minimum Principle

3.3.1. Optimal control problem

The optimal control problem consists in finding the optimal control $u^*(t)$ among all admissible control $u(t):[0,T]\mapsto \mathcal{U}\subseteq\mathbb{R}^m$ of the following dynamical system:

$$\dot{x}(t)=f\left(x(t),x(t),t\right) \tag{7.12}$$

driving the initial state $x(0)=x_0$ to an admissible final state $x(T)\in\mathcal{X}\subseteq\mathbb{R}^n$ (which may be free or constraint) such that the corresponding system state, denoted $x^*(t)$, satisfied the state constraints $x^*(t)\in\mathcal{X}\subseteq\mathbb{R}^n, \forall t\in[0,T]$ and such that the cost functional defined as:

$$\min_{u\in\mathcal{U}}\left\{\mathcal{J}(u)=\int_0^T\mathcal{L}\left(x(t),u(t),t\right)dt+\phi\left(x(T),T\right)\right\} \tag{7.13}$$

is minimized.

In (7.13), $\mathcal{L}\left(x(t),u(t),t\right)$ is the instantaneous cost and $\phi\left(x(T),T\right)$ represents the terminal cost of the system state at final time T. The functions $f(\cdot)$, $\mathcal{L}(\cdot)$ and $\phi(\cdot)$ are assumed to be at least once continuously differentiable with respect to all of their arguments. A such couple $\left(x^*(t),u^*(t)\right)$, if existing, is called *optimal solution*.

3.3.2. Basis on Pontryagin's Minimum Principle

The PMP is known as a very powerful tool in optimal control theory (Pontryagin et al., 1962; Kirk, 1970). This principle provides a set of necessary conditions for the optimality of a solution of an optimal control problem. In what follows, the PMP for optimal control problems with a fixed final time T and state $x(T)$ and without state constraints ($\mathcal{X} \equiv \mathbb{R}^n$) will be introduced. This kind of optimal problem is directly related to the design of vehicle energy management strategy considered in this work. An interesting overview on optimal control with state constraints can be found in (Hartl et al., 1995).

The PMP requires the definition of Hamiltonian $\mathcal{H}: \mathcal{X} \times \mathcal{U} \times \mathbb{R}^n \times [0,T] \mapsto \mathbb{R}$ as:

$$\mathcal{H}(x(t),u(t),\lambda(t),t) = \mathcal{L}(x(t),u(t),t) + \lambda^T(t) f(x(t),u(t),t) \tag{7.14}$$

where $\lambda(t)$ is called co-state (or adjoint state) vector associated with the dynamical system (7.12). The PMP is stated as follows. If $(x^*(t),u^*(t)): [0,T] \mapsto \mathcal{X} \times \mathcal{U}$ is the optimal solution, then there exists co-state vector $\lambda(t)$ such that the following conditions hold:

$$\dot{x}^*(t) = \frac{\partial \mathcal{H}}{\partial \lambda}(x^*(t),u^*(t),\lambda^*(t),t) = f(x^*(t),u^*(t),t) \tag{7.15}$$

$$x^*(0) = x_0; \qquad \lambda^*(T) = \left.\frac{\partial \phi}{\partial x}\right|_{t=T} \tag{7.16}$$

$$\dot{\lambda}^*(t) = -\frac{\partial \mathcal{H}}{\partial x}(x^*(t),u^*(t),\lambda^*(t),t) = -\frac{\partial \mathcal{L}}{\partial x}(x^*(t),u^*(t),t) - \left[\frac{\partial f}{\partial x}(x^*(t),u^*(t),t)\right]^T \lambda^*(t) \tag{7.17}$$

$$\mathcal{H}(x^*(t),u^*(t),\lambda^*(t),t) \leq \mathcal{H}(x^*(t),u(t),\lambda^*(t),t); \quad \forall t \in [0,T]; \quad \forall u(t) \in \mathcal{U} \tag{7.18}$$

In the case where the final state $x(T)$ is fixed as $x(T) = x_T$, the condition (7.16) can be replaced by:

$$x^*(0) = x_0; \qquad x^*(T) = x_T \tag{7.19}$$

It is worth noting that the PMP is derived using the calculus of variations, see (Kirk, 1970) for more details. It only requests the local minimization of the Hamiltonian $\mathcal{H}(\cdot)$ with respect to the control $u(t)$. As previously stated, the set of conditions given in (7.15)-(7.18) are only necessary for

optimality and, in general, not sufficient. However, in some specific cases where the candidate of optimal solution obtained from PMP is the unique solution satisfying the necessary and boundary conditions, then global optimality is guaranteed by PMP. Note also that exact mathematical models are needed when dealing with the PMP since this principle solves analytically the optimal problem. However, only simplified models are usually used for control purpose in real-world applications. This fact may lead to sub-optimal solutions. Moreover, the solution of the differential equations (7.15) and (7.17) depends on the boundary conditions of the state and co-state vectors which are not always available. For example, the knowledge on driving conditions over the entire optimization horizon $[0,T]$ is not available when designing optimal *online strategies* for vehicle energy management.

4. Case Studies

This work deals with two case studies:

- Case study 1: single storage electric power system
- Case study 2: dual storage electric power system

The vehicle architecture is the same for both cases, see Figure 7.9. Some notations used in this work are given in Table 7.1.

Variable	Description	Unit	Variable	Description	Unit
T_w	Wheel torque	Nm	ω_w	Wheel speed	rpm
T_{ice}	ICE torque	Nm	ω_{ice}	ICE speed	rpm
T_{alt}	Alternator torque	Nm	ω_{alt}	Alternator speed	rpm
T_{ps}	Primary shaft torque	Nm	ρ	Gear ratio of the reducer	--
η_{gb}	Gearbox efficiency	--	k	k^h gear of the gearbox	--
Q_{lhv}	Constant fuel energy density	kJ/kg	$R(k)$	Gearbox ratio of the k^{th} gear	--

Table 7.1.Some notations of vehicle variables used in this work

In this vehicle architecture, the alternator is connected to the engine with a fixed gear ratio. "Electric System" block in Figure 7.9 consists of battery, all onboard consumers (auxiliaries and electrical supercharger) and eventually supercapacitor and DC/DC converter for Case study 2.

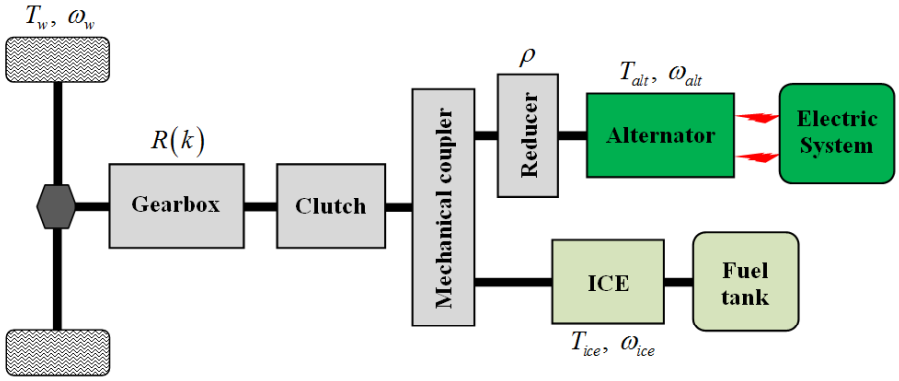

Figure 7.9. Representation of the studied vehicle architecture

In what follows, the optimization problem will be formulated for this studied vehicle. However, as previously stated, the formulation can be easily generalized to a large family of parallel hybrid electric vehicles.

4.1. Problem Formulation

4.1.1. Control objective

The goal of optimal control is to minimize the fuel consumption over the driving cycle in the time optimization horizon $[0,T]$, then the cost function is expressed by:

$$\mathcal{J} = \int_0^T Q_{lhv}\dot{m}_{fuel}\left(T_{ice}(t),\omega_{ice}(t)\right)dt = \int_0^T P_{fuel}\left(T_{ice}(t),\omega_{ice}(t)\right)dt \tag{7.20}$$

where $P_{fuel}\left(T_{ice}(t),\omega_{ice}(t)\right)$ is the fuel power and the instantaneous fuel consumption of ICE $\dot{m}_{fuel}\left(T_{ice}(t),\omega_{ice}(t)\right)$ is known at a given engine speed ω_{ice} and torque T_{ice}. In some cases, the pollutant emissions can be also integrated by modifying the cost function (7.20) as follows:

$$\mathcal{J}' = \int_0^T \left(P_{fuel}\left(T_{ice}(t),\omega_{ice}(t)\right) + \sum_{i=1}^{n} \alpha_i \dot{m}_i\left(T_{ice}(t),\omega_{ice}(t)\right) \right) dt \tag{7.21}$$

where α_i are weighting factors and the instantaneous pollutant emission rates $\dot{m}_i\left(T_{ice}(t),\omega_{ice}(t)\right)$ (in general NO_x, CO, HC) are given by static LUTs. In this work, we are only interested in the cost function of the form (7.20).

4.1.2. Constraints

a. Vehicle architecture constraints

The mechanical relations between torques and speeds of the considered vehicle architecture represented in Figure 7.9 are given by the equations:

$$\begin{cases} T_w(t) = R\left(k(t)\right)\eta_{gb}\left(T_{ice}(t) + \rho T_{alt}(t)\right) = R\left(k(t)\right)\eta_{gb}T_{ps}(t) \\ \omega_w(t) = \dfrac{\omega_{ice}(t)}{R\left(k(t)\right)} = \dfrac{\omega_{alt}(t)}{\rho R\left(k(t)\right)} \end{cases} \tag{7.22}$$

The driving cycle is usually defined by the couple $\left(\omega_w(t),k(t)\right)$. Indeed, when $\omega_w(t)$ and $k(t)$ are known, the torque requested at the wheels $T_w(t)$ can be easily derived for the vehicle longitudinal dynamics equation (Sciarretta & Guzzella, 2007). In this work, engaged gear $k(t)$ at each moment is chosen by the driver. Then, it can be noticed from (7.22) that, with a given driving cycle, neither the engine speed nor the alternator speed can be chosen by the energy management strategy, the only degree of freedom of the studied architecture is the alternator torque (or ICE torque).

b. Mechanical constraints

Due to the physical limitations of the ICE and the alternator, their speeds and torques are subject to the following constraints:

$$\begin{cases} \omega_{ice,\min} \le \omega_{ice}(t) \le \omega_{ice,\max} \\ \omega_{alt,\min} \le \omega_{alt}(t) \le \omega_{alt,\max} \end{cases} \tag{7.23}$$

and

$$\begin{cases} T_{ice,\min}\left(\omega_{ice}(t)\right) \le T_{ice}(t) \le T_{ice,\max}\left(\omega_{ice}(t)\right) \\ T_{alt,\min}\left(\omega_{alt}(t)\right) \le T_{alt}(t) \le T_{alt,\max}\left(\omega_{alt}(t)\right) \end{cases} \tag{7.24}$$

By taking into account the physical alternator torque limits, the engine torque limits at each instant t are given as follows, where the primary shaft torque $T_{ps}(t) = T_{ice}(t) + \rho T_{alt}(t)$ is derived from the driving cycle:

$$T_{ice}(t) \in \mathcal{T}_{ice} = \left\{ T_{ice}(t) : \underline{T_{ice,\min}}\left(\omega_{ice}(t)\right) \le T_{ice}(t) \le \overline{T_{ice,\max}}\left(\omega_{ice}(t)\right) \right\} \tag{7.25}$$

where

$$\begin{cases} \underline{T_{ice,\min}}\left(\omega_{ice}(t)\right) = \max\left\{ T_{ice,\min}\left(\omega_{ice}(t)\right), T_{ps}(t) - \rho T_{alt,\max}\left(\omega_{alt}(t)\right) \right\} \\ \overline{T_{ice,\max}}\left(\omega_{ice}(t)\right) = \min\left\{ T_{ice,\max}\left(\omega_{ice}(t)\right), T_{ps}(t) - \rho T_{alt,\min}\left(\omega_{alt}(t)\right) \right\} \end{cases} \tag{7.26}$$

c. Electric power system constraints

As mentioned above, the only difference between the two considered case studies lies in their energy storage systems. Case study 1 deals only with the battery, see Figure 7.10. The optimization problem formulation in this case is the same as for conventional hybrid electric vehicles with only one system state coming from the battery dynamical system:

$$\dot{SOC}_{bat}(t) = -\frac{I_{bat}\left(SOC_{bat}(t)\right)}{Q_{bat,0}}; \qquad SOC_{bat}(0) = SOC_{bat,0} \tag{7.27}$$

where the initial state of charge of the battery $SOC_{bat,0}$ is given.

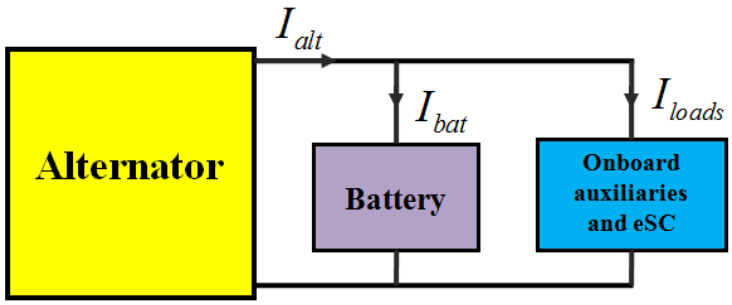

Figure 7.10. Sketch of the electric structure of Case study 1

From the electric structure in Figure 7.10, the battery current can be computed as:

$$I_{bat}(t) = I_{alt}(t) - I_{loads}(t) \tag{7.28}$$

where the electric load current $I_{loads}(t)$ is known and represents all onboard auxiliary demand including the consumption of eSC. The current delivered by the alternator $I_{alt}(t)$ can be easily derived from the optimal alternator torque at each time step. It is noticed from (7.28) that if the alternator is optimally controlled, then, the battery use is also indirectly optimized in the sense of energy efficiency.

For Case study 2, both battery and supercapacitor are considered. They are linked by a DC/DC converter. The electric structure of this case is depicted in Figure 7.11. In this case, the dynamics of the supercapacitor should be considered together with (7.27) for optimization problem to fully take advantage of all electric structure potential:

$$\dot{U}_c(t) = -\frac{I_{sc}(U_c(t))}{C_{sc}}; \qquad U_c(0) = U_{c,0} \tag{7.29}$$

where the initial voltage of the supercapacitor $U_{c,0}$ is given.

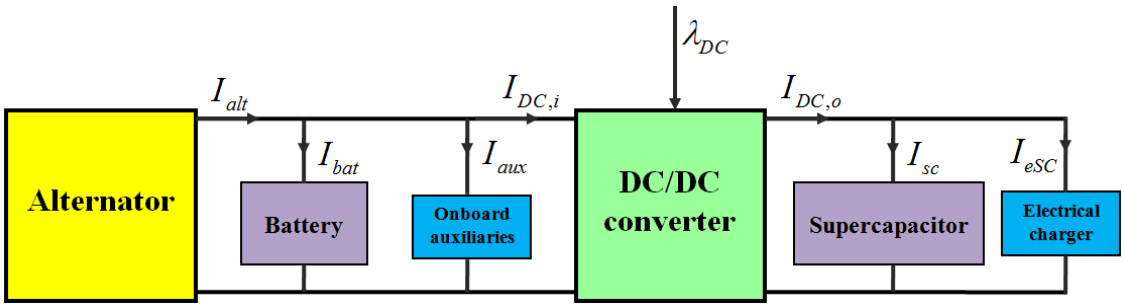

Figure 7.11. Sketch of the electric structure of Case study 2

In this work, the DC/DC converter controls its output current, i.e. $\lambda_{DC}(t) = I_{DC,o}(t)$. It is noticed that the electric structure of Case study 2 offers a second degree of freedom for optimization problem: the DC/DC output (or input) current. Indeed, if one of these two currents is optimized, the other can be easily deduced from the power relation (7.11) of DC/DC converter. The battery and supercapacitor currents are respectively computed by the following relations:

$$I_{bat}(t) = I_{alt}(t) - I_{aux}(t) - I_{DC,i}(t) \tag{7.30}$$

$$I_{sc}(t) = I_{DC,o}(t) - I_{eSC}(t) \tag{7.31}$$

The DC/DC output current is constraint by:

$$I_{DC,o}(t) \in \mathcal{I}_{DC,o} = \left\{ I_{DC,o}(t) : \underline{I_{DC,o}} \leq I_{DC,o}(t) \leq \overline{I_{DC,o}} \right\} \tag{7.32}$$

where $\underline{I_{DC,o}}$ and $\overline{I_{DC,o}}$ are respectively the minimum and maximum output current of the DC/DC converter. It is worth noting that the currents used for onboard auxiliary consumers $I_{aux}(t)$ and electrical supercharger consumption $I_{eSC}(t)$ are both known. The alternator and the DC/DC output currents are given by optimization. By optimizing the DC/DC output current, the alternator would be more efficiently exploited for energy efficiency purpose.

For safe operation and cycle life extension, the battery SOC and battery current are both limited:

$$SOC_{bat,\min} \leq SOC_{bat}(t) \leq SOC_{bat,\max} \tag{7.33}$$

$$I_{bat,\min} \leq I_{bat}(t) \leq I_{bat,\max} \tag{7.34}$$

In the case of supercapacitor, the voltage $U_c(t)$ and the current $I_{sc}(t)$ are subject to the following constraints:

$$U_{c,\min} \leq U_c(t) \leq U_{c,\max} \tag{7.35}$$

$$I_{sc,\min} \leq I_{sc}(t) \leq I_{sc,\max} \tag{7.36}$$

Both battery and supercapacitor are considered as energy buffer systems. Therefore, the charge sustaining condition should be fulfilled by EMS for both of them. Concretely, one should have $\Delta SOC_{bat} \approx 0$ and $\Delta U_c \approx 0$ where:

$$\Delta SOC_{bat} \triangleq SOC_{bat}(T) - SOC_{bat}(0) \tag{7.37}$$

$$\Delta U_c \triangleq U_c(T) - U_c(0) \tag{7.38}$$

4.2. Application of Pontryagin's Minimum Principle

Next, the PMP will be applied to the two cases. Only offline optimal solutions will be considered in this subsection. Thereafter, for simplicity, the explicit time-dependence of the variables is omitted except for confusing situations.

4.2.1. Case study 1: Single storage electric power system

Taking into account (7.20) and (7.27), the Hamiltonian in this case is defined as:

$$\mathcal{H}\left(SOC_{bat}, T_{ice}, \lambda_1\right) = P_{fuel}\left(T_{ice}, \omega_{ice}\right) - \lambda_1 \frac{I_{bat}\left(SOC_{bat}\right)}{Q_{bat,0}} \tag{7.39}$$

where the battery current $I_{bat}\left(SOC_{bat}\right)$ is computed by (7.28). The necessary conditions of optimality as described in equations (7.15)-(7.18) become in this case as:

$$\dot{SOC}^*_{bat} = \frac{\partial \mathcal{H}(\cdot)}{\partial \lambda_1} = -\frac{I_{bat}\left(SOC^*_{bat}\right)}{Q_{bat,0}}; \quad SOC^*_{bat}(0) = SOC_{bat,0} \tag{7.40}$$

$$\dot{\lambda}^*_1 = -\frac{\partial \mathcal{H}(\cdot)}{\partial SOC_{bat}} = \frac{\lambda^*_1}{Q_{bat,0}} \frac{\partial I_{bat}\left(SOC^*_{bat}\right)}{\partial SOC_{bat}} \tag{7.41}$$

$$SOC^*_{bat}(T) \approx SOC_{bat,0} \tag{7.42}$$

$$SOC_{bat,\min} \le SOC^*_{bat} \le SOC_{bat,\max} \tag{7.43}$$

$$\mathcal{H}\left(SOC^*_{bat}, T^*_{ice}, \lambda^*_1\right) \le \mathcal{H}\left(SOC^*_{bat}, T_{ice}, \lambda^*_1\right); \quad \forall t \in [0,T]; \quad \forall T_{ice} \in \mathcal{T}_{ice} \tag{7.44}$$

Several comments can be made regarding these optimality conditions. First, the conditions (7.40) and (7.41) provide respectively the dynamics of the system state and its associated co-state. However, neither an initial condition nor a final condition on the co-state are available. Second, it is important to emphasize that when the charge sustaining condition, guaranteed by (7.42), is required for the EMS, the battery usually operates only in a small range of SOC (Kim et al., 2011). As a consequence, the open circuit voltage and the internal resistance of the battery may not vary so much in this range. Therefore, from (7.5), it can be concluded that the battery current $I_{bat}\left(SOC_{bat}\right)$ is not significantly affected by the variation of battery SOC. Combining this fact with condition (7.41), it follows that:

$$\dot{\lambda}_1 \approx 0 \quad \Rightarrow \quad \lambda_1 = \lambda_{10} \tag{7.45}$$

where the constant λ_{10} has to be determined. This assumption has been exploited in many other previous works (Delprat et al., 2004; Sciarretta & Guzzella, 2007; Kim et al., 2011). Third, our studied battery has an important nominal capacity $Q_{bat,0}$, then, the state constraints (7.43) will never

be violated. Fourth, at each instant t, the optimal control T_{ice}^{*} minimizing the Hamiltonian can be exhaustively searched in the torque admissible set $\mathcal{T}_{ice}$ defined in (7.25). This can be numerically done by testing all torque possibilities of the set $\mathcal{T}_{ice}$ at each time step. Hence, the constraints on the control variable T_{ice} is "naturally" considered. Fifth, it is clear that the optimal solution at each instant t depends on the initial conditions of the system state $SOC_{bat,0}$ and the co-state λ_{10}. The former initial condition is given, however, the latter on is not known *a priori*. From (7.16), the value of λ_{10} depends on boundary condition of the terminal cost at final time T, i.e. the future information of the driving conditions. Indeed, the determination/estimation of this value is crucial to reach the optimal solution as close as possible. For offline situations where driving cycles are given in advance, the value of λ_{10} can be iteratively computed by a "root finding algorithm" (Delprat et al., 2004). The goal is to determine the value of λ_{10} that satisfies the charge sustaining condition $SOC_{bat}^{*}(T) \approx SOC_{bat,0}$. The overall PMP-based algorithm to find out the optimal control sequence T_{ice}^{*} for a given driving cycle can be summarized in Figure 7.12. There are three different loops in this algorithm. The "time-loop" allows covering the whole driving cycle. At each time step t, the "control-loop" aims at searching the optimal ICE torque that minimizes the Hamiltonian. The "lambda-loop" is used to adapt the constant value λ_{10} so that the charge sustaining condition holds at the end of the driving cycle.

Finally, when the optimal control T_{ice}^{*} is determined for each time step, the corresponding optimal alternator torque can be easily deduced from the expression of primary shaft torque $T_{ps} = T_{ice}^{*} + \rho T_{alt}^{*}$.

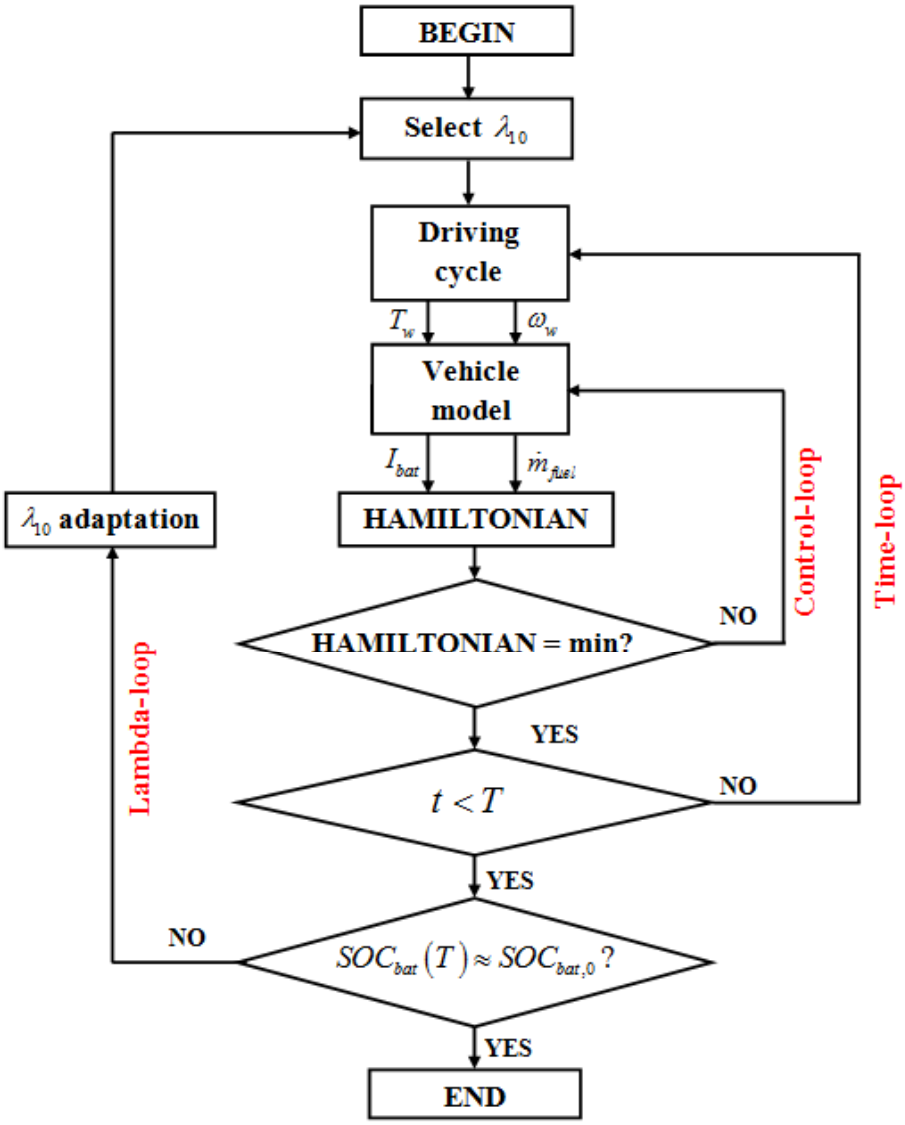

Figure 7.12. Offline optimal resolution algorithm for a given driving cycle

4.2.2. Case study 2: Dual storage electric power system

In this case, two dynamical systems (7.27) and (7.29) are available for the energy storage system. As previously highlighted, the constraints on battery SOC (7.43) is not really critical for optimization problem. However, the supercapacitor may quickly charge and discharge due to its low specific energy compared to the battery. Hence, the state constraints (7.35) of the supercapacitor should be taken into account. To this end, a new dummy variable has been introduced whose dynamics is defined as (Kirk, 1970):

$$\dot{X}_d \triangleq T(U_c) \tag{7.46}$$

where the function $T(U_c)$ in (7.46) is defined as:

$$T(U_c)=\left[U_c-U_{c,\min}\right]^2 sg\left(U_{c,\min}-U_c\right)+\left[U_{c,\max}-U_c\right]^2 sg\left(U_c-U_{c,\max}\right) \tag{7.47}$$

and the function $sg(\cdot)$ in (7.47) is given as:

$$sg(x)\triangleq\begin{cases}0, & x<0\\ 1, & x\geq 0\end{cases} \tag{7.48}$$

Note that $\dot{X}_d(t)\geq 0,\ \forall t\in[0,T]$ and $\dot{X}_d(t)=0$ only for times when the state constraints (7.35) are satisfied. The new dummy variable $X_d(t)$:

$$X_d(t)=\int_0^t \dot{X}_d(t)\,dt+X_d(0) \tag{7.49}$$

is required to satisfy the two boundary conditions: $X_d(0)=0$ and $X_d(T)=0$. This fact implies once again that $X_d(t)=0,\ \forall t\in[0,T]$. However, it is possible only if the state constraints (7.35) are satisfied for all $t\in[0,T]$.

Taking into account the dynamics (7.27), (7.29) and (7.46), the augmented Hamiltonian for the Case study 2 is defined as follows:

$$\begin{aligned}\mathcal{H}_a\left(SOC_{bat},U_c,T_{ice},I_{DC,o},\lambda_1,\lambda_2\right)=P_{fuel}\left(T_{ice},\omega_{ice}\right)-\lambda_1\frac{I_{bat}\left(SOC_{bat}\right)}{Q_{bat,0}}\ \cdots\\ -\lambda_2\frac{I_{sc}\left(U_c,I_{DC,o}\right)}{C_{sc}}+\lambda_d T\left(U_c\right)\end{aligned} \tag{7.50}$$

Then, the necessary optimality conditions are given by (7.40)-(7.43) together with the following ones:

$$\dot{U}_c^*=\frac{\partial\mathcal{H}_a(\cdot)}{\partial\lambda_2}=-\frac{I_{sc}\left(U_c^*,I_{DC,o}^*\right)}{C_{sc}};\quad U_c^*(0)=U_{c,0} \tag{7.51}$$

$$U_c^*(T)\approx U_{c,0} \tag{7.52}$$

$$U_{c,\min}\leq U_c^*\leq U_{c,\max} \tag{7.53}$$

$$\dot{X}_d^* = \frac{\partial \mathcal{H}_a(\cdot)}{\partial \lambda_d} = \left[U_c^* - U_{c,\min}\right]^2 sg\left(U_{c,\min} - U_c^*\right) + \left[U_{c,\max} - U_c^*\right]^2 sg\left(U_c^* - U_{c,\max}\right)$$
$$X_d^*(0) = 0 \tag{7.54}$$

$$\dot{\lambda}_2^* = -\frac{\partial \mathcal{H}_a(\cdot)}{\partial U_c} = \frac{\lambda_1^*}{Q_{bat,0}} \frac{\partial I_{bat}\left(SOC_{bat}^*\right)}{\partial U_c} + \frac{\lambda_2^*}{C_{sc}} \frac{\partial I_{sc}\left(U_c^*, I_{DC,o}^*\right)}{\partial U_c} \cdots$$
$$-2\lambda_d^*\left[U_c^* - U_{c,\min}\right] sg\left(U_{c,\min} - U_c^*\right) - 2\lambda_d^*\left[U_{c,\max} - U_c^*\right] sg\left(U_c^* - U_{c,\max}\right) \tag{7.55}$$

$$\dot{\lambda}_d^* = -\frac{\partial \mathcal{H}_a(\cdot)}{\partial X_d} \tag{7.56}$$

$$\mathcal{H}_a\left(SOC_{bat}^*, U_c^*, T_{ice}^*, I_{DC,o}^*, \lambda_1^*, \lambda_2^*, \lambda_d^*\right) \le \mathcal{H}_a\left(SOC_{bat}^*, U_c^*, T_{ice}, I_{DC,o}, \lambda_1^*, \lambda_2^*, \lambda_d^*\right);$$
$$\forall t \in [0,T]; \quad \forall \left(T_{ice}, I_{DC,o}\right) \in \mathcal{T}_{ice} \times \mathcal{I}_{DC,o} \tag{7.57}$$

As in Case study 1, $\lambda_1 = \lambda_{10}$, $\forall t \in [0,T]$ and at each instant t, the optimal controls $T_{ice}^*(t)$ and $I_{DC,o}^*(t)$ minimizing the Hamiltonian can be exhaustively searched in the torque and current admissible sets $\mathcal{T}_{ice}$ and $\mathcal{I}_{DC,o}$ defined respectively in (7.25) and (7.32).

Since X_d does not appear explicitly in $\mathcal{H}_a(\cdot)$, then, it can be deduced from (7.56) that:

$$\dot{\lambda}_d^* = -\frac{\partial \mathcal{H}_a(\cdot)}{\partial X_d} = 0 \quad \Rightarrow \quad \lambda_d^* = \lambda_{d0} \tag{7.58}$$

where λ_{d0} is the constant to be determined. Note that if the supercapacitor has an important capacitance C_{sc}, its state constraints (7.35) will be then trivial. In this case, λ_{d0} can be set equal to 0, which means that supercapacitor state constraints are not taken into account.

From the supercapacitor current $I_{sc}(U_c)$ expression in (7.9), it follows that:

$$\frac{\partial I_{sc}(U_c)}{\partial U_c} = -\frac{I_{sc}(U_c)}{\sqrt{U_c^2 - 4R_{sc}P_{sc}}} \tag{7.59}$$

Then, the condition (7.55) can be rewritten as:

$$\dot{\lambda}_2^* = \frac{-\lambda_2^* I_{sc}\left(U_c^*\right)}{C_{sc}\sqrt{\left(U_c^*\right)^2 - 4R_{sc}P_{sc}}} \cdots \\ -2\lambda_{d0}\left[U_c^* - U_{c,\min}\right] sg\left(U_{c,\min} - U_c^*\right) - 2\lambda_{d0}\left[U_{c,\max} - U_c^*\right] sg\left(U_c^* - U_{c,\max}\right) \tag{7.60}$$

The trajectory λ_2^* is obtained by integrating both sides of (7.60) which $\lambda_2^*(0) = \lambda_{20}$ has to be determined.

The optimization problem of Case study 2 is now reduced to the choice of the three values λ_{10}, λ_{20} and λ_{d0} in such a manner that both boundary conditions (charge sustaining conditions) (7.42) and (7.52) are satisfied. However, using a "root finding algorithm" as in Case study 1 to iteratively compute these three values would not be appropriate due to excessive time computation. A simple method, which is much effective in terms of time computation, will be proposed latter. Although this method only offers sub-optimal control sequences of T_{ice}^* and $I_{DC,o}^*$, however, it can be directly used for online implementation.

4.2.3. Physical interpretation of Hamiltonian

This subsection aims at pointing out the physical meaning of the Hamiltonians and the co-states in the previous definitions (7.39) and (7.50). To this end, only Hamiltonian of Case study 2 is considered since it is of a more general form than the one in (7.39).

Let us define the following variables:

$$s_1 \triangleq -\frac{\lambda_1}{U_{oc}\left(SOC_{bat}\right)Q_{bat,0}}; \quad s_2 \triangleq -\frac{\lambda_2}{U_c C_{sc}} \tag{7.61}$$

Then, the expression of the Hamiltonian in (7.50) can be rewritten as:

$$\mathcal{H}_a\left(SOC_{bat}, U_c, T_{ice}, I_{DC,o}, s_1, s_2\right) = P_{fuel}\left(T_{ice}, \omega_{ice}\right) + s_1 P_{bat,i}\left(SOC_{bat}\right) \cdots \\ + s_2 P_{sc,i}\left(U_c, I_{DC,o}\right) + \lambda_d T\left(U_c\right) \tag{7.62}$$

where $P_{fuel}\left(T_{ice}, \omega_{ice}\right)$, $P_{bat,i}\left(SOC_{bat}\right)$ and $P_{sc,i}\left(U_c, I_{DC,o}\right)$ are respectively the fuel power, the inner battery power and the inner supercapacitor power. The physical meaning of the Hamiltonian becomes clearer with (7.62). Indeed, this is the sum of the weighted powers of all energy sources available in

the vehicle. In other words, the Hamiltonian represents an *equivalent fuel power*; and the variables s_1 and s_2 are used to converts the inner battery power and the inner supercapacitor power into the equivalent quantities of fuel power. That is why these variables are usually referred to *equivalence factors* (Paganelli et al., 2002; Sciarretta et al., 2004). The more these variables are important, the more expensive the electric energy is. So, it is more beneficial to recover the energy by regenerative braking. On the contrary, the lower these variables are, the cheaper the electric energy is also. As a consequent, it is more beneficial to use the electric machine to generate the energy (for the case of hybrid vehicles).

In the cases where the state constraints are present, the dynamics $\dot{X}_d$ indicates these constraints are whether or not violated. Then, the term $\lambda_d \dot{X}_d = \lambda_{d0} \dot{X}_d$ is incorporated into the Hamiltonian as a penalty function. The constant λ_{d0} should be selected to be very high such that the supercapacitor state lies in its bound limits in very short time. Since there is no penalty if the state remains between its upper and lower limits, the energy management strategies can make full use of the supercapacitor over the allowable range.

5. Implementation and Results Analysis

In this section, some issues directly related to the implementation of the developed energy management strategies into the simulator are first discussed. Next, a simple idea to derive a causal EMS for real-time applications is presented. Then, to show the performance of the developed strategies in terms of energy consumption efficiency, they will be also compared to a baseline strategy where the energy storage system (ESS: battery and/or supercapacitor) will be practically never charged or discharged. As a consequent, the alternator will be always activated to generate all energy needed for onboard electric demand. Note also that these baseline strategies, provided by VALEO, will not be detailed for confidential reason.

When analyzing the simulation results, it is worth noting that both battery and supercapacitor are oversized with respect to the real needs in this project. So, the corresponding SOC varies in a small range. As a consequent, the management of the state constraints is not really a critical problem.

5.1. Implementation

5.1.1. How to use the optimal control sequences?

The developed EMSs provide, in both case studies, the engine torque and also the alternator torque. They are often used as reference signals to control the ICE and the alternator, respectively.

However, in this project, the ECU is designed by another industrial partner and only optimal alternator torque T_{alt}^{*} will be used to control the reference voltage of the alternator. The control scheme of the alternator is illustrated in Figure 7.13.

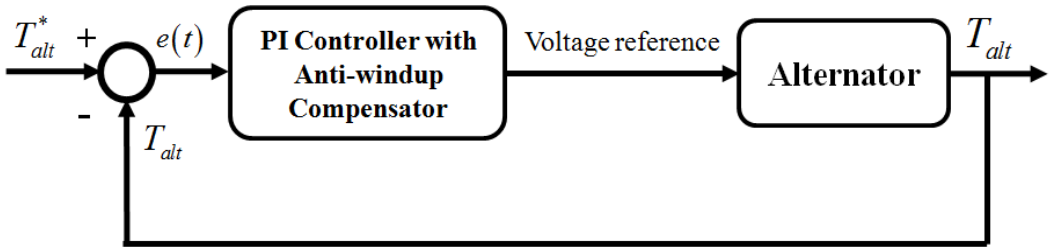

Figure 7.13. Control scheme of the alternator

For Case study 2, the EMS provides also the optimal control sequence $I_{DC,o}^{*}$ which will be used to control the DC/DC converter as shown in Figure 7.11.

One can remark that the approach used in our work does not require any modifications of the vehicle structure (drive train and electric power system). The only simple task for implementation is to replace the existing controller(s) of the baseline strategy with those developed in this chapter.

5.1.2. Online adaptation

As previously emphasized, it is possible to obtain the optimal solutions only when all information of the entire driving cycle is available *a priori*. In subsection 4.2, we also showed that the optimization problems consist finally in determining the constant λ_{10} for Case study 1 and constants λ_{10} and λ_{20} for Case study 2 with a "root finding algorithm". However, these strategies are not causal and cannot be applicable for real-world applications. Therefore, an adaptation of these strategies for online implementation is necessary. Over the years, a great deal of efforts has been investigated to cope with online strategies based on non-causal optimal ones (Sciarretta & Guzzella, 2007). The crucial point of this problem is to find out an appropriate way to adapt the co-state(s) in such a manner that the behavior of causal strategies is as close as possible to the corresponding optimal solution. For simplicity and for computation efficiency, the so-called "λ-control" method is adopted in this work (Delprat et al., 2002; Koot, 2006; Kessels, 2007). This method is based on a feedback control which is easy to implement, see Figure 7.14.

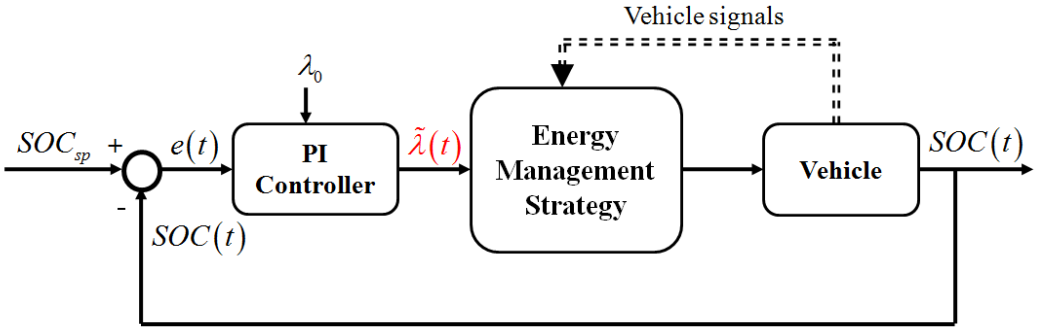

Figure 7.14. Online estimation of the co-state $\tilde{\lambda}$

The expression of the estimated $\tilde{\lambda}$ is given as:

$$\tilde{\lambda} = \lambda_0 + K_p\left(SOC_{sp} - SOC\right) + K_i\int_0^t\left(SOC_{sp} - SOC\right) \tag{7.63}$$

where SOC_{sp} is the SOC set point of the considered energy system storage. This value is given as $SOC_{sp} = SOC(0)$ if the charge sustaining condition is considered. K_p, K_i are the gains of the PI controller and λ_0 is the initial guess.

It can be noticed that the idea of the "λ-control" method is simply to keep the SOC of each energy storage system in a reference range of variation defined by SOC_{sp}. In other words, the feedback "λ-control" aims at preventing the overcharge or depletion of the considered ESS in long term, however, its SOC may "freely" vary in short term. For this reason, the PI controller gains should be selected rather low. A detail on this discussion can be found in (Koot, 2006).

5.2. Simulation Results

5.2.1. Driving cycle

In the framework of vehicular energy management, the energy consumption (and/or pollutant emissions) performance is usually evaluated on a driving cycle. In general, the driver has to follow a vehicle speed reference, given as a function of time, while the gearbox ratios are imposed or not. This allows to compare the considered performance of different vehicle architectures or different energy management strategies in the same driving conditions. The choice of gearbox position, when given, is usually made by a tradeoff between the energy consumption and driving comfort.

The driving cycles can be classified into two categories: normalized driving cycles and real-world driving cycles (Sciarretta & Guzzella, 2007). The former imposed by some standards aims at

measuring the "official" consumption of the vehicles and/or their pollutant emissions. Although the normalized cycles are not representative of real-world driving conditions, the results of different vehicle architectures and/or energy management strategies obtained with these driving cycles can be easily analyzed and interpreted. A well-known example of this category is NEDC (New European Driving Cycle). The cycles of the latter category represent the real driving conditions. In this work, we will consider exclusively the Artemis Road cycle (André, 2004). It allows achieving a realistic evaluation of the results issued from the developed energy management strategies. The vehicle speed and gear position of this real-world driving cycle are shown in Figure 7.15.

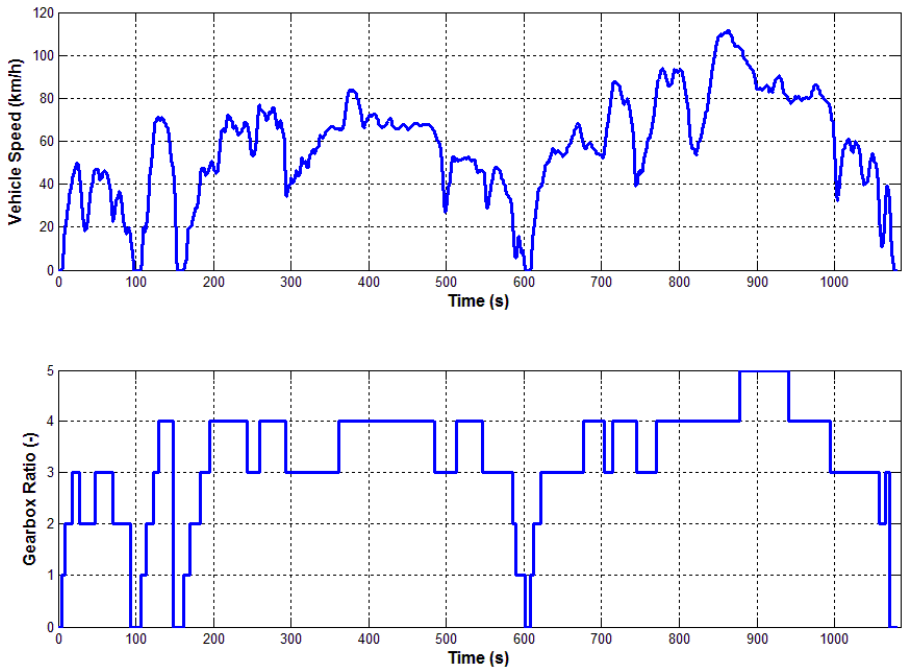

Figure 7.15. Artemis Road cycle: vehicle speed (up) and imposed gearbox ratio (bottom)

For all simulations presented hereafter, the tracking performance of the vehicle with respect to the speed reference of the considered driving cycle is always perfectly guaranteed.

5.2.2. Case study 1

The following strategies are implemented and their results will be compared:

- BL1: Baseline strategy for Case study 1 where the battery is not practically used, so the alternator power is almost equal to the required electric load.
- PMP1: PMP-based optimal strategy for Case study 1 with a given driving cycle.
- RT1: Real-time strategy for Case study 1 with $\tilde{\lambda}_1$ estimated by (7.63).

The desired and the realized alternator torques obtained from PMP1 strategy are presented in Figure 7.16. It can be noticed that the alternator toque, which is indirectly imposed by the voltage reference of the electric power system, globally tracks the optimal alternator torque provided by the PMP1 strategy. However, the alternator has its own dynamics. Hence, the realized torque tends to 0 after a certain time for each alternator activation. This problem, which is unavoidable, will degrade the fuel saving performance of the PMP1 strategy. Indeed, the alternator can take some electric energy which is unscheduled by PMP1 strategy.

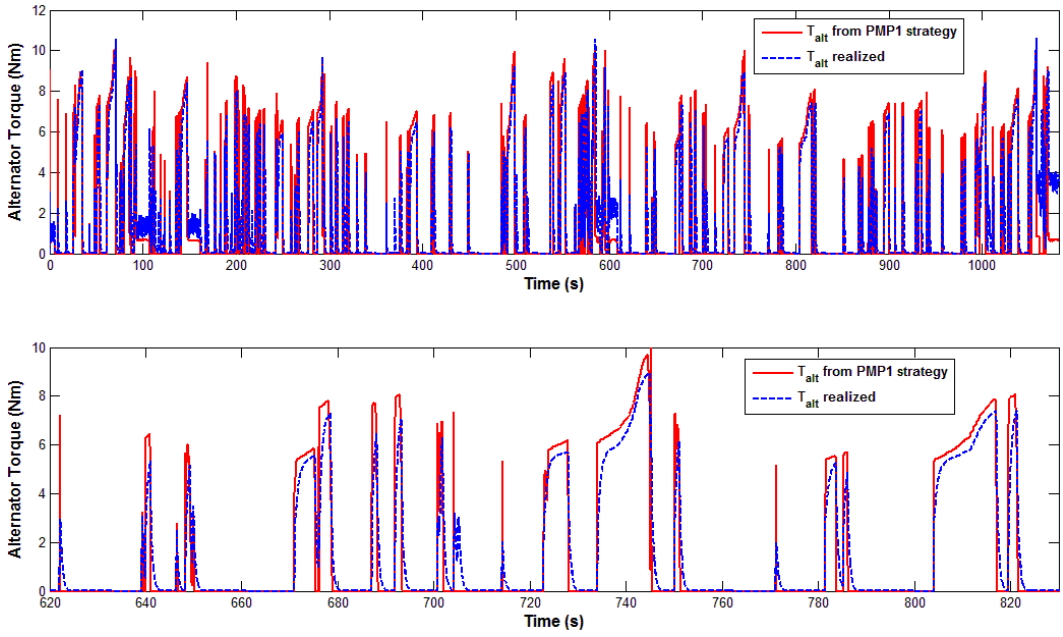

Figure 7.16. Optimal alternator toque provided by PMP1 strategy and real alternator provided by simulator for all the driving cycle (up) and their zooms (bottom)

Figure 7.17 shows the comparison of realized alternator torques between PMP1 and BL1 strategies. As previously stated, BL1 tries to maintain a constant alternator voltage, such that the battery is practically not used and all onboard electric load energy is directly supplied by the alternator. Hence, the alternator will be always activated for this strategy and this can increase the fuel consumption. Concerning PMP1 strategy, it schedules the alternator activation at appropriate moments (deceleration phases, battery charging) and with appropriate quantities of torque. In such a manner, PMP1 strategy can help to recover a certain amount of "free energy" coming from regenerative braking. In addition, with this optimal strategy, the alternator can be also used to shift the operating point of the ICE to other regions that require relative less fuel. Moreover, the battery will be better exploited as shown in Figure 7.18.

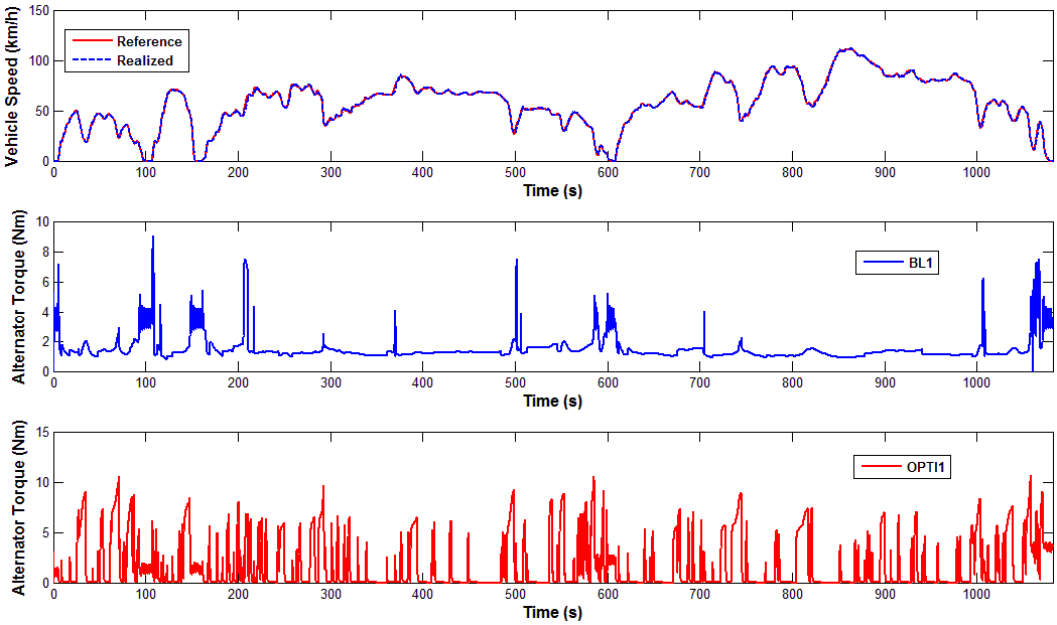

Figure 7.17. Comparison of realized alternator torques between BL1 and PMP1 strategies

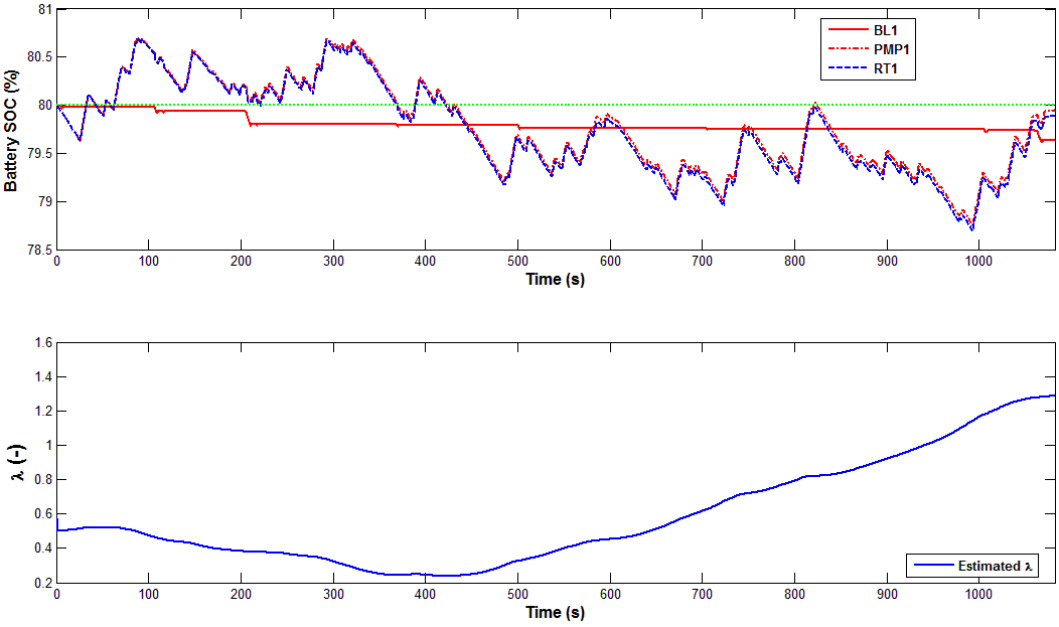

Figure 7.18. Battery state of charge for different strategies (up); trajectory of estimated $\tilde{\lambda}_1$ corresponding to RT1 strategy (bottom)

From Figure 7.18, it can be observed that if the co-state $\tilde{\lambda}_1$ is fine tuned, then RT1 strategy has the same behaviors as PMP1 strategy although it does not need any information on the future of driving cycle. Table 7.2summarizes the energy consumption of the considered strategies, and the fuel saving of PMP1 and RT1 strategies with respect to BL1 strategy for Artemis Road cycle. This table shows

that the proposed strategies (OPTI1 and RT1) are not only effective to reduce the fuel consumption but also can guarantee the sustaining charge condition of the battery.

Strategy	Fuel Use [g]	Fuel Saving [%]	ΔSOC_{bat} [%]
BL1	700.072	0	0.361
OPTI1	685. 597	2.068	0.056
RT1	685.776	2.042	0.111

Table 7.2. Summary of energy consumption for different strategies of Case study 1

5.2.3. Case study 2

As previously stated, searching offline optimal solution with "root finding algorithm" can be too expensive in terms of simulation time. Hence, this will be not presented here and only two strategies are implemented and compared in this case:

- BL2: Baseline strategy for Case study 2 uses only the supercapacitor. The DC/DC converter is controlled by a heuristic strategy of industrial partner. This strategy aims at guaranteeing that the voltage in the supercapacitor side is always superior to the one in the battery side and the supercapacitor energy is always kept between a certain level.
- RT2: Real-time strategy for Case study 2 with $\tilde{\lambda}_1$ and $\tilde{\lambda}_2$ estimated by (7.63).

The results of BL2 and RT2 strategies are compared in Figure 7.19. The same comments on the alternator activation can be done as in Case study 1, i.e. the alternator is mostly activated by RT2 strategy to recover regenerative braking energy. Moreover, RT2 strategy also activates the DC/DC converter more often than BL2 strategy to charge the supercapacitor at appropriate moments. As a consequent, both energy storage systems (ESS) are better exploited in RT2 strategy than in BL2 strategy as shown in Figure 7.20.

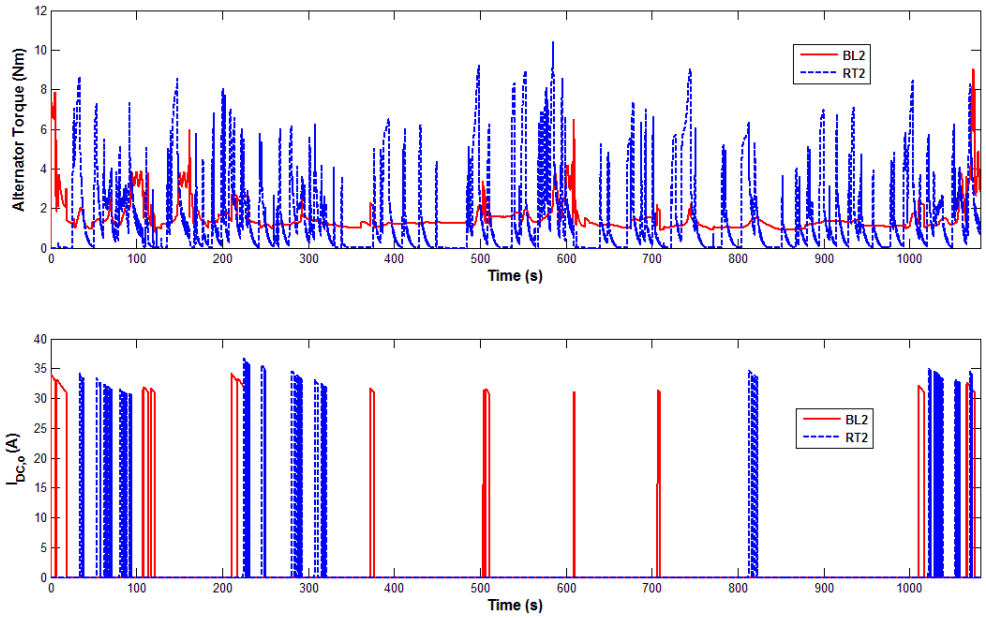

Figure 7.19. Comparison of realized alternator torques and DC/DC converter output current between BL2 and RT2 strategies

It can be also observed from Figure 7.20 that the charge sustaining conditions for both ESSs are guaranteed by RT2 strategy whereas BL2 strategy cannot fulfill this condition for the supercapacitor. Indeed, BL2 strategy only has tendency to charge the supercapacitor. Moreover, as previously stated, the use of the battery is very limited in this case, in particularly, the battery SOC with BL2 strategy is almost constant for the entire driving cycle.

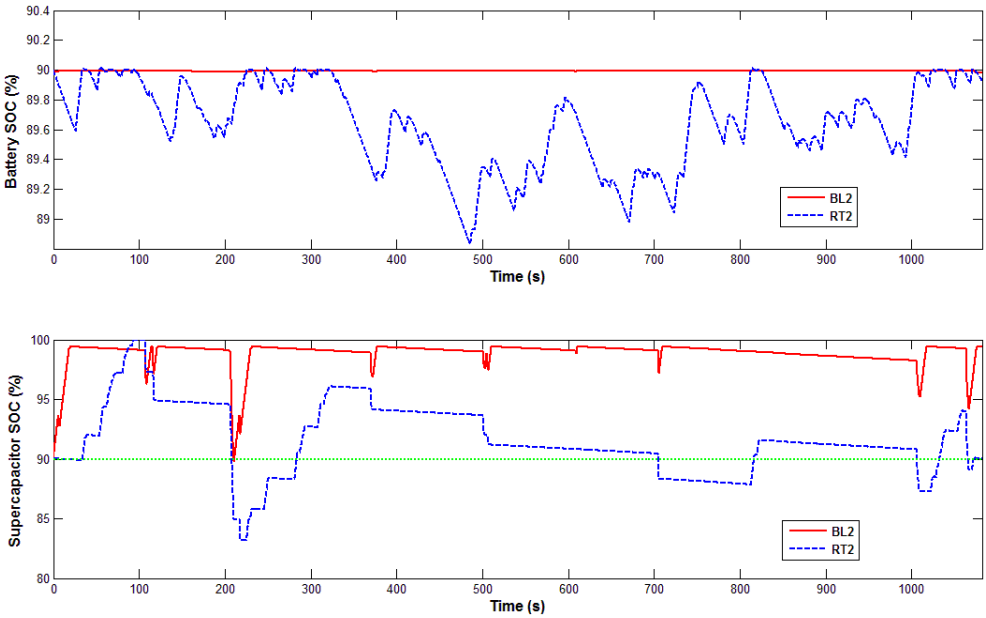

Figure 7.20. Comparison of ESS state of charges between BL2 and RT2 strategies

Figure 7.21 shows that supercapacitor voltage always remains in its operating range, i.e. it is always higher than the battery voltage as imposed by the electric power system and lower than the supercapacitor voltage maximal value (16.2V). Thanks to the penalty function $\lambda_d \dot{X}_d = \lambda_{d0} \dot{X}_d$ incorporated into the Hamiltonian, the supercapacitor voltage only touches its upper limit for a very short time (around 100s) of the driving cycle.

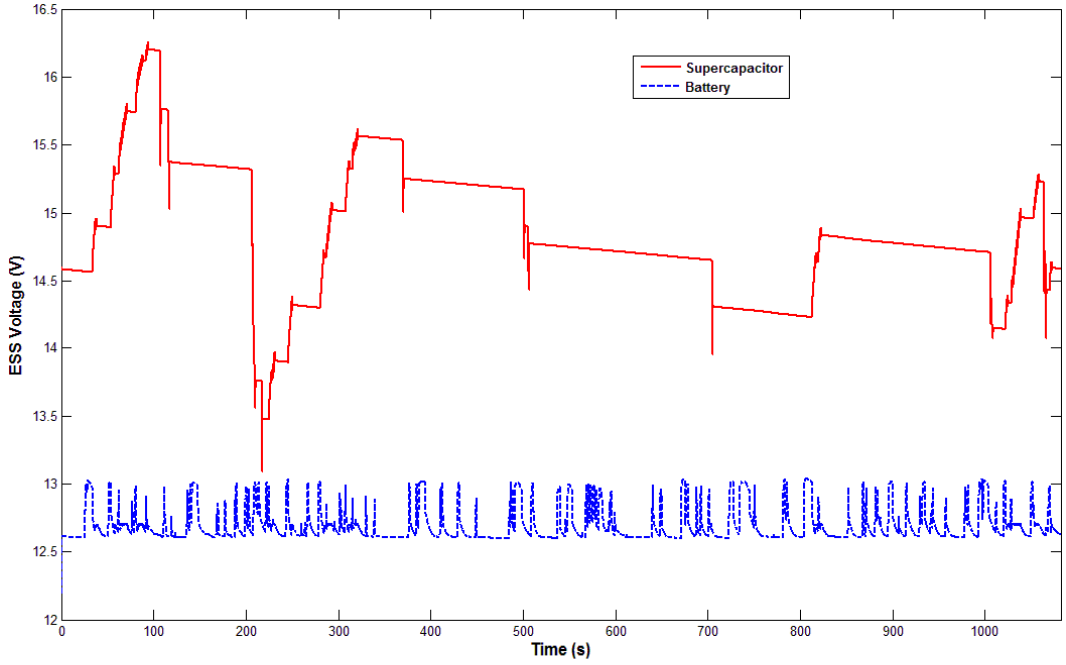

Figure 7.21. Voltages of energy storage systems for RT2 strategy

Table 7.3 summarizes the energy consumption of both strategies, and the fuel saving of RT2 strategy with respect to BL2 strategy for Artemis Road cycle. From the results, it can be concluded that the RT2 strategy is effective for fuel consumption reduction.

Strategy	Fuel Use [g]	Fuel Saving [%]	ΔSOC_{bat} [%]	ΔSOC_{sc} [%]
BL2	701.819	0	0.019	9.394
RT2	690.322	1.634	0.076	0.054

Table 7.3. Summary of energy consumption for different strategies of Case study 2

As can be seen, the results obtained on this unique cycle are very promising. However, several tests with other driving cycles would be necessary to show that the extra energy consumption of eSC

would be compensated with some effective energy management strategies (note that the eSC is practically only activated in low load region).

6. Concluding Remarks

In this work, PMP-based strategies are developed to control "optimally" the vehicular electric power systems. We have shown that this approach has several advantages for real-time implementation. First, causal strategies, which can mimic the behavior of optimal solution, can be easily obtained with a simple feedback control scheme. Second, it is very efficient in terms of time computation because it is based on the instantaneous minimization of the Hamiltonian. The effectiveness of the approach is pointed out through several simulation results for both case studies. Most of fuel saving comes from regenerative braking which is "free" energy. Despite the additional cost for hardware investments, the dual storage electric power system offers a limited fuel saving performance compared to single storage electric power system for the given parameter values in the simulator AMESim. However, this electric structure may be used to reduce the capacity of the battery since it is not practically used or it would be more interesting for electric hybrid vehicles with "stop and start" operation.

Finally, this systematic approach can be directly applied for parallel HEV or can be also generalized to a large family of HEVs with some minor adaptation.

PERSPECTIVES

In order to conclude this thesis, some possible directions for future research are addressed. A distinction is made between application and theory.

***Application*.**

First, to validate the effectiveness of both control approaches for turbocharged air system of a SI engine proposed in Part II, their implementation in an engine test bench is necessary. For this point, we do hope that the test bench in our lab would be soon available.

Second, for the moment the control approach proposed in Chapter 6 is implemented in the simulator with a simple anti-windup scheme to deal with input saturation problem. However, the study on how to theoretically take into account this saturation problem into the control design would be necessary.

Third, there exists many others air system architectures in automotive industry such as dual stage turbocharging systems, air systems with exhaust gas recirculation (EGR) or variable valve timing (VVT), etc. In particular, the hybridization of powertrains may also lead to the introduction of electric systems in air systems such as turbo compound systems or electrical superchargers as in Sural'Hy project. These systems will require the development of new control strategies. However, we believe that the systematic control approaches proposed in this thesis are flexible enough to easily be adapted to these new technologies because they are based on the description of the interactions between the different subsystems and their decoupling. Apart from automotive framework, it is worth noting that the theoretical design tools proposed in Part I and Chapter 6 are also very powerful to deal with a large class of nonlinear systems.

Fourth, the energy management strategies developed in Part III are all validated with a dynamic simulator AMESim. However, they need also to be implemented in the real vehicle developed in the

project framework. Throughout this thesis, all powertrain components of the vehicle are provided according to some study carried out by others industrial partners. Therefore, no optimization on the component dimensioning is dealt with. However, it would be interesting to dimension some components of the electric power system such as alternator, battery, supercapacitor or DC/DC converter by using the experimental design method together with the developed strategies. Another interesting point would be to consider the optimal engine torque provided by the developed strategies as a torque reference and incorporated it in the ECU for the engine control task.

Theory.

First, Lyapunov-based anti-windup strategy is a recent approach to reduce the input saturation effects in modern control theory. Many studies have been investigated in the literature for linear systems. However, this approach in the case of nonlinear system is still an open research topic. To our knowledge, the one-step design method proposed in Chapter 4 is one of the first results in Takagi-Sugeno control framework which can deal with a large class of nonlinear systems. As previously stated, the derived conditions may be conservative. The relaxation of these design conditions is currently under study.

Second, we believe that two-step design method using Takagi-Sugeno models would be also worth being investigated.

Finally, in the collaboration framework with Prof. Michio Sugeno, we have begun to study the piecewise bilinear (PB) model (Sugeno, 1999) and its related control issues. This kind of model offers an unified representation (in the sense of approximation) of a large class of nonlinear systems. From industrial point of view, PB modeling is a powerful tool to approximate a general nonlinear system and the resulting PB model can be also considered as dynamic look-up-table which is very easily implementable. These facts are interesting for both nonlinear control theory and real-world applications. However, up to now, PB model is still an "unknown domain" in control theory. Indeed, most of works related to PB model deal with feedback linearization control technique. However, from our viewpoint, the control approach based on PB model would become really attractive for researchers if we can find out the way to derive their stability/stabilization conditions directly from the Lyapunov stability theorem. The works in (Sugeno, 1999; Sugeno & Taniguchi, 2004) bring some guidelines for this problem which remains an open research topic.

RÉSUMÉ ÉTENDU EN FRANÇAIS

Introduction Générale et Contexte de la Thèse

A ce jour, la conception des véhicules modernes doit répondre à plusieurs défis qui sont souvent contradictoires. D'une part, les législations sur les émissions polluantes imposées par les gouvernements au niveau international sont de plus en plus sévères en raison de préoccupations environnementales. D'autre part, les exigences des clients en termes de performance et d'efficacité pour leurs nouveaux véhicules ont également fortement augmenté. Tous ces objectifs doivent être satisfaits à un coût abordable et avec une haute fiabilité pour les véhicules produits en série. La technique dite de downsizing (réduction de la cylindrée) et l'hybridation électrique sont deux technologies de l'industrie automobile qui sont connues comme des solutions prometteuses pour atteindre ces objectifs.

La technique de downsizing consiste à réduire la cylindrée du moteur tout en gardant les mêmes performances en termes de couple et de puissance que le moteur initial plus important et, en même temps, permet de garantir une amélioration du rendement global du moteur (Leduc et al., 2003). Cette technologie repose sur l'utilisation d'un turbocompresseur pour augmenter la densité des gaz à l'admission du moteur. Malheureusement, la présence du turbocompresseur dans le système d'air provoque le phénomène bien connu de "turbo lag" (qui augmente avec la taille du turbo), c'est à dire une dynamique lente de la pression d'admission (et donc du couple moteur) et le manque de couple moteur à bas régime moteur. Ce phénomène peut être compensé en utilisant une turbine à géométrie variable, ou en intégrant d'autres dispositifs qui vise à aider le turbocompresseur principal à bas régime, comme un autre turbocompresseur, un compresseur mécanique/électrique. En outre, une stratégie de contrôle des systèmes d'air turbocompressé est également cruciale pour obtenir un temps de réponse rapide tout en limitant les dépassements sur le couple moteur produit.

L’hybridation électrique offre de nombreuses possibilités pour améliorer l'efficacité globale des véhicules :

- l'énergie cinétique peut être récupérée (lors des décélérations) et stockée dans des systèmes de stockage d'énergie pour être utilisée plus tard de façon plus appropriée et efficace pour minimiser la consommation d'énergie globale des véhicules,
- les points de fonctionnement du moteur peuvent être déplacés vers les régions où la consommation de carburant est moins élevée,
- la cylindrée du moteur peut être réduite pour minimiser les pertes du moteur,
- le moteur peut être éteint à l'arrêt pour économiser du carburant et limiter également les émissions polluantes.

Cependant, cette technologie conduit à deux inconvénients majeurs. Le premier réside dans le coût supplémentaire induit (machines électriques plus puissantes, systèmes de stockage d'énergie plus sophistiqués, etc.) qui peut rendre le véhicule peu attrayant pour les clients potentiels. Le deuxième inconvénient est la complexité de l'architecture hybride qui rend plus complexe le développement de la stratégie de commande.

Cette thèse a été cofinancée par le groupe VALEO et la région Nord-Pas-de-Calais dans le cadre d'un projet FUI (Fonds Unique Interministériel) nommé Sural'Hy (suralimentation système hybride pour les moteurs à allumage commandé à cylindrée très réduites) labellisé par les pôles de compétitivité I-Trans et Moveo. Le projet vise à développer une solution technologique innovante pour améliorer la consommation d'énergie des moteurs automobiles. La solution proposée est la combinaison de l'hybridation électrique avec la suralimentation électrique. Cette technologie permet de répondre aux attentes des constructeurs qui cherchent des solutions pour aller plus loin dans la voie du "downsizing" de sorte que non seulement la consommation d'énergie mais aussi l'agrément du véhicule peuvent être considérablement améliorés en même temps. À cet effet, un compresseur d'air électrique (eSC) est intégré dans le système d'air turbocompressé existant. Ce dispositif électrique est associé à un système électrique avancé qui est capable de récupérer l'énergie cinétique lors des phases de freinage du véhicule. Tout l'intérêt de cette solution technologique vient des faits suivants. En premier lieu, à bas régime, la disponibilité de l’air compressé et donc du couple est quasi-instantanée. Ensuite, l'eSC peut être utilisé en complément du turbocompresseur principal afin de réduire les effets du "turbo lag". Par conséquent, le confort de conduite est amélioré. En second lieu, la consommation d'énergie de l'eSC peut être plus ou moins compensée par l'énergie "gratuite"

récupérée par le système électrique avancé du véhicule avec une stratégie de gestion d'énergie efficace. Dans ce contexte, deux sujets de recherche sont spécifiquement considérés dans cette thèse :

- Les applications automobiles concernent concrètement la commande du système d'air turbocompressé d'un moteur à allumage commandé et la gestion énergétique du système électrique du véhicule.
- Afin de répondre aux besoins de ces applications automobiles, nous avons développé dans cette thèse quelques nouveaux outils théoriques utilisant des commandes non linéaires à base des modèles polytopiques impliquant des inégalités matricielles linéaires (LMI).

Pour le premier sujet de recherche, il est à noter que la tâche de contrôle moteur dans le projet Sural'Hy est prise en charge par un autre partenaire industriel. Notre tâche pour ce projet est donc de concevoir un système de gestion énergétique pour différents systèmes électriques du véhicule. En parallèle de ce travail, la commande du système d'air turbocompressé du même moteur à allumage commandé étudié est également effectuée dans la thèse. Cependant, dans ce cas, l'eSC n'est pas encore pris en compte directement dans le système d'air.

Au cours des dernières années, les systèmes automobiles sont devenus un sujet attractif aussi bien pour les chercheurs industriels qu'académiques. En effet, les exigences au niveau de performance et les préoccupations environnementales concernant ces systèmes ont constamment augmenté - le système d'air turbocompressé des moteurs à allumage commandé est un exemple très pertinent de cette tendance. Par conséquent, les systèmes considérés sont devenus de plus en plus sophistiqués pour faire face à cette situation. Une solution à faible coût pour répondre à ces exigences est de proposer des stratégies de plus en plus efficaces de contrôle en termes de précision, de temps de réponse et de robustesse. Dans le second sujet de recherche, des outils théoriques étant capable de relever ce défi de commande sont développés. En général, ces techniques de commande sont également très puissantes pour traiter une large classe de systèmes non linéaires complexes.

Structure de la Thèse

Cette thèse est divisée en trois parties :

- Partie I : Contributions à la stabilisation des systèmes non linéaires à entrée saturée représentés sous la forme Takagi-Sugeno.
- Partie II : Nouvelles approches pour le contrôle d'un système d'air turbocompressé.
- Partie III : Stratégie de gestion de l'énergie pour les systèmes électriques du véhicule.

Chaque partie commence avec une introduction contenant un résumé détaillé de chaque chapitre. Dans ce qui suit, un aperçu rapide des trois parties et de chacun de leurs chapitres est donné.

1. Partie I : Contributions à la stabilisation des systèmes non linéaires à entrée saturée représentés sous la forme Takagi-Sugeno

Au cours des deux dernières décennies, la technique de commande basée sur les modèles Takagi-Sugeno (T-S) (Takagi & Sugeno, 1985) est devenue un sujet de recherche actif (Tanaka & Wang, 2001). En particulier, cette technique a reçu de plus en plus d'attention de la part de la communauté automaticienne (Sala et al., 2005; Feng, 2006; Guerra et al., 2009), car elle a été appliquée avec succès à de nombreuses applications d'ingénierie (Tanaka & Wang, 2001; Lauber et al., 2011; Nguyen et al., 2012a). Les modèles T-S sont inspirés de l'approche historique de la logique floue (Mamdani, 1974). Ils peuvent être interprétés comme une collection de modèles linéaires locaux interconnectés par des fonctions d'appartenance non linéaires. Ensuite, une commande basée sur le modèle T-S peut être conçue pour garantir la stabilité et certaines performances pour le système non linéaire original. Un tel modèle présente plusieurs avantages. Premièrement, le modèle T-S est une approximation universelle (Tanaka & Wang, 2001), et dans de nombreux cas, ce type de modèles peut être utilisé pour représenter exactement des systèmes non linéaires de façon globale ou semi-globale (Ohtake et al., 2001). Deuxièmement, grâce à sa structure polytopique, l'approche de commande basée sur des modèles T-S rend possible l'extension de certains outils de commande très puissants pour les systèmes linéaires au cas des systèmes non linéaires (Tanaka & Wang, 2001). Troisièmement, cette technique de commande fournit un cadre général et systématique pour traiter une large classe de systèmes non linéaires. En effet, beaucoup de conditions concernant la stabilité ou la stabilisation dans le cadre du modèle T-S sont formulées comme des contraintes LMI (inégalités matricielles linéaires) (Boyd et al., 1994; Scherer & Weiland, 2005), le problème de commande peut

alors être résolu efficacement avec des algorithmes numériques déjà disponibles (Tanaka & Wang, 2001).

Parmi tous les phénomènes non linéaires, la saturation de la commande est inévitable dans presque toutes les applications réelles. Cet effet peut sévèrement dégrader les performances du système en boucle fermée et dans certains cas, conduire à l'instabilité du système. Motivés par cet aspect pratique de commande, beaucoup d'efforts ont récemment été consacrés aux systèmes saturés, voir par exemple (Fang et al., 2004; Tarbouriech et al., 2011) et les références qui s'y trouvent. Cependant, très peu de résultats sont disponibles pour les systèmes non linéaires.

En général, il existe deux approches principales pour traiter des problèmes de saturation d'entrée. La première prend directement en compte l'effet de saturation dans le processus de conception de la commande. À cette fin, deux techniques principales de synthèse sont considérées dans la littérature : la *loi de commande saturée* et celle *non-saturée*. Pour la deuxième technique, le domaine des états initiaux et la conception est telle que la loi de commande n'atteindra jamais la limite de saturation. Présenté par exemple dans (Tanaka & Wang, 2001; Ohtake et al., 2006), ce type de commande à faible gain est très conservatif et conduit souvent à des performances médiocres de la boucle fermée (Tarbouriech et al., 2011; Cao & Lin, 2003). Comme son nom l'indique, la loi de commande saturée (Cao & Lin, 2003) permet la saturation du signal de commande et donc autorise de meilleures performances. C'est pourquoi ce type de lois de commande sera abordé dans cette thèse. Dans la seconde approche, l'effet de saturation est traité en utilisant des compensateurs *anti-windup*. Deux types de méthodes de synthèse de contrôleurs basés sur les stratégies *anti-windup* peuvent être trouvés dans la littérature : la méthode à "*une étape*" et celle à "*deux étapes*". Pour la première méthode, la stratégie anti-windup est directement prise en compte dans le contrôleur. Par conséquent, le contrôleur et le compensateur anti-windup sont conçus simultanément (Wu et al., 2000; Mulder et al., 2009). Pour la méthode à "deux étapes", la loi de commande est tout d'abord calculée en ignorant la saturation de l'actionneur. Une fois que le contrôleur a été conçu, un compensateur anti-windup supplémentaire est intégré afin de minimiser tout effet indésirable des contraintes de saturation sur les performances en boucle fermée (Hu et al., 2008; Zaccarian & Teel, 2004; Tarbouriech et al., 2011). Dans cette thèse, nous abordons uniquement la méthode à "une étape". Dans la littérature, la plupart des travaux sur les compensateurs anti-windup sont disponibles pour les systèmes linéaires invariants dans le temps (LTI). L'ouvrage (Tarbouriech et al., 2011) offre un excellent aperçu de ces travaux. Cependant, très peu de résultats existent pour les systèmes non linéaires.

Motivés par ces constats, la partie I présente quelques contributions à la stabilisation des systèmes non linéaires soumis à saturation de l'actionneur dans le cadre de la commande basée sur les modèles T-S. Cette partie est organisée comme suit.

1.1. Chapitre 2 : État de l'art sur les modèles Takagi-Sugeno

Le chapitre 2 a pour but de présenter un rapide tour d'horizon des différents résultats concernant la stabilité et la conception de commande basée sur des modèles T-S. Ici, seuls quelques problèmes basiques concernant les modèles T-S seront couverts. L'unique objectif de ce chapitre est de montrer les différentes possibilités que les modèles T-S peuvent offrir en termes d'analyse et de conception de lois de commande pour les systèmes non linéaires. Nous n'avons pas l'intention de donner un état de l'art complet sur ce sujet, mais de fournir des informations directement liées à d'autres chapitres de cette partie. Plus d'informations peuvent être trouvées dans, par exemple, (Sala et al., 2005; Feng, 2006; Guerra et al., 2009).

Le chapitre commence par une description des modèles T-S, suivie par la procédure de construction d'un tel modèle à partir d'un modèle non linéaire ayant été obtenu à partir des lois de la physique par exemple. En général, les problèmes de conception des lois de commande basées sur les modèles T-S peuvent être formulés en termes de contraintes LMI (Boyd et al., 1994). À cette fin, quelques notions de base sur les problèmes d'optimisation convexe et les propriétés matricielles seront rappelées.

Dans le cadre des modèles T-S, la méthode directe de Lyapunov est généralement utilisée pour dériver les conditions permettant le calcul des gains du contrôleur. Pour simplifier, seuls quelques résultats classiques sur la stabilité et la stabilisation en utilisant une fonction de Lyapunov quadratique sont présentés. Un état de l'art sur les contrôleurs de retour de sortie est également donné. Parmi les nombreux résultats disponibles dans la littérature concernant les performances des contrôleurs, nous ne présentons que quelques-uns d'entre eux ayant trait directement aux travaux de thèse. Enfin, des discussions sur le conservatisme des solutions sont également présentées dans ce chapitre. En effet, il faut souligner que seules des conditions suffisantes sont obtenues en considérant des modèles T-S. Le conservatisme provient des sources suivantes :

- aucune information sur les fonctions d'appartenance non linéaires n’est exploitée à l'exception de la propriété de somme convexe;
- les conditions utilisées pour tester la réalisabilité d’une LMI paramétrée ne sont que suffisantes;

- le choix des fonctions de Lyapunov.

Différents travaux ont été consacrés à réduire ce conservatisme, voir (Sala et al., 2005; Feng, 2006) pour plus de détails, aussi nous ne développerons pas cette direction de recherche dans la thèse.

1.2. Chapitre 3 : Stabilisation des modèles T-S soumis à la saturation de commande : Approche de représentation polytopique

Le chapitre 3 présente une nouvelle méthode de conception d'un contrôleur robuste H_∞ stabilisant des systèmes T-S à commutation incertains et perturbés qui sont soumis à la saturation de la commande. À cette fin, des motivations sur le choix d'un modèle T-S à commutation au lieu d'un modèle T-S classique sont présentées. Dans ce chapitre, la non-linéarité concernant la saturation est directement prise en compte dans la conception de lois de commande sous sa forme polytopique. Deux cas seront étudiés: la commande par retour d'état (SFC) et la commande par retour de sortie statique (SOFC). La seconde méthode de Lyapunov est utilisée pour dériver des conditions de conception, qui sont formulés comme un problème d'optimisation LMI. Ensuite, la conception du contrôleur revient à résoudre un ensemble de conditions LMI avec des outils numériques. En comparaison avec les résultats existant dans la littérature, la méthode proposée ne fournit pas seulement une procédure de conception simple et efficace, mais aussi permet d'obtenir des contrôleurs moins conservatifs en maximisant le domaine d'attraction. De cette façon, les performances de la boucle fermée peuvent être améliorées.

Le contrôleur est basé sur le concept PDC (Parallel Distributed Compensation) (Tanaka & Wang, 2001) et la prise en compte de la performance H_∞ garantissant l'atténuation des perturbations. En utilisant la théorie de stabilité de Lyapunov, les conditions de conception sont établies pour les deux catégories de lois de commande : SFC et SOFC. Le point clé de la méthode proposée est d'obtenir des conditions de conception sous forme LMI. Ainsi, les gains du contrôleur peuvent être calculés de manière efficace avec des outils numériques (Gahinet et al., 1995). À notre connaissance, très peu de résultats portent sur les modèles T-S à commutation incertains et perturbés, surtout avec l'approche SOFC. La méthode proposée peut être appliquée à une large classe de systèmes à commutation non linéaires et constitue la principale contribution de ce chapitre.

1.3. Chapitre 4 : Stabilisation des modèles T-S soumis à la saturation de commande : Approche basée sur la stratégie anti-windup

Dans le cadre de la commande basée sur les modèles T-S, la commande par retour d'état utilisant le concept de compensation parallèle distribué (PDC) (Wang et al., 1996) est généralement appliquée afin de dériver des conditions de conception (Tanaka & Wang, 2001; Guerra & Vermeiren, 2004). Cependant, les mesures des différents états du système ne sont pas toujours disponibles dans de nombreux cas pratiques. Par conséquent, la commande par retour de sortie a été intensivement étudiée dans la littérature, voir (Feng, 2006) pour un aperçu. La plupart des travaux concerne la conception des contrôleurs basés sur les observateurs (Tanaka et al., 1998; Liu & Zhang, 2003; Lin et al., 2005). Toutefois, le principe de séparation n'est plus applicable lorsque les variables de prémisse ne sont pas toutes mesurables (Nguang & Shi, 2003; Guerra et al., 2006). En particulier, l'approche observateur-contrôleur devient beaucoup plus compliquée lorsqu'il s'agit de systèmes non linéaires soumis à la saturation de la commande et à des contraintes sur l'état. Ce problème de commande est peu traité dans la littérature (Ding, 2009).

Motivé par ces aspects de commande, le chapitre 4 porte sur le développement d'une nouvelle approche pour concevoir simultanément un contrôleur par retour de sortie dynamique (DOFC) et un compensateur anti-windup pour un système non linéaire donné. À cette fin, le système non linéaire perturbé soumis à la saturation de l'actionneur et aux contraintes sur l'état est représenté sous la forme T-S et le DOFC proposé dans (Li et al., 2000) est adopté. En utilisant la seconde méthode de Lyapunov, la conception du contrôleur est formulée comme un problème d'optimisation multi-objectif convexe permettant la spécification de plusieurs performances souvent contradictoires. Un exemple est également donné pour illustrer l'efficacité de l'approche proposée.

La conception du contrôleur basé sur l'anti-windup en présence de perturbations à énergie bornée et de contraintes sur l'état est une contribution originale dans le cadre de commande T-S. Cette méthode proposée fournit un outil systématique pour traiter une très large classe de systèmes non linéaires, ce qui est notre contribution majeure pour ce travail.

2. Partie II : Nouvelles approches pour le contrôle d'un système d'air turbocompressé

Aujourd'hui, les concepteurs de moteurs automobiles modernes doivent relever plusieurs défis qui sont souvent contradictoires. D'une part, les nouvelles normes concernant les émissions polluantes imposées par les gouvernements au niveau international sont de plus en plus strictes en raison des préoccupations environnementales. D'autre part, les exigences des clients en termes de performance

et de rendement sont également de plus en plus sévères. Tous ces objectifs doivent être satisfaits à faible coût et haute fiabilité pour des véhicules de série. Le downsizing (réduction de la cylindrée du moteur) est une solution très prometteuse pour atteindre ces objectifs. En effet, la combinaison de la suralimentation avec le downsizing est devenue une technologie clé pour améliorer les performances du moteur telles que l'économie de carburant, la réduction des pertes de pompage pour augmenter le rendement du moteur ou l'amélioration du confort de conduite. Les systèmes de contrôle efficaces de la boucle d'air du moteur permettent de profiter pleinement des potentiels de cette technologie. Dans ce contexte, la partie II propose deux nouvelles approches pour commander un système d'air turbocompressé d'un moteur à l'allumage commandé.

2.1. Chapitre 5 : Commande multi-objective basée sur les modèles Takagi-Sugeno à commutation pour le système d'air suralimenté

Le chapitre 5 porte sur la modélisation du système d'air d'un moteur à allumage commandé et propose un nouveau contrôleur robuste H_∞ à commutation pour ce système complexe. D'abord, un aperçu rapide sur les moteurs à l'allumage commandé et sur la modélisation d'un système d'air turbocompressé est donné. Ensuite, nous proposons de considérer ce modèle complexe comme un système à commutation afin de simplifier le modèle de commande et, en même temps, de tenir compte de la stratégie minimisant les pertes par pompage du moteur. Puis, la conception du contrôleur robuste est directement basée sur les résultats théoriques concernant le modèle T-S à commutation présentés dans le chapitre 3. Le contrôleur à commutation proposé traite facilement les non-linéarités complexes et facilite considérablement l'analyse de la stabilité globale de l'ensemble du système d'air turbocompressé. Par rapport aux résultats actuels dans la littérature, la méthode proposée limite significativement les efforts de calibration sur toute la plage de fonctionnement du moteur avec des performances très satisfaisantes de la boucle fermée. Enfin, cette approche peut être généralisée pour les autres systèmes d'air turbocompressés plus complexes avec quelques adaptations.

2.2. Chapitre 6 : Commande linéarisante robuste pour le système d'air turbocompressé d'un moteur à l'allumage commandé: Vers une approche minimisant la consommation de carburant

La commande du système d'air turbocompressé d'un moteur à l'allumage commandé est connue comme un problème très intéressant dans l'industrie automobile. Au fil des ans, de nombreuses approches ont été proposées dans la littérature pour traiter ce problème de commande. Cependant, jusqu'à maintenant, c'est encore un sujet de recherche très actif dans l'industrie. Les difficultés rencontrées lorsqu'on commande ce système sont principalement dues aux faits suivants. Tout

d'abord, il y a beaucoup de non-linéarités complexes impliquées dans ce système multivariable. Ensuite, il n'est pas facile de prendre en compte la stratégie minimisant la consommation de carburant (Eriksson et al., 2002) dans la conception du contrôleur lorsque l'on considère l'ensemble du système. Dans le chapitre 5, un état de l'art concernant ce problème de commande est donné. Nous avons également proposé un contrôleur robuste basé sur les modèles Takagi-Sugeno à commutation permettant de s'affranchir des difficultés mentionnées. Bien que ce contrôleur non linéaire donne des performances très satisfaisantes en boucle fermée, il pourrait sembler complexe du point de vue industriel. Dans ce chapitre, nous proposons une deuxième approche basée sur la commande linéarisante robuste pour le système d'air turbocompressé qui est beaucoup plus simple (dans le sens de la conception et de la mise en œuvre) et peut atteindre pratiquement le même niveau de performances que le contrôleur proposé dans le chapitre 5.

La commande linéarisante est un outil simple et systématique pour la conception des lois de commande des systèmes non linéaires. L'idée de base est de transformer (totalement ou partiellement) les systèmes non linéaires en ceux linéaires de sorte que les techniques de commande linéaires peuvent être appliquées par la suite. Cependant, il est bien connu que cette technique est basée sur le principe de l'annulation exacte des non-linéarités. Par conséquent, elle exige des modèles de haute qualité. Ce fait est directement lié à la propriété de robustesse en boucle fermée par rapport aux incertitudes de modélisation. À cette fin, une nouvelle commande robuste pour traiter des incertitudes/perturbations sera proposée. Par rapport à certains autres résultats existants sur la commande linéarisante robuste (Ha & Gilbert, 1987; Kravaris & Palanki, 1988; Khalil, 2002), la méthode proposée est non seulement simple et constructive, mais aussi permet d'obtenir facilement des gains du contrôleur en résolvant un problème d'optimisation convexe (Boyd et al., 1994). Par ailleurs, cette méthode peut être appliquée à une large classe de systèmes non linéaires qui sont linéarisables et possèdent des dynamiques internes stables. Enfin, l'analyse de la stabilité de la dynamique interne sera également illustrée par notre application concernant le contrôle de moteur à la fin de ce chapitre.

A notre connaissance, c'est la deuxième approche de commande non linéaire multivariable qui peut garantir la stabilité de l'ensemble du système d'air turbocompressé en boucle fermée, tout en tenant compte de la stratégie de minimisation de carburant après (Nguyen et al., 2012a) et le premier contrôleur non linéaire qui est directement basé sur le modèle complet de ce système. En outre, l'approche de contrôle proposée dans ce travail pourrait également limiter les capteurs coûteux et/ou les observateurs/estimateurs complexes en exploitant au maximum possible les informations

disponibles. L'idée est d'estimer toutes les variables nécessaires à la conception du contrôleur par des cartographies statiques issues des mesures du banc d'essais. Deux stratégies de contrôle du système d'air turbocompressé sont présentées dans ce chapitre : la stratégie d'optimisation du confort de conduite et celle d'optimisation de consommation de carburant. La simplicité et l'efficacité de ces deux stratégies indiquent clairement que l'approche proposée dans ce chapitre est très pertinente notamment dans le contexte industriel. En effet, par le biais de cette application réelle, nous tenons à souligner que la commande linéarisante robuste proposée dans ce chapitre pourrait être un outil non linéaire intéressant pour des applications industrielles.

Le travail dans le chapitre 6 présente nos premiers résultats réalisés en collaboration avec le professeur Michio Sugeno, chercheur émérite du European Centre for Soft Computing, en Espagne. Nous tenons à remercier l'aide précieuse du professeur Marie-Thierry Guerra, directeur du LAMIH.

3. Partie III : Stratégie de gestion de l'énergie pour les systèmes électriques du véhicule

La troisième partie est composée du chapitre 7. Ce chapitre porte sur le travail directement lié à notre tâche dans le projet Sural'Hy avec d'autres partenaires industriels.

3.1. Motivations

Au fil des ans, la demande de consommation d'énergie électrique dans les véhicules conventionnels est devenue de plus en plus importante. Cela est dû au fait que les clients du secteur automobile sont plus exigeants en termes de performances, de confort et de sécurité pour leurs nouveaux véhicules. Par conséquent, le nombre de dispositifs auxiliaires alimentés par le réseau électrique du véhicule a constamment augmenté dans les véhicules modernes, par exemple les suspensions actives, les freins électriques, etc. Cette demande croissante a tendance à doubler ou tripler la consommation électrique dans les prochaines années (Soong et al., 2001). Outre améliorer l'efficacité des composants électriques, une stratégie de gestion de l'énergie efficace est également cruciale afin de minimiser la consommation d'énergie globale du véhicule.

Dans notre projet, une particularité du véhicule étudié consiste en la présence d'un compresseur électrique (E-charger) dans le système d'air turbocompressé du moteur à l'allumage commandé. Ce dispositif vise à aider le turbocompresseur principal à réduire les effets de "turbo lag", c'est-à-dire, la dynamique lente du couple moteur et le manque de couple à faibles régimes. En conséquence, le confort de conduite est nettement amélioré. L'énergie consommée par l'E-charger provient soit de l'alternateur soit du système de stockage d'énergie du système électrique du véhicule. À cette fin, le véhicule est équipé d'un alternateur avancé qui peut être contrôlé en puissance. A noter que cet

alternateur est directement couplé à l'arbre primaire du véhicule et, par conséquent, le point de fonctionnement du moteur peut être déplacé en commandant la puissance de sortie de l'alternateur, ce qui offre un degré de liberté pour l'optimisation de l'énergie comme dans le cas des véhicules hybrides classiques (Koot, 2006). Toutefois, cet alternateur à faible capacité est exclusivement utilisé pour fournir l'énergie au système électrique et ne peut pas aider le moteur thermique pour propulser le véhicule. Il est à noter aussi que l'alternateur considéré peut également récupérer l'énergie cinétique pendant les phases de freinage régénératif. Cette "énergie gratuite" est ensuite stockée dans le système de stockage et sera utilisée ultérieurement à des moments appropriés.

D'après les remarques ci-dessus, il est clair que la gestion de l'énergie devient primordiale pour améliorer le rendement énergétique global du véhicule étudié. En effet, un des objectifs du projet est aussi de savoir si l'énergie consommée par l'E-charger pourrait être totalement compensée par le gain d'énergie obtenu avec une stratégie de gestion de l'énergie efficace.

3.2. But de la partie III

Le but de ce travail est de développer des stratégies de gestion de l'énergie qui optimisent le flux d'énergie des systèmes électriques du véhicule considéré. Grâce à ces stratégies, la consommation d'énergie globale du véhicule sera réduite au minimum dans toutes les situations de conduite. Les stratégies développées doivent répondre à plusieurs objectifs. Tout d'abord, lorsque les conditions de conduite sont parfaitement connues à l'avance, elles sont capables d'offrir une solution optimale globale. Cependant, la connaissance sur l'ensemble du cycle de conduite n'est malheureusement pas disponible pour les applications en temps réel. Ainsi, le second objectif de ces stratégies est que leurs adaptations aux situations de conduite réelles soient simples et les stratégies causales résultant ressemblent le plus fidèlement possible à celles optimales globales. Ensuite, les stratégies développées doivent être simples pour être implémentées facilement et peu couteuses en termes de calcul. Puis, les stratégies sont basées sur une approche systématique afin qu'elles puissent être applicables à une large gamme de dimensions des composants sans avoir besoin des calibrations couteuses. Pour toutes ces raisons, les stratégies développées seront basées sur une approche de contrôle optimal avec des modèles des composants physiques du véhicule.

Dans ce travail, deux systèmes électriques pour la même structure du véhicule seront considérés. Le véhicule est équipé d'un groupe motopropulseur conventionnel avec une boîte manuelle à 5 vitesses. L'alternateur est relié au moteur thermique par un réducteur avec un rapport fixe. La seule

différence entre ces systèmes électriques consiste dans leurs systèmes de stockage d'énergie. Le flux de puissance des deux études de cas est décrit ci-dessous.

3.2.1. Cas 1: Système de stockage d'énergie simple

Ce système de stockage d'énergie se compose uniquement de la batterie comme système dynamique. Les composants connectés au système électrique dans ce cas sont la batterie, l'alternateur, les auxiliaires à bord et l'E-charger. Pour la simplicité, tous les auxiliaires électriques sont modélisés par un seul consommateur d'énergie. En ce qui concerne l'E-charger, il est commandé par le calculateur du moteur qui est hors du contexte de ce travail. Cependant, son profil de consommation d'énergie est connu et sera considéré comme une entrée pour les stratégies développées. Les flux de puissance dans ce cas sont représentés dans la figure suivante où le sens des flèches correspondant au sens de l'échange d'énergie entre les différents composants :

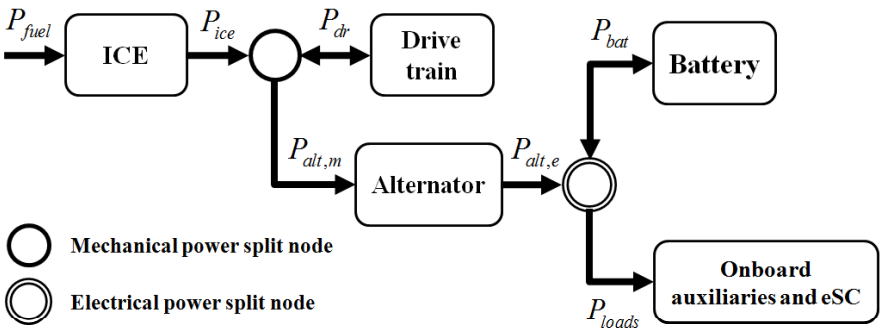

Système électrique du véhicule pour le Cas 1

Ce cas offre un seul degré de liberté pour l'optimisation qui vient de l'architecture mécanique du véhicule. La stratégie de gestion de l'énergie vise à contrôler "optimalement" l'alternateur dans le sens de l'efficacité énergétique. En conséquence, la batterie sera chargée ou déchargée de façon temporaire pour produire la quantité d'énergie appropriée pour le système électrique. La stratégie considère la batterie comme un tampon d'énergie et son état de charge doit être maintenu à la fin du cycle de conduite.

3.2.2. Cas 2 : Système de stockage d'énergie avancé

Outre les composants présents dans le système électrique du Cas 1, une supercapacité est également disponible dans ce cas comme un second système de stockage dynamique. Les deux sources d'énergie (batterie et supercapacité) sont reliées entre eux grâce à un convertisseur DC/DC. Il est à noter que le Cas 1 n'est rien d'autre qu'un cas particulier du Cas 2 où la supercapacité et le

convertisseur DC/DC sont retirés du système électrique. Un schéma concernant les flux de puissance dans ce cas est représenté comme suit :

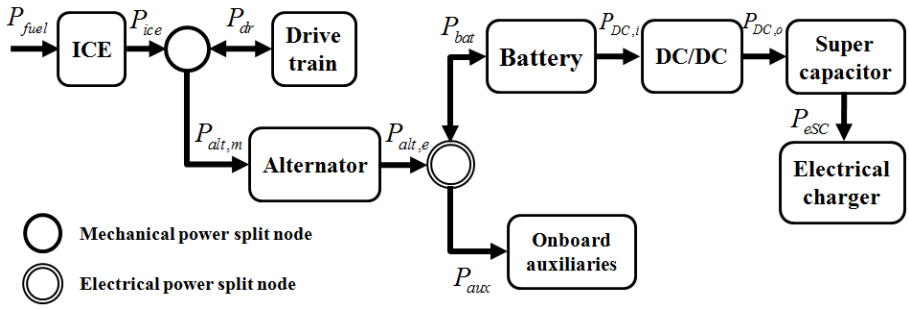

Système électrique du véhicule pour le Cas 2

Pour ce deuxième cas, deux degrés de liberté sont disponibles pour l'optimisation. Le premier vient de l'architecture mécanique du véhicule comme dans le Cas 1, tandis que le seconde vient du système électrique. Dans ce cas, la batterie et la supercapacité sont considérées comme des tampons de l'énergie et les conditions sur les charges soutenues devraient être vérifiées pour chacune d'elles. Cependant, l'utilisation de la batterie doit être limitée, c'est à dire qu'il est principalement utilisé pour la demande de bord auxiliaire lorsque cela est vraiment nécessaire.

Enfin, toutes les stratégies développées dans cette partie sont évaluées dans un environnement de simulation avancé sous AMESim. Le problème de la gestion de l'énergie considéré dans ce travail est très similaire à celui des véhicules électriques hybrides (VEH). Par conséquent, les stratégies développées peuvent être appliquées directement aux VEH de structure parallèle. Elles sont aussi facilement généralisées à d'autres types de véhicules hybrides avec quelques modifications mineures.

Perspectives

Dans la conclusion de cette thèse, quelques directions possibles pour de futures recherches sont proposées. Cela concerne les applications automobiles considérées ainsi que la théorie sur la technique de commande à base des modèles Takagi-Sugeno à entrée saturée.

Applications automobiles.

Premièrement, il est nécessaire d'implémenter sur un banc d'essai moteur les deux approches de commande pour le système d'air turbocompressé d'un moteur d'essence proposées dans la Partie II afin de valider leur efficacité. Pour ce point, le banc d'essai dans notre laboratoire sera utilisé.

Deuxièmement, l'étude sur la prise en compte de la saturation de commande dans l'approche de commande proposée au chapitre 6 serait également nécessaire.

Troisièmement, dans l'industrie automobile, il existe beaucoup d'autres architectures de systèmes d'air comme les systèmes de suralimentation à double étage, les systèmes d'air avec la recirculation des gaz d'échappement (EGR) ou les soupapes à distribution variable (VVT), etc. En particulier, l'hybridation de motorisation peut également conduire à l'introduction de systèmes électriques dans les systèmes d'air tels que les compresseurs électriques comme c'est le cas dans le projet Sural'Hy. Ces systèmes nécessitent le développement de nouvelles stratégies de commande. Cependant, nous croyons que les approches systématiques de commande proposées dans cette thèse sont suffisamment flexibles pour être facilement adaptées à ces nouvelles technologies. En dehors du cadre automobile, il est à noter que les outils de commande théoriques proposés dans la Partie I et le chapitre 6 sont également très intéressants pour traiter une large classe de systèmes non linéaires.

Quatrièmement, les stratégies de gestion de l'énergie développées dans la Partie III sont toutes validées sur un simulateur dynamique sous AMESim. Cependant, elles doivent également être implémentées dans le véhicule réel développé dans le cadre du projet. Tout au long de cette thèse, tous les composants du groupe motopropulseur du véhicule sont fournis selon des études préliminaires réalisées par d'autres partenaires industriels. Par conséquent, aucune optimisation concernant le dimensionnement des composants n'a été complètement traitée. Toutefois, il serait intéressant de dimensionner certains composants du système électrique du véhicule comme l'alternateur, la batterie, le supercondensateur ou le convertisseur DC/DC en utilisant la méthode de plan d'expériences ainsi que les stratégies développées. Un autre point intéressant serait de considérer

le couple moteur optimal fourni par les stratégies développées comme une référence de couple et de l'incorporer dans le calculateur pour la tâche de contrôle du moteur.

Théorie.

Premièrement, l'utilisation de la stratégie "anti-windup" basée sur les fonctions de Lyapunov, pour réduire les effets de saturation est très récente dans l'automatique moderne. De nombreux travaux sont disponibles dans la littérature pour les systèmes linéaires. Cependant, cette approche est encore un sujet de recherche très ouvert dans le cas des systèmes non linéaires. À notre connaissance, l'approche de commande à "une étape" proposée dans le chapitre 4 est l'un des premiers résultats dans le cadre de la technique de commande basée sur des modèles Takagi-Sugeno. Cette méthode peut est utilisée pour une grande classe de systèmes non linéaires. Comme indiqué précédemment, les conditions pour concevoir le contrôleur peuvent être conservatives. La relaxation de ces conditions est actuellement à l'étude.

Deuxièmement, nous pensons que la méthode de commande à "deux étapes" où le contrôleur est supposé connu avant de concevoir le gain "anti-windup" en utilisant des modèles Takagi-Sugeno serait très intéressante à étudier. La comparaison entre ces deux approches serait également importante.

Enfin, dans le cadre de la collaboration avec le Professeur Michio Sugeno, nous avons commencé à étudier les modèles bilinéaires par morceaux (PB) (Sugeno, 1999) et ses problèmes de commande. Ce type de modèles offre une représentation unifiée (dans le sens d'approximation) d'une grande classe de systèmes non linéaires. Du point de vue industriel, la modélisation bilinéaire par morceaux est un outil puissant pour approximer un système non linéaire général, et le modèle de PB qui en résulte peut être également considéré comme une cartographie dynamique facilement implémentable. Ces faits sont intéressants à la fois pour la théorie de commande non linéaire et pour les applications réelles. Toutefois, jusqu'à présent, les modèles PB sont encore un "terrain inconnu" dans le monde de l'automatique. En effet, la plupart des travaux liés aux modèles PB est actuellement basée sur la commande linéarisante. Cependant, de notre point de vue, la technique de commande basée sur les modèles PB deviendrait vraiment attirante pour les chercheurs scientifiques si nous arrivions à trouver un moyen de dériver les conditions de stabilité/stabilisation directement à partir du théorème de stabilité de Lyapunov. Les travaux proposés dans (Sugeno, 1999; Sugeno & Taniguchi, 2004) apportent quelques lignes directrices, mais ce problème reste ouvert.

BIBLIOGRAPHY

Ambühl, A., Sundström, O., Sciarretta, A. & Guzzella, L., 2010. Explicit Optimal Control Policy and Its Practical Application for Hybrid Electric Powertrains. *Control Engineering Practice*, 18(12), pp.1429-39.

André, M., 2004. The ARTEMIS European Driving Cycles for Measuring car Pollutant Emissions. *Science of The Total Environment*, 334-335, pp.73-84.

Bellman, R.E., 1957. *Dynamic Programming*. Princeton, USA: Princeton University Press.

Borutzky, W., 2010. *Bond Graph Methodology: Development and Analysis of Multidisciplinary Dynamic System Models*. Springer.

Boyd, S., Ghaoui, L.E., Feron, E. & Balakrishnan, V., 1994. *Linear Matrix Inequalities in System and Control Theory*. Philadelphia: Society for Industrial and Applied Mathematics (SIAM).

Cao, Y.Y. & Lin, Z., 2003. Robust Stability Analysis and Fuzzy-Scheduling Control for Nonlinear Systems Subject to Actuator Saturation. *Transactions on Fuzzy Systems*, 11(1), pp.57-67.

Castelan, E.B., Tarbouriech, S., Gomes da Silva Jr, J.M. & Queinnec, I., 2006. $\mathcal{L}_2$-Stabilization of Continuous-Time Linear Systems with Saturating Actuators. *International Journal of Robust and Nonlinear Control*, 16, pp.935-44.

Chadli, M. & Guerra, T.M., 2012. LMI Solution for Robust Static Output Feedback Control of Discrete Takagi-Sugeno Fuzzy Models. *IEEE Transactions on Fuzzy Systems*, 20(6), pp.1160-65.

Chen, S.S. et al., 2005. Robust Static Output-Feedback Stabilization for Nonlinear Discrete-Time Systems with Time Delay via Fuzzy Control Approach. *Trans. Fuzzy Systems*, 13, pp.263-72.

Colin, G., Chamaillard, Y., Bloch, G. & Corde, G., 2007. Neural Control of Fast Nonlinear Systems: Application to a TCSI Engine with VCT. *Transaction on Neural Networks*, 18(4), pp.1101-14.

Dabo, M., Langlois, N. & Chafouk, H., 2009. Dynamic Feedback Linearization Applied to Asymptotic Tracking: Generalization about the Turbocharged Diesel Engine Outputs Choice. In *American Control Conference*. St. Louis, 2009.

Daubler, L., Bessai, C. & Predelli, O., 2007. Tuning Strategies for Online-Adaptive PI Controller. *Oil & Gas Science and Technology - Rev. IFP*, 62(4), pp.493-500.

Delmotte, F., Guerra, T.M. & Ksantini, M., 2008. Continuous Takagi-Sugeno's Models: Reduction of the Number of LMI Conditions in Various Fuzzy Control Design Technics. *IEEE Transactions on Fuzzy Systems*, 15(3), pp.426-38.

Delprat, S., Guerra, T.M. & Rimaux, J., 2002. Optimal Control of a Parallel Powertrain: from Global Optimization to Real Time Control Strategy. In *IEEE Vehicular Transportation Systems*. Atlantic City, USA, 2002.

Delprat, S., Lauber, J., Guerra, T.M. & Rimaux, J., 2004. Control of a Parallel Hybrid Powewtrain: Optimal Control. *IEEE Transactions on Vehicular Technology*, 53(3), pp.872-81.

Ding, B., 2009. Quadratic Boundedness via Dynamic Output Feedback for Constrained Nonlinear Systems in Takagi-Sugeno's Form. *Automatica*, 45, pp.2093-98.

Dong, J. & Yang, G.H., 2008. State Feedback Control of Continuous-Time T-S Fuzzy Systems via Switched Fuzzy Controllers. *Information Sciences*, 178, pp.1680-95.

El Ghaoui, L. & Scorletti, G., 1996. Control of Rational Systems Using Linear-Fractional Representations and Linear Matrix Inequalities. *Automatica*, 32(9), pp.1273-84.

Eriksson, L., 2007. Modeling and Control of Turbocharged SI and DI Engines. *Oil & Gas Science and Technologies*, 62(4), pp.523-38.

Eriksson, L., Frei, S., Onder, C. & Guzzella, L., 2002. Control and Optimization of Turbocharged SI Engines. In *15th IFAC World Congress*. Barcelona, Spain, 2002.

Fang, H., Lin, Z. & Hu, T., 2004. Analysis of Linear Systems in the Presence of Actuator Saturation and $\mathcal{L}2$ Disturbances. *Automatica*, 40, pp.1229-38.

Feng, G., 2003. Controller Synthesis of Fuzzy Dynamic Systems Based on Piecewise Lyapunov Functions. *IEEE Transactions on Fuzzy Systems*, 11(5), pp.605-12.

Feng, G., 2006. A Survey on Analysis and Design of Model-Based Fuzzy Control Systems. *IEEE Transactions Fuzzy Systems*, 14(5), pp.676-97.

Gahinet, P., Nemirovski, A., Laub, A.J. & Chilali, M., 1995. LMI Control Toolbox. *The Math Works Inc*.

Gomes da Silva, J.M. & Tarbouriech, S., 2005. Antiwindup Design with Guaranteed Regions of Stability: An LMI-Based Approach. *IEEE Transactions on Automatic Control*, 50(1), pp.106-11.

Gorzelic, P. et al., 2012. A Coordinated Approach for Throttle and Wastegate Control in Turbocharged Spark Ignition Engines. In *24th Chinese Control and Decision Conference*. Taiyuan, China, 2012.

Grimm, G.a.H.J.a.P.I., Teel, A.R., Turner, M.C. & Zaccarian, L., 2003. Antiwindup for Stable Linear Systems with Input Saturation: an LMI-Based Synthesis. *IEEE Transactions on Automatic Control*, 48(9), pp.1509-25.

Guelton, K., Bouarar, T. & Manamanni, N., 2009. Robust Dynamic Otput Feedback Fuzzy Lyapunov Stabilization of Takagi-Sugeno Systems — A Descriptor Redundancy Approach. *Fuzzy Sets and Systems*, (160), pp.2796-811.

Guerra, T., Kruszewski, A. & Lauber, J., 2009. Discrete Tagaki–Sugeno Models for Control: Where Are We? *Annual Reviews in Control*, 33(1), pp.37-47.

Guerra, T.M., Kruszewski, A., Vermeiren, L. & Tirmant, H., 2006. Conditions of Output Stabilization for Nonlinear Models in the Takagi-Sugeno's Form. *Fuzzy Sets and Systems*, 157(9), pp.1248-59.

Guerra, T.M. & Vermeiren, L., 2004. LMI-Based Relaxed Nonquadratic Stabilization Conditions for Nonlinear Systems in the Takagi-Sugeno's Form. *Automatica*, 40(5), pp.823-29.

Guzzella, L. & Onder, C., 2004. *Introduction to Modeling and Control of Internal Combustion Engine Systems*. Springer.

Ha, I.J. & Gilbert, E.G., 1987. Robust Tracking in Nonlinear Systems. *IEEE Transactions on Automatic Control*, 32(9), pp.763-71.

Hartl, R.F., Sethi, S.P. & Vickson, R.G., 1995. A Survey of the Maximum Principles for Optimal Control Problems with State Constraints. *SIAM Review*, 37(2), pp.181-218.

Heywood, J., 1988. *Internal Combustion Engine Fundamentals*. McGraw-Hill, Inc.

Hofman, T., 2007. *Framework for Combined Control and Design Optimization of Hybrid Vehicle Propulsion Systems*. PhD Thesis. Technische Universiteit Eindhoven.

Hong, S.K. & R., L., 2000. An LMI-Based Fuzzy Control System Design with T-S Framework. *Information Sciences*, 123, pp.163-79.

Huang, D. & Nguang, S.K., 2006. Robust H∞ Static Output Feedback Control of Fuzzy Systems: an ILMI Approach. *Transactions on Systems, Man, and Cybernetics*, Part-B, 36(1), pp.216-22.

Hu, T., Teel, A.R. & Zaccarian, L., 2008. Anti-Windup Synthesis for Linear Control Systems with Input Saturation: Achieving Regional, Nonlinear Performance. *Automatica*, 44, pp.512-19.

Isidori, A., 1989. *Nonlinear Control Systems*. Springer Verlag.

Johansson, M., Rantzer, A. & Arzen, K.E., 1999. Piecewise Quadratic Stability of Fuzzy Systems. *IEEE Transactions on Fuzzy Systems*, 7(6), pp.713-22.

Jung, M., Glover, K. & Christen, U., 2005. Comparison of Uncertainty Parameterisations for H-infinity Robust Control of Turbocharged Diesel Engines. *Control Engineering Practice*, 13(1), pp.15-25.

Karnik, A., Buckland, J. & Freudenberg, J., 2005. Electronic Throttle and Wastegate Control for Turbocharged Gasoline Engines. In *American Control Conference*. Portland, 2005.

Kau, S.W. et al., 2007. Robust H∞ Fuzzy Static Output Feedback Control of T-S Fuzzy Systems with Parametric Uncertainties. *Fuzzy Sets and Systems*, 158(2), pp.135-46.

Kessels, T.J.B.A., 2007. *Energy Management for Automotive Power Nets*. PhD Thesis. Technische Universiteit Eindhoven.

Khalil, H.K., 2002. *Nonlinear Systems*. 3rd ed. Prentice Hall.

Khargonekar, P.P., Nagpal, I.M. & Poollag, K.R., 1990. Control of Linear Systems with Nonzero Initial Conditions. In *29th IEEE Conference Decision and Control*. Honolulu, HI, 1990.

Kim, N., Cha, S. & Peng, H., 2011. Optimal Control of Hybrid Electric Vehicles Based on Pontryagin's Minimum Principle. *IEEE Transactions on Control Systems Technology*, 19(5), pp.1279-87.

Kim, E., Park, M., Ji, S. & Park, M., 1997. A New Approach to Fuzzy Modeling. *IEEE Transactions on Fuzzy Systems*, 5(3), pp.328-37.

Kirk, D.E., 1970. *Optimal Control Theory: An Introduction*. Englewood Cliffs : Prentice-Hall.

Koot, M.W.T., 2006. *Energy Management for Vehicular Electric Power Systems*. PhD Thesis. Technische Universiteit Eindhoven.

Koot, M. et al., 2005. Energy Management Strategies for Vehicular Electric Power Systems. *IEEE Transactions on Vehicular Technology*, 54(3), pp.771-82.

Kothare, M.V., Campo, P.J., Morari, M. & Nett, C.N., 1994. A Unified Framework for the Study of Anti-Windup Designs. *Automatica*, 30(12), pp.1869-83.

Kravaris, C. & Palanki, S., 1988. A Lyapunov Approach for Robust Nonlinear State Feedback Synthesis. *IEEE Transactions on Automatic Control*, 33(12), pp.1188-91.

Lake, T. et al., 2004. Turbocharging Concepts for Downsized DI Gasoline Engines. In *SAE Conference*., 2004.

Lauber, J., Guerra, T.M. & Dambrine, M., 2011. Air-Fuel Ratio Control in a Gasoline Engine. *International Journal of Systems Science*, 42(2), pp.277-86.

Leduc, P., Dunbar, B., Ranini, A. & Monnier, G., 2003. Downsizing of Gasoline Engine: an Efficient Way to Reduce CO2 Emissions. *Oil & Gas Science and Technology*, 58(1), pp.115-27.

Lee, K.R., Jeung, E.T. & Park, H.B., 2001. Robust Fuzzy H_∞ Control for Uncertain Nonlinear Systems via State Feedback: an LMI Approach. *Fuzzy Sets and Systems*, 120(1), pp.123-34.

Lendek, Z., Guerra, T.M., Babuška, R. & De Schutter, B., 2010. *Stability Analysis and Nonlinear Observer Design Using Takagi-Sugeno Fuzzy Models*. Studies in Fuzziness and Soft Computing.

Liberzon, D., 2003. *Switching in Systems and Control*. Boston, MA: Birkhauser.

Lin, C.C., Peng, H., Grizzle, J.W. & Kang, J.M., 2003. Power Management Strategy for a Parallel Hybrid Electric Truck. *IEEE Transactions on Control Systems Technology*, 1(6), pp.839-49.

Lin, C., Wang, Q.G. & Lee, T.H., 2005. Improvement on Observer-Based H_∞ Control for T-S Fuzzy Systems. *Automatica*, 41, pp.1651-56.

Liu, X. & Zhang, Q., 2003. New Approaches to Controller Designs Based on Fuzzy Observers for T-S Fuzzy Systems via LMI. *Automatica*, 39(9), pp.1571-82.

Li, J., Wang, H.O. & Tanaka, K., 2000. Dynamic Parallel Distributed Comp ensation for Takagi-Sugeno Fuzzy Systems: An LMI Approach. *Information Sciences*, 123(3-4), pp.201-21.

Lofberg, J., 2004. YALMIP: a Toolbox for Modeling and Optimization in MATLAB. In *IEEE International Symposium on Computer Aided Control Systems Design*. Taipei, 2004.

Lo, J.C. & Lin, M.L., 2003. Robust H_∞ Nonlinear Control via Fuzzy Static Output Feedback. *Transactions Circuits Systems*, 50(11), pp.1494-502.

Mamdani, E.H., 1974. Application of Fuzzy Algorithms for Control of Simple Dynamic Plant. *Proceedings of the Institution of Electrical Engineers*, 121(12), pp.1585-88.

Mansouri, B. et al., 2009. Output Feedback LMI Tracking Control Conditions with H_∞ Criterion for Uncertain and Disturbed T-S Models. *Information Sciences*, 179, pp.446-57.

Moraal, P. & Kolmanovsky, I., 1999. Turbocharger Modeling for Automotive Control Applications. *SAE Technical Paper Series*, no. 1999-01-0908.

Moulin, P., 2010. *Air Systems Modeling and Control for Turbocharged Engines*. PhD Thesis. MINES Paristech.

Moulin, P. & Chauvin, J., 2011. Modeling and Control of the Air System of a Turbocharged Gasoline Engine. *Control Engineering Practice*, 19(3), pp.287-97.

Moulin, P., Chauvin, J. & Youssef, B., 2008. Modeling and Control of the Air System of a Turbocharged Gasoline Engine. In *IFAC World Conference*. Seoul, 2008.

Mozelli, L.A., Palhares, R.M., Souza, F.O. & Mendes, E.M.A.M., 2009. Reducing Conservativeness in Recent Stability Conditions of T-S Fuzzy Systems. *Automatica*, 45(6), pp.1580-83.

Mulder, E.F., Tiwari, P.Y. & Kothare, M.V., 2009. Simultaneous Linear and Anti-Windup Controller Synthesis Using Multiobjective Convex Optimization. *Automatica*, 45, pp.805-11.

Nguang, S.K. & Shi, P., 2003. Fuzzy Hinf Output Feedback Control of Nonlinear Systems under Sampled Measurements. *Automatica*, 39(12), pp.2169-74.

Nguyen, A., Lauber, J. & Dambrine, M., 2012a. Switching Fuzzy Control of the Air System of a Turbocharged SI Engine. In *IEEE International Conference on Fuzzy Systems*. Brisbane, Australia, 2012a.

Nguyen, A.T., Lauber, J. & Dambrine, M., 2012b. Modeling and Switching Fuzzy Control of the Air Path of a Turbocharged Spark Ignition Engine. In *IFAC Workshop on Engine and Powertrain Control, Simulation and Modeling*. Paris, France, 2012b.

Nguyen, A.T., Lauber, J. & Dambrine, M., 2012c. Robust H∞ Control Design for Switching Uncertain System: Application for Turbocharged Gasoline Air System Control. In *51st Conference on Decision and Control*. Maui, Hawaii, USA, 2012c.

Ohtake, H., Tanaka, K. & Wang, H.O., 2001. Fuzzy Modeling via Sector Nonlinearity Concept. In *Joint 9th IFSA World Congress and 20th NAFIPS International Conference*. Vancouver, Canada, 2001.

Ohtake, H., Tanaka, K. & Wang, H.O., 2006. Switching Fuzzy Controller Design Based on Switching Lyapunov Function for a Class of Nonlinear Systems. *Transactions Systems, Man, and Cybernetics, Part B*, 36(1), pp.13-23.

Ortner, P. & del Re, L., 2007. Predictive Control of a Diesel Engine Air Path. *IEEE Transactions on Control Systems Technology*, 15(3), pp.449-56.

Paganelli, G. et al., 2002. Optimal Control Theory Applied to Hybrid Fuel Cell Powered Vehicle. In *15th IFAC World Congress*. Barcelona, 2002.

Petersen, I.R., 1987. A Stabilization Algorithm for a Class of Uncertain Linear Systems. *Systems & Control Letters*, 8(4), pp.351-57.

Pontryagin, L.S., Boltyanskii, V.G., Gamkrelidze, R.V. & Mishchenko, E.F., 1962. *The Mathematical Theory of Optimal Processes*. New York: Interscience Publishers.

Poursamad, A. & Montazeri, M., 2008. Design of Genetic Fuzzy Control Strategy for Parallel Hybrid Electric Vehicles. *Control Engineering Practice*, 16(7), pp.861-73.

Rhee, B.J. & Won, S., 2006. A New Lyapunov Function Approach for a Takagi-Sugeno Fuzzy Control System Design. *Fuzzy Sets and Systems*, 157(9), pp.1211-28.

Rousseau, G., 2008. *Hybrid Vehicles and Optimal Control*. PhD Thesis (in French). MINES Paristech.

Sala, A. & Arino, C., 2007. Asymptotically Necessary and Sufficient Conditions for Stability and Performance in Fuzzy Control: Applications of Polya's Theorem. *Fuzzy Sets Systems*, 158, pp.2671–86.

Sala, A. & Arino, C., 2009. Polynomial Fuzzy Models for Nonlinear Control: A Taylor Series Approach. *IEEE Transactions on Fuzzy Systems*, 17(6), pp.1284-95.

Sala, A., Guerra, T. & Babuska, R., 2005. Perspectives of Fuzzy Systems and Control. *Fuzzy Sets and Systems*, 156(3), pp.432-44.

Sala, A., Guerra, T.M. & Babuska, R., 2005. Perspectives of Fuzzy Systems and Control. *Fuzzy Sets and Systems*, 156(3), pp.432-44.

Sastry, S., 1999. *Nonlinear Systems*. Springer.

Scherer, C., Gahinet, P. & Chilali, M., 1997. Multiobjective Output-Feedback Control via LMI Optimization. *IEEE Transactions on Automatic Control*, 42(7), pp.896-911.

Scherer, C. & Weiland, S., 2005. *Linear Matrix Inequalities in Control*. Lecture Notes, Delft University.

Schouten, N.J., Salman, M.A. & Kheir, N.A., 2002. Fuzzy Logic Control for Parallel Hybrid Vehicles. *IEEE Transactions on Control Systems Technology*, 10(3), pp.460-68.

Sciarretta, A., Back, M. & Guzzella, L., 2004. Optimal Control of Parallel Hybrid Electric Vehicles. *IEEE Transactions on Control Systems Technology*, 12(3), pp.352-63.

Sciarretta, A. & Guzzella, L., 2007. Control of Hybrid Electric Vehicles: a Survey of Optimal Energy Management Strategies. *IEEE Control Systems Magazine*, 27(2), pp.60-70.

Serrao, L., Onori, S. & Rizzoni, G., 2009. ECMS as a Realization of Pontryagin's Minimum Principle for HEV Control. In *American Control Conference*. St. Louis, MO, 2009.

Šiljak, D.D. & Stipanović, D.M., 2000. Robust Stabilization of Nonlinear Systems: The LMI Approach. *Mathematical Problems in Engineering*, 6(5), pp.461-93.

Sontag, E. & Wang, Y., 1995. On Characterizations of the Input to State Stability Property. *Systems and Control Letters*, 24, pp.351-59.

Soong, W., Ertugrul, N., Lovelace, E. & Jahns, T., 2001. Investigation of Interior Permanent Magnet Offset-Coupled Automotive Integrated Starter/Alternator. In *Industry Applications Conference*. Chicago, IL, USA, 2001.

Sugeno, M., 1999. On Stability of Fuzzy Systems Expressed by Fuzzy Rules with Singleton Consequents. *IEEE Transactions on Fuzzy Systems*, 7(2), pp.201-24.

Sugeno, M. & Kang, G.T., 1988. Structure Identification of Fuzzy Model. *Fuzzy Sets and Systems*, 28(1), pp.15-33.

Sugeno, M. & Taniguchi, T., 2004. On Improvement of Stability Conditions for. Continuous Mamdani-Like Fuzzy Systems. *IEEE Transactions on Systems, Man, and Cybernetics, Part B: Cybernetics*, 34(1), pp.120-31.

Sundström, O., 2009. *Optimal Control and Design of Hybrid Electric Vehicles*. PhD Thesis. ETH Zurich.

Syrmos, V.L., Abdallah, C.T., Dorato, P. & Grigoriadis, K., 1997. Static Output Feedback: a Survey. *Automatica*, 33(2), pp.125-37.

Takagi, T. & Sugeno, M., 1985. Fuzzy Identification of Systems and Its Applications to Modeling and Control. *Transactions on Systems, Man and Cybernetics*, 15(1), pp.116-32.

Tanaka, K., Ikeda, T. & Wang, H.O., 1998. Fuzzy Regulators and Fuzzy Observers: Relaxed Stability Conditions and LMI-Based Design. *IEEE Transactions on Fuzzy Systems*, 4(2), pp.1-16.

Tanaka, K., Iwasaki, M. & Wang, H.O., 2001. Switching Control of an R/C Hovercraft: Stabilization and Smooth Switching. *Transactions on Systems, Man and Cybernetics*, 31(6), pp.853-63.

Tanaka, K. & Sugeno, M., 1992. Stability Analysis and Design of Fuzzy Control Systems. *Fuzzy Sets and Systems*, 45(2), pp.135-56.

Tanaka, K. & Wang, H.O., 2001. *Fuzzy Control Systems Design and Analysis: a Linear Matrix Inequality Approach*. New York: Wiley, Wiley-Interscience.

Taniguchi, T. & Sugeno, M., 2012. Robust Stabilization of Nonlinear Systems Modeled with Piecewise Bilinear Systems Based on Feedback Linearization. In *IPMU*. Sicily, 2012.

Taniguchi, T., Tanaka, K., Ohtake, H. & Wang, H.O., 2001. Model Construction, Rule Reduction, and Robust Compensation for Generalized Form of Takagi-Sugeno Fuzzy Systems. *Transactions on Fuzzy Systems*, 9(4), pp.525-38.

Taniguchi, T., Tanaka, K. & Wang, H.O., 2000. Fuzzy Descriptor Systems and Nonlinear Model Following Control. *IEEE Transactions on Fuzzy Systems*, 8(4), pp.442-52.

Tarbouriech, S., Garcia, G., Gomes da Silva Jr., J.M. & Queinnec, I., 2011. *Stability and Stabilization of Linear Systems with Saturating Actuators*. London: Springer-Verlag.

Teel, A.R. & Kapoor, N., 1997. The L2 Anti-Windup Problem: Its Definition and Solution. In *European Control Conference*, 1997.

Tuan, H., Apkarian, P., Narikiyo, T. & Yamamoto, Y., 2001. Parameterized Linear Matrix Inequality Techniques in Fuzzy Control System Design. *Transactions on Fuzzy Systems*, 9(2), pp.324-32.

Utkin, V., Chang, H., Kolmanovsky, I. & Cook, J., 2000. Sliding Mode Control for Variable Geometry Turbocharged Diesel Engines. In *American Control Conference*. Chiacago, 2000.

Wang, H.P., Bosche, J., Tian, Y. & El Hajjaji, A., 2011. Two Loop based Dynamical Feedback Stabilization Control of a Diesel Engine with EGR & VGT. In *50th IEEE Conference on Decision and Control and European Control Conference,* Orlando, USA, 2011.

Wang, H.O., Tanaka, K. & Griffin, M., 1996. An Approach to Fuzzy Control of Noninear Systems: Stability and Design Issues. *IEEE Transactions on Fuzzy Systems*, 4, pp.14-23.

Wei, X. & del Re, L., 2007. Gain Scheduled H∞ Control for Air Path Systems of Diesel Engines Using LPV Techniques. *IEEE Transactions on Control Systems Technology*, 15(3), pp.406-15.

Wu, F., Grigoriadis, K.M. & Packard, A., 2000. Anti-windup Controller Design Using Linear Parameter Varying Control Methods. *International Journal of Control*, 73(12), pp.1104-14.

Xu, S. & Lam, J., 2005. Robust H_∞ Control for Uncertain Discrete-Time-Delay Fuzzy Systems via Output Feedback Controllers. *Transactions Fuzzy Systems*, 13, pp.82-93.

Yoneyama, J., 2006. Robust H_∞ Control Analysis and Synthesis for Takagi–Sugeno General Uncertain Fuzzy Systems. *Fuzzy Sets and Systems*, 157(16), pp.2205-23.

Yoneyama, J., 2007. Robust Stability and Stabilization for Uncertain Takagi-Sugeno Fuzzy Time-Delay Systems. *Fuzzy Sets and Systems*, 158(2), pp.115-34.

Yoneyama, J., Nishikawa, M., Katayama, H. & Ichikawa, A., 2000. Output Stabilization of Takagi-Sugeno Fuzzy Systems. *Fuzzy Sets and Systems*, 111(2), pp. 253-266.

Zaccarian, L. & Teel, A.R., 2004. Nonlinear Scheduled Anti-Windup Design for Linear Systems. *IEEE Transactions on Automatic Control*, 49(11), pp.2055-61.